



University of **HUDDERSFIELD**

University of Huddersfield Repository

Olabode, Olaide Felix

CORE TEMPERATURE MEASUREMENT USING ULTRASOUND FOR HIGH PRECISION MANUFACTURING PROCESSES

Original Citation

Olabode, Olaide Felix (2021) CORE TEMPERATURE MEASUREMENT USING ULTRASOUND FOR HIGH PRECISION MANUFACTURING PROCESSES. Doctoral thesis, University of Huddersfield.

This version is available at <http://eprints.hud.ac.uk/id/eprint/35676/>

The University Repository is a digital collection of the research output of the University, available on Open Access. Copyright and Moral Rights for the items on this site are retained by the individual author and/or other copyright owners. Users may access full items free of charge; copies of full text items generally can be reproduced, displayed or performed and given to third parties in any format or medium for personal research or study, educational or not-for-profit purposes without prior permission or charge, provided:

- The authors, title and full bibliographic details is credited in any copy;
- A hyperlink and/or URL is included for the original metadata page; and
- The content is not changed in any way.

For more information, including our policy and submission procedure, please contact the Repository Team at: E.mailbox@hud.ac.uk.

<http://eprints.hud.ac.uk/>

**CORE TEMPERATURE MEASUREMENT USING
ULTRASOUND FOR HIGH PRECISION MANUFACTURING
PROCESSES**

OLAIDE FELIX OLABODE

A thesis submitted to the University of Huddersfield in partial fulfilment of the requirements
for the degree of Doctor of Philosophy

The University of Huddersfield

2021

Copyright Statement

- i. The author of this thesis (including any appendices and/or schedules attached to this thesis) owns any copyright in it (the “Copyright”) and he has given The University of Huddersfield the right to use such Copyright for any administrative, promotional, educational, and/or teaching purposes.
- ii. Copies of this thesis, either in full or in extracts, may be made only in accordance with the regulations of the University Library. Details of these regulations may be obtained from the Librarian. This page must form part of any such copies made.
- iii. The ownership of any patents, designs, trademarks and any and all other intellectual property rights except for the Copyright (the “Intellectual Property Rights”) and any reproductions of copyright works, for example graphs and tables (“Reproductions”), which may be described in this thesis, may not be owned by the author and may be owned by third parties. Such Intellectual Property Rights and Reproductions cannot and must not be made available for use without permission of the owner(s) of the relevant Intellectual Property Rights and/or Reproductions.

Abstract

During manufacturing processes, workpiece temperature may vary due to factors arising from the process such as tool/workpiece friction. Workpiece temperature may also vary due to the environmental conditions and these variations can affect the dimensional accuracy of the manufactured workpiece. The surface temperature of a part being manufactured can vary significantly from the core temperature, especially during dry cutting processes or when the environmental conditions are changing rapidly. It is known that the expansion of a part is controlled by its average temperature and can be influenced more by the core temperature of the part than the surface temperature due to the relative material volumes. Therefore, to effectively control or compensate for the effects of temperature variation as it relates to material expansion, there is a need to measure the core temperature of the workpiece accurately. Due to the harsh nature of many manufacturing environments, the required accuracy and resolution for temperature measurement in precision manufacturing are rarely achieved.

The aim of this research is to measure core temperature of workpieces during manufacturing processes with accuracy and resolution based on industry requirements. The main research objectives include simulating the chosen temperature measurement method to determine its suitability, designing a system for core temperature measurement, and using the designed system for core temperature measurement during a manufacturing process.

In this thesis, after reviewing the different temperature measurement methods with greater emphasis on those applicable to the manufacturing process, the ultrasonic thermometry was chosen for further study. The speed of sound in any medium depends on the temperature of the medium. Hence, if the length and time of travel of an ultrasonic wave can be measured, the speed, and consequently the temperature, can be measured. Since the ultrasonic method gives the average of the travel path, the core temperature can be obtained.

To verify these theories and determine the cost-effective technique of ultrasonic measurement for the present task, the MATLAB k-Wave toolbox was used for simulating the two main techniques of ultrasonic measurement – the pulse-echo and phase-shift methods. Using steel as the medium of propagation, the simulation results showed that both techniques can be used for the present task. However, further analysis of the results showed that the phase-shift technique could be the cost-effective option. Therefore, the phase-shift technique was chosen for the bench tests. Controlled heating of a steel test part was performed using a liquid bath calibrator and a reference temperature sensor for accurate comparison. The results showed that the measured temperature values using the phase-shift ultrasonic method agree with the reference PT100 measurements with the required resolution and accuracy. The phase-shift card used in this method is a cost-effective solution that eliminates the need for the expensive pulser-receivers used for the ultrasonic pulse-echo method.

Thereafter, the setup was used on a computer numeric control machine while incrementally introducing different levels of uncertainty to the manufacturing process. The results show that the phase-shift ultrasonic thermometry method measures workpiece temperature during subtractive manufacturing processes with accuracy of ± 1 °C. The setup was also used on a coordinate measuring machine during dimensional inspection. This test was set up to compare the calculated expansion based on core and surface temperature measurements with the measured expansion. The results show that the surface temperature-based expansion error is approximately 0.5 μm more than that of the core temperature. Finally, the created setup was used on an aluminium workpiece. The temperature measurement has error values within ± 0.45 °C when compared with the reference PT100 readings with standard deviation of 0.1 °C.

This is the first time that ultrasonic thermometry has been used to measure temperature of metal components being machined and is a novel solution to the significant challenges of part temperature measurement during machining.

Acknowledgements

I would like to thank God; the fountain of wisdom, understanding, and true knowledge for granting me all that I required to complete this doctoral study. I received insights and inspiration throughout my PhD journey through His grace and favour. I would also like to appreciate my amazing supervisors who patiently led me through each stage and ensured that I received the best support and guidance throughout my doctoral study. It is such a privilege to have been supervised by Dr Simon Fletcher, Professor Andrew Peter Longstaff, and Dr Naeem Mian.

I would like to deeply appreciate Dr Simon Fletcher. Thank you for helping me find my feet, for teaching me how to carry out a research work, and for steadying me throughout the journey. Thank you for literally opening your door to me. Thank you for supporting me to present my work properly, for asking the tough questions, for modelling hard work and dedication to me, and for the numerous things I have probably not mentioned. Thank you so much and I do not take any of these for granted.

I would also like to specially thank Professor Andrew Longstaff. Sir, thank you for creating an enabling environment for this research from the outset of my doctoral study. Thank you for genuinely being interested in my welfare and for your insistence on quality research. I am forever thankful for the opportunity you gave me to learn how to teach and supervise students.

I would like to thank Dr Naeem Mian for his support which he readily offered whenever I needed it. I would like to specially appreciate Mr Andrew Bell. Thank you for instilling in me the awareness of safety in the workshop and for teaching me about the CNC. Thank you for answering all my numerous questions. Thank you for guiding me through all my cutting trials. I am truly grateful for all your help.

I would like to acknowledge the funding I received from the School of Computing and Engineering – University of Huddersfield and the EPSRC Future Metrology Hub which helped me to fully focus on my research without the need to worry about my finances.

I would like to thank Dr Kwame Akowua who mentored me through my first year and for his guidance throughout the journey. I would like to thank Mr Tom Furness for his help with the CMM experiment and general research advice. I would also like to thank my colleagues at the ECMPG research group for their support throughout my doctoral study.

My special thanks also go to my examiners Dr James Williamson, Professor Bruce Drinkwater, and Dr Peter Mather who provided me with detailed comments and constructive criticisms of my research.

On a personal note, I would like to specially appreciate my fantastic wife, Dr Oluwaseun Eniola Olabode for her love, care, support, and encouragement throughout the PhD journey. I am grateful for your strength, for not losing focus during our most trying times. Thank you for handling trials and adversity with such resilience and remaining graceful all through. Thank you for being my personal quality control officer. Thank you for your numerous sacrifices for us and for believing in this approach to life. I am proud of what you have achieved. I love you and I am grateful for you. To Gloria and Bezalel Oyeoluwa Olabode, you mean so much to me.

I would like to thank my parents, Mr Felix Olabode Abegunde and Mrs Esther Bolatito Abegunde for their prayers, love, and support. I am grateful for all you have given to me in life. Thank you for giving your all and for providing the platform I needed to be whatever I wanted to be. Thank you for teaching me the principles of planning ahead of time. I would like

to thank my adorable siblings, Fiyinfoluwa, Oluwadamilola, and Emmanuel. Thank you for your love, prayers, and support. I also want to appreciate Dr MBO, Mrs Titilola, Matthew, and Mercy Adegbile for their prayers and support.

I am grateful to my friends and other members of my family for their love, prayers, and support. Thank you.

Olaide Felix Olabode

July 2021.

Contents

Abstract	2
Acknowledgements	3
List of Figures	10
List of Tables	14
Glossary of Terms	15
Nomenclature	17
Chapter 1	19
1 Introduction	19
1.1 Motivation	23
1.2 Aim	23
1.3 Objectives	23
1.4 Novel Contributions	24
1.4.1 Journal Article Published from Thesis Findings	25
1.4.2 Conference Papers and Presentations from Thesis	25
1.5 Scope of Research	26
1.6 Thesis Structure	27
Chapter 2	29
2 Review of Previous Research	29
2.1 Temperature Measurement Techniques	29
2.2 Temperature Measurement in Metal Cutting Processes	32

2.3	Acoustic Thermometry.....	34
2.3.1	Acoustic Velocity.....	34
2.4	Ultrasound.....	35
2.4.1	Ultrasonic Thermometry	36
2.5	Temperature Dependence of Ultrasonic Velocity	38
2.6	Ultrasonic Velocity Measuring Methods	39
2.7	Phase-shift Method.....	40
2.8	Pulse-echo Method.....	41
2.9	Modifications and Combinations of Pulse-echo and Phase-shift Methods.....	43
2.10	Ultrasonic Transducers, Signal Generation, and Data Acquisition Electronics.....	45
2.10.1	Ultrasonic Transducers	45
2.10.2	Signal Generation and Data Acquisition Electronics.....	48
2.11	Summary of Literature Review	51
Chapter 3	53
3	Methodology.....	53
3.1	Ultrasonic Simulation.....	53
3.1.1	Ultrasonic Time-of-flight Simulation	56
3.1.2	Ultrasonic Phase-shift Simulations	65
3.2	Ultrasonic Couplants.....	70
3.3	Signal Generation and Acquisition	72
3.3.1	Waveform Generation.....	72

3.3.2	Ultrasonic Transducer	74
3.3.3	Phase-shift Detection	75
3.3.4	AD8302 Phase-shift Detector	77
3.3.5	Data Acquisition	83
3.4	Summary	83
Chapter 4.....		86
4	Ultrasonic Thermometry Experiments (Controlled Heating)	86
4.1	Experiments.....	86
4.1.1	Phase Out Response.....	86
4.1.2	Experimental Setup Using Ceramic Heater	88
4.1.3	Results for Ultrasonic Thermometry (Ceramic Heater).....	90
4.2	Experiment Using Liquid Bath Calibrator	94
4.2.1	Results of Ultrasonic Thermometry (Liquid Bath Calibrator).....	98
4.3	Echo Signal Amplification	101
4.3.1	Bench Test with Signal Amplifier	106
4.4	Summary	109
Chapter 5.....		112
5	In-Process Ultrasonic Thermometry	112
5.1	Static Test (CNC Switched on)	116
5.2	Spindle Running Tests	121
5.3	Test with Cutting Fluid	124

5.4	Dry Cutting Trials	126
5.5	Wet Cutting Trials.....	129
5.6	Summary	132
Chapter 6.....		135
6	Temperature-Expansion Experiment on the Coordinate Measuring Machine and Ultrasonic Thermometry Using Aluminium.....	135
6.1	Temperature-Expansion Experiment on the CMM.....	135
6.2	Ultrasonic Thermometry on Aluminium.....	141
6.3	Summary	144
Chapter 7.....		146
7	Conclusions and Suggestions for Future Research.....	146
7.1	Conclusions	146
7.1.1	Summary of the Key Findings	148
7.1.2	Contributions to Knowledge	149
7.2	Avenues for Future Research	150
References		153
Appendix A.....		166
MATLAB Code and Results for the Pulse-Echo Thermometry Simulation		166
MATLAB Code for Speed of Sound/Expansion Effects on Time-of-flight Simulation		173
MATLAB Code and Results for the 5 MHz Phase-shift Thermometry Simulations		177
MATLAB Plots for the 1 MHz Phase-shift Thermometry Simulations		184
Appendix B		187

Unfiltered Results of In-process Ultrasonic Tests	187
Absolute Temperature Measurement for the On-CMM Experiment.....	197
Appendix C	198
1 MHz Transducer Certificate of Conformance	198
1 MHz Transducer Characterization	199
Appendix D.....	200
Cutting Routine G-Code	200

List of Figures

Figure 2.1: TOF estimation using the threshold technique [11].	42
Figure 2.2: Delay line transducer [65].	47
Figure 2.3: Dual element transducer [65].	48
Figure 2.4: Pulse-echo ultrasonic experimental setup.	49
Figure 2.5: Major blocks of a typical pulser-receiver [66].	49
Figure 3.1: Overview of the input structures and fields used for the simulations [74].	56
Figure 3.2: Setup of the ultrasonic source and sensors for pulse-echo simulation	60
Figure 3.3: Recorded tone burst.	61
Figure 3.4: Simulation of time-of-flight for 0.1 °C resolution for 25 °C to 25.2 °C.	62
Figure 3.5: Simulation of time-of-flight for 0.1 °C resolution for 25.3 °C to 25.5 °C.	63
Figure 3.6: Effect of change in speed and expansion on TOF	64
Figure 3.7: Setup of the ultrasonic source and sensors for phase-shift simulation	66
Figure 3.8: Simulation of phase-shift for 25 °C using 5 MHz frequency.	68
Figure 3.9: Simulation of phase-shift for 25 °C using 1 MHz frequency.	69
Figure 3.10: Spectrum M2i.6022-exp arbitrary waveform generator	73
Figure 3.11: SBench 6 Easy Generator	73
Figure 3.12: Amgaze 5 MHz dual element piezo-electric transmitter/receiver transducer	74
Figure 3.13: 0.1° Phase-shift test on Agilent Technologies high-speed oscilloscope	75
Figure 3.14: (a) - Picture of AD8302 Phase detector. (b) - AD8302 functional block diagram	77
Figure 3.15: Phase output vs phase difference [101].	78
Figure 3.16: Phase detector input signals (yellow and green) and AD8302 output signal (blue)	79

Figure 3.17: Phase detector input signals (yellow and green) and filtered output signal (blue)	80
Figure 3.18: AD 8302 Phase-out vs phase difference for 5 MHz signals	82
Figure 4.1: AD 8302 Phase-out vs phase difference for 5 MHz (2 V, 40 mV) signals	87
Figure 4.2: Ultrasonic phase-shift thermometry experimental set-up	89
Figure 4.3: Ultrasonic experimental set-up devices	89
Figure 4.4: Results of 20 to 30 °C temperature range in steps of 1 °C	91
Figure 4.5: Residual plot of 20 to 30 °C	92
Figure 4.6: Results of 21.5 to 23.5 °C temperature range in steps of 0.1 °C	93
Figure 4.7: Residual plot of 21.5 to 23.5 °C	94
Figure 4.8: TCS 140 Liquid bath calibrator	95
Figure 4.9: AD 8302 Phase-out vs phase difference for 5 MHz (2 V, 5 mV) signals	96
Figure 4.10: Ultrasonic phase-shift thermometry experimental set-up using liquid bath calibrator	97
Figure 4.11: Results of 20 to 30 °C range in steps of 1 °C for 100 mm steel	98
Figure 4.12: Residual plot of 20 to 30 °C for 100 mm steel	99
Figure 4.13: Results of 20 to 21 °C range in steps of 0.1 °C for 100 mm steel	100
Figure 4.14: Residual plot of 20 to 21 °C for 100 mm steel	100
Figure 4.15: THS3202 pin assignments [106]	102
Figure 4.16: Echo signal amplifier design	102
Figure 4.17: Analog Devices DUAL-SO-8 evaluation board [107]	103
Figure 4.18: Schematic of evaluation board [107]	104
Figure 4.19: Populated signal amplifier	105
Figure 4.20: Input signal to amplifier	105
Figure 4.21: Signal output from amplifier	106

Figure 4.22: PT100 Workpiece temperature readings	107
Figure 4.23: Ultrasonic phase difference readings	107
Figure 4.24: Ultrasonic workpiece temperature readings	108
Figure 4.25: Deviation of ultrasonic readings from PT100 readings	109
Figure 5.1: CNC and data acquisition setup for ultrasonic thermometry	112
Figure 5.2: Transducer and PT100 spacing on workpiece.....	113
Figure 5.3: Improvised mechanical clamp for the ultrasonic transducer.....	114
Figure 5.4: Echo signal after clamping	115
Figure 5.5: PT100 and Ultrasonic thermometry results of static test 1	116
Figure 5.6: Residuals of PT100 and ultrasonic thermometry for static test 1.....	117
Figure 5.7: PT100 and ultrasonic thermometry static test 1 result after filtering	119
Figure 5.8: Results of the extended static test.....	120
Figure 5.9: Results for spindle running at 1000 rpm	122
Figure 5.10: Results for spindle running at 5000 rpm	123
Figure 5.11: Effect of cutting fluid on ultrasonic thermometry.....	125
Figure 5.12: Direction of cut perpendicular to the transducers.	126
Figure 5.13: Results of dry cutting trials	128
Figure 5.14: Wet cutting trials 1-3.....	130
Figure 5.15: Wet cutting trials 4-5.....	131
Figure 6.1: Experiment setup on the CMM.	136
Figure 6.2: On-CMM PT100 and ultrasound results	138
Figure 6.3: Core and surface temperature values.....	139
Figure 6.4: Part dimension and expansion.....	139
Figure 6.5: Part expansion	140
Figure 6.6: Error: Calculated vs measured.	140

Figure 6.7: Aluminium propagation medium	141
Figure 6.8: Results of ultrasonic thermometry on aluminium trials 1-3.....	142
Figure 6.9: Results of ultrasonic thermometry on aluminium (trials 3-4)	143

List of Tables

Table 3.1: Result of simulation for quantisation of sampling frequency.....	59
Table 3.2: Phase-shift simulation result for 5 MHz frequency.....	68
Table 3.3: Phase-shift simulation result for 1 MHz frequency.....	69
Table 3.4: Acoustic impedances of some common media.....	71
Table 3.5: 0.1° Test on AD8302 phase-shift detector.....	81
Table 3.6: AD 8302 Phase-out vs phase difference for 5 MHz signals.....	82
Table 4.1: AD 8302 Phase-out vs phase difference for 5 MHz (2 V, 40 mV) signals.	87
Table 4.2: AD 8302 Phase-out vs phase difference for 5 MHz (2 V, 5 mV) signals.	96
Table 4.3: Component values for signal amplifier.....	104
Table 5.1: Dry cutting trial errors and standard deviation.....	129
Table 5.2: Wet cutting trial errors and standard deviation.....	132
Table 6.1: Aluminium trial errors	144

Glossary of Terms

AC	Alternating Current
ADC	Analog to Digital Converter
AWG	Arbitrary Waveform Generator
BFSK	Binary Frequency Shift Keyed
CTE	Coefficient of Linear Thermal Expansion
CNC	Computer Numerical Control
CSV	Comma Separated Values
DC	Direct Current
DREAM	Discrete Representation Array Modelling
EMF	Electromotive Force
FFT	Fast Fourier Transform
FPGA	Field-programmable Gate Array
GUM	Guide to the Expression of Uncertainty in Measurement
HIFU	High-intensity Focused Ultrasound
LVM	LabVIEW Measurement
MFCW	Multiple Frequency Continuous Wave Method
MO	Mineral Oils
NDT	Non-destructive Testing
PC	Personal Computer

PCI	Peripheral Component Interconnect
PCIe	Peripheral Component Interconnect Express
PID	Proportional Integral Derivative
PT100	Platinum Resistance Thermometer
RTDs	Resistance Temperature Detectors
SFAI	Swept-frequency acoustic interferometry
SMA	SubMiniature Version A
SNR	Signal to Noise Ratio
TOF	Time of Flight
UT	Ultrasonic Testing
VCO	Voltage Controlled Oscillator

Nomenclature

A	Amplitude
c	Velocity of sound
C_{\min}	Minimum ultrasonic velocity
dx	Spacing of grid points in x Cartesian direction
E	Young's modulus
f	Frequency of ultrasonic signal
f_{\max}	Maximum ultrasonic frequency
$H[u(t)]$	Hilbert transform of $u(t)$
l	Distance of travel of ultrasonic wave
L	Original length
n	Integer number of wave periods
N_x	Number of grid points in x Cartesian direction
p	Pressure of medium
ppw	Points per wavelength
s	Specific entropy
T	Temperature of medium
t	Time
t_array	Array of time values
$u(t)$	Function
V_{in}	Voltage In
V_{out}	Voltage Out
x_{size}	Size of computational grid
$y(t)$	Sine wave
α_L	Linear coefficient of thermal expansion
Δf	Difference between two frequencies
ΔL	Change in length
Δr	Spacing between two resonance peaks
ΔT	Change in temperature
$\Delta \phi$	Difference between phase-shifts
ρ	Density of medium

Ω	Ohm
Φ	Phase
φ	Phase-shift between transmitted and received signals

Chapter 1

1 Introduction

Temperature variations during manufacturing processes affect both the dimensional accuracy and surface integrity of workpieces [1–3]. These two specifications are indicators of the conformance of the manufactured workpieces to the design intent. Therefore, there is the need to have a temperature control system or a system in place to compensate for the effect of temperature variation.

There is no exact temperature variation value for manufacturing processes in literature, this is due to the different factors that influence the manufacturing process such as the type of workpiece material, type of manufacturing process, and the environmental condition during the process. However, 1 μm resolution is typically required in the manufacturing of standard precision parts on the CNC machines. Considering an aluminium part component of 200 mm in length with expansion coefficient of 25 $\mu\text{m}/\text{m}^\circ\text{C}$, a thermal expansion of 1 μm can occur with an average temperature rise of 0.2 $^\circ\text{C}$. Therefore, a target resolution of 0.1 $^\circ\text{C}$ will meet the requirement for 1 μm resolution.

Many manufacturing environments can be very harsh. In the case of subtractive production processes, heat is generated, metal swarf and coolant are often present on the workpiece being machined. Traditional methods of temperature measurement during manufacturing such as the thermocouple, resistance temperature detectors, and infrared thermometry all measure the surface temperature of the part which is impractical due to the changing surface condition during machining and is not always indicative of the material's core temperature [4, 5]. In order to give a more accurate representation of the workpiece temperature, the average core temperature of the workpiece needs to be known. This is because the core temperature of the workpiece has a significant influence on the average temperature which determines the

dimensional expansion of the workpiece, which could in turn impact on the accuracy of the manufactured workpiece.

During inspection of manufactured components, the process is similar. Typically, a high accuracy temperature sensor such as a Platinum Resistance thermometer (Example is a PT100 with ± 0.1 °C accuracy) is placed on the surface or edge of a part being measured. Previous processes before the inspection can mean that temperature gradients exist, increasing uncertainty in the CMM temperature compensation of more than 0.18 °C [6] on a small component which will increase with size and mass.

The speed of sound in any medium depends on the temperature of such medium. This relationship has been used in different types of applications such as flaw detection (e.g., cracks and inhomogeneity) in non-destructive testing, thickness gauging, and imaging for medical purposes. The spectrum of sound wave mostly used for these purposes is the ultrasound – sound wave above 20 kHz. In many ultrasound applications, the sound wave is generated using an ultrasonic transducer which is excited by an electronic pulser. The wave is transmitted through the medium of interest with the aid of a couplant [7]. The return wave is then captured with a receiver. With the knowledge of the time of travel and the distance of travel, the ultrasonic velocity can be calculated.

Two of the main methods of time-of-flight ultrasonic measurements are the pulse-echo method and the phase-shift method. With the pulse-echo method, discrete ultrasonic pulses are used to measure ultrasonic time-of-flight, while the phase-shift method makes use of continuous ultrasonic waves [8]. Peak detection technique is used in pulse-echo method to measure the time-of-flight. However, in phase-shift method, the difference between the phase of the sent and received signals is used to compute the ultrasonic velocity. There are variations of both the

pulse-echo and the phase-shift method which are used to either increase the resolution of measurement, measurement range or both. These are reviewed in Section 2.9.

Although temperature measurement (especially in solids) is not the traditional application of ultrasound, ultrasonic techniques have been used for measurement of air temperature in the literature [9]. As the speed of sound in solids is approximately 20 times higher than in air, there is a need for an analogue to digital converter with higher sampling rate for metals when compared to air. Some pulser-receivers have integral analogue to digital converters, however, there are other configurations with pulser-receivers being separate from the analogue to digital converters. The sampling rate of pulser-receivers referred to in this thesis is the sampling rate of the analogue to digital converters integrated with pulser-receivers. Ihara et al. found that the relationship between ultrasonic velocity and temperature in a steel medium can be given as:

$$c(T) = (-0.636T + 5917.6) \text{ m/s} \quad (1.1)$$

Where $c(T)$ is the temperature dependent ultrasonic velocity and T is the temperature [10].

Using equation (1.1), the ultrasonic velocity will be 5901.7 m/s for a steel of 25 °C average temperature and 5901.6 m/s for a 25.1 °C steel. This velocity difference will cause a difference of 0.57 ns to the signal transit time in a 200 mm steel part. To correctly capture this signal, a pulser-receiver of over 3.5 GS/s needs to be used. However, in air, the ultrasonic velocity and temperature relationship is given as:

$$c(T) = 20.06 * \sqrt{T + 273.15} \text{ m/s} \quad (1.2)$$

Where $c(T)$ is the temperature dependent ultrasonic velocity and T is the temperature [11].

With equation (1.2), the ultrasonic velocity will be 346.38 m/s for air medium of 25 °C and 346.43 m/s for 25.1 °C. The velocity difference will cause a difference of 83.34 ns to the transit

time of an ultrasonic signal traveling through a 200 mm path. A pulser-receiver of over 24 MS/s is required to sample this signal correctly.

Quotes obtained for different pulser-receivers from vendors show that a typical pulser-receiver for resolving 0.1 °C in air medium can be gotten for £3,400 while the cost for a metallic medium can reach £17,000. Therefore, the required equipment needed for ultrasonic measurement in solids are more expensive than in air for similar ultrasonic thermometry application.

This thesis focuses on creating a novel method for core temperature measurement of metals during manufacturing processes. In this thesis, the existing methods of temperature measurement are reviewed. Based upon the potential use of ultrasound for core temperature measurement of metals, both the pulse-echo and the phase-shift method were simulated in MATLAB using k-Wave toolbox (k-Wave is a toolbox for time domain ultrasound simulations). The simulations showed that both methods can resolve 0.1 °C change in temperature with the appropriate transmitting and receiving frequencies. However, the equipment needed for pulse-echo are more expensive than for the phase-shift method. Hence, the phase-shift method was chosen for the purpose of this thesis. Simulations also showed that the time-of-flight is influenced by both ultrasonic velocity and material expansion, however, ultrasonic velocity has the greater influence on time-of-flight. Based upon these findings, experiments were based on ultrasonic velocity.

Initial ultrasonic experiments were performed in laboratory conditions on a steel plate with controlled heating. The results show that the method can resolve 0.1 °C change in temperature. Further experiments were performed on the Computer Numeric Control (CNC) before and during cutting. The results of the experiments were compared to results obtained from a PT100 temperature detector inserted in a hole drilled into the workpiece.

1.1 Motivation

The main goal of manufacturing activities is to deliver products that meet customer specifications. Two of such specifications are the dimensional accuracy and surface integrity of manufactured workpieces. Temperature variation during manufacturing processes influences the ability of the manufacturing processes to meet these specifications. When temperature is monitored and its effect compensated for, the productivity of the manufacturing process will improve through reduction in rejects and less rework. Although there has been growth in on-machine inspection, there is no convenient solution for measuring workpiece temperature to the level of accuracy required in precision manufacturing. This is because the existing measurement methods can only measure the surface temperature which is subject to measurement uncertainty. Therefore, a novel technique and equipment setup needs to be created to measure workpiece temperature during manufacturing with accuracy and resolution meeting precision manufacturing requirements.

1.2 Aim

The aim of this research is to create a novel temperature measurement system that measures the core workpiece temperature with accuracy and resolution that satisfy the requirements for precision manufacturing processes.

1.3 Objectives

- This research project will review existing temperature measurement methods used during metal cutting processes and other unused methods in order to identify potential techniques applicable to this research.

- Simulations of wave behaviour in metals and detection methods will be carried out to establish the best method which achieves the specified accuracy and resolution. This method will be chosen for in-process temperature measurement during metal cutting processes based on the findings from the research work.
- Experiments will be performed to use the preferred simulated method for workpiece core temperature measurements.
- The research will establish a cost-effective method of measuring the core temperature of workpieces during metal cutting process.
- The research will attempt to achieve accuracy and resolution based on industry requirements for the evaluated workpiece temperature variation during manufacturing processes.
- The research will evaluate the impact of machining on workpiece temperature measurement.
- In-process temperature sensors, electronics, data acquisition, and processing system adapted for metal cutting processes will be created.

1.4 Novel Contributions

- Creation of a new method for precision core temperature measurement of metals using an ultrasonic phase-shift method.
- Creation of a method for core temperature measurement in subtractive manufacturing processes.
- Creation of MATLAB tools to simulate ultrasonic pulse-echo and phase-shift thermometry measurements.

- Comparison of the effects of change in ultrasonic velocity and material dimension (expansion) on ultrasonic time-of-flight.
- Evaluation of the suitability of phase-shift technique and pulse-echo technique in temperature measurement applications for manufacturing processes.
- Amplification of ultrasonic echo signals using high speed amplifier for phase-shift ultrasonic measurements.
- Application of core temperature measurement on coordinate measuring machines to reduce uncertainty during dimensional inspection.
- Creation of a functional method for ultrasonic transducer coupling in manufacturing environment.

1.4.1 Journal Article Published from Thesis Findings

O. F. Olabode, S. Fletcher, A. P. Longstaff, and N. S. Mian, “Precision core temperature measurement of metals using an ultrasonic phase-shift method,” *J. Manuf. Mater. Process.*, vol. 3, no. 3, 2019.

1.4.2 Conference Papers and Presentations from Thesis

O. F. Olabode, S. Fletcher, A. P. Longstaff, and N. S. Mian, “Core temperature measurement in subtractive manufacturing processes,” in *Laser Metrology and Machine Performance XIII - 13th International Conference and Exhibition on Laser Metrology, Machine Tool, CMM and Robotic Performance, LAMDAMAP 2019*, 2019.

O. F. Olabode, S. Fletcher, A. P. Longstaff, and N. S. Mian, "Precision Core Temperature Measurement of Metals for Use in Manufacturing Applications," in *Special Interest Group Meeting: Thermal Issues*, 2020.

1.5 Scope of Research

It is necessary to state that the scope of this research was limited to relative temperature measurement during machining processes for a simple geometry i.e., a continuous rectangular structure representative of a simple workpiece. The term 'workpiece' refers to the piece of material that is being worked on and is sometimes referred to as a 'part' or 'component'. During the machining processes, the ultrasonic transducer is coupled to the workpiece at a position where the propagated ultrasonic wave covers the length of the workpiece.

The length of workpieces used in this research was limited to 200 mm. The choice of material length was made based typical material sizes used in the research group and on the limitations of typical dual element ultrasonic transducers. In applications where a longer range is desired, appropriate transducers can be procured and used based on the developed method detailed in this thesis.

It is also important to state that the temperature range considered in this research falls below 50 °C which is well above the range expected in precision manufacturing.

The metals used in this research are steel and aluminium. Steel was chosen based on its prevalence in both manufacturing processes and published results of ultrasonic experiments. The previous studies on ultrasonic measurement in steel provide the needed assumptions and equations for ultrasonic simulations. The simulations provided a basis for the choice of

experimental methodology which was used in this research. After successfully using steel for the tests, a test on aluminium part was also carried out.

1.6 Thesis Structure

This thesis is structured into seven chapters. Chapter one is the thesis introduction. In the second chapter of the thesis, relevant literature to this research are reviewed. Chapters three to seven detail the original contribution of this research. A more detailed breakdown of the thesis is given below.

Chapter one introduces the thesis, it also provides the topic domain, background, and problem definition.

Chapter two reviews the relevant literature relating to traditional temperature measurement methods, the methods that have been used in metal cutting applications, literature relating to ultrasound and its use for thermometry, and uncertainty evaluation in measurement.

Chapter three presents the methodology. The details of the ultrasonic simulation materials, methods, and results are given. In this chapter, the methodology and results of simulation justifying the choice of ultrasonic phase-shift method are presented. This chapter also shows the effects of ultrasonic velocity and material expansion on ultrasonic time-of-flight. Based upon the simulation, the methodology for the ultrasonic experiments was developed and discussed.

Chapter four presents the ultrasonic experiments in a laboratory. It details ultrasonic thermometry experiment using controlled heating. The results provide insight into the ideal results to be expected from subsequent experiments and setup as well as the limitations of the method. The chapter also provides the details of the ultrasonic setup used for a larger workpiece

(liquid bath calibrator). The chapter also contains the details of the high-speed amplifier developed to amplify the echo signal for in-process experiments.

Chapter five provides the details of the ultrasonic thermometry experiments on a CNC machine. Results of ultrasonic thermometry were obtained in different conditions on the machine, these include dry and wet cutting conditions as well as non-cutting conditions.

Chapter six details the method adopted for using the ultrasonic thermometry on a coordinate measuring machine and the calculated expansion based on the core and surface temperature of the workpiece. The use of ultrasonic thermometry on an aluminium part is also detailed in this chapter.

Chapter seven contains the discussions and conclusion of the thesis. Future research direction is also suggested in this chapter.

Chapter 2

2 Review of Previous Research

This chapter provides the review of relevant literature to this research. First, temperature measurement techniques are reviewed. Thereafter, the methods that have been used in metal cutting processes are individually reviewed. Considering their features and limitations, ultrasonic thermometry, a potential temperature measurement technique is reviewed. Different methods used in ultrasonic thermometry, their variations, components, and the equipment required to carry out the measurement process are also reviewed. Finally, the summary of the reviewed literature is provided.

2.1 Temperature Measurement Techniques

Temperature variation during cutting processes affects both the dimensional accuracy and surface integrity of manufactured workpieces. Attempts to measure both the machine tool and workpiece temperature are described in extant literature [12–14]. The techniques used usually depend on the type of material being machined, the type of manufacturing process, and the level of accuracy required. In this section, these previously used methods are evaluated as they provide useful guides for selecting the appropriate method for solving the present task.

Temperature measurement differs substantially from many other types of measurement processes. The fact that the temperatures of two bodies do not sum up algebraically when they are in contact makes establishing a standard for absolute temperature measurement difficult [15]. Temperature measurement techniques can be divided into broad classes based on their principles of operation. Some of the common principles used in temperature measurement are thermoelectric effect, resistance change, sensitivity of a semiconductor device, radiation thermometry, thermal expansion, acoustic thermometry, and colour change [15].

The thermoelectric or Johann Seebeck effect refers to the generation of electromotive force at the junction of two dissimilar conductors experiencing thermal gradient [16]. Thermocouples are regarded as versatile, simple to use, and are made in different sizes while covering different ranges of measurement. They are also one of the common sensors used in industrial temperature measurement [15]. Thermistors and resistance temperature detectors (RTDs) work based on the principle of change in resistance. Thermistors have been shown to have higher sensitivity than RTDs [17], however, thermistors are not suitable for temperature measurements above 300 °C while RTDs can measure up to 660 °C [15, 18, 19]. A main limitation of both the RTDs and thermistors is that they require full immersion in the medium of measurement in order to work accurately [15]. Thermocouples are considered to be the most versatile temperature sensor, the Platinum RTDs are considered to be the most stable and are commonly found on the Coordinate Measurement Machines (CMMs) for measuring the temperature of a component being inspected. Finally, thermistors are regarded as the most sensitive of the three types of temperature measurement devices [20].

Some temperature detectors are classed as semiconductor devices. Semiconductor devices give temperature sensitive characteristics that can be used for temperature indication. These devices include diodes and integrated circuit transistors. In semiconductor thermometers, the voltage across the p-n junction increases when temperature decreases. The relationship between the voltage and temperature is the basis for measuring temperature with the sensitivity of semiconductor devices. The typical temperature range for a semiconductor device is – 55 to +150 °C with accuracy of ± 0.8 °C [16]. Major limitations of semiconductor devices are the range of measurement and the extra external power supply these devices need in order to work [15].

Radiation thermometers absorb electromagnetic radiation from objects and convert it to signal that can be read [21]. Optical pyrometers and radiation detectors are based on the principle of

absorption of electromagnetic radiation. However, infrared detectors are able to obtain temperature distribution of a body whereas optical pyrometers only provide the single point temperature at the device's focal point [15]. Advantages of radiation thermometers include their ability to obtain the temperature of an object non-invasively, have very high detection rates, and their ability to measure very high temperatures. However, because radiations from bodies vary with the nature of the surface of the body, there is a need for careful calibration and consideration that any surface contamination would reduce performance [15].

The use of the thermal expansion of an object to determine its temperature is based on the understanding that the dimension of matter changes when the temperature is varied. The liquid-in-glass thermometer, bimetallic strip, and the pressure thermometer are built upon this principle. The liquid-in-glass thermometer is used in many applications, but the need to read the position of the curved meniscus introduces error. The bimetallic thermometer also requires careful design as errors can be easily introduced if the helix's expansion is distorted. The pressure thermometer requires protection from the measurement environment, hence, error due to the distance of separation is introduced [15].

Acoustic thermometry is based on the variation of a medium's speed of sound due to temperature [22]. One of the main advantages of acoustic thermometry is the possibility of obtaining temperature measurements in environments of extreme temperature conditions where other sensors may not work [23]. The temperature measurement obtained with acoustic sensors is the overall measurement through the acoustic wave path. This gives the advantage of obtaining the average temperature of the medium through which the acoustic wave passes which cannot be obtained with conventional temperature sensors [23]. Ultrasound is a type of acoustic wave with sound frequencies above the upper limit of human hearing (nominally 20 kHz) [24].

2.2 Temperature Measurement in Metal Cutting Processes

Metal cutting is one of the most important aspects of manufacturing and there have been advancements in optimising the rate of metal cutting. With new technologies, cutting speed, feed rate, and depth of cut have all been optimised over time for different manufacturing needs. However, with increments in these parameters comes an increase in heat generation near the tool-workpiece interface [25]. In order to achieve dimensional accuracy and surface integrity of the manufactured workpiece, there is a need for a form of temperature control and/or compensation for the dimensional changes caused by increase in temperature due to heat generation. This requirement for dimensional accuracy, and the need to understand temperature influence on tool life has led to several attempts at measuring or estimating both tool and workpiece temperatures [25].

Most of the methods described in literature for measuring temperature arising from cutting zones have dealt with the cutting tool [25]. One of the challenges of taking workpiece temperature is the difficulty of placing a conventional sensor on the workpiece surface due to varying shapes and sizes resulting in the sensor being placed a significant distance away from the cutting zone. Furthermore, the harsh machining environment introduces other factors such as vibration, presence of coolant, swarf, and lubricant on workpieces. These challenges increase the uncertainty of measurement. As such, the methods reviewed in this section are limited to those applicable to workpiece temperature measurement during the machining process.

One of the methods used for temperature measurement in metal cutting is the tool/workpiece thermocouple. This method makes use of the tool and workpiece as the elements of thermocouple and using the electromotive force generated at the interface of the two elements, the temperature is measured [26]. The main difficulties reported in literature concerning the

use of the tool/workpiece thermocouple pair are the parasitic electromotive force (EMF) from secondary joints, the necessity for accurate calibration of tool and workpiece as thermocouple pair, the need to isolate the thermocouple from the environment, and the lack of clarity on what temperature the EMF represents [27, 28]. Because the temperature measurement given by the tool/workpiece thermocouple arrangement does not represent the core workpiece temperature, this method cannot be used to solve the present task.

The surface temperature of a workpiece can be obtained by measuring the radiation from the surface of the material. However, only the temperature of the exposed surface can be obtained using this method. Radiation methods are complicated and there is a need for extreme care in using the radiation pyrometer. There are optical pyrometers which measure thermal radiation in visible spectrum and radiation/infrared sensors which can measure radiation in the infrared region. Infrared sensors have been used to measure workpiece surface temperature and this technique was first used in dry cutting conditions and thereafter modified for use when cutting fluid is applied [25]. A major limitation of infrared thermometers is their accuracy which is typically stated as or lower than ± 2 °C [29, 30]. However, a higher level of accuracy is required for precision temperature measurement.

Thermographic phosphor sensors' operation is based upon the difference in emission decay time of phosphor materials at different temperature values [31]. The surface for which temperature is to be measured is coated with a phosphor material and thereafter, light is directed to the surface. The inorganic phosphor then emits light containing the temperature information which is gotten from the emission decay time. The main advantages of the thermographic phosphor method is that they can be used in harsh environments non-intrusively [32]. However, they can only be used to measure the surface temperature of parts [31, 32].

RTDs such as PT100 have also been used to measure workpiece temperature during cutting and calibrate other temperature measurement systems [30, 33]. However, as with all the other temperature measurement methods previously used in metal cutting, the RTD can only be used for surface temperature measurement. Therefore, a main gap in the reviewed literature is the lack of a temperature measurement method developed for core temperature measurement of metals during manufacturing processes.

2.3 Acoustic Thermometry

From all the reviewed temperature measurement principles and techniques, none can give a direct indication of the average, or internal temperature of a medium or body such as a workpiece. Although thermocouples are widely used in metal cutting processes, it can neither give the core temperature of the workpiece nor is it suitable for in-process monitoring due to its slow response [34]. However, the acoustic thermometry gives the overall temperature of the entire path of the acoustic wave. Hence, the rest of the literature review will focus on acoustic thermometry. Acoustic velocity will be reviewed in the next section.

2.3.1 Acoustic Velocity

Sound as a vibrational wave travels through different media at a velocity that is dependent on the properties of that medium. Therefore, equations for the speed of sound in a medium depends on the type of medium of propagation of the ultrasonic wave. The theoretical equation relating the acoustic velocity to the properties of the medium of propagation is given as [35]:

$$c^2 = \left(\frac{\partial p}{\partial \rho} \right)_s \quad (2.1)$$

where c is the isentropic velocity of sound, p is the pressure of the medium, ρ is the medium's density, and s is the specific entropy.

The medium of sound propagation can be gas, liquid, or solid. For solid medium of propagation, the longitudinal wave velocity depends on the Young's modulus and the density of the medium as given in equation (2.2):

$$c = \sqrt{\frac{E}{\rho} \frac{1 - \mu}{(1 + \mu)(1 - 2\mu)}} \quad (2.2)$$

where c is the longitudinal acoustic velocity in the medium, E is the Young's modulus of the medium, ρ is the medium's density, and μ is the Poisson's ratio [36].

Bulk shear waves travel are another type of ultrasonic wave that travel at different speeds from the longitudinal wave, however, the longitudinal wave is used in this thesis because of its propagation pattern.

2.4 Ultrasound

Ultrasound has similar propagation features when compared with audible sound. Generally, ultrasound is regarded as sound wave with frequency above 20 kHz – this is above the upper limit of human hearing [37]. One main benefit of using ultrasound rather than audible sound is that ultrasound, being of higher frequency, gives a better resolution than the lower frequency

audible sound [38, 39]. However, attenuation is higher with higher frequency even though the attenuation of ultrasound is lower in solid media when compared to air [40, 41].

Ultrasound has been used in different fields such as medicine, where it has been used as both a diagnostic and a therapeutic tool [42–44] and in chemistry, ultrasound is used to enhance different chemical processes, which is known as sonochemistry [45]. One main use of ultrasound in engineering is its application to non-destructive testing (NDT) of materials, such as the detection of crack, void, and porosity in materials [46].

Although ultrasound is widely used for NDT applications, these NDT techniques rely on detecting changes in the internal structure of materials due to defects. However, for temperature measurement, the setup needs to be able to give temperature readings even without defects. Therefore, these past methods are not directly suitable for temperature measurement of workpieces.

Another use of ultrasound mentioned in literature is in temperature measurement of various medium which will be reviewed in the next section.

2.4.1 Ultrasonic Thermometry

Ultrasound has been used for temperature measurement in air [47, 48]. Huang et al. proposed an ultrasonic thermometer based on measurement of ultrasonic velocity in air [49]. Their method achieved accuracy of ± 0.05 °C within transducer distance of 10 cm. The main limitation of the method used as it relates to the present research is that the used ultrasonic frequency of 40 kHz will not give the needed measurement resolution in steel as the ultrasonic velocity in steel is higher than in air. Similar works by Tsai et al. achieved an accuracy of ± 0.4

°C for a range of 0 °C to 80 °C [47, 48]. However, this was also achieved with an ultrasonic frequency of 40 kHz which will not give sufficient resolution in metals.

Pernot et al. used the ultrasonic time-of-flight technique to estimate temperature of biological tissues [50]. Their method makes use of pulser-receiver for a 1.5 MHz transducer during high-intensity focused ultrasound (HIFU). Using the pulse-echo method will present the challenge of the cost associated with appropriate pulser-receiver for metallic medium. Another medium for which ultrasonic thermometry has been used is water. Zhou et al. used phase-shift of a single-frequency continuous wave for measuring the temperature of distilled water [51]. Using a signal frequency of 1 MHz, the measurement error stayed within ± 0.04 °C. Phase-shift method is an alternative to the pulse-echo method, and it is further reviewed in section 2.7.

Ultrasound has been used for measuring the temperature of some solid materials. Following a numerical simulation, Ihara et al. performed an experiment to measure the internal temperature profile of a 30 mm steel plate using the pulse-echo method [52]. The experiment was carried out using a 5 MHz transducer for ultrasonic measurement and five thermocouples for reference temperature measurement. Although the paper does not provide the details of the pulser-receiver used, the error in their measurement results (ultrasound – thermocouple) reached 2 °C in 5 seconds of material heating. Their plot also suggests that this error will increase over increased heating time. Another limitation of the work is that it was carried out on a 30 mm steel and using the same setup on a bigger part will increase signal attenuation. Furthermore, the work does not state the resolution that can be achieved using the setup. However, the plot of the results suggests that the resolution could be approximately 1 °C. The achieved accuracy and resolution are much lower than that required in precision measurements. It is also expected that the accuracy will further reduce in the harsh manufacturing environment.

Another ultrasonic thermometry experiment described in literature was carried out on silicone rubber of 30 mm thickness [34]. A 2.25 MHz ultrasonic transducer was used for the pulse-echo signal transmission and reception. Five thermocouples were used for measuring the reference temperature while sampling the ultrasonic echo signal at 100 MHz. The measurement error from the plot of thermocouple and ultrasound readings reached 8 °C at material temperature of 80 °C. Although the resolution achieved is not stated in the paper as the focus was more on the agreement of results at relatively high temperature of 80 °C, the plotted results suggest that the resolution is lower than 1 °C. The achievable resolution and accuracy of the method are the main limitations as it applies to this research.

Finally, a similar work also used the pulse-echo method with a 2 MHz transducer for temperature measurement of a steel plate [10]. The results show that the accuracy is below 5 °C. The setup and application used also suggest that the achievable resolution is below 1 °C.

2.5 Temperature Dependence of Ultrasonic Velocity

Both the Young's modulus and density presented in equation (2.2) are temperature dependent, hence, the ultrasonic velocity is temperature dependent. However, the relationship between the ultrasonic velocity and temperature is often determined experimentally [53].

In order to estimate the temperature of a material from ultrasonic velocity through experimentation, the time of travel and length of the material are used. If ultrasonic wave is propagated through a material of known length, the time of travel of the ultrasound can be measured. The relationship between the transit time, ultrasonic velocity, and material temperature is given as equation (2.3):

$$t_L = \int_0^L \frac{1}{c(T)} dx \quad (2.3)$$

where t_L is the transit time, L is the distance of travel of the ultrasonic wave, and $c(T)$ is the ultrasonic velocity [34].

The use of transit time has been widely applied and the next section covers the related research.

2.6 Ultrasonic Velocity Measuring Methods

As explained in section 2.5, in ultrasonic thermometry, temperature is obtained by measuring the acoustic velocity. Hence, the main methods of ultrasonic velocity measurement will be reviewed in this section.

Ultrasonic velocity measurement methods can be broadly classified into two groups based on their fundamental principles of operation. The first method makes use of continuous waves while the other uses discontinuous waves [8]. The method that makes use of continuous wave is known as the phase-shift method which utilises the phase-shift between the transmitted and received ultrasonic signals for measurement [54]. The time of travel of the ultrasonic wave can be computed from the indicated phase-shift which in turn can be used to estimate the ultrasonic velocity and consequently the material temperature.

The method that uses discontinuous waves is known as the pulse-echo method and it uses discrete ultrasonic pulses. Pulsed signals are generated using ultrasonic transmitters and when the transmitted ultrasonic wave encounters a medium of different density, it is reflected. The reflected signal also known as the echo is detected by the ultrasonic receiver. The ultrasonic time of travel between the transmitter and receiver is used to compute the ultrasonic velocity and the material temperature. The time of travel depends on the length of the material and the physical properties of the material of which temperature is a crucial part [8].

Both the phase-shift and the pulse-echo methods have their strengths and weaknesses. Modifications as well as combination of both methods have been proposed and developed to exploit the strengths of the methods and compensate for their weaknesses. In the next sections, the two methods as well as their modifications will be reviewed.

2.7 Phase-shift Method

The phase-shift method uses the difference in the phase of steady-state frequency ultrasonic waves between transmitted and received signals for ultrasonic time of travel measurement. This description was given by Huang et al. [55]. They used the phase-shift method for distance measurement in air. Although the application of ultrasound in their work is different from the present research, the background information on the phase-shift method provides a basis for possible application in solids with an adapted setup.

For an ultrasonic wave of a known frequency travelling through a known distance, the phase difference between the transmitted and the received signal can be used to obtain the ultrasonic velocity through the medium of propagation. The equation relating the phase-shift to the ultrasonic velocity is given as:

$$L = \left(n + \frac{\varphi}{2\pi}\right) \frac{c}{f} \quad (2.4)$$

where L is the distance of travel of the ultrasonic wave, n is the integer number of wave periods, φ is the phase-shift between the transmitted and the received signals, c is the ultrasonic velocity in the medium, and f is the frequency of the signals as defined in [49].

The phase-shift method was used for temperature measurement of a silicon sample by Abdelmejeed et al. [56]. Using a voltage-controlled oscillator (VCO), pulse generator, 1.6 GHz

transducers, a 20 GS/s oscilloscope, and MATLAB for computing the phase-shift between the sent and received signals, they developed a temperature measurement system for a 650 μm silicon. The temperature measurement was from 30 – 120 $^{\circ}\text{C}$ with 17 m°C resolution. The main limitations of their work are the used setup and method of computation of the phase-shift. Apart from the cost of the standalone VCO, pulse generator and oscilloscope, the sent and received signals need to be exported to MATLAB for the phase-shift to be computed. Another limitation of their solution is the very small material size of 650 μm used. In manufacturing applications for which a solution needs to be created in this thesis, part sizes are much larger than what was described in the reviewed article.

A major advantage of the phase-shift method is that it reduces the type of attenuation caused by short-burst transmissions. However, it has start/stop envelope problems which only disappears during continuous operation [49]. Another limitation of the phase-shift method is that the measurable range without phase ambiguity is only from 0 to one wavelength (2π radians) [11]. This means that for steel, with ultrasonic velocity of 5890 m/s, and a 1 MHz transducer, measurement can only be made over a 5.89 mm length of material without phase ambiguity. Although lower frequencies can increase the measurement range, this is at the expense of the resolution and this has resulted in hybrid methods described in section 2.9.

2.8 Pulse-echo Method

Ultrasonic measurement using the pulse-echo method is commonly used in manufacturing industry for non-destructive testing (NDT). The pulse-echo method uses the principle of time-of-flight (TOF) where a pulse is sent through a medium and the pulse is reflected by an obstacle which is usually an object or an environment of different physical properties [57]. The time-

of-flight of the ultrasonic wave and the distance of travel are used to calculate the ultrasonic velocity [49]. The relationship between these three is given as:

$$c = \frac{L}{TOF} \quad (2.5)$$

where c is the ultrasonic velocity, L is the distance of travel of the ultrasonic wave, and TOF is the time-of-flight [11].

Different techniques of estimating the TOF are described in literature, the threshold and the cross-correlation techniques are two of the common techniques [11]. The threshold technique measures the TOF by comparing the time of the pulse generation with the time the echo signal first crosses a pre-set threshold level. This is shown in Figure 2.1.

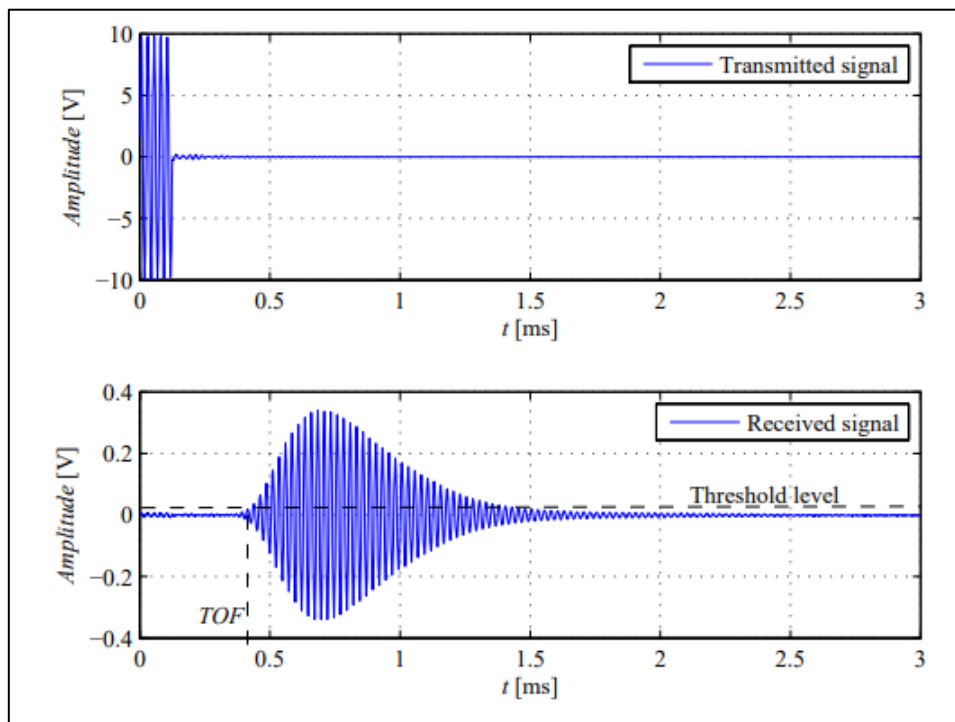


Figure 2.1: TOF estimation using the threshold technique [11].

The threshold technique is best for systems with high signal-to-noise ratio (SNR) and the accuracy also depends on the chosen threshold level [11]. Due to the low-bandwidth

transducers used for air medium, the rise-time of the echo signal is usually long and this creates a bias in the results obtained by simple thresholding [57].

The cross-correlation technique works by cross correlating both the transmitted and received signals. The TOF is taken as the time when the cross-correlated result reaches its maximum [11]. This technique has better performance with low SNR signals when compared with the threshold technique for the air medium as described in literature [11, 57]. The cross-correlation technique was used for temperature measurement in a 30 mm steel sample by Ihara et al. [52]. However, as previously stated in section 2.4.1, the setup used suggests that the obtained results are of resolution lower than 1 °C.

2.9 Modifications and Combinations of Pulse-echo and Phase-shift Methods

There are many forms of modifications as well as combinations of the pulse-echo and phase-shift methods described in literature. The aim of the modifications is to exploit the strengths of the presented methods to meet the needs of specified tasks. Gueuning et al. developed an algorithm which combined the cross-correlation technique of pulse-echo method and phase-shift method. They achieved better resolution even with a relatively low sampling rate [39]. Although the resolution was improved, the used setup was for air, and the application was for distant measurement. For temperature measurement in metals, the used setup will not deliver the required resolution and accuracy as previously stated in section 2.4.1.

The two-frequency and multiple-frequency phase-shift methods adopt the principle of increasing the number of frequencies considered for the phase-shift estimation. This has the potential of significantly increasing the range of measurement and improving measurement resolution as proven in the work of Huang et al. [55]. They showed that if only one frequency

of 40 kHz is used, the maximum achievable range is 8.5 mm. By increasing the frequencies to three, they were able to measure over a range of 1500 mm with accuracy of ± 0.05 mm. The multiple-frequency method has also been used for temperature measurement in air and using three frequencies, the measurement error remained within ± 0.4 °C[47]. The phase-shift method will be further explored in subsequent chapters. The equation for the two-frequency continuous wave method is given as:

$$c = \frac{2\pi\Delta f l}{\Delta\varphi} \quad (2.6)$$

where c is the ultrasonic velocity, Δf is the difference of the two frequencies ($f_1 - f_2$), l is the distance of travel of the ultrasonic wave, and $\Delta\varphi$ is the difference between the phase-shifts [48]. $\Delta\varphi$ is defined by the following equations:

$$\text{if } \varphi_1 > \varphi_2, \Delta\varphi = \varphi_1 - \varphi_2,$$

$$\text{if } \varphi_1 < \varphi_2, \Delta\varphi = \varphi_1 + 2\pi - \varphi_2.$$

The multiple-frequency continuous wave method's equation relates ultrasonic velocity to phase-shift [58], and it is given as:

$$l = \text{Int} \left[\frac{\Delta\varphi_1}{2\pi} * \frac{\Delta f_2}{\Delta f_1} \right] * \frac{c}{\Delta f_2} + \text{Int} \left[\frac{\Delta\varphi_2}{2\pi} * \frac{f_1}{\Delta f_2} \right] * \frac{c}{f_1} + \frac{\varphi_1}{2\pi} * \frac{c}{f_1} \quad (2.7)$$

Another ultrasonic measurement method is the multi-frequency amplitude modulation based ultrasonic system described by Hill et al. [38] which increases the achievable range of ultrasonic measurements in air. Using this method, Hill et al. were able to increase the maximum measurement range from 4.3 mm to 410 mm in air. As with many previously reviewed methods used for air medium, the higher ultrasonic velocity in solids when compared with air means that the setup is not directly suited for ultrasonic measurement in solids.

Another method described in the literature is the binary frequency shift keyed (BFSK) method [41, 48]. With the BFSK method, on reception of the pulse, an approximate TOF is computed based on the time at which the change between the discrete frequency occurs. BFSK is usually combined with phase-shift for increased accuracy, however, the use of BFSK in literature has been for air medium.

There are several other methods described in literature which vary based on the medium of propagation and the aim of the measurement. Among the other methods are the pulse-echo overlap method [59, 60] and pulse superposition method [61].

2.10 Ultrasonic Transducers, Signal Generation, and Data Acquisition Electronics

In order to carry out ultrasonic measurement on solid materials, there is a need to define and correctly choose the ultrasonic transducers, signal generation, and data acquisition equipment to be used. In this section, the individual components and equipment needed for ultrasonic measurements will be reviewed.

2.10.1 Ultrasonic Transducers

The first sandwich ultrasonic transducer was developed by Professor Paul Langevin during the first world war [62, 63]. Based on the Curie's piezoelectric effect, he embedded piezoelectric rings between two metals, which he used for high intensity vibration [63]. Modifications and improvements on the initial design have been described in literature [63]. Some solid materials produce electricity under pressure and also produce mechanical vibration when electricity is applied. This piezoelectric and converse piezoelectric effect is utilised in the making of

transducers which can serve as transmitters and receivers of ultrasonic signals [62]. Transducers of various sizes, shapes, and frequencies have been developed for use in different applications. Ultrahigh frequency transducers can achieve very high resolutions in NDT applications and transducers of up to 300 MHz have been made [64]. However, for ultrasonic temperature measurement applications, apart from the frequency of the transducer, the speed of the acquisition electronic needs to be significantly higher for high resolution to be achieved as shown in the introduction.

Apart from classifying ultrasonic transducers based on the materials they are made from; transducers can also be grouped based on how they are used and the type of ultrasonic signals they transmit. Types of transducers relevant for use on a metallic workpiece include the standard contact, the angle beam, immersion, the delay line, and the dual element transducers [24]. All the transducers listed apart from the immersion transducer – which is designed to be immersed in water, are contact transducers and are designed to be used in direct contact with the workpiece [65]. The standard contact is a single element transducer with a relatively larger element size and is mostly used for flaw detection, speed of sound measurement, and thickness measurement [24]. The delay line, shown in Figure 2.2, is designed to introduce a delay between the generation of the ultrasonic wave and the reception of the echo wave. By introducing the delay, the transducer can complete sending before it receives the reflected echo wave [65].

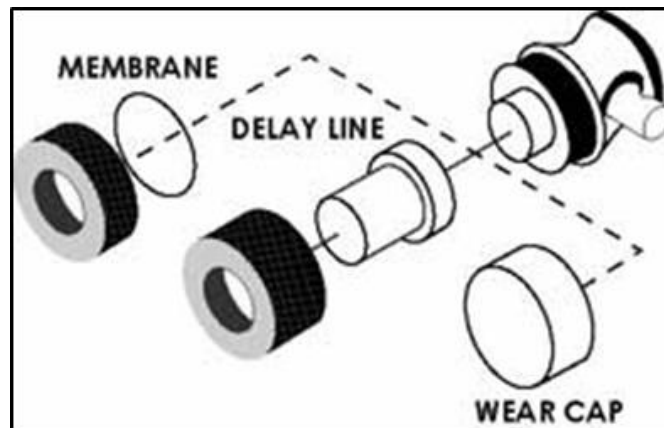


Figure 2.2: Delay line transducer [65].

The angle beam transducers are used to introduce refracted ultrasonic waves into the workpiece. These are ideal for applications where angled wave is desirable [65].

The dual element transducer or simply ‘duals’ contains two elements with each being independent of the other. The main advantage of the dual element transducer is that because one element serves as the transmitter while the other acts as the receiver, only one transducer is needed even for a phase-shift method where the signal is continuously being generated. The two elements in duals are separated by an acoustic barrier and are both slightly angled towards each other so that the transmitted and received waves have a ‘V’ shaped path as shown in Figure 2.3.

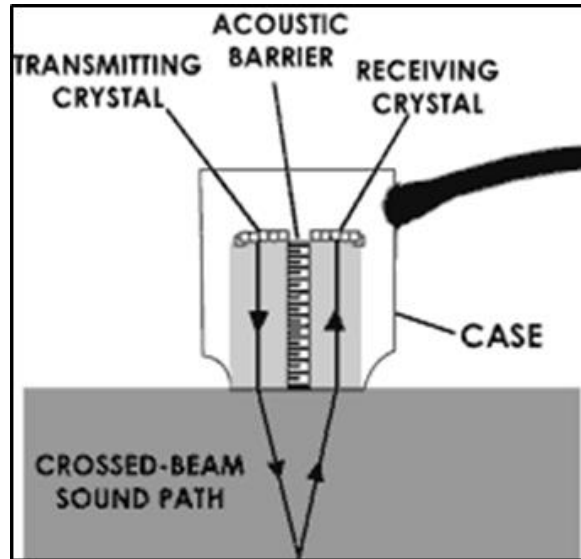


Figure 2.3: Dual element transducer [65].

Each element in the dual is independently wired to a connector. This makes it possible for continuous waves needed for phase-shift ultrasonic thermometry to be sent and received using only one transducer as the two connectors can be connected to a phase detector simultaneously.

2.10.2 Signal Generation and Data Acquisition Electronics

Signal generation and data acquisition electronics are important parts of ultrasonic experiments. Different types of electronics have been described in extant literature. A common setup used in pulse-echo ultrasonic thermometry in solids is described by Ihara et al. [10]. The transducer is connected to a pulser-receiver which in turn is connected to an analogue/digital conversion board and then to a personal computer (PC) as shown in Figure 2.4.

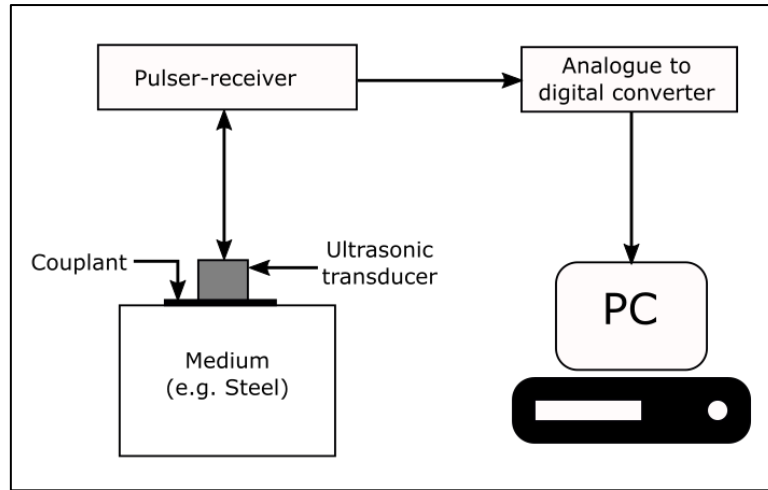


Figure 2.4: Pulse-echo ultrasonic experimental setup.

The pulser-receiver plays an important role in the pulse-echo ultrasonic setup. The achievable resolution of measurement depends on the centre frequency of the transducer and sampling rate of the pulser-receiver. The major blocks of a typical pulser-receiver described by Sharma et al. is shown in Figure 2.5 [66]. It is worth mentioning that there are other configurations of pulser-receivers and that some pulser-receivers generate the signal digitally.

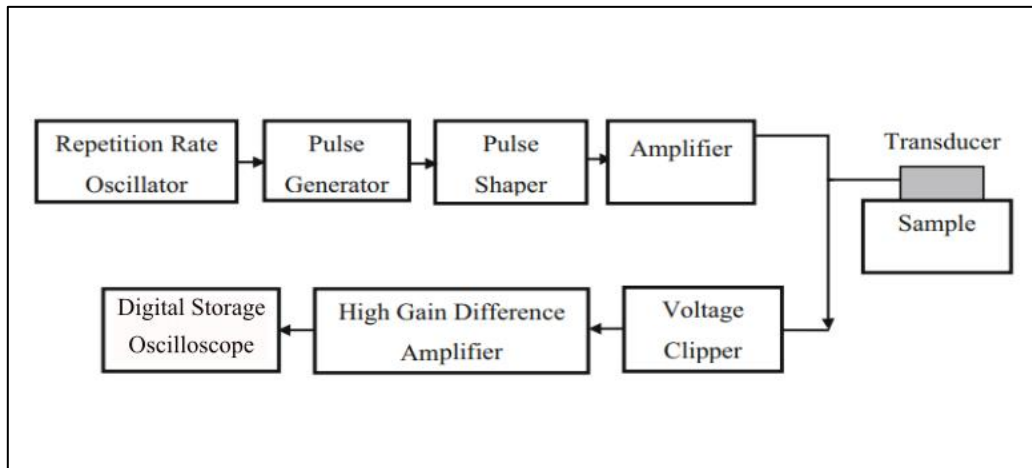


Figure 2.5: Major blocks of a typical pulser-receiver [66].

The frequency set by the repetition rate oscillator is used in generating the pulse which is then shaped, amplified, and sent to the transmitting probe of the transducer.

In the continuous wave method, a function generator is used to generate the input signal such as a sinusoid [47, 58]. The generated signal is sent to the transducer as well as a phase detector. The received signal from the transducer is amplified and then sent to the phase detector as well. The phase detector computes the difference in phase between the transmitted and received signals.

Different approaches, techniques, and devices for detecting the phase difference between transmitted and received ultrasonic signals have been described in literature. Microcontroller based phase digitisers were used for distance measurement in air [39]. However, the microcontrollers were 8-bit analogue to digital converters with a sampling rate of 40 kHz which is sufficient for distance measurement applications in air but too low for precision temperature measurement in solids. Another method used is the detection of phase with the FPGA digital phase detector [67]. This FPGA based solution was also used for temperature measurement in air with the frequency of 40 kHz which is much lower than that needed for precision temperature measurement in metals as described in the introduction. Kumar et al. also designed and implemented a phase detector on FPGA. However, the ADC used could only sample at 1.5 MS/s [68]. The need for an ADC for the use of FPGA as a phase detector also increases the complexity and cost of the setup. Reddyhoff et al. used a PCI based digitising card in a PC to acquire transmitted and received signals. Thereafter, they performed signal processing in LabVIEW using fast Fourier transform (FFT) to produce the phase spectrum for an oil film medium [69]. One of the limitations of their measurement setup is that they used pulser-receiver for generation of voltage pulses. For precision temperature measurement in metallic medium, the pulser-receiver required needs to be of high sampling rate (up to 3.5 GHz) as shown in the introduction and this has an associated increase in the cost of the setup.

Another approach for extracting ultrasonic pulse-echo information is the use of time-to-voltage analogue converters. With this method, the converter generates voltage values equivalent to

the time-of-flight. Wells et al. used this method for extracting diagnostic information of soft tissues [70]. However, they only considered ultrasonic velocity of 1500 m/s, which is the velocity of sound in soft tissues. Time-to-digital converters such as the Texas Instruments TDC7200 has resolution of 55 ps stated in its datasheet [71]. However, the converter is mostly used for fluid applications.

2.11 Summary of Literature Review

Thermocouples are commonly used for tool and workpiece temperature measurement. However, like other methods of temperature measurement involving discrete surface mounted sensors used for tool and workpiece temperature measurement, the thermocouple cannot give a true indication of the core temperature of the workpiece.

Ultrasonic thermometry works based on the dependence of ultrasonic velocity on material temperature. With the knowledge of both transit time and length of material through which an ultrasonic wave is propagated, the ultrasonic velocity can be determined. One main use of ultrasound in engineering is in NDT for flaw detection, the main limitations of the NDT techniques in relation to this research is that unlike in NDT where testing is based on detecting changes due to detected flaw, the temperature measurement system needs to be able to give temperature readings even without flaw in the material. There are two main ultrasonic measurement methods, the phase-shift, and the pulse-echo method. Both methods as well as combination and modification of the methods have been used for different applications including for temperature measurement. However, none of the setups or methods described in literature has been used for precision temperature measurement of metals or indeed for temperature measurement during manufacturing processes.

To properly transmit ultrasound to a workpiece from a transducer, the air present at the boundary of the transducer and the workpiece needs to be dispelled. This is because of the low acoustic impedance of air which makes it difficult to efficiently transmit ultrasound to metals since metals have high acoustic impedance. To dispel the air, ultrasonic couplants are used. There is no existing solution/research into couplants for temperature measurement during precision manufacturing, due to this, this research will include couplant analysis in the methodology chapter.

Microcontrollers and FPGAs have been used to measure the phase-shift between transmitted and received signals, however, they are not able to resolve phase-shift caused by a 0.5 °C change in temperature in steel. This is because they are limited to applications where lower ultrasonic frequencies are utilised. In some other studies, digitisers were used to record the signal attributes, thereafter the signal was processed to extract the phase information.

This literature review has shown that there is currently no method for core temperature measurement of metal components during high precision manufacturing scenarios such as machining and inspection.

With growing interest in on-machine inspection during manufacturing, the lack of a core temperature measurement technique for workpieces during manufacturing is an identified gap. Hence, there is a need to develop a method suited for precision ultrasonic thermometry in the harsh manufacturing environment. Based on the findings from literature, the methodology for this research was developed and is discussed in the next chapter.

Chapter 3

3 Methodology

Before deciding on the experimental methodology to be adopted in this thesis, having a simulation of the identified methods from the reviewed literature can give a better understanding of the strengths and weaknesses of each method and help to determine the initial parameters for the ultrasonic experiments. Therefore, ultrasonic simulations were carried out and discussed in this chapter.

There is no existing couplant solution found in literature for the present research, due to this, a couplant analysis is done to determine an appropriate couplant for this research. Thereafter, the devices and equipment choices for ultrasonic experiments are detailed and preliminary tests to determine their suitability were performed.

3.1 Ultrasonic Simulation

Several numerical methods, commercially available and open-source software have been utilised and described in extant literature for the simulation of ultrasonic wave propagation and reception. One of the industry standard software is CIVA by EXTENDE. Early works to develop the CIVA software started in the early 90s and since its release for commercial use, it has been widely adopted for different ultrasonic simulation applications in power, aerospace, oil and gas, and mechanical industries [72]. Due to CIVA's extensive use, different authors have carried out validation works for the software [72, 73] and several modules have been created. The module of interest is the ultrasonic testing (UT) module which comes at over £9000 for academic use. It is therefore appropriate to review open-source software in order to establish if the simulation objectives can be achieved without the use of a premium software.

K-wave is an open-source MATLAB and C++ toolbox developed for time domain acoustic and ultrasonic simulations [74]. The functions of the software are based on the k-space pseudospectral method and are able to model pressure and velocity sources, arbitrary detectors, and a detailed time-domain model of the propagation of ultrasonic waves [74].

Martin et al. performed a quantitative validation of the k-Wave software [75] and their results showed that k-Wave can predict fields close to the experimental uncertainty. The k-Wave toolbox has been used in several published studies. For example, Hladky et al. solved a modelling problem focused on the propagation of a modulated ultrasonic wave in a nonlinear medium with k-Wave [76]. Another study showed that k-Wave predicts the behaviour of transmitted and received signals with expected accuracy [77].

Other ultrasonic studies such as quantification of excess ultrasonic attenuation [78], modelling of defects in an ultrasonic inspection [79], and simulation of railway inspection [80] are some of the fields where k-Wave toolbox has been used.

There are other ultrasonic simulation software reviewed and tried such as SIMSONIC [81], the Discrete Representation Array Modelling (DREAM) [82], and Field II [83]. These ultrasonic simulation tools are all freely available open-source software. They are like k-Wave in their use as MATLAB toolbox software. However, the k-Wave is more user friendly with an active support forum and extensive research coverage.

In this chapter, the simulations performed to determine the potential acquisition parameters for precision temperature measurement will be discussed. The first simulation is of the ultrasonic pulse-echo based thermometry; this is because the pulse-echo method is the traditional ultrasonic measurement method for common applications such as NDT. The choice of simulation methods, parameters such as the speed of sound in the medium of interest, and the underlying assumptions such as the equation relating the ultrasonic velocity to temperature are

all retrieved from extant literature. References are provided in the following sections as and when the parameters are used.

Based on the findings from the literature review, there are limitations arising from resolving the time-of-flight in metals to a resolution that would be suitable for temperature measurement in manufacturing. Typically, a 1 μm resolution is used in manufacturing of standard precision parts on CNC machines, as well as compensation of errors on machines with such functionality. Considering a small to medium sized aluminium component of 200mm in length, a thermal expansion of 1 μm can occur with an average temperature increase of just 0.2 $^{\circ}\text{C}$ (assuming (Expansion coefficient of 25 $\mu\text{m}/\text{m}/^{\circ}\text{C}$). A target resolution of 0.1 $^{\circ}\text{C}$ was therefore chosen and used in defining some of the settings and the discussions in this chapter.

In order to determine the requirements for existing ultrasonic measurement methods, ultrasonic simulations were required. These were designed to understand the behaviour of ultrasonic waves in the media of interest and the required parameters for achieving desired resolutions of temperature measurement. Furthermore, both material expansion and change in ultrasonic velocity affect the ultrasonic time-of-flight in a material. Hence, there is a need to differentiate these individual effects on TOF. Based on this, the effects of expansion and change in speed due to temperature on TOF were simulated.

The simulations were performed in MATLAB with the k-Wave MATLAB toolbox. k-Wave is an open-source toolbox for time domain acoustic and ultrasound simulations. K-Wave gives a real-time ultrasonic information of the medium during simulation as well as the wave propagation plot [74].

In all the simulations, steel was chosen as the transmission medium because of its prevalence both in ultrasonic measurement literature and in manufacturing practice. The underlying equation required to simulate the ultrasonic speed-temperature relationship, which had to be

obtained experimentally, was obtained from the work of Ihara et al. [10]. This equation is only provided for steel in the literature, hence the choice of steel as the medium of propagation.

3.1.1 Ultrasonic Time-of-flight Simulation

The first simulation was set up to observe the pulse-echo method. A nominal material length of 200 mm (steel) was chosen. This part size is typically made in the University workshop and is compatible with the fixturing used. In simulation however, this can be varied to observe the effect of expansion on TOF as will be discussed under the section for expansion simulation.

Certain parameters need to be set correctly in k-Wave to obtain reliable simulation results. k-Wave makes use of a computational grid which is defined by calling the `kgrid` function for simulating the propagation of ultrasonic waves. The grid determines how the continuous ultrasonic medium is split into an even mesh of grid nodes [74]. It is at these discrete grid nodes that the governing equations are solved. k-Wave offers other functions that can be called for simulation. The fields used in this simulation and for subsequent simulations are shown in Figure 3.1 and discussed thereafter.

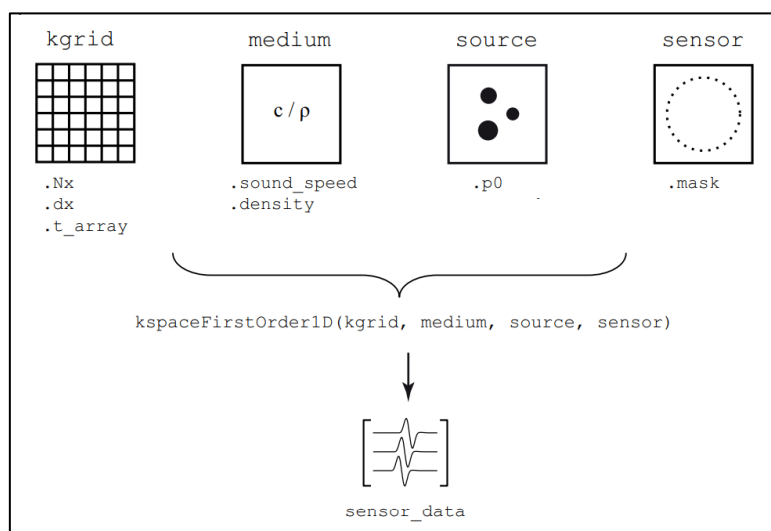


Figure 3.1: Overview of the input structures and fields used for the simulations [74].

N_x is the number of grid points with spacing dx in the x Cartesian direction. dx and N_x are chosen based on the size of the computational grid, the minimum ultrasonic velocity, the maximum frequency, and the number of points per wavelength required [74].

The number of points per wavelength is chosen to be above 2 to satisfy the Nyquist requirement. The equations for determining the optimal spacing and grid size are given in equations (3.1) and (3.2).

$$dx = \frac{C_{min}}{ppw * f_{max}} \quad (3.1)$$

$$N_x = round(\frac{x_{size}}{dx}) \quad (3.2)$$

Where dx is the grid spacing, C_{min} is the minimum ultrasonic velocity in the grid, ppw is the number of points per wavelength, and f_{max} is the maximum ultrasonic frequency. N_x is the number of grid points and x_{size} is the size of the computational grid.

The `t_array` parameter defines the array of time values, and it is over these values that the ultrasonic simulation is run. This can be set to populate automatically or manually using the `makeTime` function. When being set manually, the function must be evenly set. This is achieved by passing the `kgrid`, sound speed, and end time argument into the `makeTime` function.

The ultrasonic medium must also be defined. Nominal ultrasonic velocity or an equation representing the change in ultrasonic velocity over time and the density of the material need to be provided. In this simulation, the equation relating the change in ultrasonic velocity to temperature was used, this is given as equation (1.1).

The ultrasonic source is the third input structure. Using the `source.p0` function, the location and the properties of the initial pressure distribution of the ultrasonic source can be set. In these simulations, the source location is defined to simulate the position of the ultrasonic transmitter. For the pulse-echo simulations, the source was defined as a tone burst and k-Wave provides a function that can be called to generate a tone burst. The `toneBurst` function requires the following arguments: sampling frequency, tone burst frequency, and tone burst cycles. The tone burst frequency was chosen to be 5 MHz to simulate a transducer of 5 MHz centre frequency. This value was chosen as 5 MHz transducers are easy to obtain due to their prevalence in thickness gauging applications.

Ultrasonic couplants such as epoxy provide a fixed coupling of the transducer to the solid medium of propagation. Because of their higher acoustic impedance than air, they aid the transmission of ultrasonic signals. A detailed couplant analysis is provided in Section 3.2. For this simulation, epoxy was used. Using sound speed of 3070 m/s for epoxy, equation (1.1) for steel, density of 1800 kg/m³ for epoxy, and 8030 kg/m³ for steel, the physical properties of the media of propagation was set. The grid point spacing dx was chosen as 1.023e-04 m with N_x (number of grid points) chosen as 7.776e+03, these were chosen based on equations (3.1) and (3.2) respectively.

For a 5 MHz transducer, sampling above 10 MHz will satisfy the Nyquist theorem. However, to resolve a 0.1 °C temperature change, there is a need to reconstruct the signal with increased sampling frequency using signal processing (Fourier interpolation). The simulation tool being used (K-Wave) is however a time-domain simulation tool. Therefore, a simulation to determine the required sampling frequency in time domain was carried out. To determine the optimal sampling frequency which was related to the time step dt as $1/dt$, an iterative simulation was carried out to resolve 0.1 °C for a 200 mm steel part starting with frequency of 1 GHz. 1 GHz was chosen as the starting point because initial calculations in the introduction showed that

approximately 3.5 GHz sampling frequency is needed. The result of the simulation is given in Table 3.1.

Table 3.1: Result of simulation for quantisation of sampling frequency

Temperature (°C)	Sampling Frequency (GHz)				
	1	2	3	4	5
	Time-of-flight (μ s)				
25	33.876	33.876	33.8767	33.8765	33.8764
25.1	33.876	33.8765	33.877	33.877	33.8768
25.2	33.877	33.877	33.8773	33.8773	33.8772
25.3	33.877	33.8775	33.8777	33.8775	33.8776
25.4	33.877	33.8775	33.878	33.878	33.878
25.5	33.878	33.878	33.8783	33.8783	33.8784

The result shows that with 1 GHz sampling frequency, the achievable resolution is 0.3 °C as there is no change in the time-of-flight results from 25.2 °C to 25.4 °C. For 2 GHz, the achievable resolution is 0.2 °C as there is no change in the time-of-flight from 25.3 °C to 25.4 °C. 3 GHz and 4 GHz resolved 0.1 °C, however, the rate of change of the time-of-flight due to temperature change was not uniform through the simulations. 5 GHz sampling frequency gave uniform results; therefore, 5 GHz was chosen for the time-of-flight simulations.

To capture the transit time of the ultrasonic wave, the pulse needs to be recorded at a minimum of two points. These points are defined by the sensor structure which takes a location argument for its mask function. The transit time is taken as the difference between the time of ultrasonic pulse reaching the two sensors. In the simulations, the separation distance is set to represent the material length in the direction of ultrasonic propagation.

The sensors were set to be 200 mm apart and centralised in an 800 mm grid to prevent reflections from the grid boundaries reaching the grid's area of interest. The sensor positions are shown in Figure 3.2.

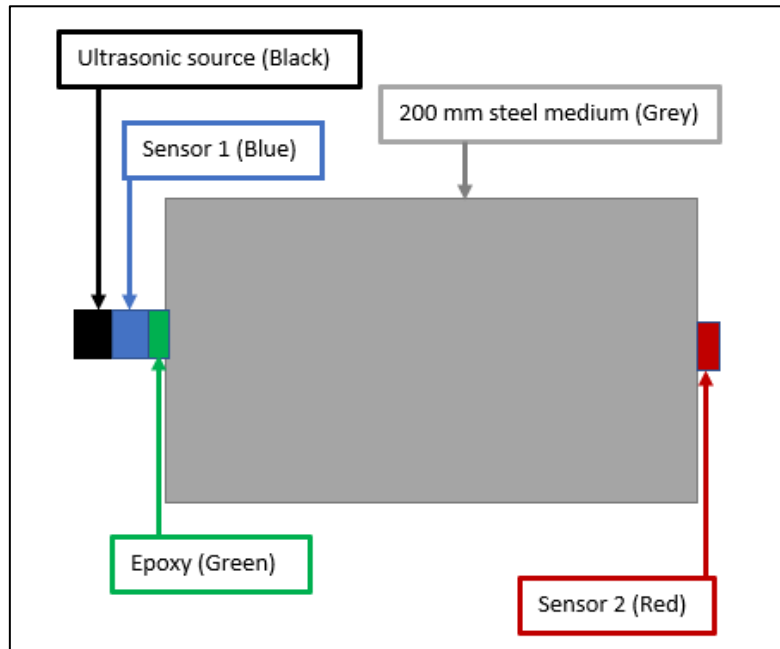


Figure 3.2: Setup of the ultrasonic source and sensors for pulse-echo simulation

Figure 3.2 shows the propagation of the ultrasonic wave. The pulse is generated at the position of the source (-101 mm) and is propagated in all directions. The first sensor at -100 mm is used to capture the time the pulse reaches that position. The second sensor is positioned at +100 mm to represent a 200 mm part. The recorded tone burst is shown in Figure 3.3.

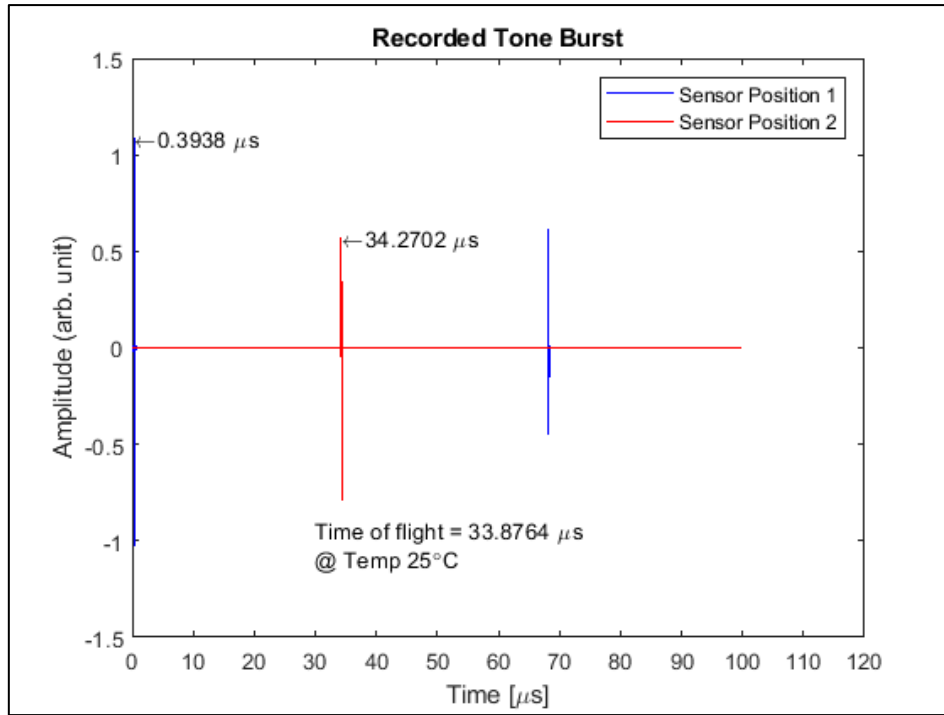


Figure 3.3: Recorded tone burst.

The recorded tone burst for 25 °C shows that the ultrasonic pulse reached the first sensor at 0.3938 μs and the second sensor at 34.2702 μs . This was used to compute the time (33.8764 μs). The threshold technique of TOF method was used in all the time-of-flight in the simulations. One set of simulations was run over the range of 25 °C to 25.5 °C, the time-of-flight changed accordingly with the same set of parameters given above. The ultrasonic velocity was changed based on equation (1.1). The full code is given in Appendix A and the results of the simulations are given in Figure 3.4 and Figure 3.5.

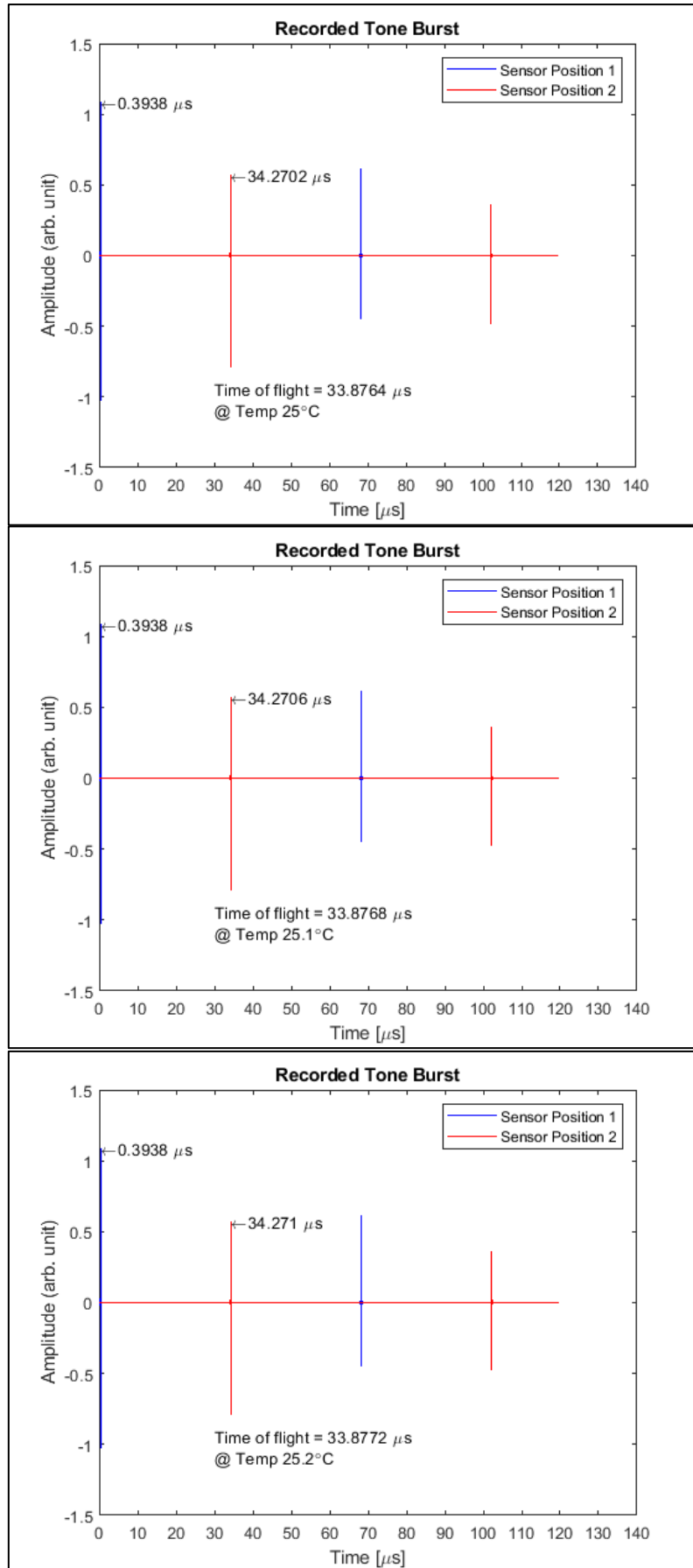


Figure 3.4: Simulation of time-of-flight for 0.1 $^{\circ}$ C resolution for 25 $^{\circ}$ C to 25.2 $^{\circ}$ C.

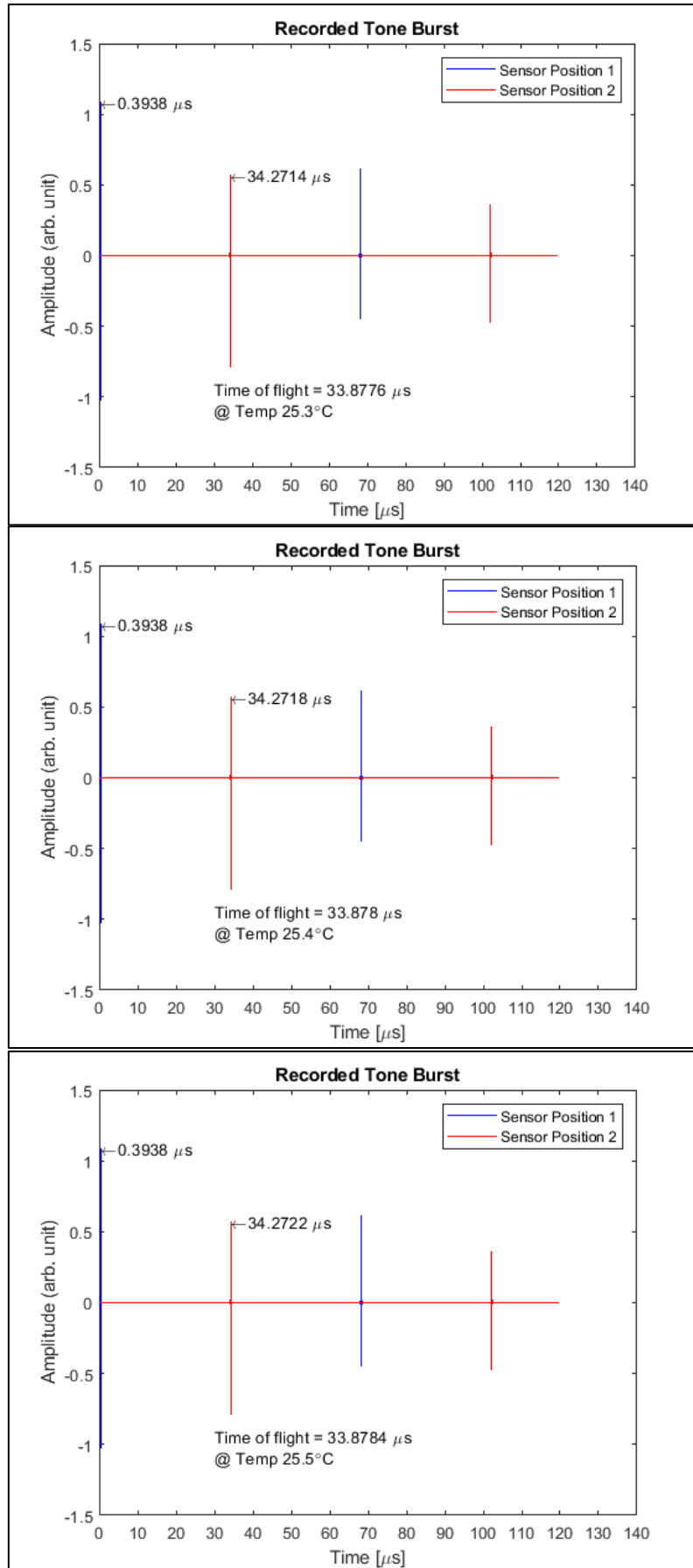


Figure 3.5: Simulation of time-of-flight for 0.1 $^{\circ}\text{C}$ resolution for 25.3 $^{\circ}\text{C}$ to 25.5 $^{\circ}\text{C}$.

Change in temperature affects the dimension of the material (thermal expansion or contraction) as well as the ultrasonic velocity through the material. Both change in dimension and change in ultrasonic velocity will affect the TOF of ultrasonic wave, differentiation of which is crucial for this research. The next simulation shows the individual effects of change in ultrasonic velocity and change in dimension. The velocity and expansion effects were simulated by varying velocity with temperature while holding dimension constant and varying dimension while holding the velocity constant, respectively.

The ultrasonic velocity was varied based on equation (1.1), while the expansion was varied using equation (3.3).

$$\Delta L = \alpha_L \Delta T L \quad (3.3)$$

where ΔL is change in length, α_L is linear coefficient of thermal expansion which is taken as $12.3 \mu\text{m}/\text{m}^\circ\text{C}$ for EN24T steel [84], ΔT is change in temperature, and L is the original length.

The result of the simulation is given in Figure 3.6.

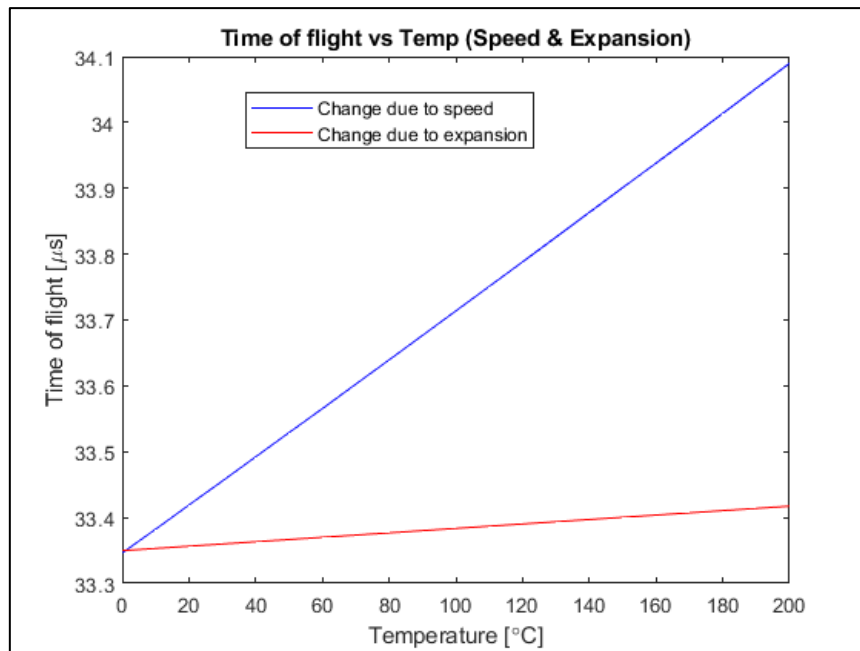


Figure 3.6: Effect of change in speed and expansion on TOF

The relationship between ultrasonic velocity and temperature is approximately linear over the range of 200 °C [10], the typical precision manufacturing temperature falls within this range. It can be seen from Figure 3.6 that time-of-flight varied more due to change in velocity than the expansion of the material. This simulation validates that ultrasonic TOF can be estimated from change in velocity of sound or from material expansion or both. From the result, using just the ultrasonic velocity, TOF estimation can be made with compensation made for expansion where required. This result will be a guide for experimental methodology, providing a basis for focusing on ultrasonic velocity for determining ultrasonic TOF.

The results of the time-of-flight simulations show that pulser-receiver of 5 GHz sampling frequency is required to measure temperature change with resolution of 0.1 °C. Enquiries were made to know the cost of acquisition devices meeting this sampling specification. One card that meets this specification is the Acqiris U5310A PCIe card with a budgetary price of £16,700. Tribosonics was also contacted, however, their £9,600 xSCAN can only achieve a sampling frequency of 100 MHz. Ultratek's USB-UT350 costs £3,300 but its digitiser can only sample at 50 MHz.

The associated cost with the pulse-echo method makes it infeasible for the present task. In the next section, the phase-shift method will be simulated.

3.1.2 Ultrasonic Phase-shift Simulations

The phase-shift simulations are similar to the pulse-echo simulations. The main differences are the type of ultrasonic pressure source and the need for phase difference calculation which is different from the peak-detection technique used in the pulse-echo simulations. Also, because the recorded signals at the sensor positions are used to compute the phase-shift, a medium of

single density was used to prevent the overlapping caused by the reflections at the boundaries. The simulations were carried out with the properties of steel and not the couplant for the phase-shift simulations (section 3.2 covers the importance of couplants).

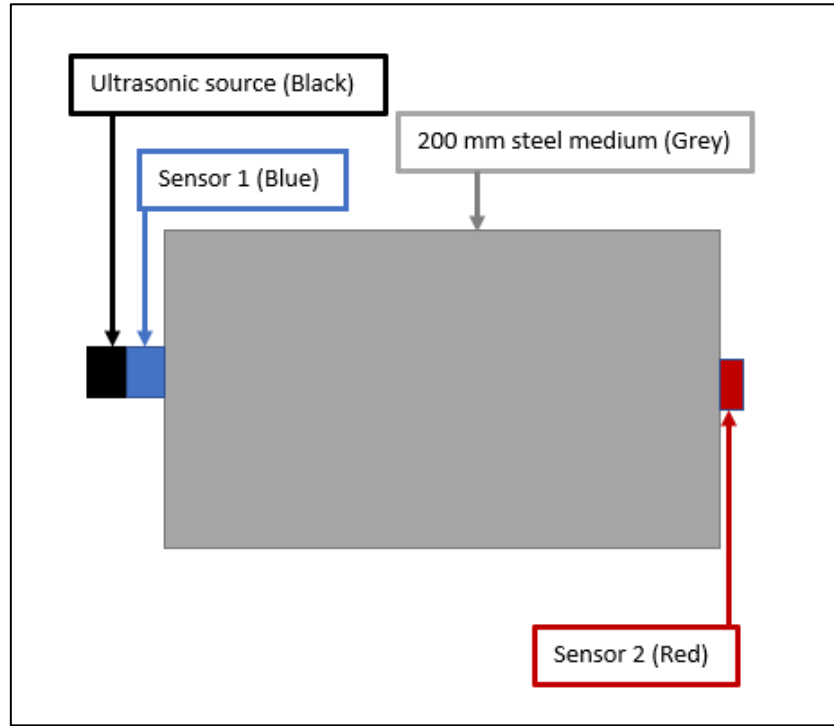


Figure 3.7: Setup of the ultrasonic source and sensors for phase-shift simulation

The source was defined using the basic sine wave equation given as:

$$y(t) = A\sin(2\pi ft + \Phi) \quad (3.4)$$

Where A is the amplitude, f is the wave frequency, t is time, and Φ is phase.

For the simulations, the frequency was defined for each simulation to represent transducer frequency and the time was set with the kgrid time array.

In order to extract the phase information from the simulation results, there is the need to use a specialised function for extracting time domain information. The Hilbert transform is one of such functions. For a given function $u(t)$, its Hilbert transform $H[u(t)]$ is given as:

$$H[u(t)] = u(t) * \frac{1}{\pi t} = \frac{1}{\pi} \int_{-\infty}^{\infty} \frac{u(\tau)}{t - \tau} d\tau = \frac{1}{\pi} \int_{-\infty}^{\infty} \frac{u(t - \tau)}{\tau} d\tau. \quad (3.5)$$

The Hilbert transform of the function $u(t)$ is the convolution of $u(t)$ with the signal $1/\pi t$ [85].

The Hilbert transform is related to the original signal by a phase-shift of 90° , this is because the Hilbert transform introduces a phase-shift of 90° to the original signal [86]. MATLAB offers a function for computing the Hilbert transform of a signal, Therefore, the MATLAB Hilbert transform function was used for the phase-shift simulations. The output of the function has the original data as the real part and the Hilbert transform as the imaginary part. This output is sometimes referred to as the analytic signal. The analytic signal is useful for calculating instantaneous properties of a time series signal at any instance in time [87]. This attribute is needed for obtaining the phases of the transmitted and received signals, this is then used to compute the phase difference between both signals. After the Hilbert transform of the signals, the signals' phases are obtained using the unwrap and angle functions. Thereafter, the angle of the received signal is subtracted from the transmitted signal. The phase-shift simulation was carried out for temperature range 25 to 25.5 °C in steps of 0.1 °C. The results are shown in Figure 3.8 and Table 3.2. Figure 3.8 is a zoomed in plot that shows the actual phase-shift. The full plot for all the simulation is provided in Appendix A.

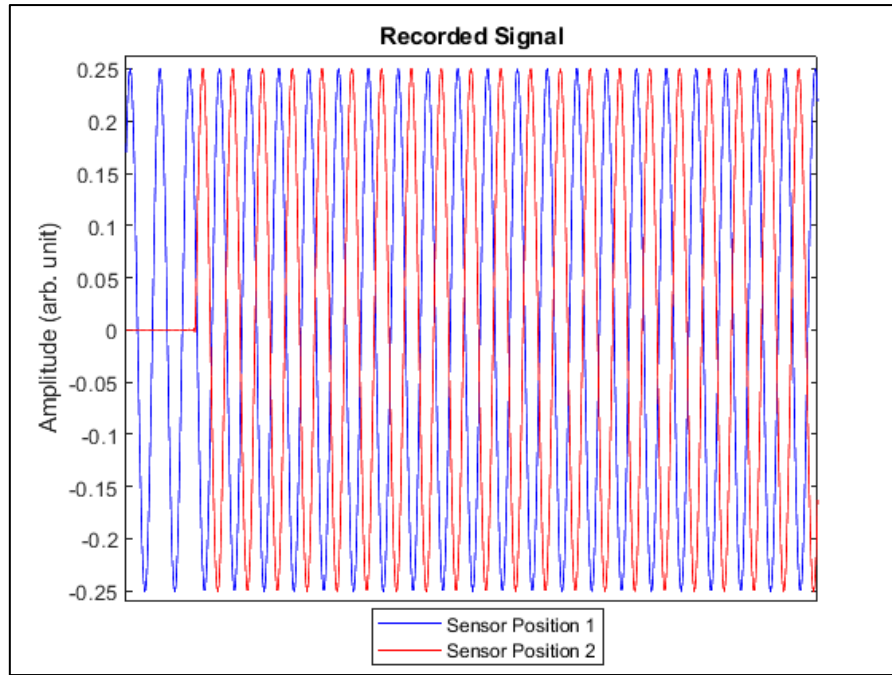


Figure 3.8: Simulation of phase-shift for 25 °C using 5 MHz frequency.

Table 3.2: Phase-shift simulation result for 5 MHz frequency.

Temperature (°C)	Phase-shift (5 MHz) (°)	Used ultrasonic velocity (m/s)
25	-200.628	5901.7
25.1	-199.971	5901.636
25.2	-199.313	5901.573
25.3	-198.657	5901.509
25.4	-197.999	5901.446
25.5	-197.341	5901.382

Table 3.2 shows a phase-shift of -200.628° in a 200 mm steel part at 25 °C. The phase-shift changed to -199.971° at 25.1 °C. The simulation results show that a 0.1 °C change in temperature caused the phase of a 5 MHz ultrasonic signal to shift by 0.66° in a 200 mm part.

In cases where a larger temperature range needs to be measured, a lower frequency transducer can increase the measurable range. However, this will come with the cost of lower

measurement resolution. Another commonly used transducer is the 1 MHz transducer. Phase-shift simulation was done using a 1 MHz transducer, the result is shown in Figure 3.9.

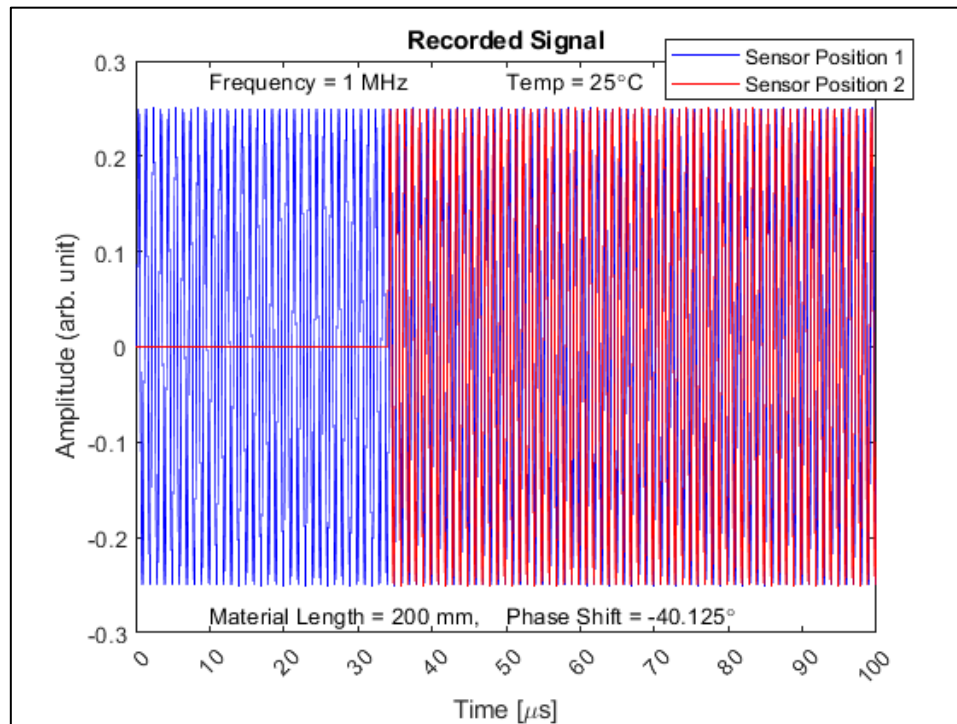


Figure 3.9: Simulation of phase-shift for 25 °C using 1 MHz frequency.

The phase of the 1 MHz signal shifted by -40.125° in a 200 mm steel at 25 °C. To know the resolution of the 1 MHz transducer with respect to temperature, the simulation was repeated in steps of 0.1 °C from 25 °C to 25.5 °C. The result is given in Table 3.3.

Table 3.3: Phase-shift simulation result for 1 MHz frequency.

Temperature (°C)	Phase-shift (1 MHz) (°)	Used ultrasonic velocity (m/s)
25	-40.125	5901.7
25.1	-39.994	5901.636
25.2	-39.863	5901.573
25.3	-39.731	5901.509
25.4	-39.599	5901.446
25.5	-39.468	5901.382

Table 3.3 shows that a 0.1 °C change in temperature will shift the phase of a 1 MHz ultrasonic signal by 0.13° in a 200 mm steel.

The 5 MHz transducer gives 0.53°/0.1 °C of sensitivity than the 1 MHz transducer. Both the phase-shifts of the 1 MHz and 5 MHz transducers are large enough to be measured by a phase-detector. (Section 3.3.4 covers the AD8302 phase-shift detector). The simulation codes and results are provided in Appendix A.

The phase-shift simulations have provided an approximate sensitivity of the phase-shift to temperature, this will be used in the experiments. The 5 MHz transducer was chosen for use in the laboratory experiments because of its higher sensitivity and because of the ease of sourcing them from different commercial vendors. This will help to clarify if the approach is suitable for on-machine testing.

3.2 Ultrasonic Couplants

Ultrasonic couplants are used to aid the transmission of ultrasonic wave from the transducer to the medium of ultrasonic wave propagation. The use of a couplant is necessary if the medium of propagation is solid as this helps to remove any air from the surface of both the transducer and the solid material. Air causes significant loss in transmission due to the low acoustic impedance of air compared to the transducer and the solid medium [88]. The acoustic impedance of air is about 5 orders of magnitude lower than that of the ultrasonic transducer and steel [89]. Ultrasonic couplants with high impedance significantly improve the transmission of ultrasonic signals [90].

There are different types of couplants. The suitability of couplants to an application generally depends on the type and requirement of the task at hand. Liquid couplants are generally used

with smooth surfaces and examples of this are silicone oil and propylene glycol. One of their major limitations is their low acoustic impedance. They are however very efficient in forcing air out. More viscous couplants like gel and grease are better suited for rougher surfaces and they provide higher acoustic impedance than less viscous couplants [91].

Adhesives such as Cyanoacrylate (super glue) are commonly used because they eliminate the need for clamping and their acoustic transmission is better than many other adhesives. However, previous studies have shown that there is a risk of damaging the transducer during removal of the transducer [92–94]. As such super glue would only be ideal for a permanent fixing of the ultrasonic transducer.

Epoxy resin is another adhesive couplant for use with a metallic medium of propagation [95]. Epoxy resins are stable and they have relatively high acoustic impedance when compared with other couplants and it has also been shown that epoxy bonds can be broken off when they are no longer needed [96]. Based on the reviewed couplant types, epoxy has the qualities needed for use in the present study. Its strength, good transmission, and reusability are desirable for the present task.

The acoustic impedances of air, water, and some other media are given in Table 3.4 [97–99].

Table 3.4: Acoustic impedances of some common media

Medium	Impedance ($\text{kg.m}^{-2}\text{s}^{-1}$)
Air	0.4×10^3
Water	1.5×10^6
Epoxy	2.6×10^6
PZT (ceramic)	3×10^7
Stainless steel	4.7×10^7
Steel	4.8×10^7

Other couplants include special couplants for very high temperature and shear wave transmission [88], but these are designed for operating parameters that are outside the scope of this research.

3.3 Signal Generation and Acquisition

The adopted methodology for the laboratory experiments is based on the findings, gaps identified in the literature and the results of the simulation. Thus, the phase-shift method was adopted as it offers the potential for higher resolution without the need for an expensive pulser-receiver. The choice of devices and equipment for waveform generation, propagation and phase-shift detection, and logging will now be discussed.

3.3.1 Waveform Generation

For the phase-shift experiment, a continuous waveform rather than pulses is required. A spectrum M2i.6022-exp arbitrary waveform generator (Spectrum Instrumentation, Ahrensfield, Grosshansdorf, Germany) was chosen because of its availability, performance, and PCIe form factor enabling high speed PC data logging. It has a maximum clock speed of 62.5 MS/s as specified in the data sheet [100]. The waveform generator comes with a software - SBench 6. SBench 6's base license is able to output up to 7 MHz. The waveform generator can also be used with LabVIEW and MATLAB. The M2i.6022-exp waveform is shown in Figure 3.10.

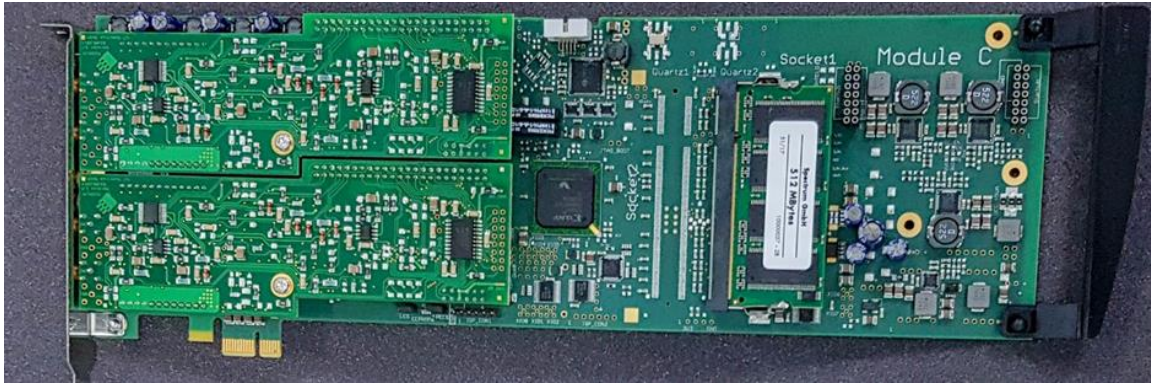


Figure 3.10: Spectrum M2i.6022-exp arbitrary waveform generator

With the Easy Generator function provided in SBench 6, the signal frequency, signal type, amplitude, and phase-shift can be set. The user interface of the Easy Generator function is shown in Figure 3.11.

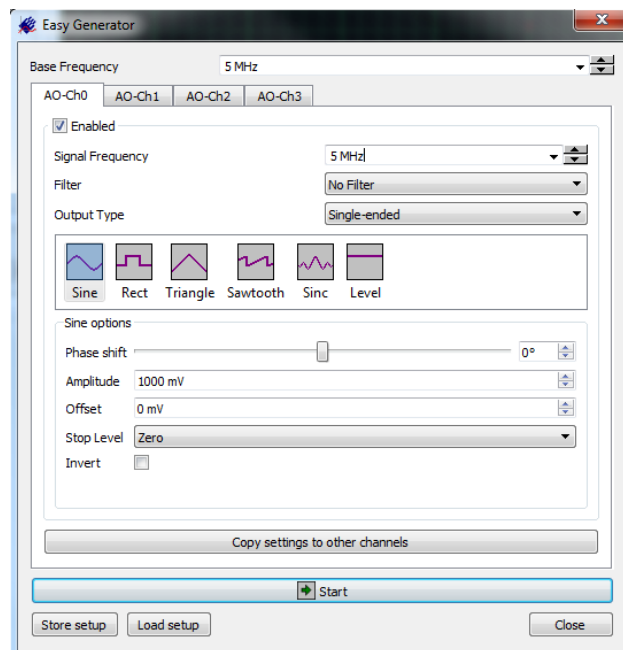


Figure 3.11: SBench 6 Easy Generator

3.3.2 Ultrasonic Transducer

Based on the literature review (see section 2.10.1) and the requirement of the phase-shift method for the sent and received signals to be recorded simultaneously which enables dynamic phase-shift computation during an actual test, the dual element transducer was chosen for this study. The dual element transducer has two crystal elements housed in the same case, one can be used as the transmitter and the other as the receiver. The elements are separated by an acoustic barrier and the transmitted and received signal form a 'V' shape as shown in Figure 3.12. To determine the feasibility of using the method being developed, before procuring a relatively high-end transducer, an off the shelf 5 MHz transducer sold with Amgaze Digital Ultrasonic Thickness Gauge was procured. The gauge and the transducer cost £75, while similar transducers from NDT vendors are quoted for £350. There is still the need to use a properly characterised transducer, however, a readily available and affordable transducer will help to determine the feasibility of the developed method. A 5 MHz transducer was used as this frequency has been used in simulations where it provided good results. Figure 3.12 shows the travel pattern of ultrasonic wave transmitted and received by a dual element transducer.

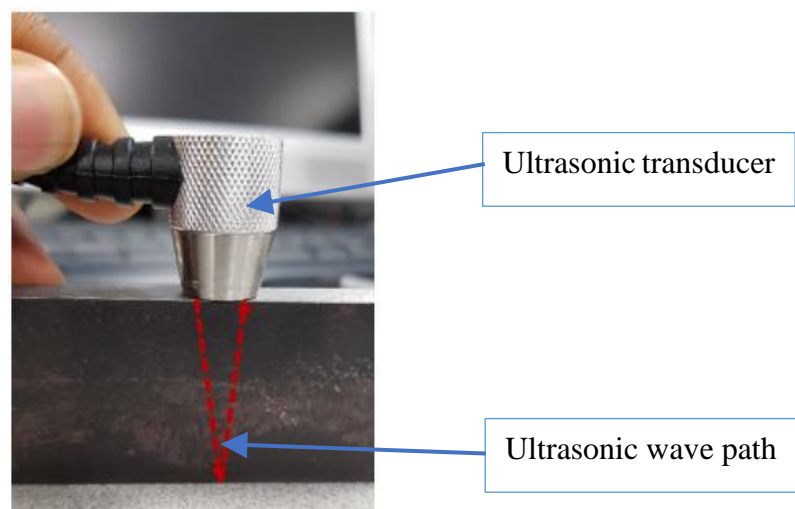


Figure 3.12: Amgaze 5 MHz dual element piezo-electric transmitter/receiver transducer

3.3.3 Phase-shift Detection

The result of the phase-shift simulation given in Table 3.3 shows that 0.1°C change in temperature caused a phase-shift of 0.13° . A test was set up in the electronics laboratory to determine if the high specification oscilloscope can be used to measure 0.1° phase-shift.

Keysight 33500B series waveform generator with two channels was used to generate two 5 MHz sine waveforms (Keysight waveform generator was only used for the preliminary phase-shift test, ultrasonic thermometry experiments were performed using the Spectrum waveform generator). The first waveform's phase is set to 0° and the second waveform was synced with the first and its phase set to 0.1° . The two waveforms were sent to an Agilent Technologies InfiniiVision MSO-X 3034A mixed signals oscilloscope able to sample at 4 GSa/s as shown in Figure 3.13.

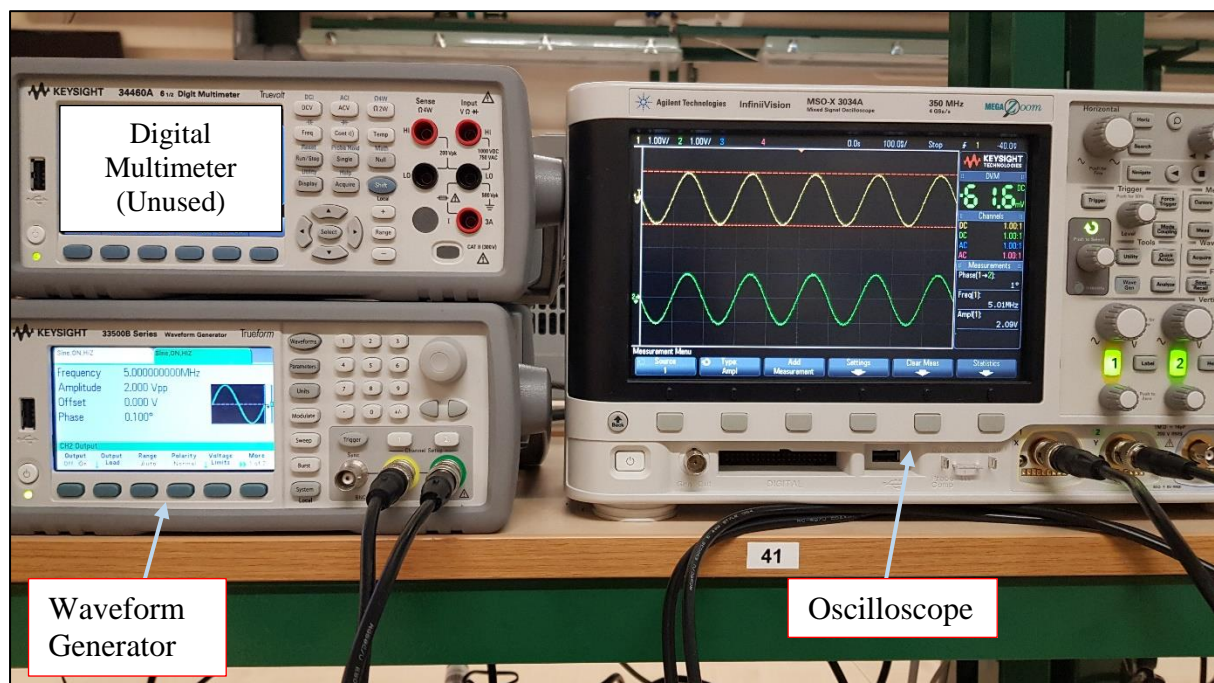


Figure 3.13: 0.1° Phase-shift test on Agilent Technologies high-speed oscilloscope

The test showed that the oscilloscope is unable to resolve 0.1° phase-shift as the highest resolution of the oscilloscope is 1° . Another limitation of using this high-speed oscilloscope is the lack of functionality for dynamically utilising the phase-shift measurements, this functionality is required for in-process temperature measurement.

None of the reviewed phase-shift detection solutions from section 2.10.2 is suitable for the present task. Therefore, phase-shift detection solutions were further researched. The main requirements used for identifying a potential solution were its ability to resolve 0.1° phase-shift, functionality for dynamically outputting the phase-shift measurement, and a cost lower than the that of pulser-receiver. The AD8302 phase-shift detector was identified as a potential solution for the present task.

The AD8302 evaluation board is a fully integrated board for measuring phase-shift information for several send/receive applications [101, 102]. The board comes in a small footprint and is ideal for in-situ monitoring in a non-invasive fashion [103]. Apart from a single supply of 2.7-5.5 V as supply voltage, the board does not require any other external component to serve as a phase detector. Within the range of $0-180^\circ$, the detector is able to measure accurately with the range scaled to $10 \text{ mV}/^\circ$ [101]. The main limitation of the AD8302 is the ambiguity of voltage value. However, in applications where relative rather than absolute measurement is required, the lack of knowledge of the actual phase value is not a major disadvantage. Although the AD8302 has not been used in precision temperature measurement applications in metals, the given specifications – the accuracy, size as well as the cost (£250) of this phase detector device make the device a potential choice for the present task.

3.3.4 AD8302 Phase-shift Detector

The AD8302 phase-shift detector compares the phases of two signals and outputs an equivalent voltage to represent the phase difference. Its stated accurate phase measurement scaling is 10 mV/Degree. Figure 3.14 shows AD8302. The two signals to be compared are sent to INPA and INPB ports respectively and this is done using SMA (SubMiniature Version A) coaxial connectors. 5 V DC power is supplied to the board through the VP port (red wire in Figure 3.14 (a)). For measurement tasks, the red switch is set to 'M'. The voltage value representing the phase-difference measurement is outputted through the SMA 'PHASE' port which can be sent through a coaxial cable for capturing or digitising. Other ports on this board are not relevant to this task as they are either used for control tasks or for signal gain measurements.

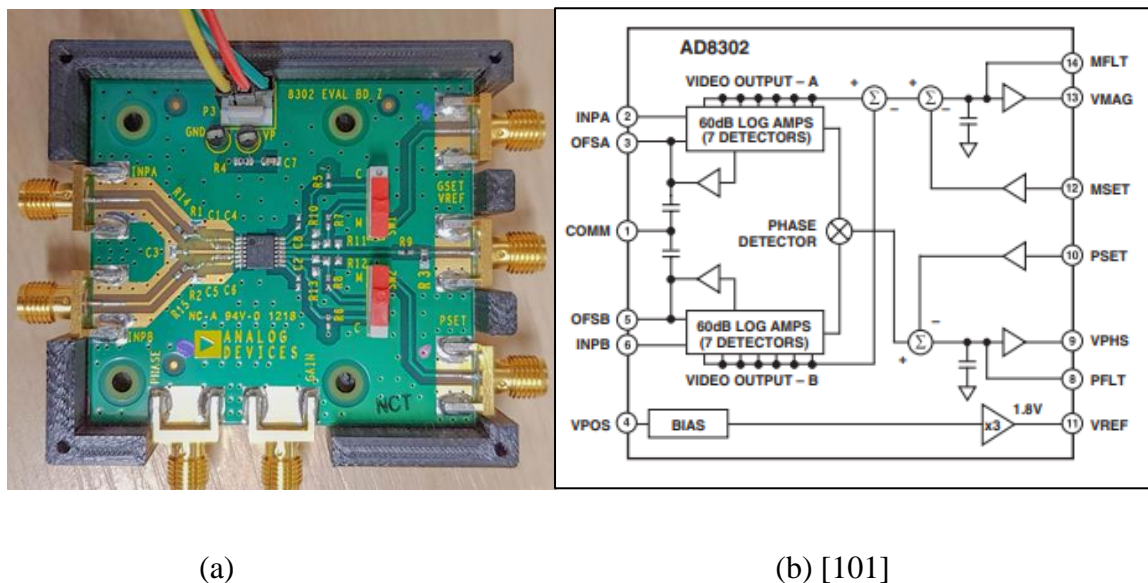


Figure 3.14: (a) - Picture of AD8302 Phase detector. (b) - AD8302 functional block diagram

One of the limitations of the phase detector board is its non-linearity at the extremes of phase values (below -150° , -20° to 20° , and above 150°) as shown in Figure 3.15. It is possible to limit the range of phase-shift used by changing the frequency if the phase-shift for the used frequency falls within the non-linear range. Another limitation of the phase-detector is the lack of distinction between the positive and negative phase difference in their indication. This

however would not impact negatively on the experiment if the extremes are avoided, this is because in the planned experiment, only the change in temperature and phase from the initial reading needs to be known and not the absolute temperature or phase. The plot shown in Figure 3.15 is from the datasheet and to verify this response, a new response will be recorded using the planned experimental setup.

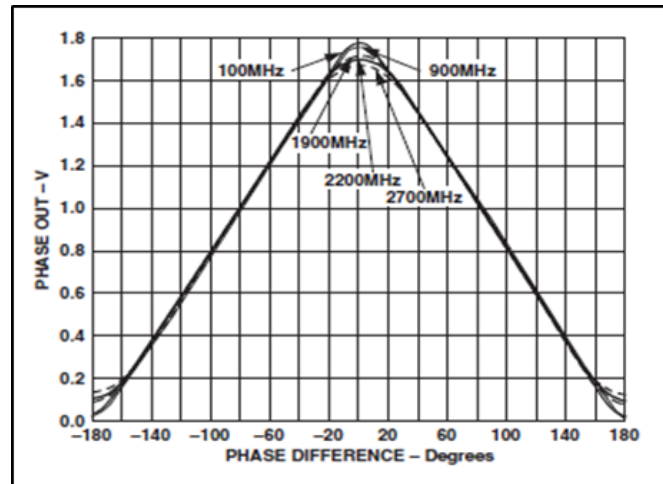


Figure 3.15: Phase output vs phase difference [101].

To better understand the nature of the voltage output signal, the waveform generator was used to generate two sinusoid signals. The signals were sent to the AD8302 board and the output from the board as well as the original signals were observed on an oscilloscope. These signals are shown in Figure 3.16.

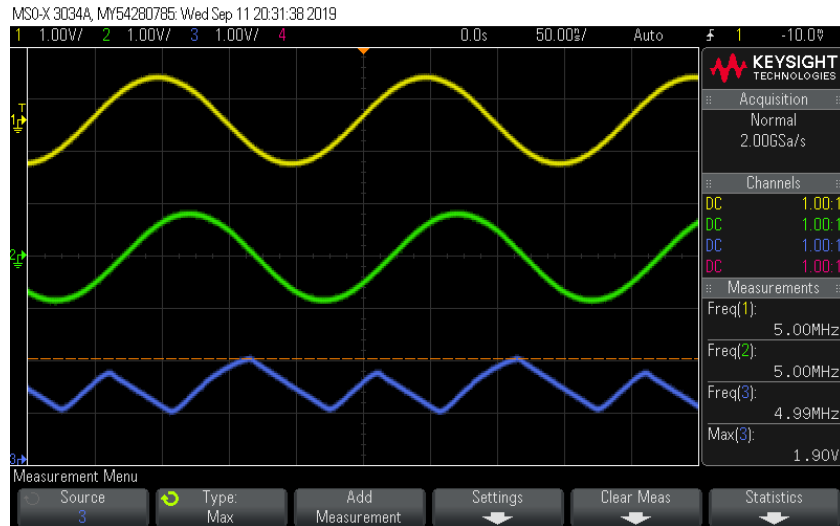


Figure 3.16: Phase detector input signals (yellow and green) and AD8302 output signal (blue)

A pure DC voltage was expected as the output of the phase detector board. However, the phase-output voltage value has some AC component of 5 MHz frequency which is the frequency of the input signal as shown in Figure 3.16. A possible cause of this is that the card has not properly filtered the output voltage before sending it out as phase values. To remove the AC component, low pass filtering was chosen. The choice of value for the low pass filter was based on the requirement for the signal voltage to be cut off. Some high-quality low pass filters previously developed in the research group were considered. A 3.4 Hz low pass filter removed the AC component; however, any low pass filter of similar frequency will give similar results. The output of the phase detector with the filter used is given in Figure 3.17

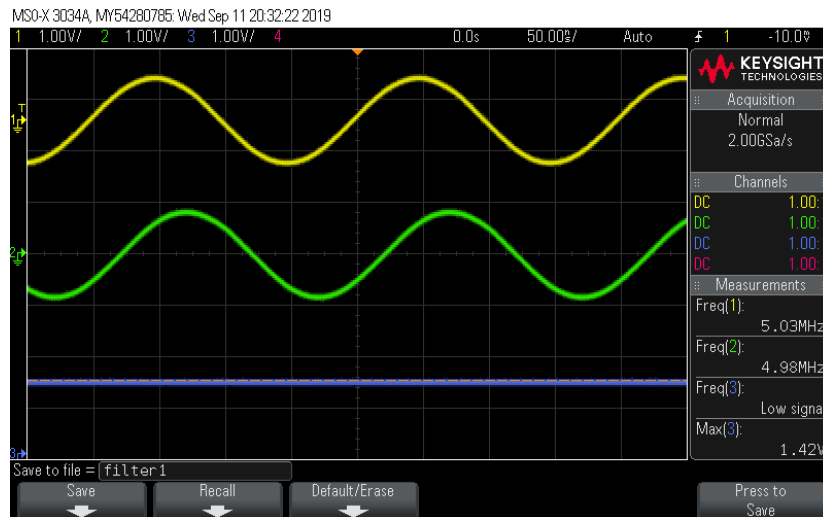


Figure 3.17: Phase detector input signals (yellow and green) and filtered output signal (blue)

From Figure 3.17, the filtered output signal (blue) has been filtered to be rid of the AC components. A test was set up to determine if the card can resolve 0.1° phase-shift. Using the waveform generator shown in Figure 3.13, two 5 MHz signals were generated. The two signals were sent to INPA and INPB ports of the phase-shift detector, the phase of the second signal was varied in steps of 0.1° and the output voltage values were recorded from the digital multimeter. The initial phase-shift was chosen to be 90° as it falls within the linear range of the phase output values as shown in Figure 3.15. The result is given in Table 3.5.

Table 3.5: 0.1° Test on AD8302 phase-shift detector

Phase-shift (°)	Trial 1 (V)	Trial 2 (V)	Trial 3 (V)	Trial 4 (V)	Trial 5 (V)
90	1.1253	1.1252	1.1253	1.1252	1.1253
90.1	1.1244	1.1244	1.1244	1.1244	1.1244
90.2	1.1236	1.1236	1.1236	1.1236	1.1236
90.3	1.1227	1.1227	1.1228	1.1227	1.1228
90.4	1.1219	1.1219	1.1220	1.1220	1.1220
90.5	1.1212	1.1212	1.1212	1.1212	1.1221

The result shows that the AD8302 board resolves the phase-shift with approximately 0.8 mV/0.1° with 60% of the readings being 0.8 mV/0.1°, 24% as 0.9 mV/0.1°, 12% as 0.7 mV/0.1°, and 4% as 1 mV/0.1°. With this result, the resolution performance exceeds the performance of the high specification oscilloscope presented in section 3.3.3. Also, because the phase-shift card's voltage output can be continuously sampled, it offers a potential solution for the present application. From the results, it can also be seen that the voltage results did not closely agree with the expected results from Figure 3.15. This could be because the given plot in the datasheet is for relatively high frequencies of 100 MHz to 2700 MHz while the test is for 5 MHz.

To determine the practical phase out versus phase difference curve that applies to the frequency of interest (5 MHz), another test was carried out to cover the range of -180° to 180° while varying the phase of one signal in steps of 40° and keeping the other phase constant. In this test, the Spectrum M2i.6022-exp arbitrary waveform generator was used (see section 3.3.1). 40° was chosen to match the steps provided in the datasheet plot. The test was repeated 5 times and the result is given in Figure 3.18 and Table 3.6. The table is provided along the plot because the individual trials cannot be identified from the plots due to close agreement of readings.

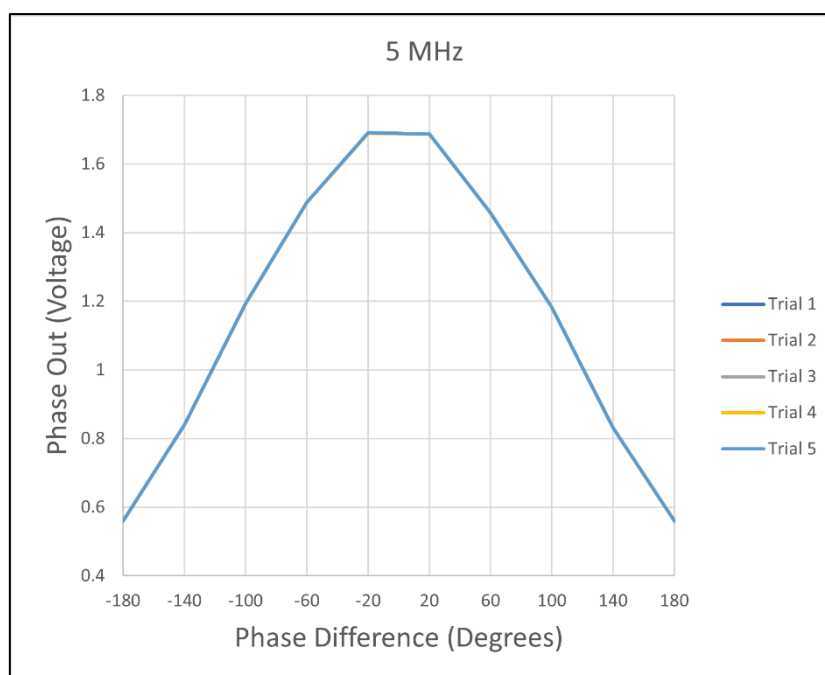


Figure 3.18: AD 8302 Phase-out vs phase difference for 5 MHz signals

Table 3.6: AD 8302 Phase-out vs phase difference for 5 MHz signals

Phase (°)	Trial 1 (V)	Trial 2 (V)	Trial 3 (V)	Trial 4 (V)	Trial 5 (V)
-180	0.5604	0.5603	0.5602	0.5602	0.5604
-140	0.8405	0.8403	0.8403	0.8404	0.8402
-100	1.1922	1.1923	1.1921	1.192	1.1921
-60	1.4886	1.4885	1.4887	1.4884	1.4886
-20	1.6906	1.6905	1.6905	1.6904	1.6906
20	1.6872	1.6871	1.6871	1.6869	1.6869
60	1.4576	1.4577	1.4575	1.4577	1.4574
100	1.1823	1.1825	1.1822	1.1823	1.1822
140	0.8313	0.8315	0.8314	0.8313	0.8314
180	0.5605	0.5604	0.5604	0.5604	0.5603

Figure 3.18 shows that the phase-out values for 5 MHz signals is approximately normally distributed. This is the ideal response provided in the AD8302 datasheet. However, the starting and ending voltage values are 0.56 V as against approximately 0.1 V given for 2200 MHz

signals in the datasheet. This difference does not affect the usefulness of the phase detector for this application because further measurements can be correlated to the relevant frequency curve to determine what phase-shift the measured voltage value represents.

3.3.5 Data Acquisition

The voltage values representing the phase difference between the sent and received signals were acquired using the NI-9239 analogue input card. The input card was chosen because of its ease of use with LabVIEW, both the input card and LabVIEW are readily available in the research group and can capture the needed data. This 24-bit card is configured in LabVIEW to sample 5000 samples at 10 kHz, this gives a sufficient number of samples to accurately represent the voltage value. The captured phase difference values are saved as .lvm files which are essentially Comma Separated Values (CSV) files with a detailed header and it is easy to extract the data to use in MATLAB or Excel.

3.4 Summary

Ultrasonic simulations to study the effect of temperature on time-of-flight were performed using MATLAB with the k-Wave toolbox. Simulations completed include pulse-echo simulations, simulations to determine the independent effects of change in ultrasonic velocity, and expansion on time-of-flight and phase-shift simulations. The results of the pulse-echo method show that with 5 GHz sampling frequency, 0.1 °C change in temperature can be measured.

The result of the simulation to determine the individual effect of material expansion and change in ultrasonic velocity on the time-of-flight shows that time-of-flight depended largely on the

change in ultrasonic velocity. Based on this result, ultrasonic thermometry can be modelled upon ultrasonic velocity while considering the uncertainty introduced by material expansion.

The phase-shift method's main disadvantage is the phase ambiguity that results when the phase difference crosses one full phase cycle. To compensate for this, the Vernier approach can be used [38]. With this approach, a lower frequency is used to identify the position in phase of the measurement, while a higher frequency is used to achieve higher resolution of measurement. With the Vernier approach, multiple frequencies can be used to increase the range and resolution of measurement. This method is referred to as the multiple frequency continuous wave method (MFCW method) and this is reviewed in section 2.9.

Comparing the pulse-echo method with the phase-shift method, although the pulse-echo method is the traditional ultrasonic measurement method in many NDT applications, for the required resolution in this study, there will be a need to sample at up to 5 GHz. The cost of a pulser-receiver able to sample at this frequency is considerably high for the intended application. To use the phase-shift method, there needs to be a dedicated way of measuring the phase-difference with a sensitivity of $0.13^\circ/0.1^\circ\text{C}$ change in temperature for 1 MHz signal in a 200 mm steel part as shown in Table 3.3. The AD8302 board is a potential device that can be used to achieve the in-process measurement of phase difference.

For phase-shift measurements, continuous rather than pulsed signal is used. To generate this signal, a PCIe based Spectrum M2i.6022-exp arbitrary waveform generator (AWG) was chosen. The AWG has a clock speed of 62.5 MS/s and it is controlled using the provided SBench 6 software. The software is used to set the signal frequency, signal type, amplitude, and the phase-shift.

The dual element transducer has two acoustically separated crystal elements in the same housing. Because one element can be used as the transmitter and the other as receiver, the dual

element was chosen for the phase-shift experiments. A 5 MHz transducer was chosen because of its resolution and availability. For phase-shift measurement, the AD8302 phase detector compares two signals and outputs their phase difference as voltage values. The phase detector's measurement scaling is $10 \text{ mV}/^\circ$. Preliminary tests show that the phase detector resolves phase-shift of a 5 MHz signal with approximately $0.8 \text{ mV}/0.1^\circ$, which is a better resolution performance than that of the high specification oscilloscope used for the initial test. This advantage and the possibility of logging the phase difference readings are the reasons for choosing the AD8302 as the potential phase-shift measurement device. NI-9239 analogue input card was chosen for data acquisition because of its suitability for the task and availability.

Based on the simulation results and the results from the tested devices, the phase-shift method of ultrasonic measurement was chosen for the laboratory experiments. This is because the phase-shift method offers higher resolution measurements without the need for expensive pulser-receivers needed for use with the pulse-echo method.

Laboratory experiments were designed to determine the suitability of the ultrasonic phase-shift technique for precision temperature measurement in laboratory conditions. These experiments as well as the findings are discussed in Chapter 4.

Chapter 4

4 Ultrasonic Thermometry Experiments (Controlled Heating)

In this chapter, to determine the achievable accuracy and resolution of the phase-shift ultrasonic method with the proposed set-up, an experiment was designed for bench testing in a laboratory. The room has moderate temperature control to ± 2 °C.

The experimental procedure adopted to understand the temperature-phase relationship of ultrasound in steel as well as the results of experiments are also presented.

4.1 Experiments

Before performing the ultrasonic phase-shift experiments, the 5 MHz transducer was bonded to the steel part for use as the ultrasonic medium (Section 4.1.2 covers the test piece features). 5 MHz, 2 V signal was generated and sent to the transducer and the echo signal was observed. This preliminary test was performed to determine the effect of attenuation on the echo signal. It was found that the echo signal has been attenuated to 40 mV from the 2 V input signal. Due to this, another test to determine the AD8302 response using different signal voltages was carried out. The details and result are presented in the next section.

4.1.1 Phase Out Response

In order to determine the obtainable practical phase out versus phase difference curve that applies to the frequency of interest (5 MHz) and other parameters applicable to the used transducer (2 V transmitted and 40 mV echo signal voltage), the waveform generator was used to generate two signals while varying the phase of one in steps of 40° as explained in section

3.3.4 and keeping the other constant. The phase output equivalent voltage values of the AD8302 were recorded using the NI-9239 card. The result is given in Figure 4.1 and Table 4.1.

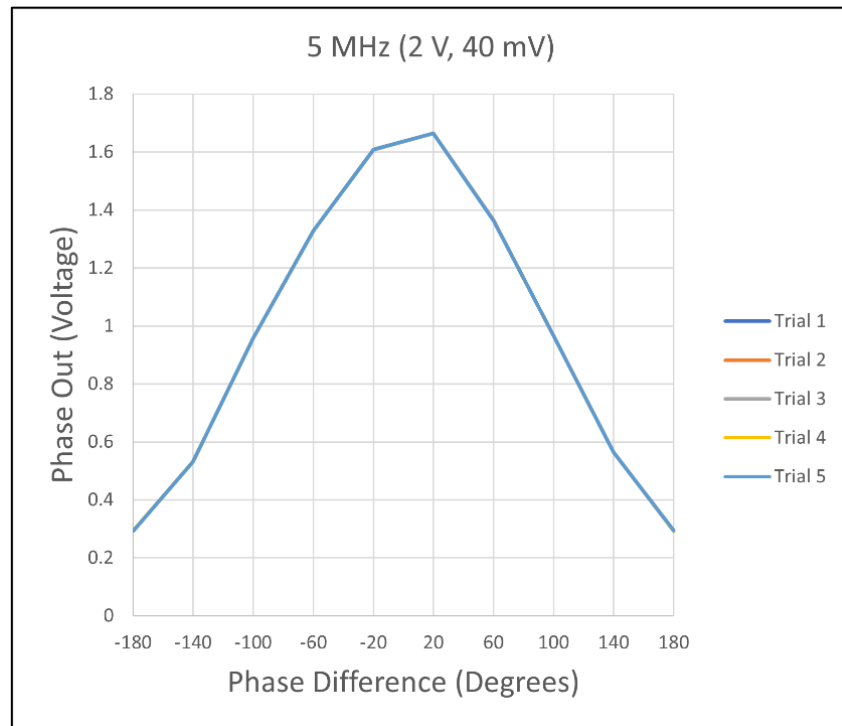


Figure 4.1: AD 8302 Phase-out vs phase difference for 5 MHz (2 V, 40 mV) signals.

Table 4.1: AD 8302 Phase-out vs phase difference for 5 MHz (2 V, 40 mV) signals.

Phase (°)	Trial 1 (V)	Trial 2 (V)	Trial 3 (V)	Trial 4 (V)	Trial 5 (V)
-180	0.2934	0.2933	0.2932	0.2935	0.2934
-140	0.5318	0.5321	0.5318	0.5319	0.5318
-100	0.9578	0.9581	0.9577	0.9575	0.9574
-60	1.3278	1.3278	1.3276	1.3278	1.3276
-20	1.6083	1.6082	1.6079	1.6082	1.6081
20	1.6644	1.6647	1.6647	1.6647	1.6648
60	1.364	1.3639	1.3638	1.3637	1.3638
100	0.9644	0.9642	0.9641	0.9643	0.9642
140	0.564	0.5641	0.5637	0.5638	0.5641
180	0.2935	0.2935	0.2933	0.2933	0.2936

The result shows that the starting phase out voltage changed from 0.5604 V for 2 V, 2V 5 MHz signals to 0.2934 V for 2 V, 40 mV 5 MHz signals. The shape of the curve however remained approximately normally distributed (Figure 4.1). This change should not affect the usefulness of the phase-detector for this task since the results can be related to the obtainable response when required.

4.1.2 Experimental Setup Using Ceramic Heater

Based on the developed methodology, an ultrasonic thermometry phase-shift experiment was set up as shown in Figure 4.2. A sinusoidal waveform was generated with the Spectrum arbitrary waveform generator and this signal was sent to both the receiving probe of the 5 MHz ultrasonic transducer and the input A of the phase detector board. The initial experiment was set up for a 15 mm EN24T steel workpiece. 15 mm was used for the initial experiment to enhance homogeneity, also the attenuation is higher in larger workpieces (Section 4.2 covers experiments on a workpiece equivalent to 200 mm ultrasonic path using liquid bath calibrator for homogeneity and section 4.3 covers amplification of attenuated signals). EN24T steel was chosen as it is commonly used in precision manufacturing in the research group and it is also readily available. The transducer was coupled to the workpiece using epoxy as couplant. The echo probe of the transducer was connected to the input B of the phase detector. The phase-out port of the phase detector board was connected to a 3.4 Hz low pass filter and the voltage output of the filter was connected to the analogue input card connected to the PC to be captured by LabVIEW. A Thorlabs HT24S2 ceramic heater controlled with an Inkbird ITC-106VH thermostatic temperature controller was used to change the temperature of the workpiece. This controller and heater combination were chosen because of the inbuilt PID control and because the temperature set point can be increased in steps of 0.1 °C. The heater has rated power of 24

W at 24 V input voltage. A calibrated Maxim DS18B20 digital temperature sensor was connected to the PC via a DS9490 to USB adapter, from which reading were captured using proprietary software and these values served as the reference temperature values. A PT100 temperature sensor was used as feedback temperature sensor for the temperature controller.

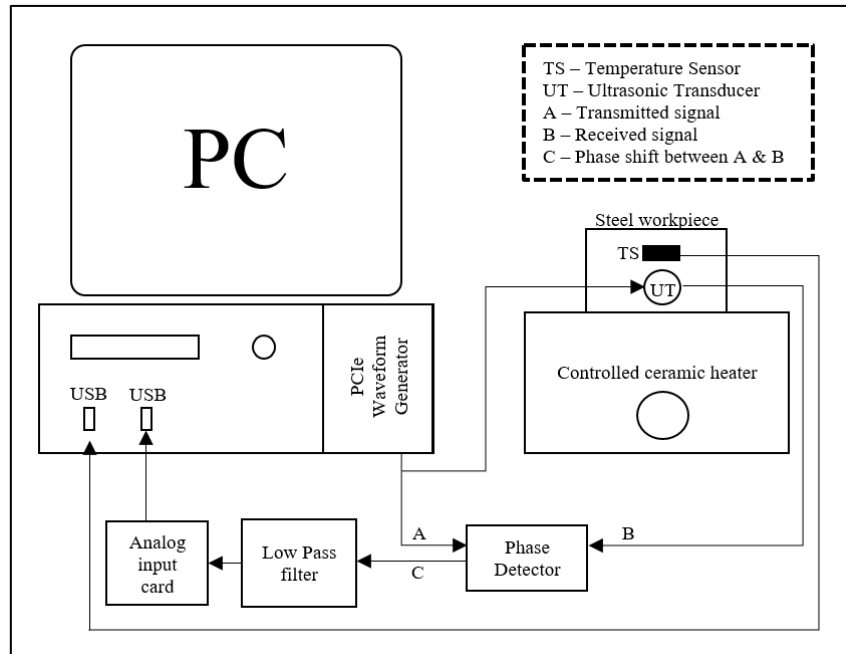


Figure 4.2: Ultrasonic phase-shift thermometry experimental set-up

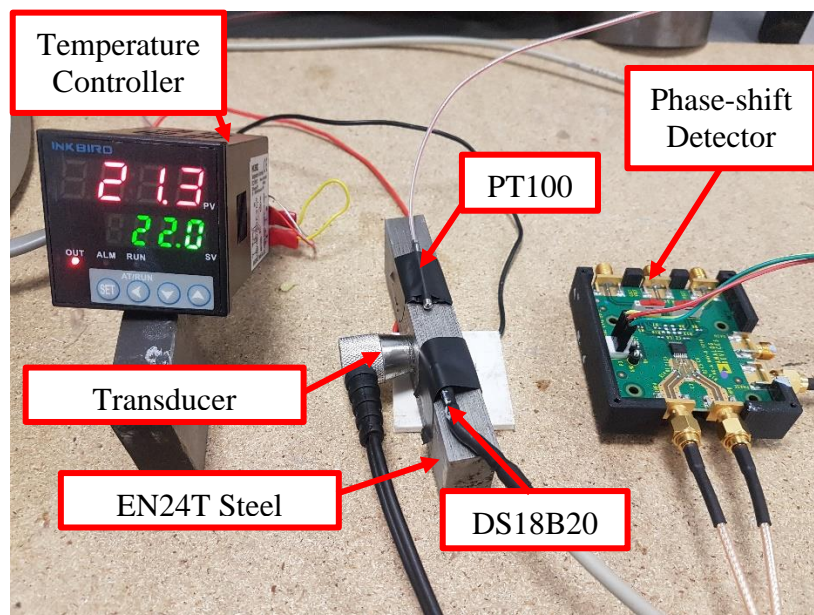


Figure 4.3: Ultrasonic experimental set-up devices

Figure 4.3 shows the temperature controller, steel part, transducer, temperature sensors, and phase-shift detector used for the ultrasonic experiments. The phase-shift experiment was designed to determine the achievable range and resolution of the method. In the first experiment, phase-shift measurement was made for a temperature range of 20 °C to 30 °C – this is a typical temperature variation range during machining in the research group. As such, this experiment was carried out with temperature varied in steps of 1 °C. 1 °C rather than 0.1 °C step was chosen for the first experiment because the range rather than the resolution is of interest and 1 °C steps give insight into the readings within this range. Thereafter, another experiment was carried out for the range of 21.5 °C to 23.5 °C in steps of 0.1 °C, this was done to observe the ability of the setup to measure temperature with resolution of up to 0.1 °C (Section 3.1 covers the justification for 0.1 °C resolution target). In both tests, the steel block was held at the set point for 20 minutes before taking the phase-shift reading, this was done to aid homogeneity in the workpiece.

4.1.3 Results for Ultrasonic Thermometry (Ceramic Heater)

The phase-shift vs temperature values obtained for both experiments using the described setup are shown in the Figure 4.4 to Figure 4.7. Figure 4.4 and Figure 4.6 show the phase-shift readings for each temperature point. For Figure 4.4, a second order polynomial fit was done in excel, this gives a reference phase-out value for each temperature point which was used for the calculation of the residuals. A linear fit was used in Figure 4.6. Figure 4.5 and Figure 4.7 show the residuals which is the deviation of each measurement reading from the predicted value (represented with a polynomial fit). The residual values were converted to their temperature equivalent values from the phase-out readings. The choice of temperature for residual presentation is based on the clarity it gives as it relates to the original measurement intent.

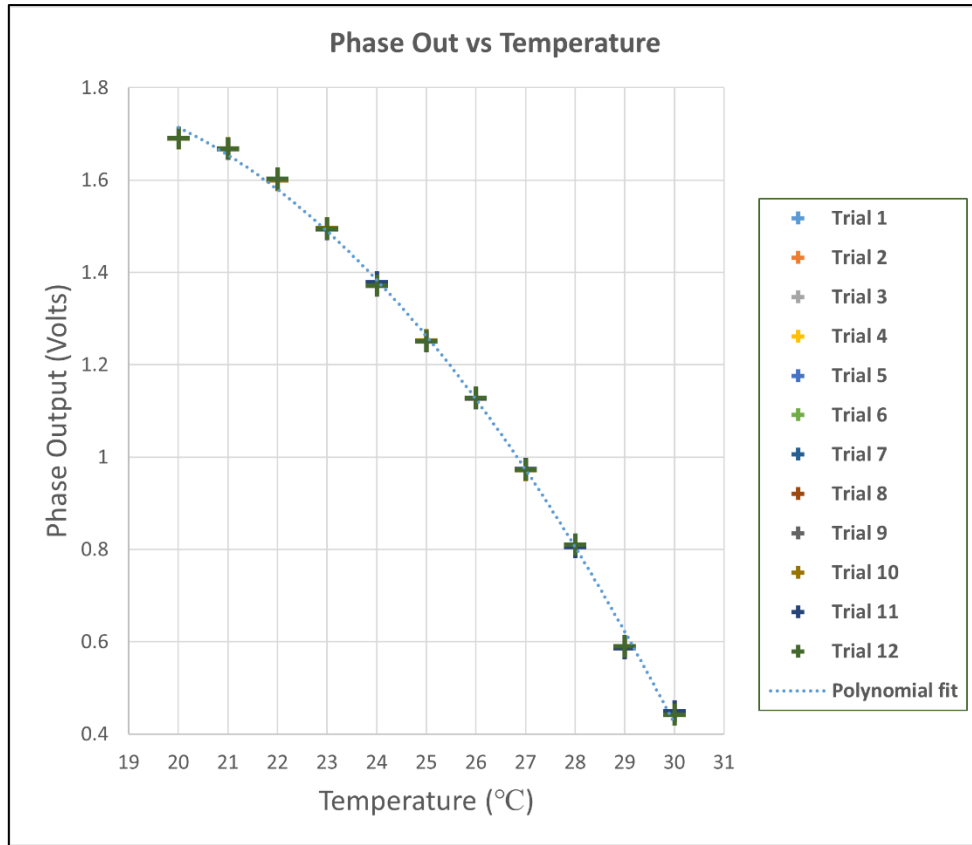


Figure 4.4: Results of 20 to 30 °C temperature range in steps of 1°C

The result shows that there is a measurable response of the phase-shift to temperature change; a 1 °C-temperature change caused an approximate phase-shift of 12.4°. The result also shows that the phase-shift curve is not linear, the shape of the curve is the right-hand part of a normally distributed curve which is the shape of the response of the phase-shift detector. To enhance linearity, a lower frequency needs to be used if a large range is to be covered (Section 5.4 covers the use of a lower frequency transducer for an increased range of measurement). The residuals of this result is given in Figure 4.5.

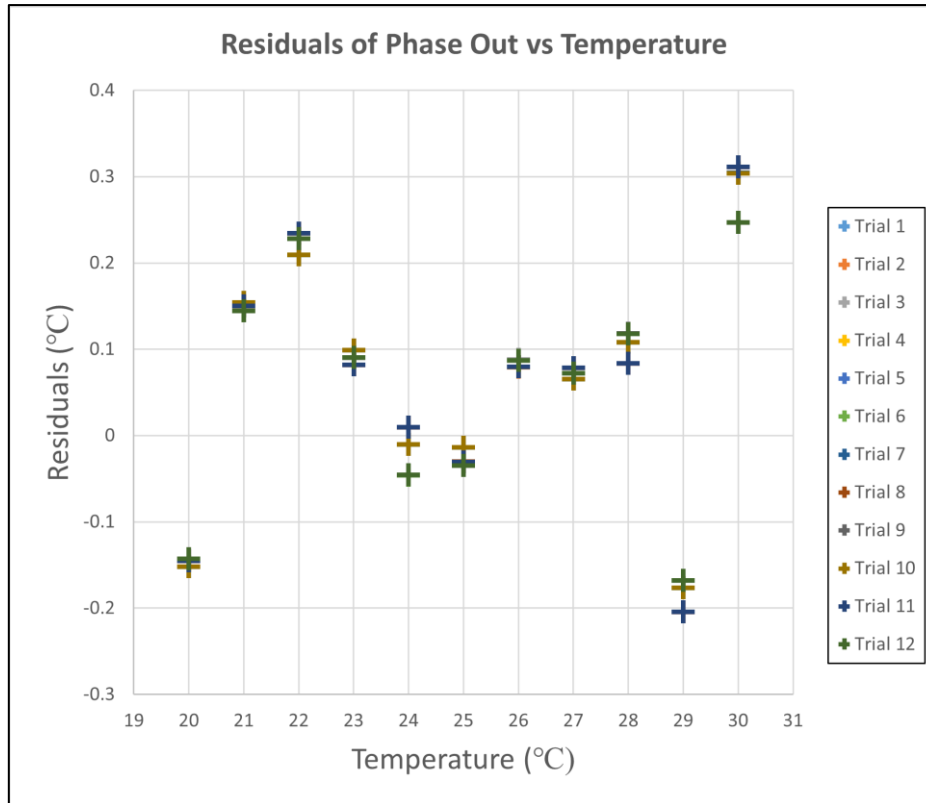


Figure 4.5: Residual plot of 20 to 30 °C

The residuals of the 20 – 30 °C phase-shift experiment show that the errors are within the range of -0.0254 V to 0.0387 V, the temperature equivalents of these are -0.2045 °C to +0.3114 °C and the standard deviation is 0.1372 °C.

The next figure shows the result of the 0.1 °C step experiment. The experiment was started from 21.5 °C to avoid the extreme part of the phase-out curve.

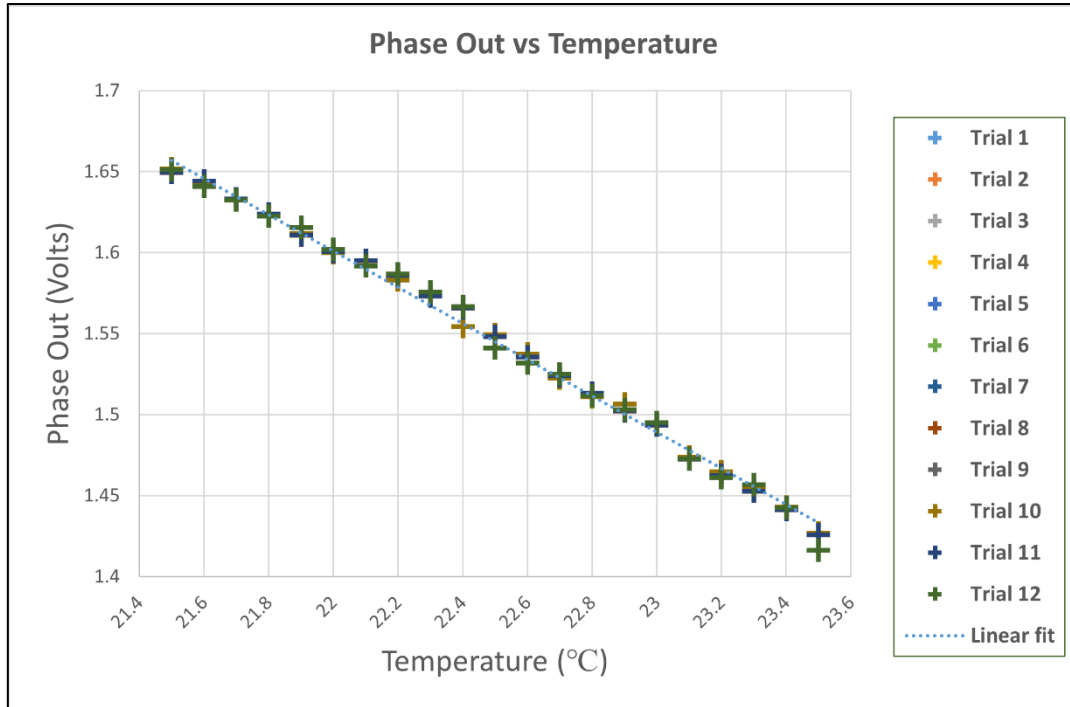


Figure 4.6: Results of 21.5 to 23.5 °C temperature range in steps of 0.1°C

Figure 4.6 shows that 0.1 °C temperature change can be measured with the setup. From the result, a 0.1 °C change caused a phase-shift approximately equal to 1.1°. The residuals of this result is presented in Figure 4.7. The error values are within the range of -0.0142 V to 0.0109 V which is equivalent to -0.1267 °C to 0.0968 °C and the standard deviation of the residuals is 0.0426 °C for the twelve trials.

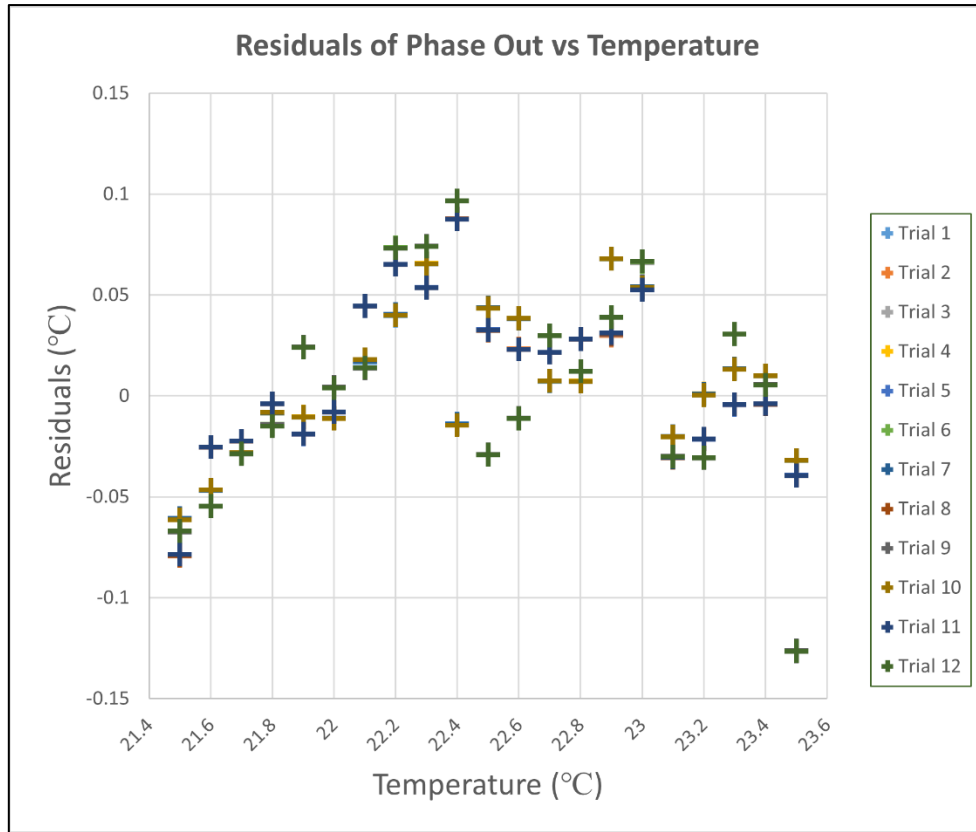


Figure 4.7: Residual plot of 21.5 to 23.5 °C

The result shows that 0.1 °C resolution can be achieved with the current setup. Another experiment was carried out by modifying the setup to use a liquid bath calibrator rather than a ceramic heater. The purpose of the modification is to get the larger workpiece closer to homogeneity of temperature by total immersion in heat source rather than spot heating that the ceramic heater provides. The new setup is described in section 4.2.

4.2 Experiment Using Liquid Bath Calibrator

The TCS 140 liquid bath calibrator (E Instruments, Langhorne, PA, USA) is a low temperature furnace (-55 °C to 140 °C) with a stability of ± 0.025 °C [104]. This will potentially provide a high accuracy temperature-controlled heating for the ultrasonic experiments. The TCS liquid bath calibrator is shown in Figure 4.8.

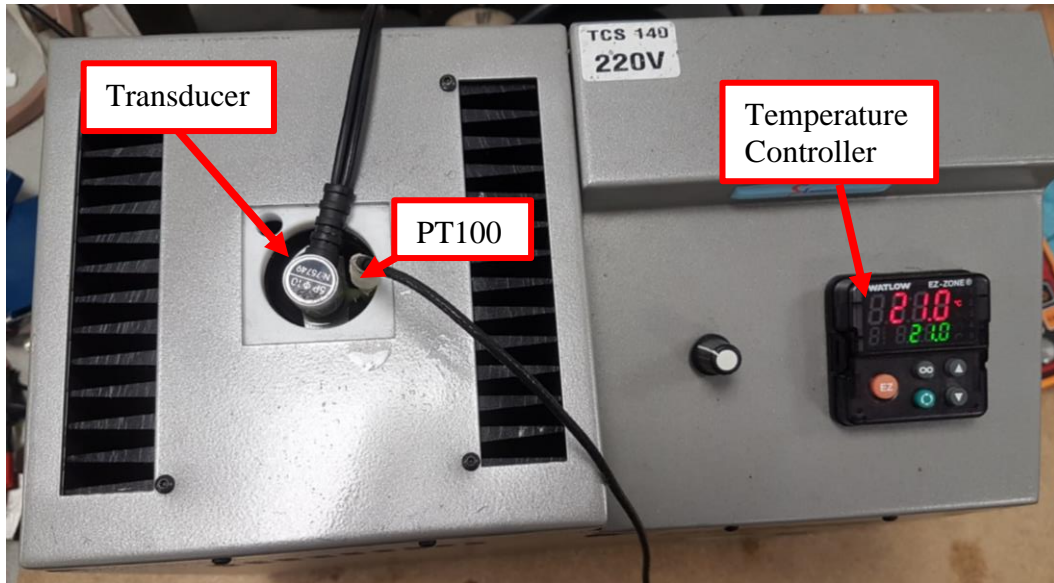


Figure 4.8: TCS 140 Liquid bath calibrator

By using the SBench software together with a Spectrum M2i.6022-exp arbitrary waveform generator (Spectrum Instrumentation, Ahrensfielder, Grosshansdorf, Germany), a 5 MHz sinusoidal waveform was generated. The generated input signal was then sent to the 5 MHz ultrasonic transducer. The transducer was coupled to a 100 mm steel. A 100 mm workpiece was used for this experiment because with a dual element ultrasonic transducer setup, a 100 mm path length is equivalent to a 200 mm path length when using two contact transducers at opposite ends as demonstrated in the simulations. To determine the level of attenuation due to the increased ultrasonic path (200 mm), the amplitude of the echo signal was measured and it was observed that the signal amplitude dropped to 5 mV. To determine if the phase-detector will work with this signal level, a phase response test was carried out using two signals of 2 V and 5 mV respectively. The result is shown in Figure 4.9 and Table 4.2.

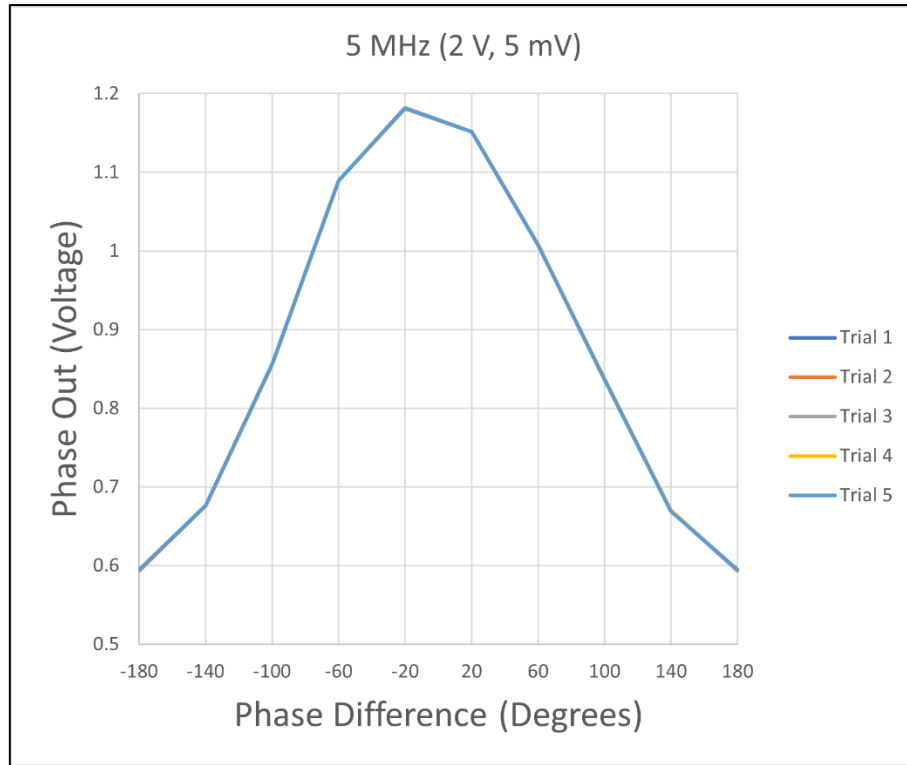


Figure 4.9: AD 8302 Phase-out vs phase difference for 5 MHz (2 V, 5 mV) signals.

Table 4.2: AD 8302 Phase-out vs phase difference for 5 MHz (2 V, 5 mV) signals.

Phase (°)	Trial 1 (V)	Trial 2 (V)	Trial 3 (V)	Trial 4 (V)	Trial 5 (V)
-180	0.5933	0.5932	0.5947	0.5947	0.5946
-140	0.6769	0.6762	0.6766	0.6766	0.6767
-100	0.8564	0.8559	0.8559	0.856	0.8564
-60	1.0889	1.0889	1.0889	1.0891	1.0892
-20	1.1818	1.1819	1.1816	1.1806	1.1815
20	1.1513	1.1516	1.1512	1.1512	1.1514
60	1.0076	1.0077	1.0073	1.0079	1.0073
100	0.8362	0.837	0.8367	0.8364	0.8367
140	0.6698	0.6703	0.6696	0.6704	0.6693
180	0.5946	0.5934	0.5934	0.5941	0.5942

The result shows that the starting phase out voltage (-180°) changed from 0.2934 V for the 2 V, 40 mV 5 MHz signals to 0.5933 for 2 V, 5 mV 5 MHz signals. The phase out voltage at 20°

also changed to 1.1513 V from 1.6644 V. The suitability of the phase detector card for ultrasonic temperature measurement at this highly attenuated echo signal level will be determined through the liquid bath calibrator experiment. The shape of the curve however remained approximately normally distributed (Figure 4.9).

Instead of the DS18B20, the temperature sensor was changed to a PT100 detector as this can be inserted into the liquid bath calibrator. The PT100 detector can also be used in the harsh manufacturing environment. The PT100 measurements were acquired using a NI-9219 universal analog card. This card was chosen because of the possibility of selecting a configuration for PT100 when using it for data acquisition. The experiment with liquid bath calibrator was set up as shown in Figure 4.10.

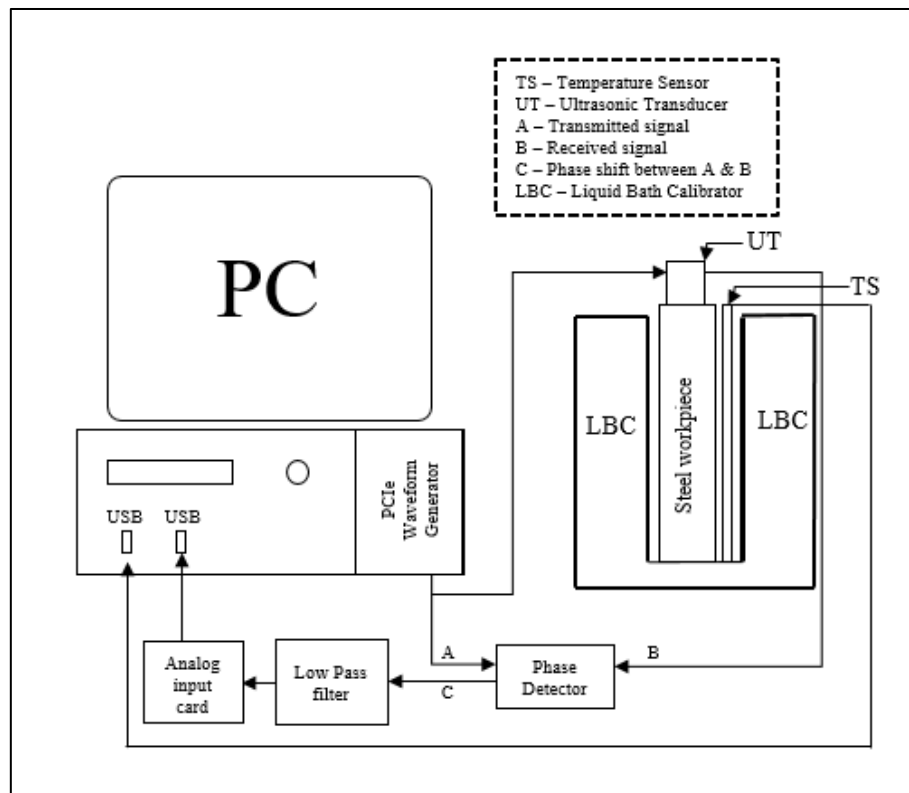


Figure 4.10: Ultrasonic phase-shift thermometry experimental set-up using liquid bath calibrator.

The workpiece was fully immersed into the liquid bath calibrator, this was done to aid temperature homogeneity in the workpiece. The echo signal was sent through the receiver probe of the transducer to the ‘port B’ of the phase detector and the computed voltage values representing the phase difference were recorded as in the previous experiment (section 4.1.2). With the TCS140 liquid bath calibrator, the temperature of the workpiece was varied in steps of 1 °C and 0.1 °C respectively and the workpiece was left for 30 minutes to attain homogeneity for the two sets of experiment as previously presented in section 4.1.2. The results of these experiments are presented in the next section.

4.2.1 Results of Ultrasonic Thermometry (Liquid Bath Calibrator)

The result of the first experiment for a temperature range of 20 °C to 30 °C in steps of 1 °C is given in Figure 4.11 and Figure 4.12. In Figure 4.11, a fourth order polynomial was used to construct the reference fit.

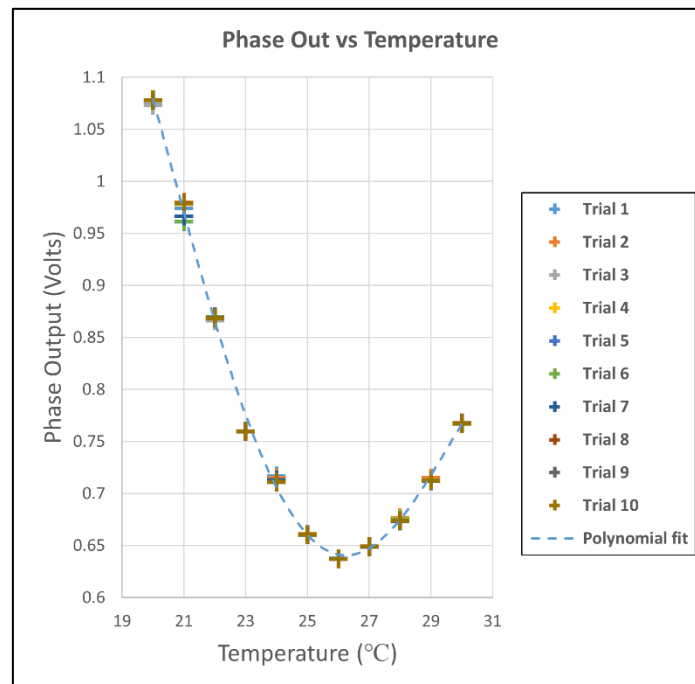


Figure 4.11: Results of 20 to 30 °C range in steps of 1 °C for 100 mm steel.

Figure 4.11 shows that the measured phase-shift values reached the non-linear part of the phase response. During a non-controlled measurement process, this non-linearity can create ambiguity. To prevent this ambiguity, a lower frequency transducer should be used. (Section 5.4 covers the use of a lower frequency transducer to obtain linear results for a 10 °C range).

The residuals of the 20 to 30 °C measurement is given in Figure 4.12.

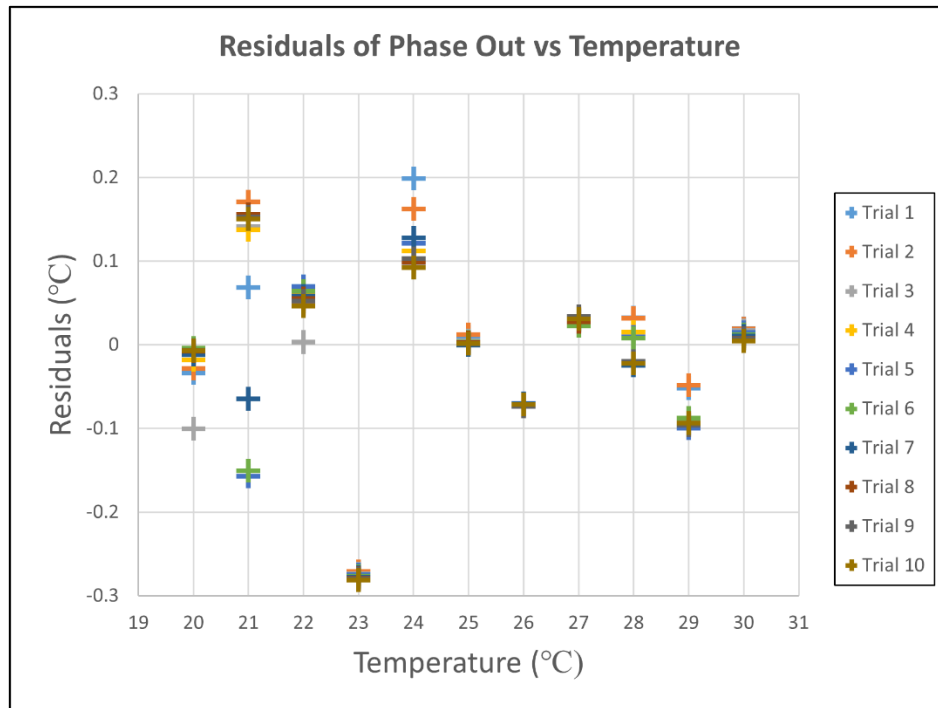


Figure 4.12: Residual plot of 20 to 30 °C for 100 mm steel

The residuals result shows that the error values are within the range of -0.2814 °C to 0.199 °C with standard deviation of 0.1076 °C.

The second experiment focused on achieving a resolution of 0.1 °C. This experiment was carried out over the range of 20 °C to 21 °C in steps of 0.1 °C. The choice of 20 °C to 21 °C is based on the linearity in this range from the previous result. The recorded phase out and residual values are given in Figure 4.13 and Figure 4.14. In Figure 4.13, a linear fit was constructed for reference phase output values.

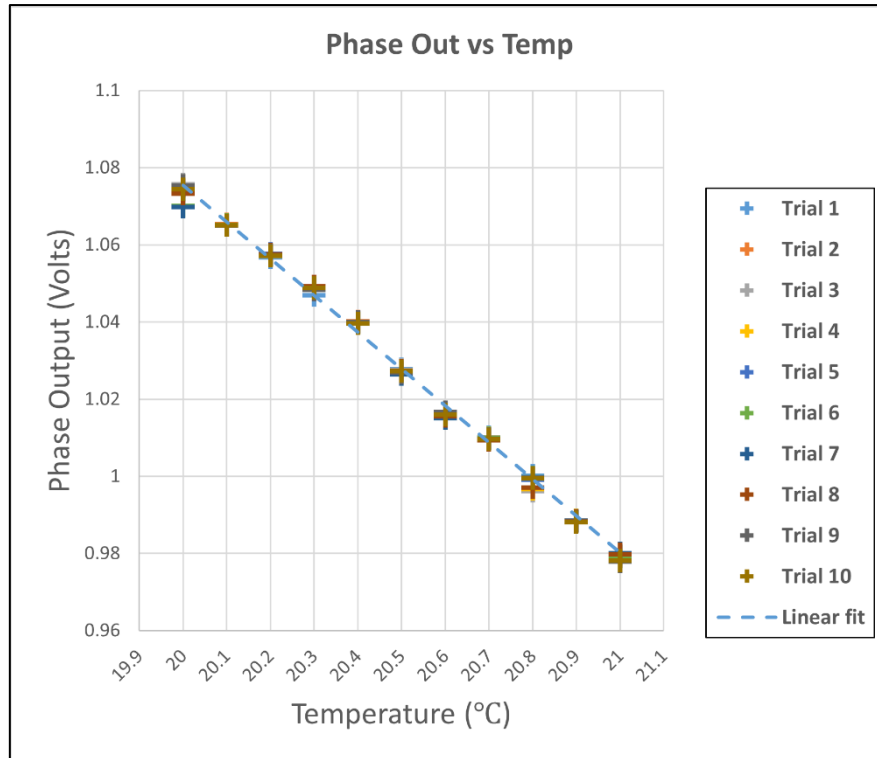


Figure 4.13: Results of 20 to 21 °C range in steps of 0.1 °C for 100 mm steel.

The result shows that 0.1 °C temperature change caused the phase to shift by approximately 0.9°. Figure 4.13 also shows that the plot of the results follows a linear path for a range of 1 °C for a 100 mm steel part using 5 MHz signal.

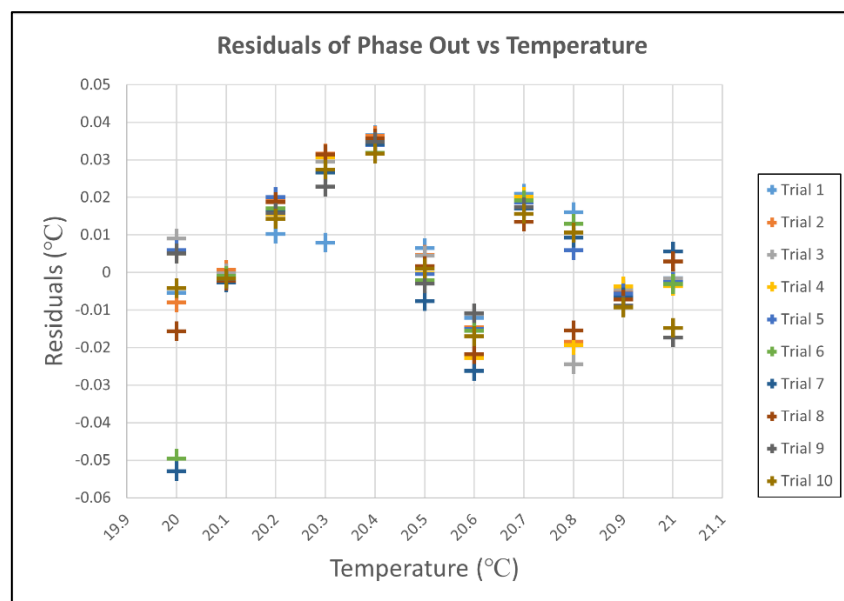


Figure 4.14: Residual plot of 20 to 21 °C for 100 mm steel.

The residuals of the results (Figure 4.14) show that the error values are within the range of -0.053 °C to +0.0365 °C with standard deviation of 0.0178 °C.

The results of the ceramic heating and the liquid bath calibrator experiments show that the core temperature measurement of steel workpiece can be performed using the created ultrasonic phase-shift method. In both 15 mm and 100 mm steel experiments, the 10 °C range measurement had results in the non-linear region of the phase response. This can be avoided by using a lower frequency transducer such as the 1 MHz transducer (see section 5.4)

The next section covers the design and development of an amplifier for the echo signal.

4.3 Echo Signal Amplification

With the 100 mm workpiece used in the liquid bath calibrator experiments, the echo signal was attenuated to 5 mV. Although the phase detector worked with 5 mV echo signal, it is possible that the noise from a manufacturing environment will have an impact on the accuracy of phase difference measurement at 5 mV echo signal. Due to this, echo signal amplification was considered.

The amplifiers considered include Texas Instruments THS3202 and the Analog Devices AD8056, they were considered because of their ability to handle the 5 MHz transducer frequency. The THS3202 is a low distortion, dual current feedback amplifier while the AD8056 is a dual voltage feedback amplifier. Both amplifiers have the potential to work for the created method. However, current feedback amplifiers are more efficient in handling high gain applications [105], therefore the THS3202 was chosen. The pin assignment of the THS3202 amplifier is given in Figure 4.15.

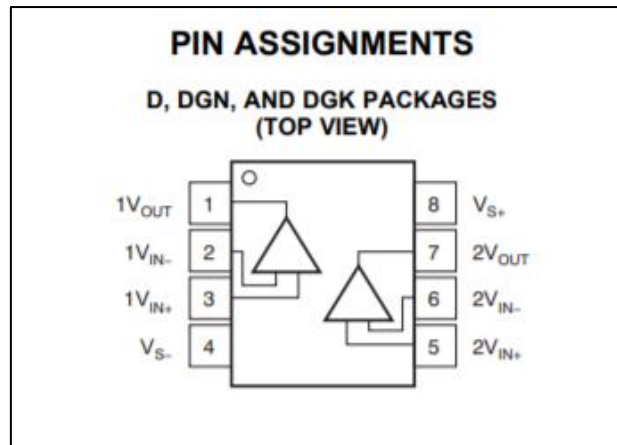


Figure 4.15: THS3202 pin assignments [106].

The initial amplifier design was made using National Instruments Multisim and it was chosen because of its availability for student use. The design is shown in Figure 4.16.

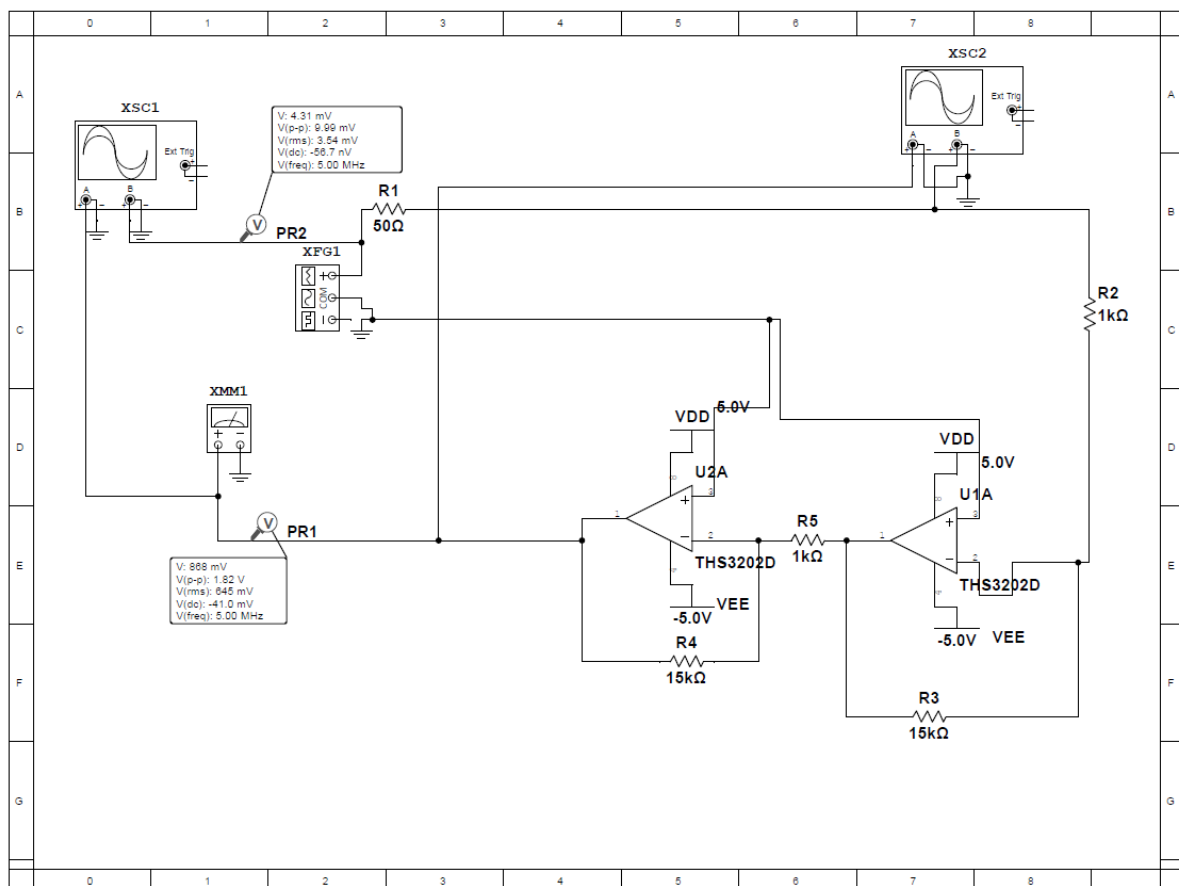


Figure 4.16: Echo signal amplifier design

Figure 4.16 shows the circuit design for a 2-stage echo signal amplifier. Using a waveform generator (XFG1), a 5 MHz, 5 mV signal was generated (This is shown on probe PR2), a 50 Ω resistor (R1) was used for impedance matching. Resistors of 15 k Ω and 1 k Ω were chosen in order to achieve a gain of 15 in a non-inverting amplifier configuration. The THS3202D amplifiers were supplied with 5 V dual voltage. The output signal (1.82 V peak to peak) can be seen on PR1. XSC1 and XSC2 are oscilloscopes used during simulation and XMM1 is a multimeter.

The simulation shows that a signal of 5 mV can be amplified to 2 V using the THS3202 high-speed amplifier.

Analog Devices DUAL-SO-8 evaluation board provides a suitable board for soldering the required components for SOIC dual amplifiers such as the THS3202. With clear layout for amplifier footprints, resistors, capacitors, power, and signals, the board can be populated in a way that preserves the signal quality. Due to these, the DUAL-SO-8 was chosen for use with the THS3202 amplifier. The evaluation board and its schematic diagram are shown in Figure 4.17 and Figure 4.18 respectively.

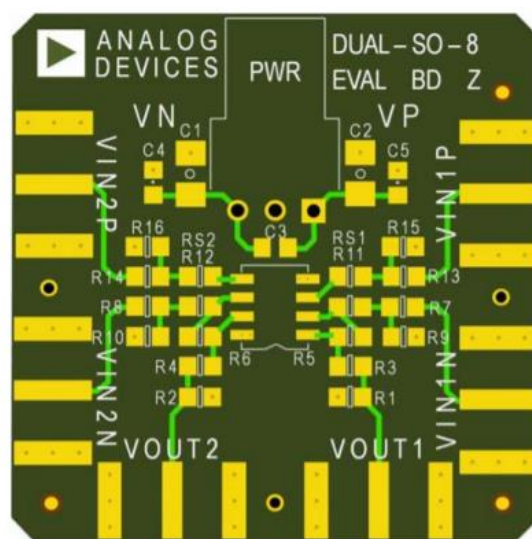


Figure 4.17: Analog Devices DUAL-SO-8 evaluation board [107].

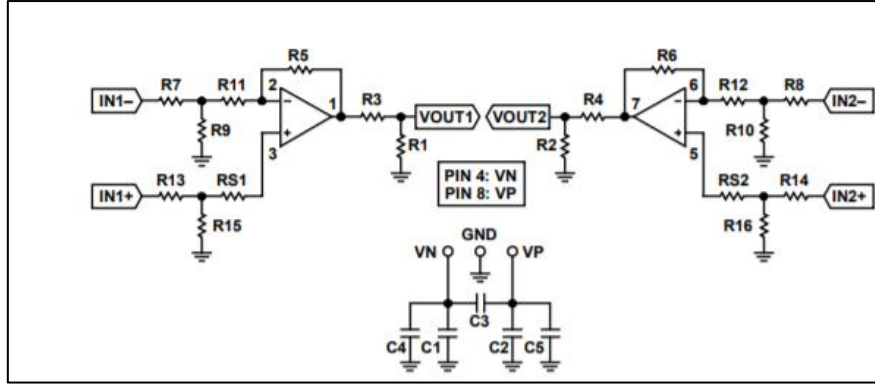


Figure 4.18: Schematic of evaluation board [107].

For a non-inverting configuration of the amplifier, the output voltage for channel 1 is given as:

$$\frac{V_{out}}{V_{in}} = \left(1 + \frac{R5}{R11}\right) \left(\frac{50\Omega}{50\Omega + R3}\right) \quad (4.1)$$

Where V_{out} is the output voltage and V_{in} is the input voltage.

Based on the information from the THS3202 datasheet, gain of 5 for each stage was chosen rather than 15. This is because a lower resistor feedback value (R5 & R6) offers more stability.

The evaluation board was populated using the following component values:

Table 4.3: Component values for signal amplifier

Reference Designator	Value	Package
C1, C2	10 μ F	C1206
C4, C5	100 nF	C0603
RS1, RS2, R9, R10, R13, R14	0 Ω	R0603
R11, R12	100 Ω	R0603
R5, R6	909 Ω	R0603
R3, R4, R15, R16	50 Ω	R0603
R1, R2, R7, R8, C3	Unused	Unused

The populated amplifier is shown in Figure 4.19.

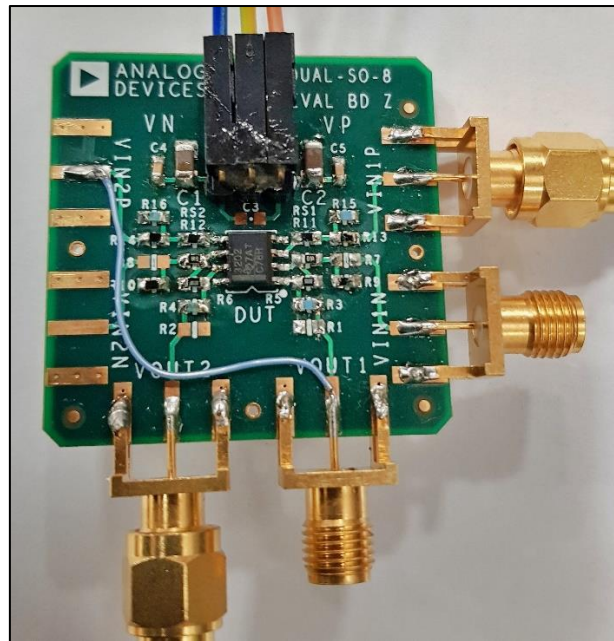


Figure 4.19: Populated signal amplifier

Using the amplifier, a typical echo signal was amplified, the input and amplified signals are shown in Figure 4.20 and Figure 4.21 respectively.

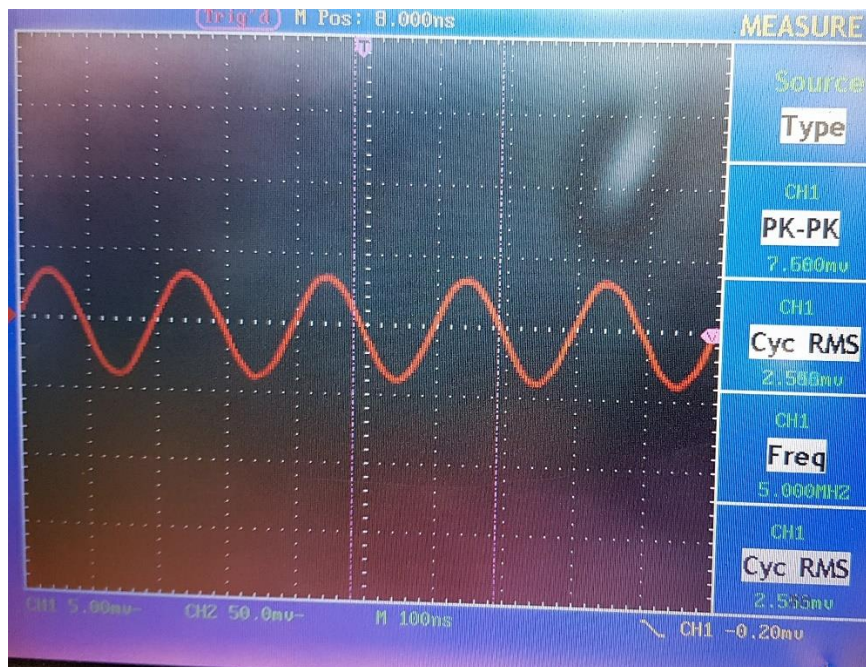


Figure 4.20: Input signal to amplifier

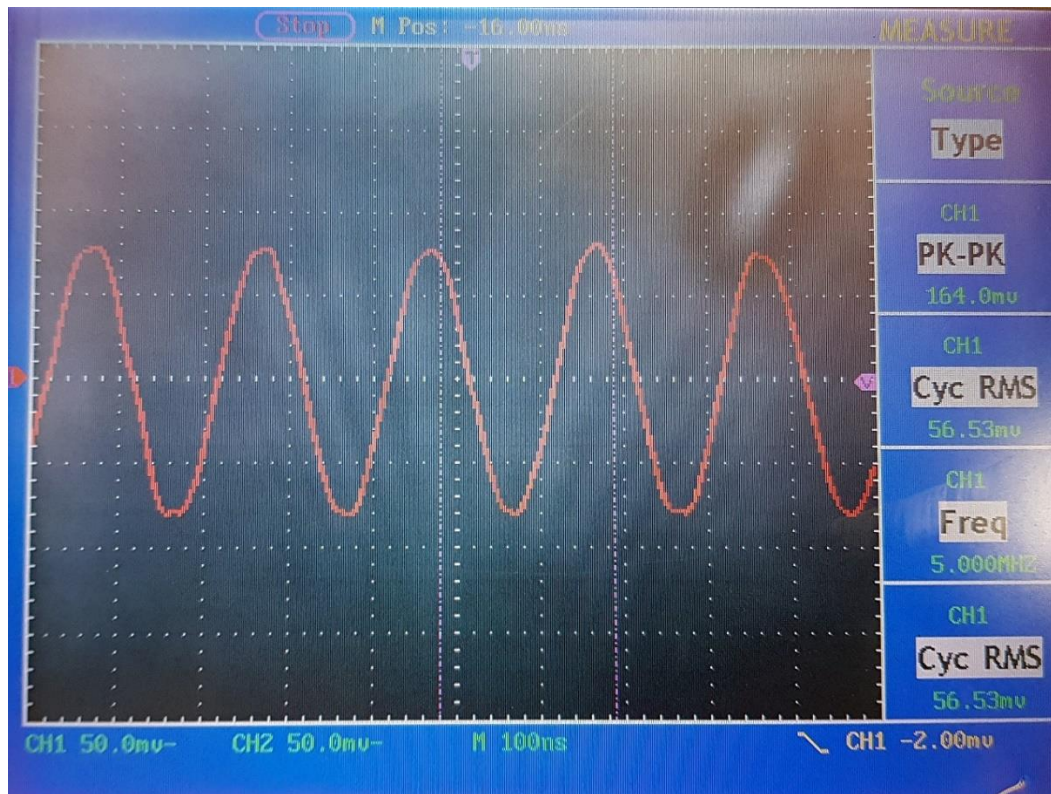


Figure 4.21: Signal output from amplifier

4.3.1 Bench Test with Signal Amplifier

Using the created ultrasonic thermometry setup and the designed and developed amplifier, a test was carried out in the CNC workshop to record a steel workpiece temperature. The recorded temperature readings captured the change in temperature due to the drop in ambient temperature from 22.07 °C to 21.69 °C over a period of approximately 30 minutes, this test was performed to observe the stability of the setup in the CNC workshop. The recorded PT100 readings and phase difference values are given in Figure 4.22 and Figure 4.23:

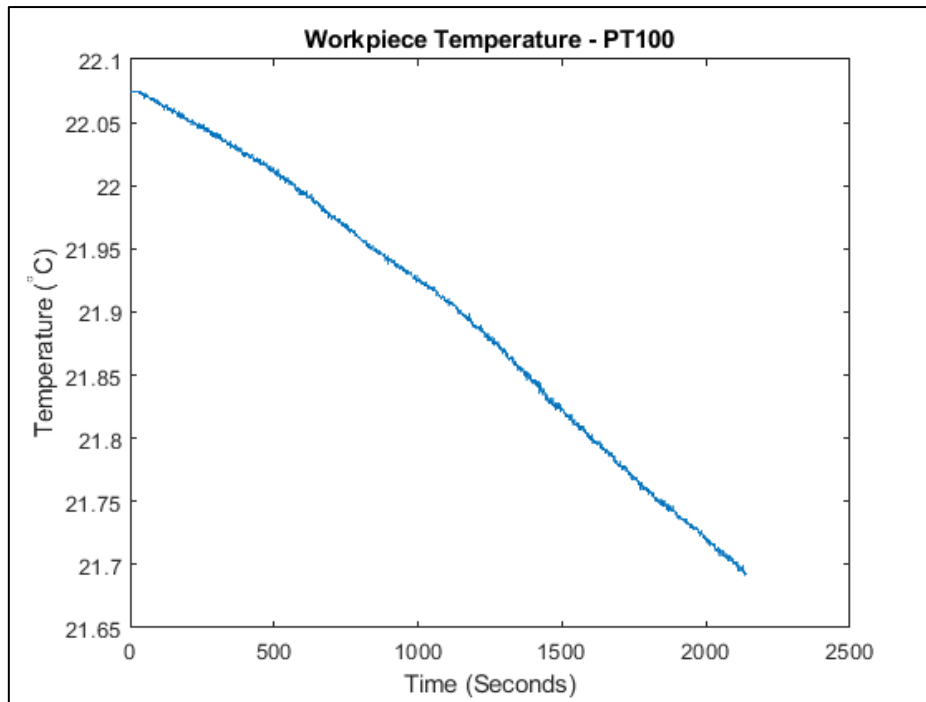


Figure 4.22: PT100 Workpiece temperature readings

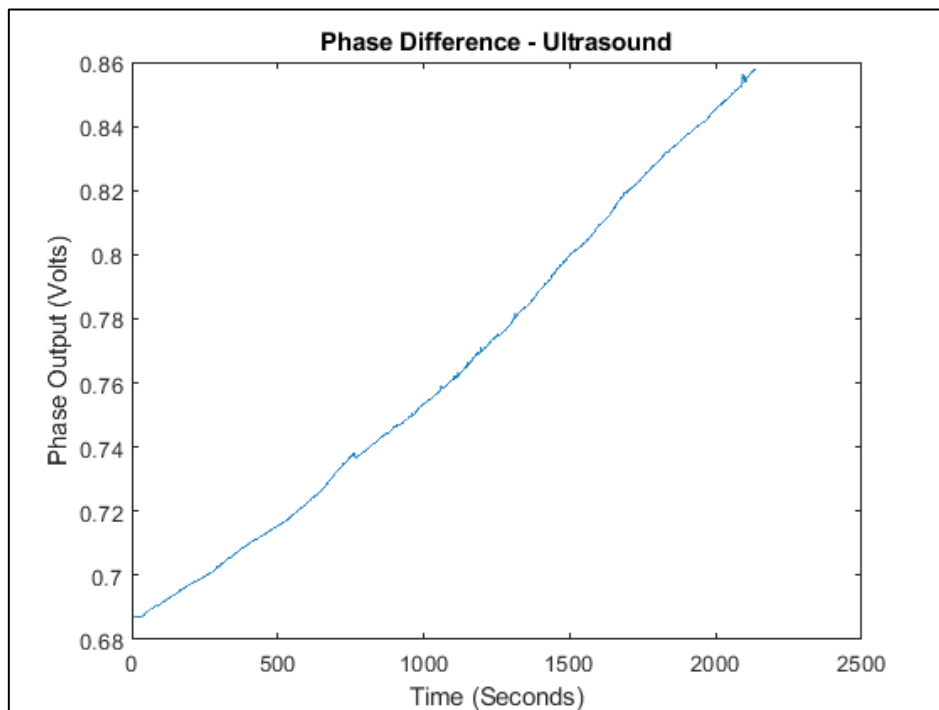


Figure 4.23: Ultrasonic phase difference readings

Using the linear interpolation function, the phase output voltage values were converted to temperature values. The linear interpolation function provides approximated values which can be directly compared with the PT100 values for error estimation and further analysis. The linear interpolation function will also be used for subsequent results. The ultrasonic temperature results are given in Figure 4.24.

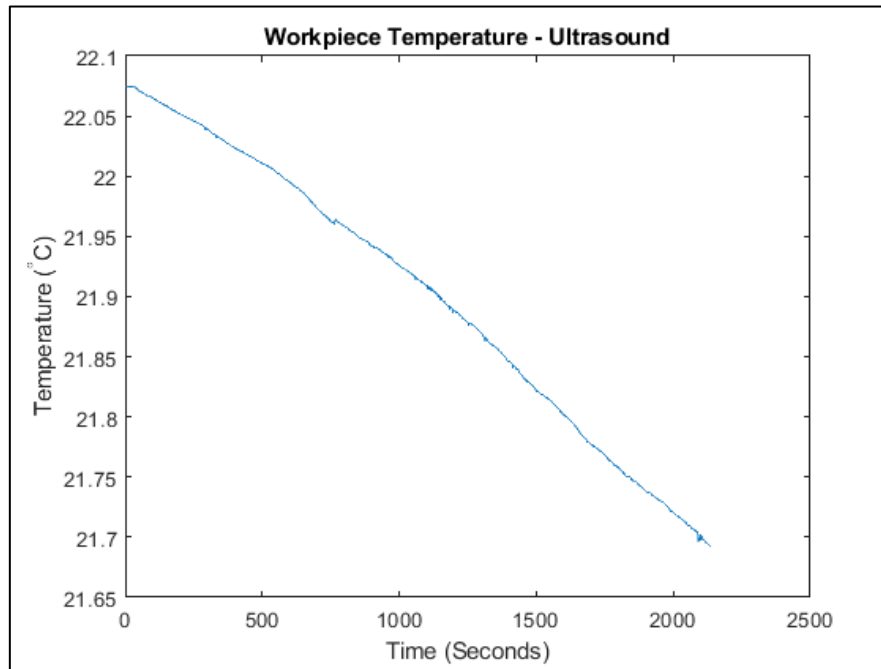


Figure 4.24: Ultrasonic workpiece temperature readings

Using the approximated values and the PT100 values, deviations of the ultrasonic readings from PT100 values were calculated. The error plot is given in Figure 4.25.

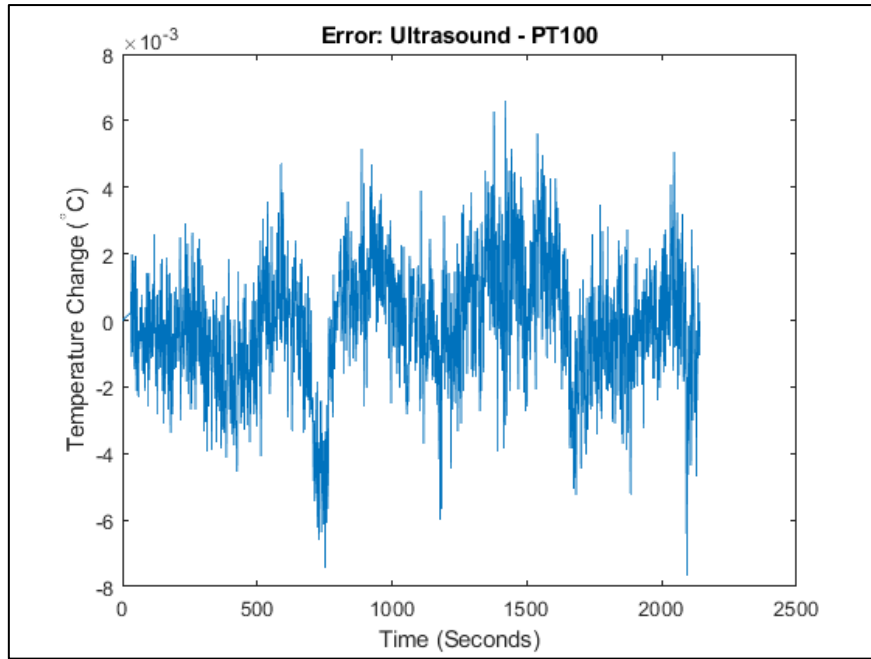


Figure 4.25: Deviation of ultrasonic readings from PT100 readings

The result showed that ultrasonic phase-shift values can be reliably obtained with the designed high-speed amplifier. The error values are within ± 0.008 °C and a further analysis of the residuals of PT100 and ultrasound readings is detailed in section 5.1. The amplified echo signal will potentially enhance signal to noise ratio during the in-process temperature measurement trials. In the next chapter, the procedures adopted for in-process ultrasonic thermometry will be detailed.

4.4 Summary

Using the created method and the described devices and equipment from the methodology section, an experiment was set up using controlled ceramic heating for ultrasonic thermometry. This test was done on a 15 mm steel part, preliminary tests show that the 40 mV attenuated echo signal is measurable using the AD8302 phase-detector board. The results of the ceramic heating experiment show that a 1 °C temperature change caused a phase-shift of 12.4° with

errors within a range of $-0.2045\text{ }^{\circ}\text{C}$ to $0.3114\text{ }^{\circ}\text{C}$. The standard deviation of the error values is $0.1372\text{ }^{\circ}\text{C}$. The $0.1\text{ }^{\circ}\text{C}$ change caused a phase-shift of 1.1° with errors within the range of $-0.1267\text{ }^{\circ}\text{C}$ to $0.0968\text{ }^{\circ}\text{C}$ and standard deviation of $0.0426\text{ }^{\circ}\text{C}$.

$0.1\text{ }^{\circ}\text{C}$ temperature resolution was achieved using the created setup. While attempting to achieve a range of $10\text{ }^{\circ}\text{C}$, it was observed that the phase-shift readings reached the non-linear part of the phase-response curve. To avoid this, a lower frequency transducer needs to be used.

After the controlled ceramic heating experiment, the size of the workpiece used for the test was increased to 100 mm . This caused the echo signal to be attenuated to 5 mV . Preliminary tests also show that the AD8302 board can measure the phase-shift of the attenuated 5 mV signal. The TCS 140 liquid bath calibrator was used to heat up the workpiece to get it closer to homogeneity. Results of the experiments show that temperature changes caused a measurable phase-shift between the transmitted and the received ultrasonic signals with errors in the $1\text{ }^{\circ}\text{C}$ steps experiment within $-0.2814\text{ }^{\circ}\text{C}$ and $0.199\text{ }^{\circ}\text{C}$ with standard deviation of $0.1076\text{ }^{\circ}\text{C}$. For the $0.1\text{ }^{\circ}\text{C}$ step, the errors of measurement are within $-0.053\text{ }^{\circ}\text{C}$ and $0.0365\text{ }^{\circ}\text{C}$ with standard deviation of $0.0178\text{ }^{\circ}\text{C}$. The $10\text{ }^{\circ}\text{C}$ range however could not be gotten in the linear region of the phase-shift response using the 5 MHz transducer.

The results show that with the described set up for ultrasonic thermometry phase-shift measurement, relative temperature change can be measured. The performance of the setup is promising as it was able to measure a $0.1\text{ }^{\circ}\text{C}$ change in temperature, this was achieved with the low-cost phase-shift detector. To do this with the pulse-echo method, an expensive pulser-receiver with cost reaching $\pounds 16,700$ is needed (section 3.1.1 covers the costs of pulser-receivers).

With the 100 mm length workpiece, the echo signal was attenuated to approximately 5 mV . This voltage value is low and may be difficult to distinguish from noise during a cutting

process. To enhance the signal strength, a THS3202 high-speed amplifier was designed and developed. The amplifier's operation was simulated in Multisim and based on the findings, the amplifier and other components were soldered to an evaluation board. The amplifier board was tested together with the ultrasonic setup. The result of the ultrasonic thermometry using the described setup and the amplifier corroborates the results gotten from the PT100 temperature detector with errors within ± 0.008 °C.

In the next chapter, the created and tested method and devices will be used on the CNC for in-process ultrasonic thermometry.

Chapter 5

5 In-Process Ultrasonic Thermometry

In Chapter 4, ultrasonic thermometry was validated in a laboratory and in relatively ideal environmental conditions. Although the previous experiments provide useful insights into the achievable range and resolution of measurement with the given transducer and workpiece pair, the additional uncertainties introduced by the harsh machining environment, which can include swarf, coolant, vibration etc, need to be investigated.

To understand the effects of the machining environment on the accuracy and resolution of the created ultrasonic thermometry method, the setup described in Chapter 4 was adapted for use on a Cincinnati CNC machine shown in Figure 5.1. This CNC machine was chosen for the test because of the ease of assembling the test equipment on the machine and the machine's availability at the time of the experiment.

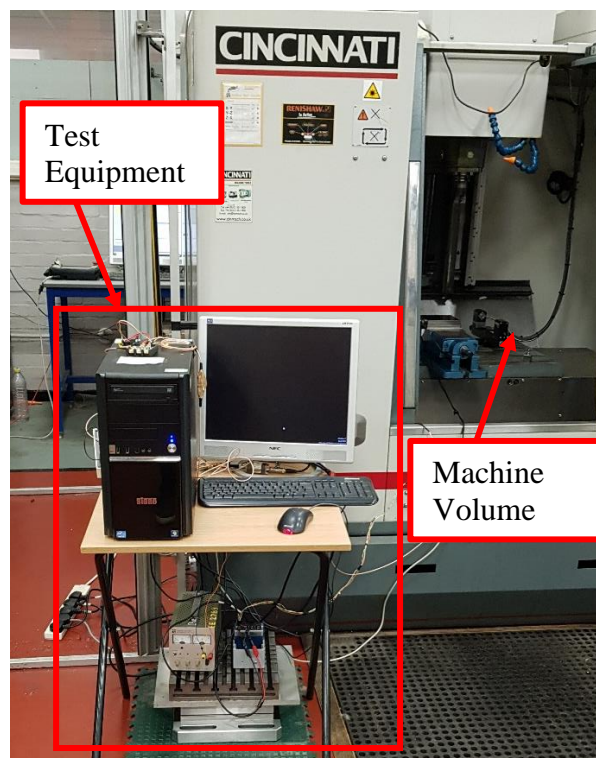


Figure 5.1: CNC and data acquisition setup for ultrasonic thermometry

A steel (EN24T) workpiece previously used in the controlled heating experiments was chosen as the medium of ultrasonic wave propagation. The workpiece was cut to the length of 120 mm, width of 120 mm, and height of 30 mm. This was done to accommodate a PT100 insert as the readings from the PT100 temperature detector will serve as the reference temperature values with which the ultrasonic measurements will be compared. A hole of diameter 6.2 mm and depth of 115 mm was drilled at the centre of the 30 mm face of the workpiece to hold the PT100. Some thermally conductive paste was applied in the hole to improve heat transfer to the sensor. The PT100 detector was inserted and glued using a glue gun, this was done to prevent sensor movement during cutting operations. The ultrasonic transducer was coupled using previously discussed epoxy (see section 3.2) at 15 mm (clearance for glue and epoxy) from the centre of the drilled hole as shown in Figure 5.2.



Figure 5.2: Transducer and PT100 spacing on workpiece.

With both the transducer and PT100 coupled to the workpiece, the workpiece was clamped to the table of the CNC. To ensure steady positioning of the transducer during machining and minimise pressure variation on the ultrasonic couplant due to machining vibration, an improvised mechanical clamp was used to fix the ultrasonic transducer in place after the epoxy bond has adequately set. The improvised clamp is shown in Figure 5.3.

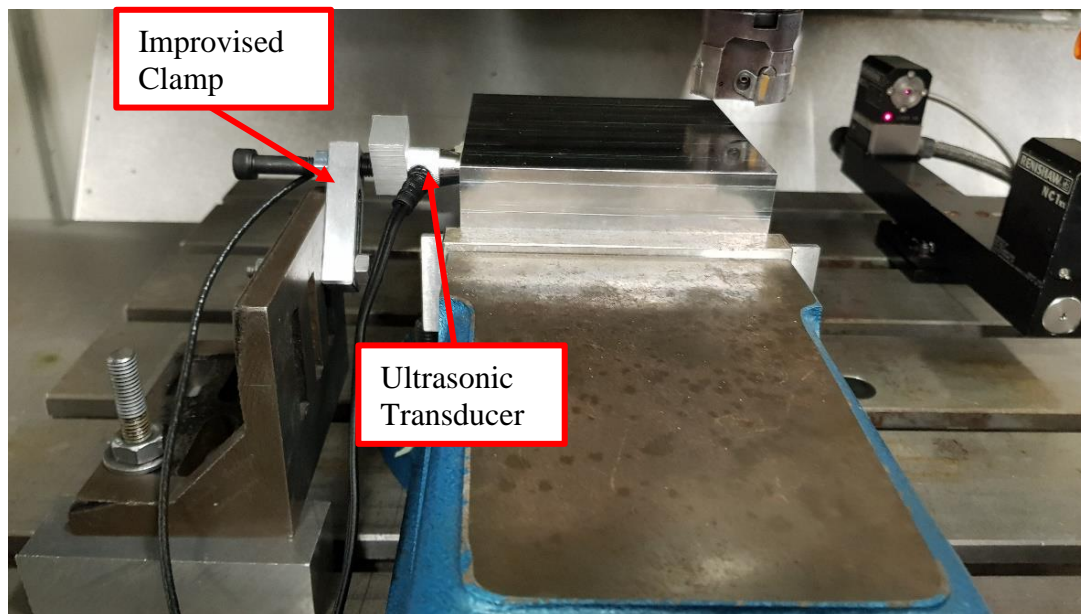


Figure 5.3: Improvised mechanical clamp for the ultrasonic transducer

After the clamp was screwed on, it was discovered that the clamping crushed the epoxy bond, this introduced air into the coupling which prevented proper ultrasonic transmission. To avoid this, the improvised clamp was screwed on before the epoxy bond was set, this improved the integrity of the bond as the echo signal showed the expected sine wave when it was observed on the oscilloscope. The echo signal after coupling is shown in Figure 5.4.

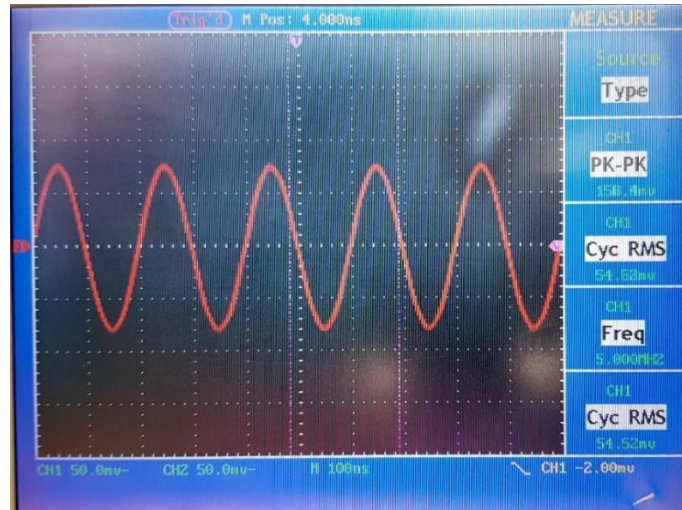


Figure 5.4: Echo signal after clamping

The following experiments were planned to systematically increase the number of uncertainties introduced to the measurement and observe the agreement of the ultrasonic thermometry results with that of the PT100.

The first experiment was designed to take the measurement while the CNC is switched on without the spindle running. This experiment will help to determine if there is any electromagnetic interference with the ultrasonic measurement. After an initial observation, the experiment was carried out over a prolonged period of approximately 13 hours. This was done to observe the consistency of the measurement result over time.

The second experiment was carried out with the CNC spindle running. The aim of this experiment is to observe the effect of the attendant vibration on the measurement result. This experiment was carried out for both 1000 rpm and 5000 rpm, these values were chosen in order to independently observe the effects of high and low speed revolution on the ultrasonic measurement. Thereafter, the effect of coolant on the measurement result was observed. The coolant was directed to the top of the workpiece from where it also flowed to the transducer.

After the coolant test, dry cutting and wet cutting tests were carried out. All the tests are discussed in detail in the subsequent sections.

5.1 Static Test (CNC Switched on)

After clamping the workpiece setup, the CNC machine was switched on. This test was set up to observe if there is any interference with the test setup from, for example, drive motors, pumps and other high power electrical systems often found on CNC machine tools. The initial data was captured for approximately 20 minutes. The result of this test is given in Figure 5.5.

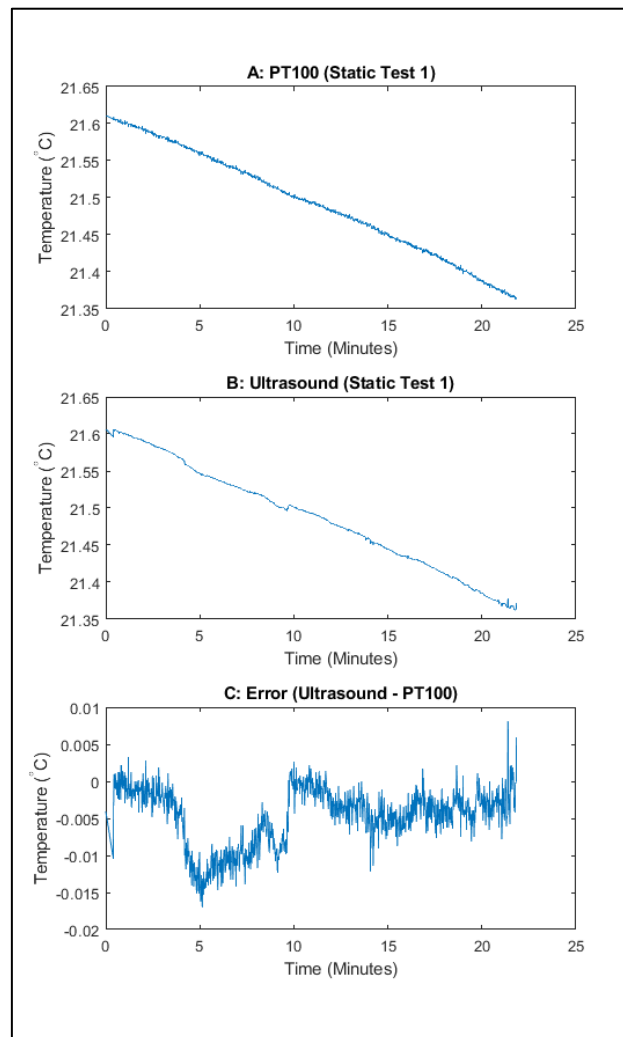


Figure 5.5: PT100 and Ultrasonic thermometry results of static test 1

The results show that the ultrasonic thermometry readings agree with the reference PT100 with an error range of $-0.017\text{ }^{\circ}\text{C}$ to $+0.0081\text{ }^{\circ}\text{C}$ and a standard deviation of $0.0039\text{ }^{\circ}\text{C}$. This is a good result; however, it is necessary to analyse both the PT100 and ultrasonic results for the observed variabilities and their individual contributions to the error result. For this, a high pass filter was considered. The high pass filter will be used to separate the slow changing temperature values from the high frequency noise. In order to select an appropriate cut-off frequency for the filter, the target resolution of $0.1\text{ }^{\circ}\text{C}$ defined in section 3.1 was taken into consideration. The chosen cut-off frequency should not cause a delay in response such that possible compensation for thermal expansion will lag more than the target resolution. For this, the typical temperature rise time during cutting was observed (section 5.4 covers the cutting trials). The temperature of a typical part will rise by $0.1\text{ }^{\circ}\text{C}$ in 0.36 seconds. This means that the cut-off frequency should not be lower than 2.8 Hz to preserve the target resolution. Therefore, a 3 Hz cut-off frequency was chosen. The high pass filter was applied to both PT100 and ultrasonic data in MATLAB and the results are shown in Figure 5.6.

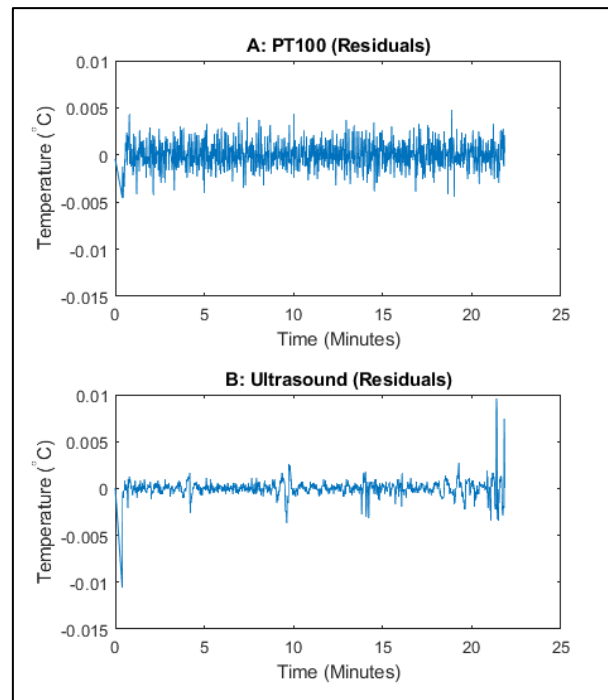


Figure 5.6: Residuals of PT100 and ultrasonic thermometry for static test 1

The results of the high pass filtering show that the standard deviation of the PT100 residual values is $0.0014\text{ }^{\circ}\text{C}$ and $0.00091\text{ }^{\circ}\text{C}$ for the ultrasound residual values. The range of the residuals is $-0.0045\text{ }^{\circ}\text{C}$ to $+0.0047\text{ }^{\circ}\text{C}$ for PT100 and $-0.0106\text{ }^{\circ}\text{C}$ to $+0.0096\text{ }^{\circ}\text{C}$ for the ultrasound readings. Although the range of the ultrasound residuals is higher than the PT100, the plot shows that this is due to the spike at the beginning and the end of the data which could be due to movements of cables while starting and stopping the experiments. These cannot reasonably be temperature readings due to thermal inertia and there is a need to filter the spikes out from the data. The standard deviation values also show that there is more variability in the PT100 data than in the ultrasound data. This could be due to the circuitry of the sensor. To remove the noise in both PT100 and ultrasound data, lowpass filter was applied, using the same 3 Hz cut-off frequency.

After filtering, the range of the error values reduced to $-0.0143\text{ }^{\circ}\text{C}$ to $0.00082\text{ }^{\circ}\text{C}$ from $-0.017\text{ }^{\circ}\text{C}$ to $+0.0081\text{ }^{\circ}\text{C}$ and the standard deviation reduced to $0.0036\text{ }^{\circ}\text{C}$ from $0.0039\text{ }^{\circ}\text{C}$. It is expected that in operations where spikes and more residual noise are likely to be present, the lowpass filter will be used to remove the noise and hence reduce the variabilities in the data. The results of the filtered data and the error plot is shown in Figure 5.7.

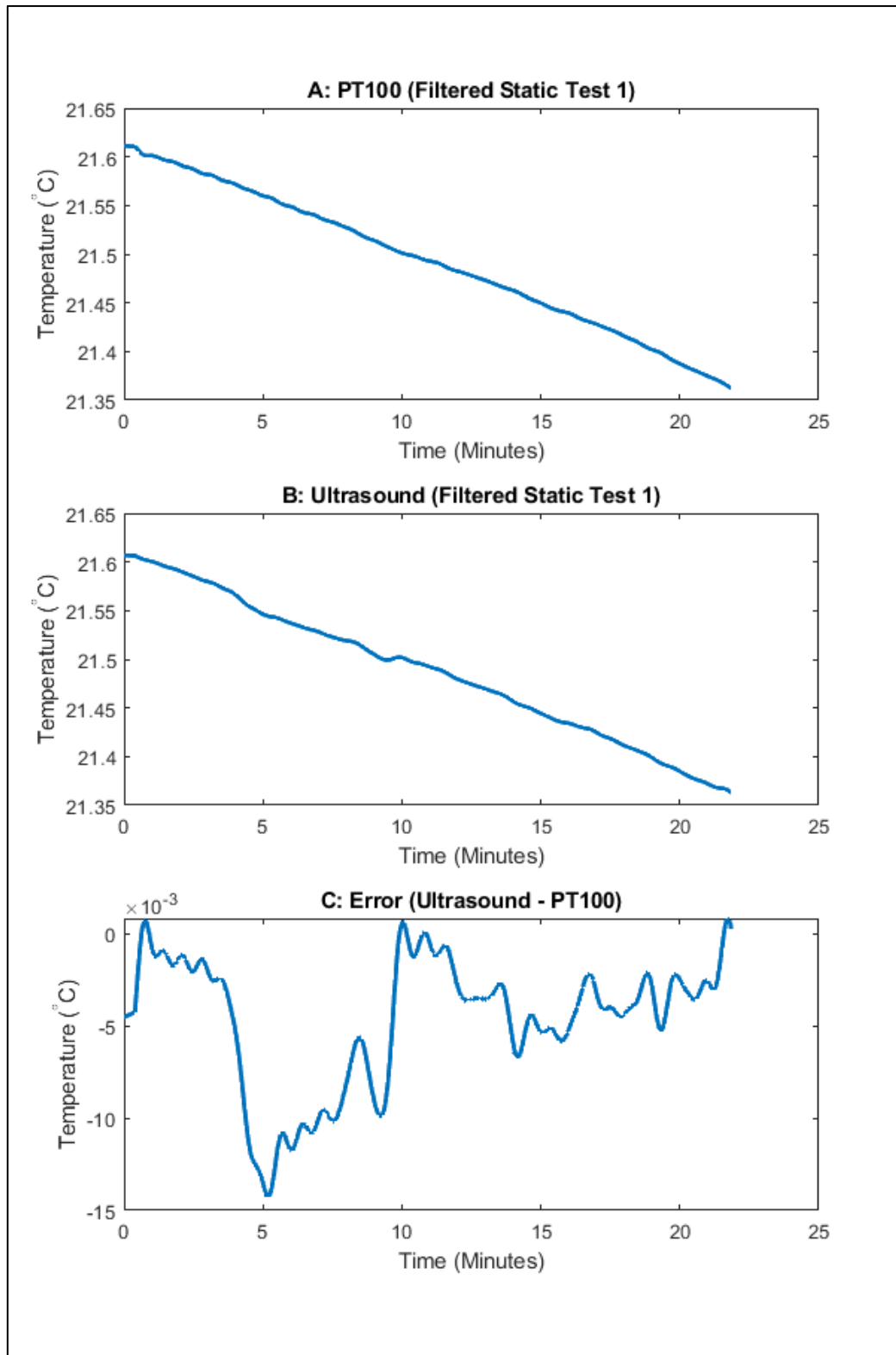


Figure 5.7: PT100 and ultrasonic thermometry static test 1 result after filtering

The same test was repeated for an extended period (approximately 13 hours). This was performed to observe how stable the readings are over an extended period that could represent a very long machining cycle.

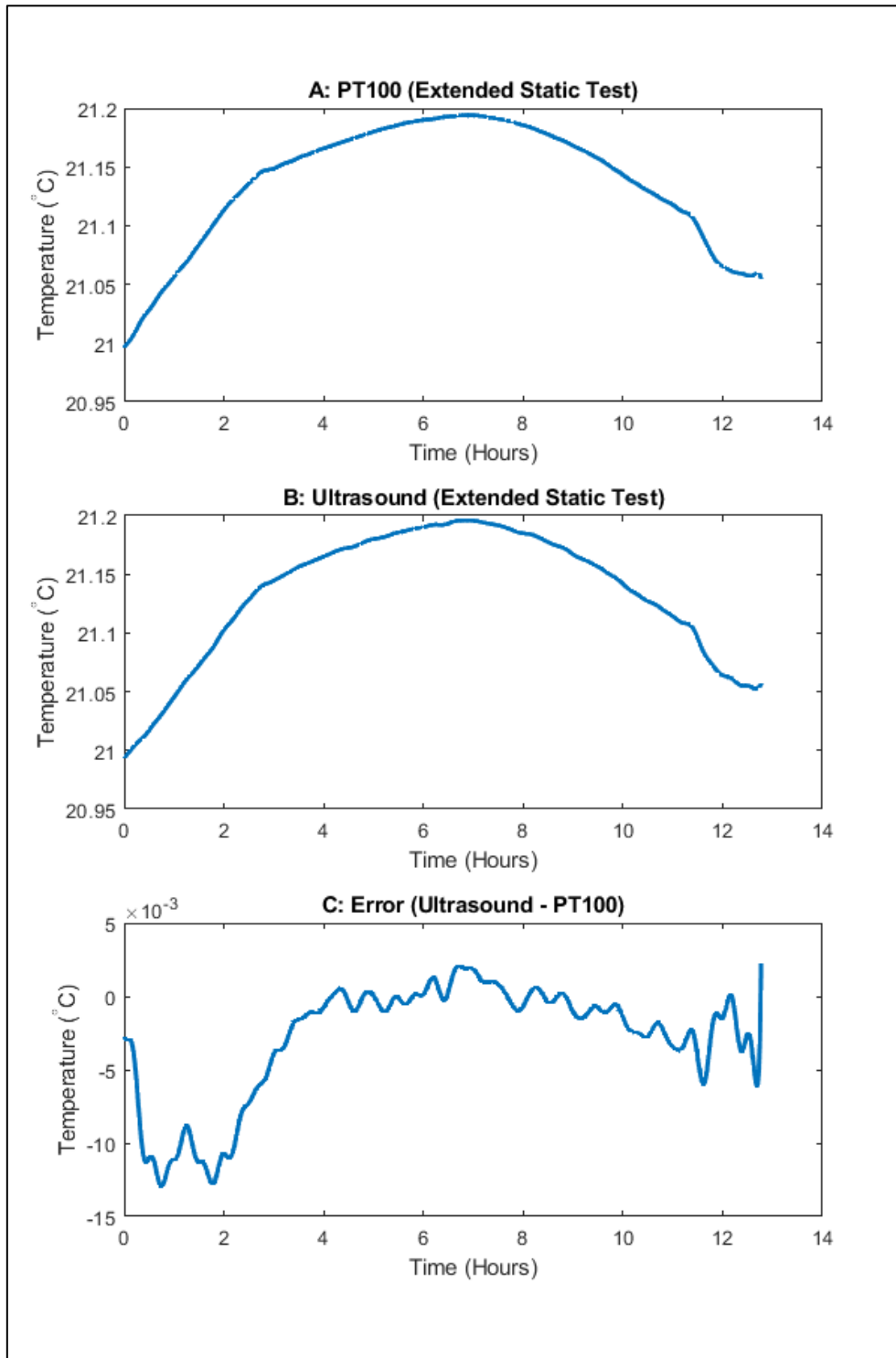


Figure 5.8: Results of the extended static test

Before filtering, the error values over 13 hours were within the range of $-0.0179\text{ }^{\circ}\text{C}$ to $+0.0089\text{ }^{\circ}\text{C}$ with standard deviation of $0.0043\text{ }^{\circ}\text{C}$ (See Appendix B for plots of unfiltered results). After filtering, the error range reduced to $-0.0130\text{ }^{\circ}\text{C}$ to $+0.0022$ with standard deviation of $0.0040\text{ }^{\circ}\text{C}$. This result shows that the ultrasonic thermometry setup is stable over time. Furthermore, none of the static test results show any observable interference with the results of the ultrasonic thermometry. In the next section, the spindle running test will be presented and the results will be discussed.

5.2 Spindle Running Tests

The aim of the spindle running tests is to observe the effects of the attendant vibration, and possibly increased electromagnetic interference on the accuracy of the ultrasonic readings. This test was planned to have two parts, a relatively low speed test of 1000 rpm and another test with higher speed of 5000 rpm which is the maximum speed for the machine. It is expected that the improvised clamping and the epoxy resin used for coupling the ultrasonic transducer to the steel workpiece will reduce the effects of the vibration on the accuracy of the ultrasonic thermometry readings both during the spindle running tests and during actual cutting. The drilled hole for the PT100 temperature detector provides a firm positioning for the PT100 and further stability was provided using the glue shown in Figure 5.2.

The results of the 1000 rpm and the 5000 rpm tests are shown in Figure 5.9 and Figure 5.10 respectively. The results show that the vibration induced by the running of the spindle does not reduce the accuracy of the measurement results. Before filtering, the error values for the 1000 rpm test were in the range of $-0.0139\text{ }^{\circ}\text{C}$ to $+0.0080\text{ }^{\circ}\text{C}$ with standard deviation of $0.0042\text{ }^{\circ}\text{C}$ and the error range for the 5000 rpm test was $-0.0105\text{ }^{\circ}\text{C}$ to $+0.0194\text{ }^{\circ}\text{C}$ with standard deviation of $0.0047\text{ }^{\circ}\text{C}$. After filtering, the error range for the 1000 rpm test reduced to $-0.0107\text{ }^{\circ}\text{C}$ to

+0.0055 °C with standard deviation of 0.0038 °C and the error range for the 5000 rpm test reduced to -0.0052 °C to +0.0126 °C with standard deviation of 0.0041 °C. The results are shown in Figure 5.9 and Figure 5.10, and the unfiltered results are shown in Appendix B.

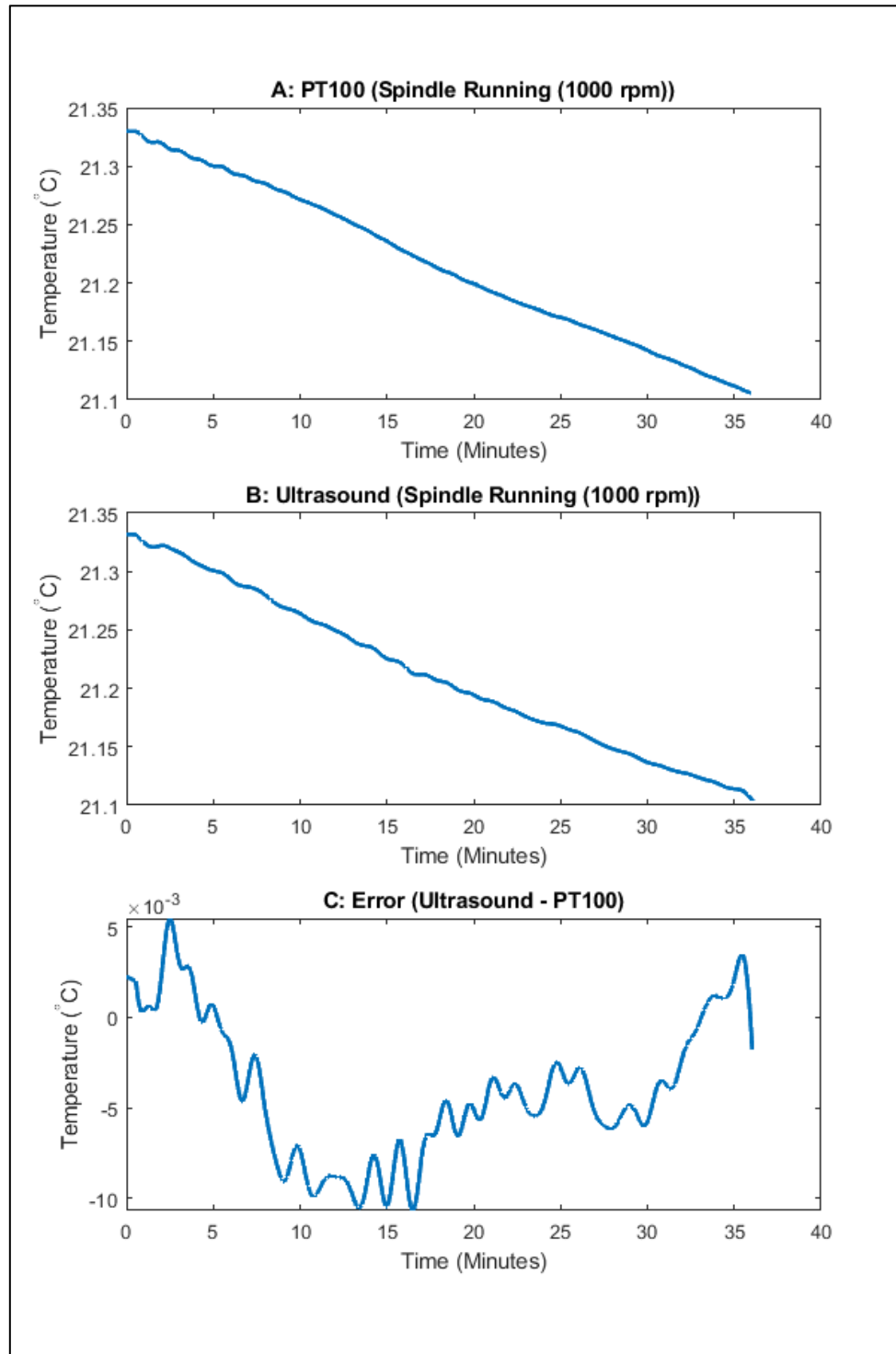


Figure 5.9: Results for spindle running at 1000 rpm

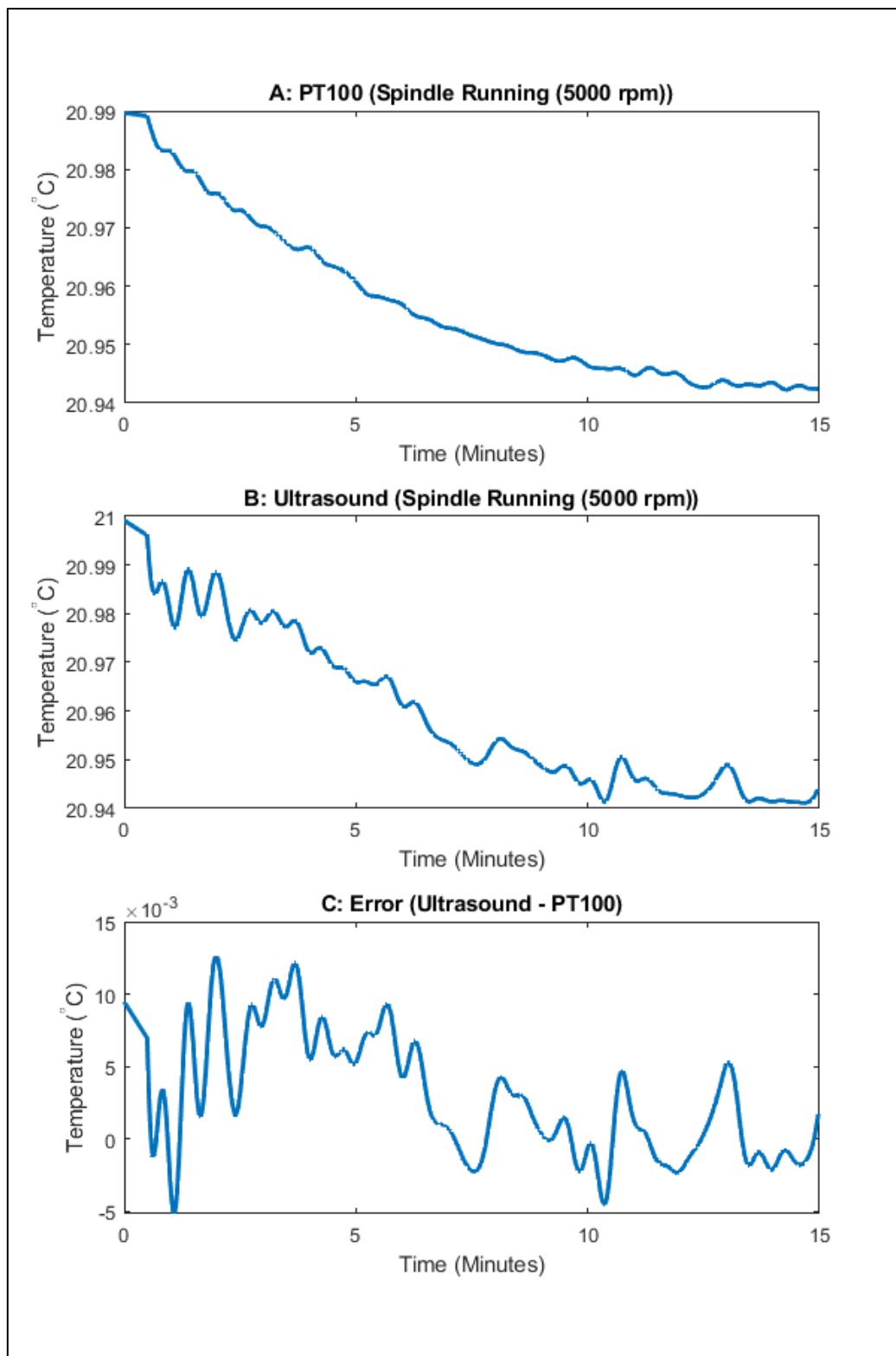


Figure 5.10: Results for spindle running at 5000 rpm

5.3 Test with Cutting Fluid

Cutting fluid used during wet cutting processes are typically used to lubricate and cool the machining region. One of the widely used cutting fluids is the petroleum based mineral oils (MO) [108]. Ultrasonic waves need to encounter a medium of different physical properties for them to be reflected. In all the tests previously described, this boundary has been steel-air interface (except for the liquid bath calibrator test which provides a consistent liquid boundary). The presence of cutting fluid adds a medium with a different type of inconsistent physical property to the steel boundary. This could add an additional uncertainty.

The cutting fluid does not provide a consistent boundary for the reflection of the ultrasonic wave. This is because the cutting fluid is flowing over the workpiece in a much more variable way than cases where the workpiece is submerged in water or other liquid. This can result in the presence of different volumes of cutting fluid at different points in time. Also, there is the possibility of air being present between the workpiece and the cutting fluid. All these factors are expected to have some effects on the results of the test.

For all the experiments with cutting fluid in this study, QUAKERCOOL 7101 BFF was used. This coolant is a mixture of mineral oil, water, salt, and additives [109]. It is the coolant used in the research group; hence it was used for the cutting trials as well. With this understanding, the test with cutting fluid was carried out. Cutting fluid was directed to flow onto the clamped workpiece for 25 minutes, it is expected that the coolant effect will be seen during this time. This took the workpiece to a stable temperature of approximately 19.1 °C. The result of the test showed that the ultrasonic thermometry readings agree with the PT100 readings with errors of the unfiltered results within the range of -0.0779 °C to +0.1450 °C and standard deviation of 0.0289 °C. Filtering reduced the error range to -0.0787 °C to +0.0989 °C with standard deviation of 0.0222 °C. This result is less accurate when compared with the previous results

from both the static and the spindle running tests as the highest standard deviation in those tests is 0.0041 °C. However, this is still considered a good result, especially because of the factors previously mentioned and because unlike the PT100 detector which is shielded from the cutting fluid by the workpiece, the ultrasonic transducer is intentionally exposed to the harsh machining environment for the purpose of experimentation. The result of the coolant effect on the ultrasonic thermometry is given in Figure 5.11 and the unfiltered result is shown in Appendix B.

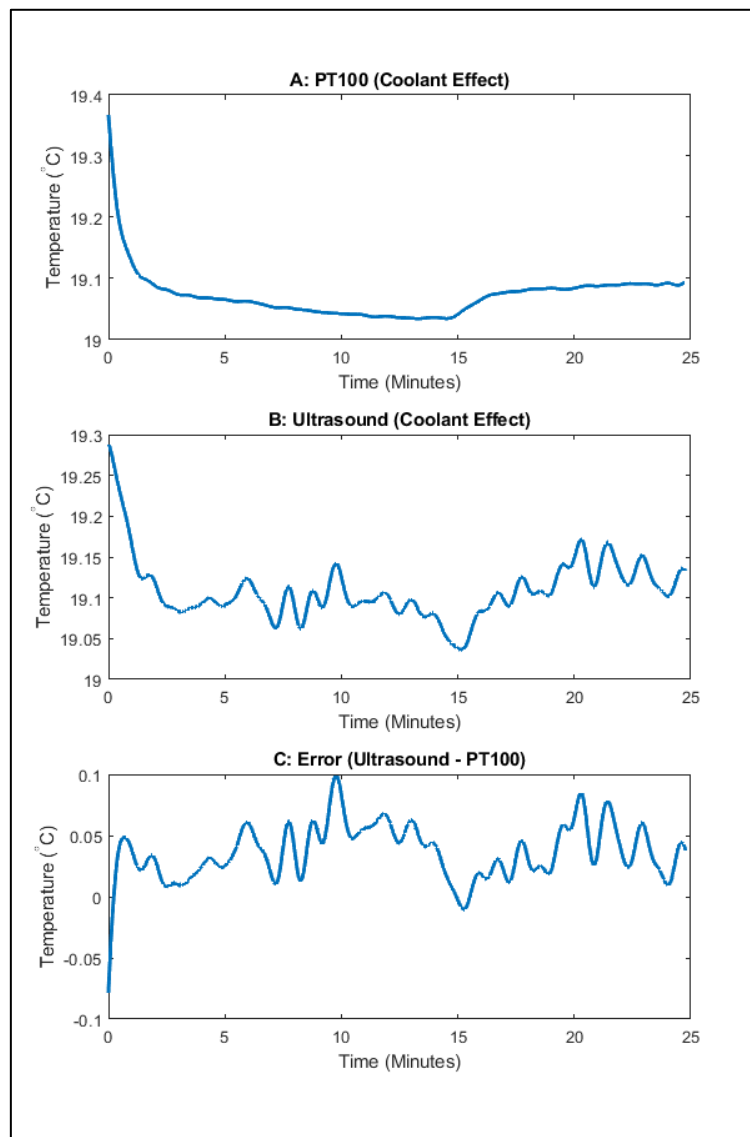


Figure 5.11: Effect of cutting fluid on ultrasonic thermometry.

5.4 Dry Cutting Trials

The results of the preliminary tests show that the ultrasonic thermometry readings agree with the reference readings with some small deviations. However, one of the key objectives of the research is to test this system during an actual cutting process. Using the same setup as previously described for the non-cutting CNC tests, a CNC cutting trial was set up. To generate sufficient heat, a 22 mm Indexable Carbide tipped 3 flute end mill was used. The cutting routine is a single pass with axial engagement of 1 mm, radial engagement of 15 mm, feed rate of 750 mm/minute, and spindle speed of 3500 rpm. These values were chosen to generate sufficient heat to provide a reasonable range of temperature measurement. The cutting direction was chosen to be perpendicular to the ultrasonic transducer and PT100 sensor to avoid lateral gradient. The direction of cut is shown in Figure 5.12.

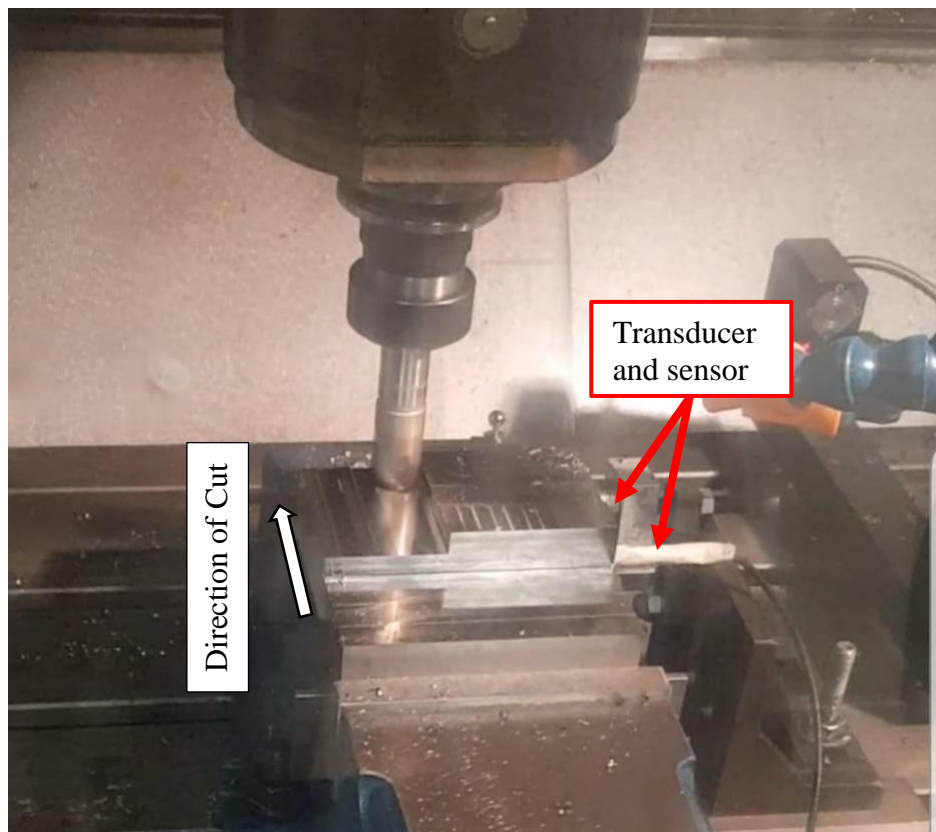


Figure 5.12: Direction of cut perpendicular to the transducers.

The initial cutting trial was carried out with the 5 MHz transducer with single pass of cutting, however, there was no sufficient span of temperature reading to allow for proper inferences to be made. Therefore, the number of cutting passes was increased to provide sufficient heat for significant temperature rise. However, the phase-shift readings from the phase detector reached the non-linear portion of the AD8302. In order to avoid the ambiguity in this region, a lower frequency transducer was considered.

A 1 MHz transducer was chosen because of its potential to achieve the range of 10 °C with results falling within the linear range. It was also the lowest frequency dual element transducer identified from vendors at the time of this experiment. For the cutting trials, an NDT Systems DVF014 transducer was chosen. The 1 MHz dual element transducer has a centre frequency of 1.038 MHz and a bandwidth of 1.465 MHz at -6dB and 1.831 MHz at -12dB. The transducer characterisation report and the certificate of conformance are provided in Appendix C.

The 1 MHz transducer was clamped using the same method as in the previous CNC experiments. The machining procedure was revised, the cutting was carried out in three passes to generate more heat. The G code is provided in Appendix D. The test data was captured before the cutting process, during the process, and the during return of the workpiece temperature to ambient temperature. Three dry cutting trials were carried out due to restricted access to the CNC. The results of these trials are shown in Figure 5.13 and the unfiltered results are presented in Appendix B.

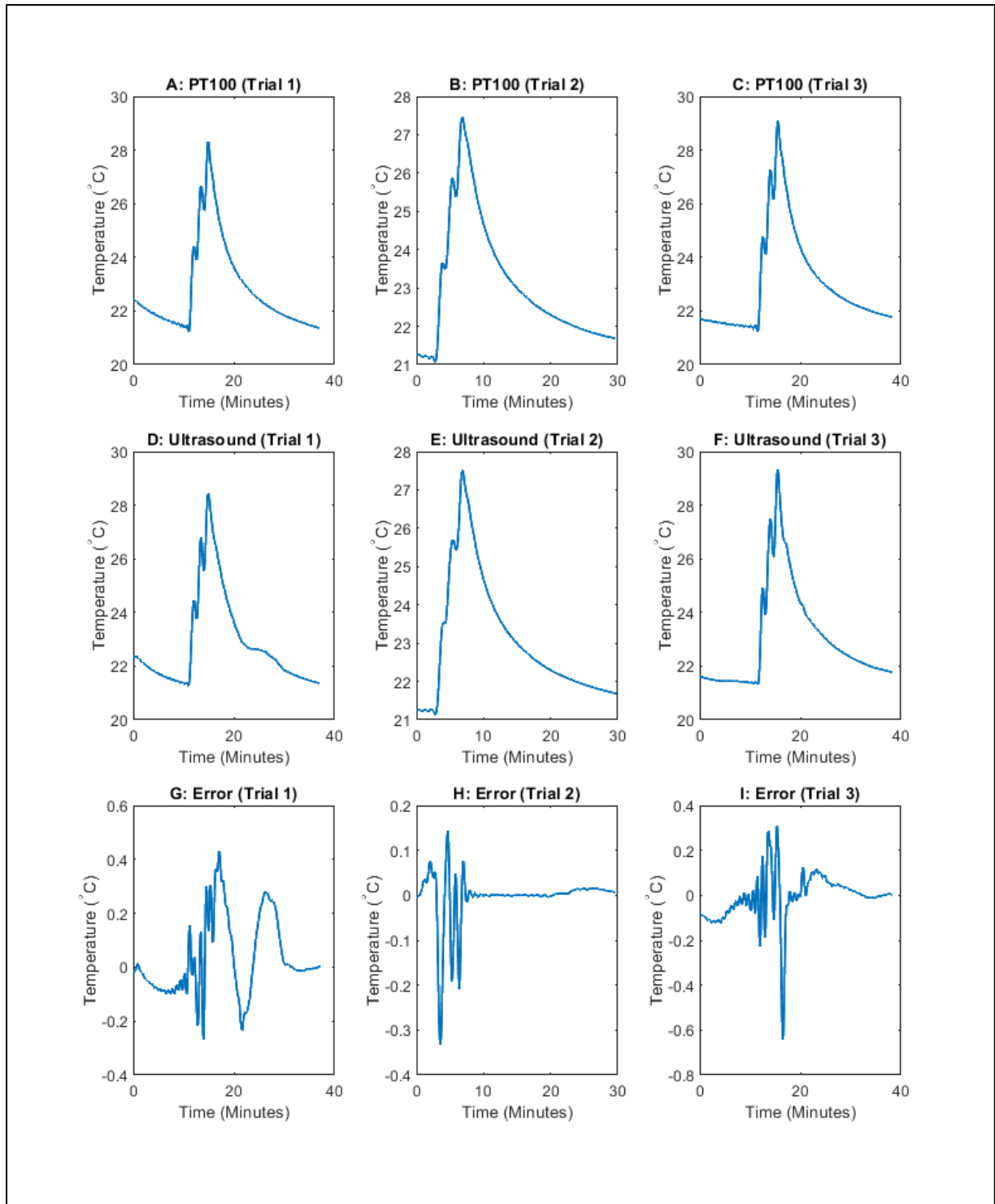


Figure 5.13: Results of dry cutting trials

The error range and standard deviation for the trials are given in Table 5.1.

Table 5.1: Dry cutting trial errors and standard deviation

Cutting Trial #	Unfiltered Results		Filtered Results	
	Error Range (°C)	Standard Deviation (°C)	Error Range (°C)	Standard Deviation (°C)
1	-0.7802/+0.8747	0.1911	-0.2677/+0.4287	0.1459
2	-0.6835/+0.6734	0.0970	-0.3337/+0.1445	0.0579
3	-0.8834/+0.8870	0.1466	-0.6408/+0.3078	0.1112

The error values for all the trials fall within ± 0.9 °C before filtering and ± 0.6 after filtering. During the cutting process, the workpiece temperature changed by 6 °C, without compensation, this will result in part error of 8.9 μm (Assuming CTE of 12.3 $\mu\text{m}/\text{m}^\circ\text{C}$ and workpiece length of 120 mm). If the highest deviation of 0.6 °C from the in-process measurement was used for compensation, the error will reduce to 0.9 μm . This shows that the method can reduce dimensional error by a factor of 10 in the given example.

From the dry cutting trials, the results show that the maximum deviation of the ultrasonic readings from the PT100 readings occurs at the cutting stage, and this is the upward rising slope in the cutting trial plots. In cases where measurement can be done when pauses are made to the actual cutting operation, the accuracy of the obtained results will be higher than those obtained during the actual cutting process.

5.5 Wet Cutting Trials

In the cutting fluid test described in Section 5.3, the results show that the presence of cutting fluid on the workpiece decreased the accuracy of the measurement result. The dry cutting results also show that during the actual cutting process, some error is introduced. With the wet cutting trials, these two effects may combine to introduce uncertainties. However, because of

the presence of the cutting fluid, the temperature rise should be less during wet cutting than in the dry cutting trial.

Wet cutting trial was carried out with the same setup as the dry cutting trial and cutting fluid was applied during cutting. The results are given in Figure 5.14 and Figure 5.15. The unfiltered result is presented in Appendix B.

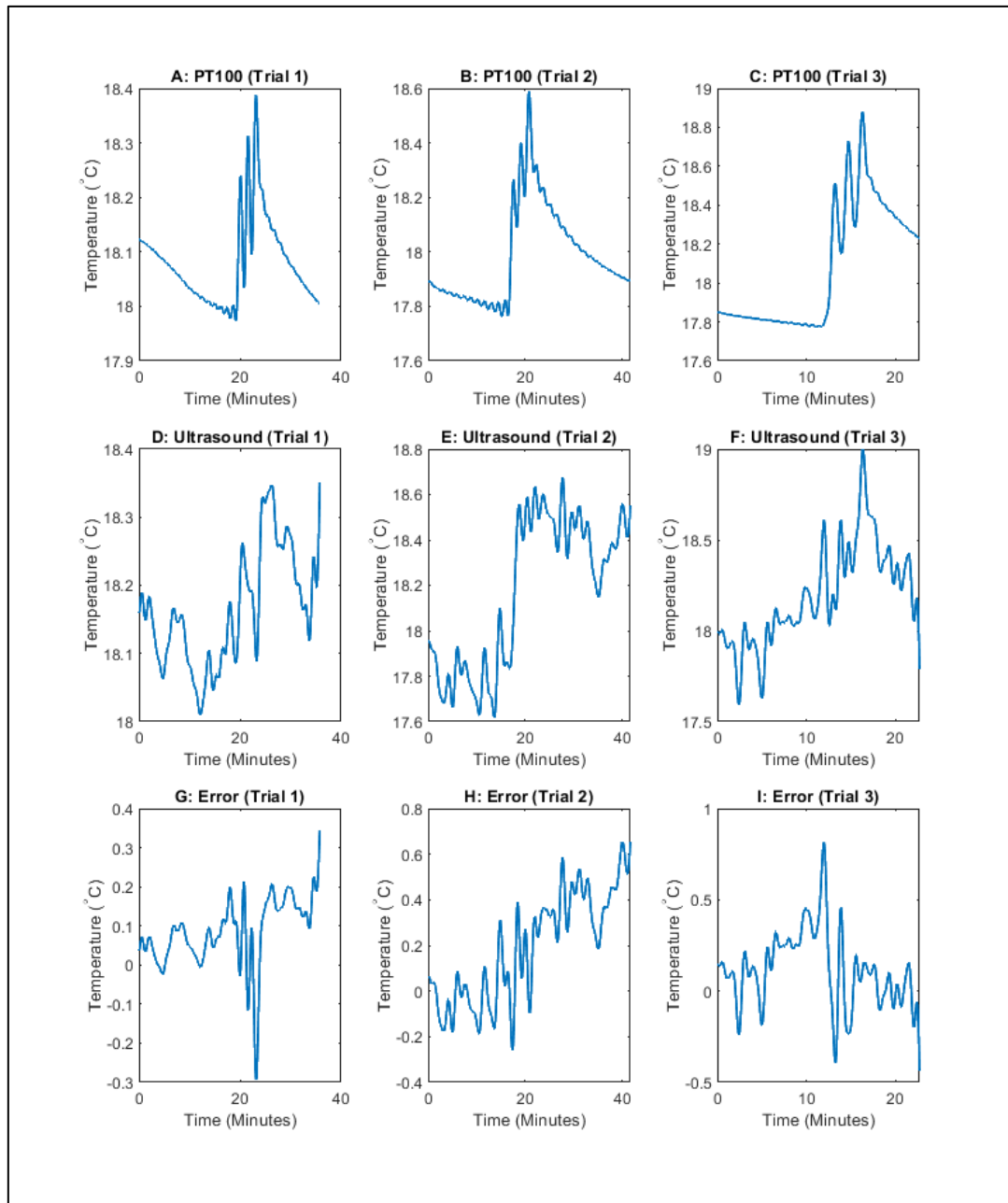


Figure 5.14: Wet cutting trials 1-3

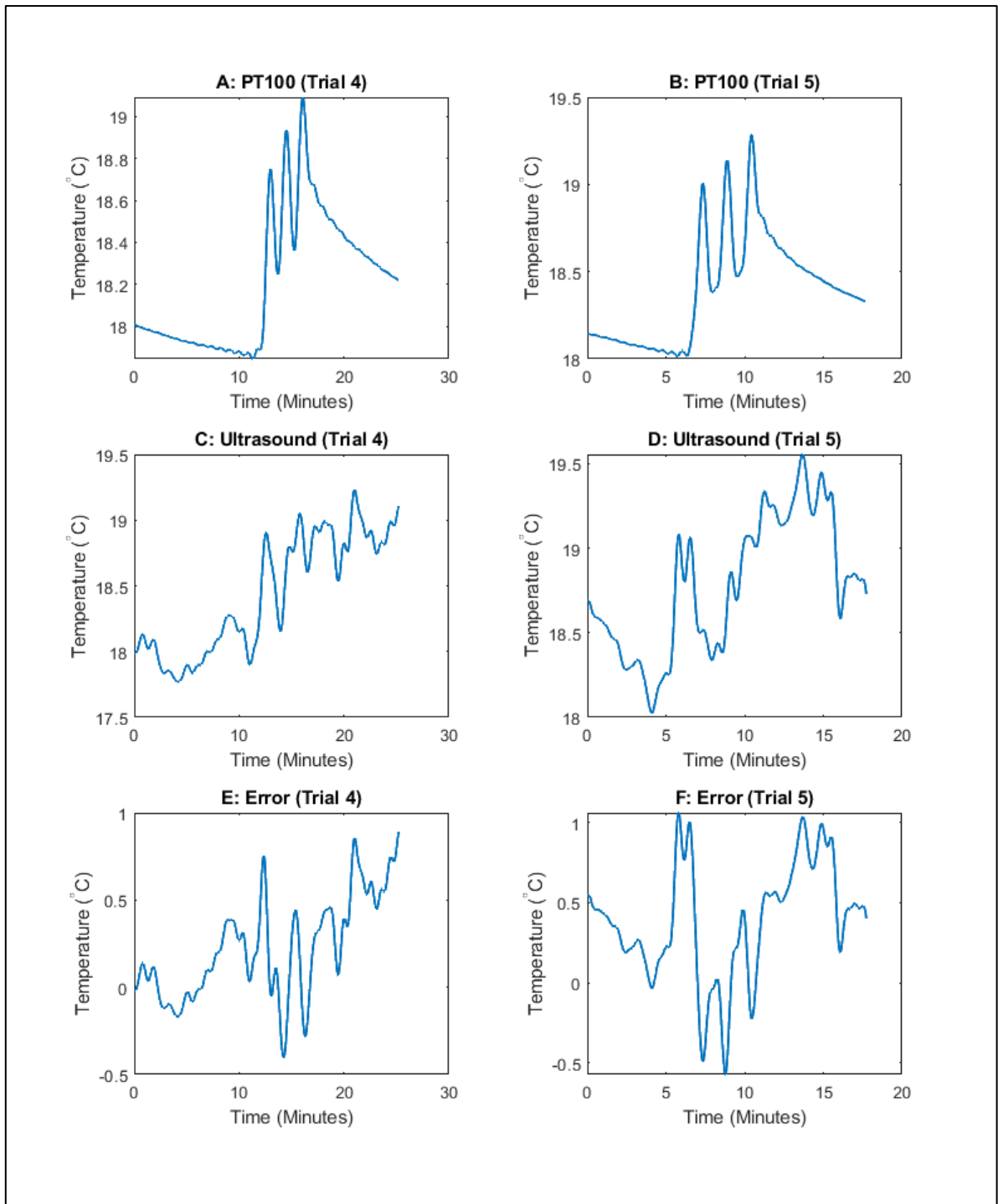


Figure 5.15: Wet cutting trials 4-5

Table 5.2: Wet cutting trial errors and standard deviation

Cutting Trial #	Unfiltered Results		Filtered Results	
	Error Range (°C)	Standard Deviation (°C)	Error Range (°C)	Standard Deviation (°C)
1	-0.3419/+0.3421	0.0934	-0.2937/+0.3458	0.0875
2	-0.2773/+0.7382	0.2454	-0.2601/+0.6567	0.2365
3	-0.4560/+0.8610	0.2122	-0.4393/+0.8144	0.2073
4	-0.7273/+1.0179	0.2963	-0.4026/+0.8942	0.2886
5	-0.9617/+1.1372	0.3735	-0.5712/+1.0591	0.3647

The plots show that there is typically less than 2 °C rise in temperature during the wet cutting process. The ultrasonic thermometry results in wet cutting are less accurate than in dry cutting with error values reaching +1 °C in one of the filtered results. There are two trials where the error values reached +1 °C before filtering, however in three other trials, the error values are all within ± 0.9 °C. These results are still potentially better than that of surface mount sensors since it is even more difficult to obtain any useful reading with conventional sensors during wet cutting processes. This is because the conventional sensors will pick up the surface temperature which will be the temperature of the cutting fluid in this case, except they are inserted in a drilled hole in the workpiece and drilling holes in every workpiece for temperature measurement is not usually feasible. With further research, optimal coupling techniques for different cutting processes as well as different materials can be established. The results of the cutting trials provide very useful input for such research.

5.6 Summary

In this chapter, the workpiece used for the CNC tests was described. A steel EN24T workpiece with dimension 120 mm x 120 mm x 30 mm was used. A hole was drilled to accommodate the

PT100 temperature detector. Using an improvised mechanical clamp, the ultrasonic transducer was secured in place with epoxy resin used as the ultrasonic couplant.

The first test that was carried out is the static CNC test. In this test, the CNC was switched on and both PT100 and ultrasonic data were captured to observe if there was any electromagnetic interference with the setup that significantly affects the accuracy of the measurement results. The results showed good agreement between the reference and ultrasound readings. This test was repeated for another 13 hours. The results also show good stability of readings over an extended period.

The spindle of the CNC was made to run, first at 1000 rpm and then at 5000 rpm. The purpose of this test is to observe the effects of vibration and possible electromagnetic interference due to the movement of the motors and operation of other high-power components present on the CNC on the results. The results show that the measurement system is not adversely affected by the running of the spindle.

A test was carried out with the cutting fluid directed to flow on to the workpiece. This test was carried out to observe the effects of the varying boundary caused by the presence of the coolant on the readings. The results show that the ultrasonic readings are 'spikier' than the PT100 readings before filtering. However, the error values were less than ± 0.15 °C and reduced to ± 0.1 °C after filtering. This is a good result especially because the cutting fluid flowed over both the workpiece and the ultrasonic transducer.

Dry cutting trials were carried out and the results show that ultrasonic thermometry in dry cutting agree with reference temperature measurement with error values within ± 0.6 °C after filtering. Using this for expansion compensation will reduce the dimensional error on the 120 mm part by more than 8 μm .

Wet cutting trials were then carried out. The presence of cutting fluid introduced more uncertainty to the measurement results. The results of two of the trials had error terms reaching +1 °C before filtering, while three other trials have the error values within ± 0.9 °C. Filtering improved the results, however one of the trials still had errors reaching +1 °C. In the next chapter, the use of the ultrasonic thermometry system on the CMM and on an aluminium workpiece will be discussed.

Chapter 6

6 Temperature-Expansion Experiment on the Coordinate Measuring Machine and Ultrasonic Thermometry Using Aluminium.

The main motivation for the ultrasonic thermometry study is to measure the core temperature of workpieces which influences the expansion of the workpiece. Although the temperature-expansion relationship is well established in extant literature, it is important to compare the link between both surface and core temperature of the workpiece with the expansion of the material. Uncertainty in coordinate metrology is very important and therefore sensitivity to internal temperature gradients may be just as significant as those during machining. This may be especially so in production scenarios where previous processes may cause the temperature of the component to vary from the 20 °C at which inspection typically occurs and there is insufficient time to allow the components to homogenise. In this chapter, an experiment performed on the Coordinate Measuring Machine (CMM) will be detailed.

In addition, in all the previous described ultrasonic thermometry experiments in this thesis, steel was used as the medium of ultrasonic wave propagation. However, it is important to establish if the created temperature measurement system is suitable for other materials. To determine this, an ultrasonic thermometry experiment was performed with aluminium being the medium of ultrasonic wave propagation. The details and results of this experiment are also presented in this chapter.

6.1 Temperature-Expansion Experiment on the CMM

The aim of the CMM experiment is to compare the expansion measurement results obtained from measuring the part dimension with the CMM probe with the calculated expansion from

the results of measuring both surface and core temperature of the workpiece. To get the required temperature rise, the part was cooled to below 10 °C. Cooling was chosen over heating as it is considered safer for the planned experiment. Using the previously described ultrasonic and PT100 devices, the experiment was setup on a ZEISS Prismo Access CMM, this is the CMM available for use in the research group. The surface temperature was measured using the on-CMM temperature sensor. The setup is shown in Figure 6.1.

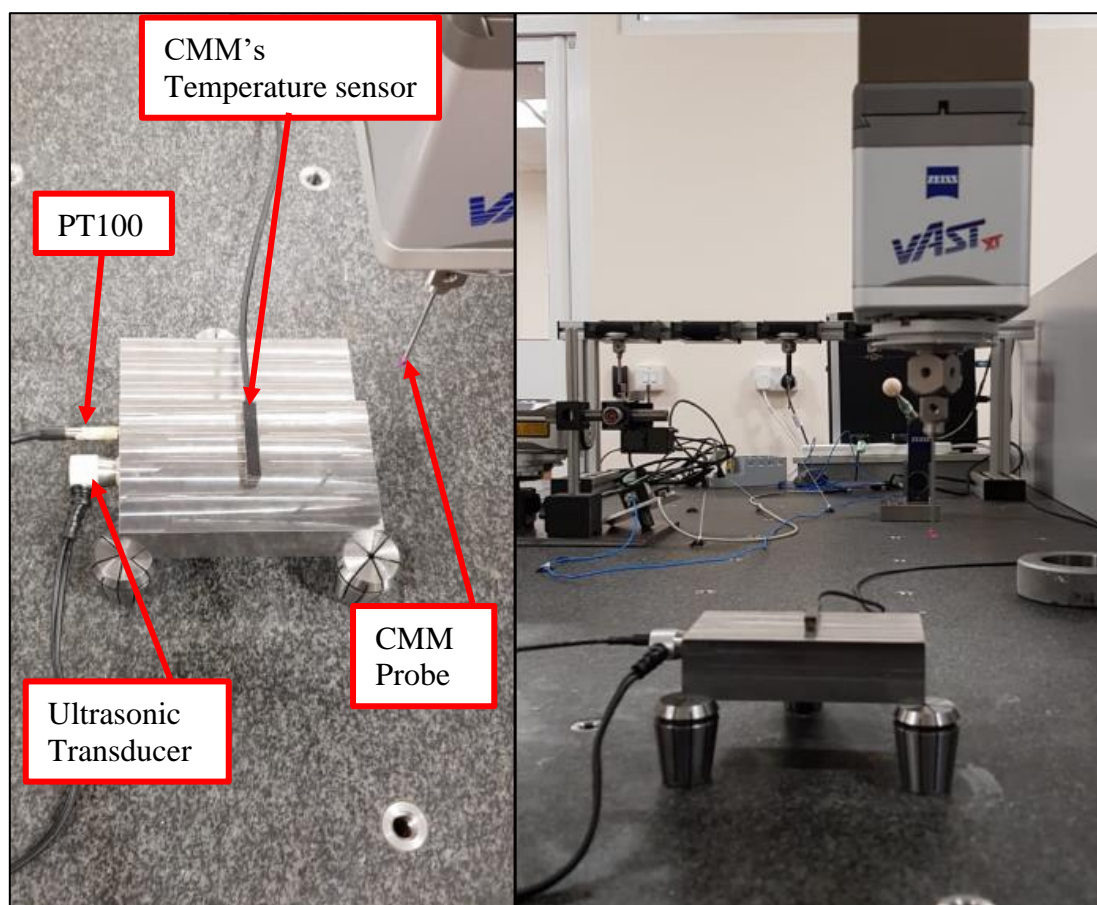


Figure 6.1: Experiment setup on the CMM.

The core and surface temperature values as well as the part dimension were recorded from 10 °C until the part reached the ambient temperature of 20 °C.

The core temperature was recorded continuously, however, the surface temperature and the part dimension were recorded at 4 minutes interval which was the approximate time taken for

the part to rise by 0.5 °C at the start of the experiment, this value was chosen to get a representative temperature profile over time and to enable the probing cycle to complete. The unfiltered results have error values within -0.2758 °C and +0.3353 °C and standard deviation of 0.0499 °C. With filtering, the error values reduced to within -0.1329 °C and +0.1354 °C with standard deviation of 0.0444 °C. The deviations are most likely the results of noise in the circuitry. However, the error values were less than 0.15 °C for the 10 °C range, this serves as a good input for material expansion analysis which will be detailed in this section. The PT100 and Ultrasound results are given in Figure 6.2 and the unfiltered results are presented in Appendix B.

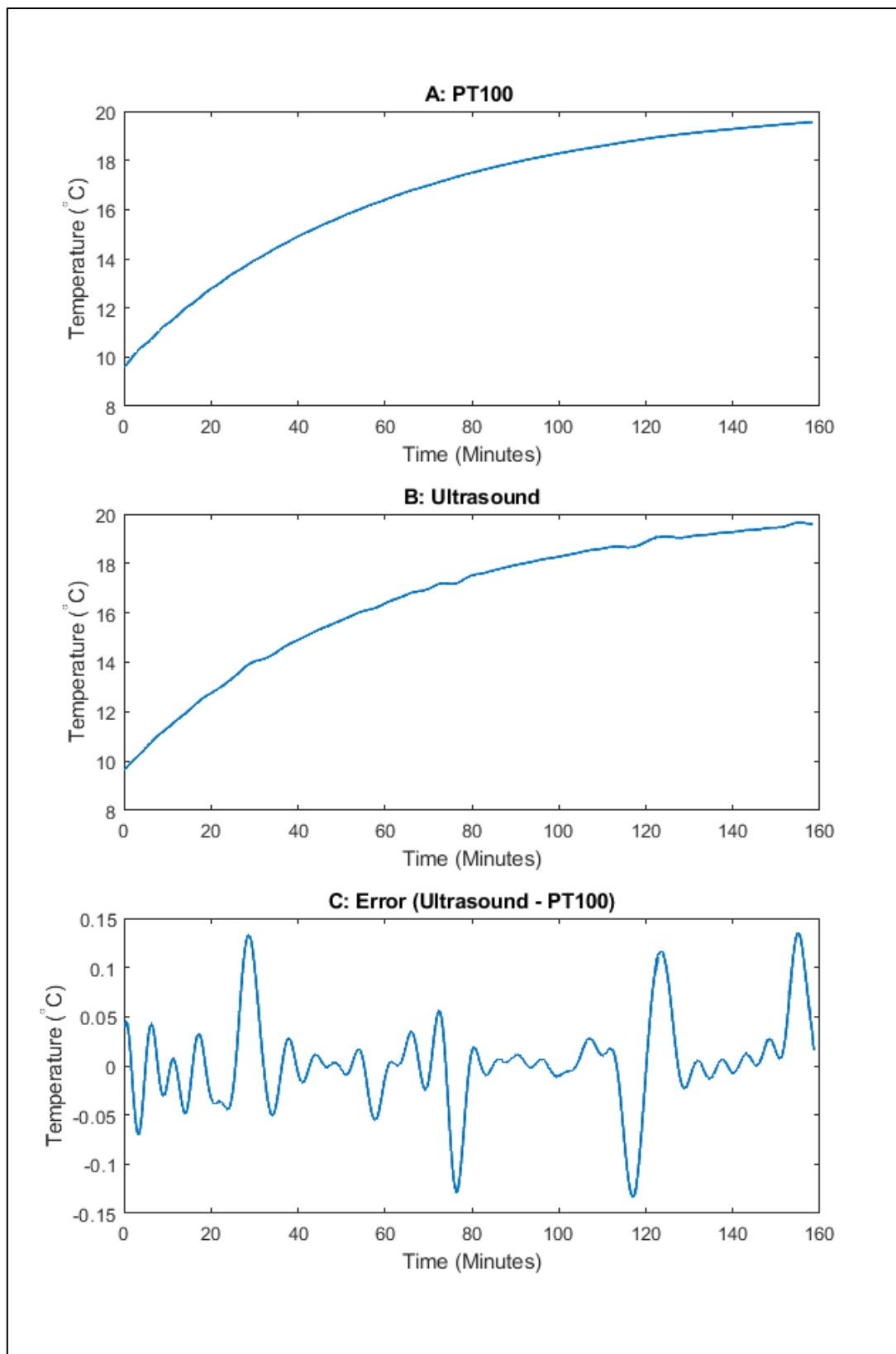


Figure 6.2: On-CMM PT100 and ultrasound results

Ultrasound result was used as the core temperature values. The core and surface temperature changes over time are given in Figure 6.3 and the absolute values are presented in Appendix B. The calculated expansion values and the CMM measured dimension values they are based on are given in Figure 6.4.

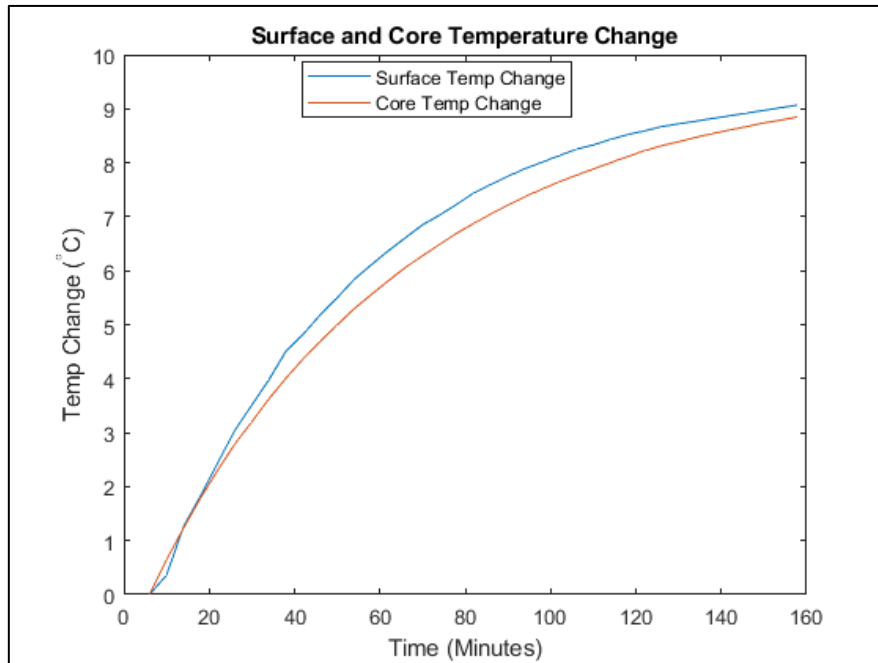


Figure 6.3: Core and surface temperature values

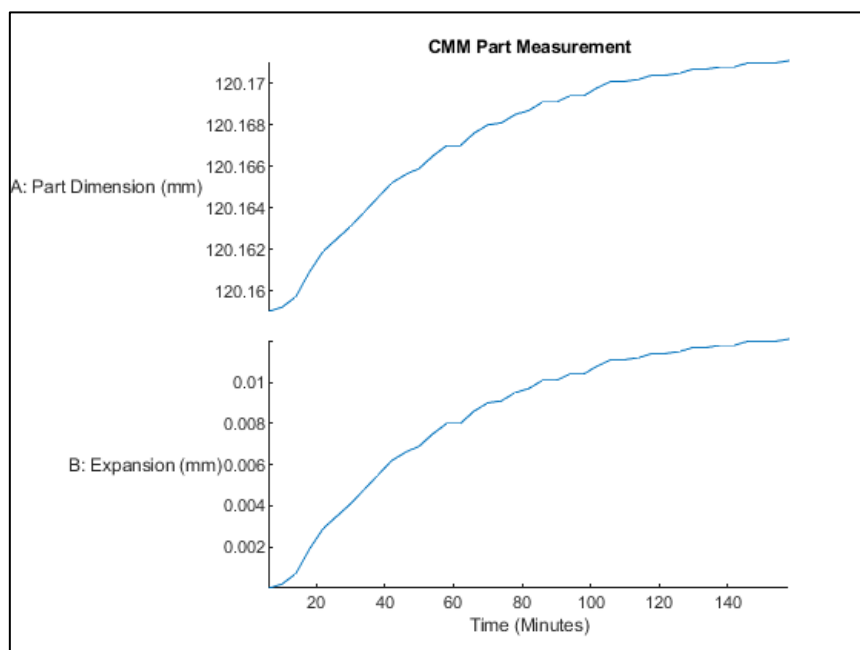


Figure 6.4: Part dimension and expansion

The expansion values based on the change of both core and surface temperature values were calculated using the linear expansion equation (3.3). The coefficient of thermal expansion for EN24T steel was taken as $12.3 \mu\text{m}/\text{m}^\circ\text{C}$ [84]. The original length of the workpiece was measured to be 120.1590 mm, the results are given in Figure 6.5 and Figure 6.6.

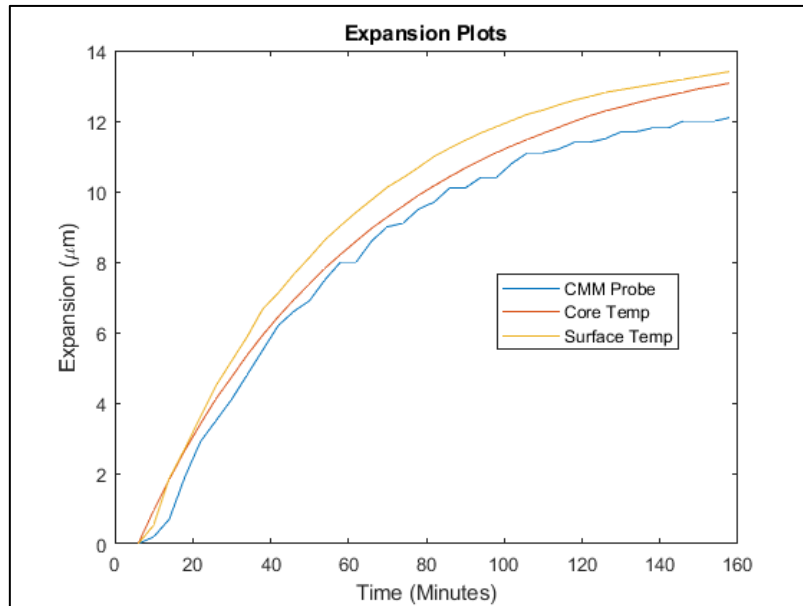


Figure 6.5: Part expansion

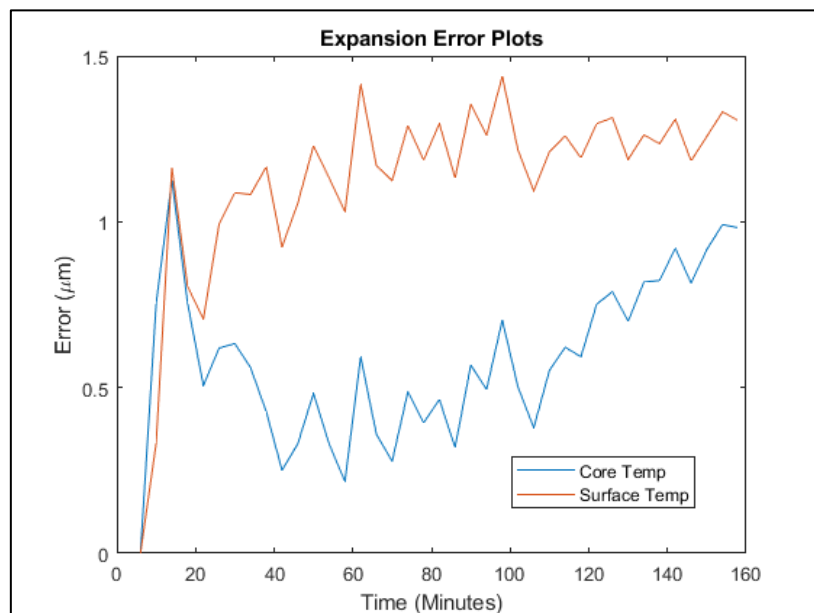


Figure 6.6: Error: Calculated vs measured.

The results show that the calculated expansion values based on the core temperature values are closer to the measured expansion when compared with the expansion values calculated from the surface temperature readings. The mean absolute error for the expansion calculation based on the core temperature is $0.58\text{ }\mu\text{m}$ while for the surface temperature is $1.1\text{ }\mu\text{m}$. The average error from the surface reading is approximately twice the error from the core temperature readings.

6.2 Ultrasonic Thermometry on Aluminium

In all the previously described ultrasonic thermometry experiments in this thesis, steel was used as the propagation medium. To find out if the created ultrasonic thermometry method can be used on other materials, an experiment was set up using aluminium as the medium of propagation. Aluminium was chosen because of its prevalence in manufacturing processes. Apart from the aluminium workpiece, this experiment was set up with the same devices and equipment used for the controlled heating experiments (This setup is described in section 4.1.2). The experiment was carried out over five trials to find out if it is repeatable. Aluminium 5080 was chosen as the workpiece because of its prevalence in manufacturing and availability. The aluminium workpiece is shown in Figure 6.7.

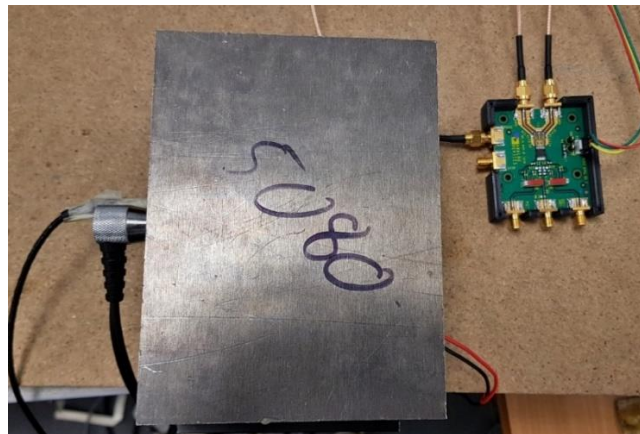


Figure 6.7: Aluminium propagation medium

The temperature values during the heating and cooling of the aluminium part were recorded.

The results of the experiments are given in in Figure 6.8, Figure 6.9 and Table 6.1.

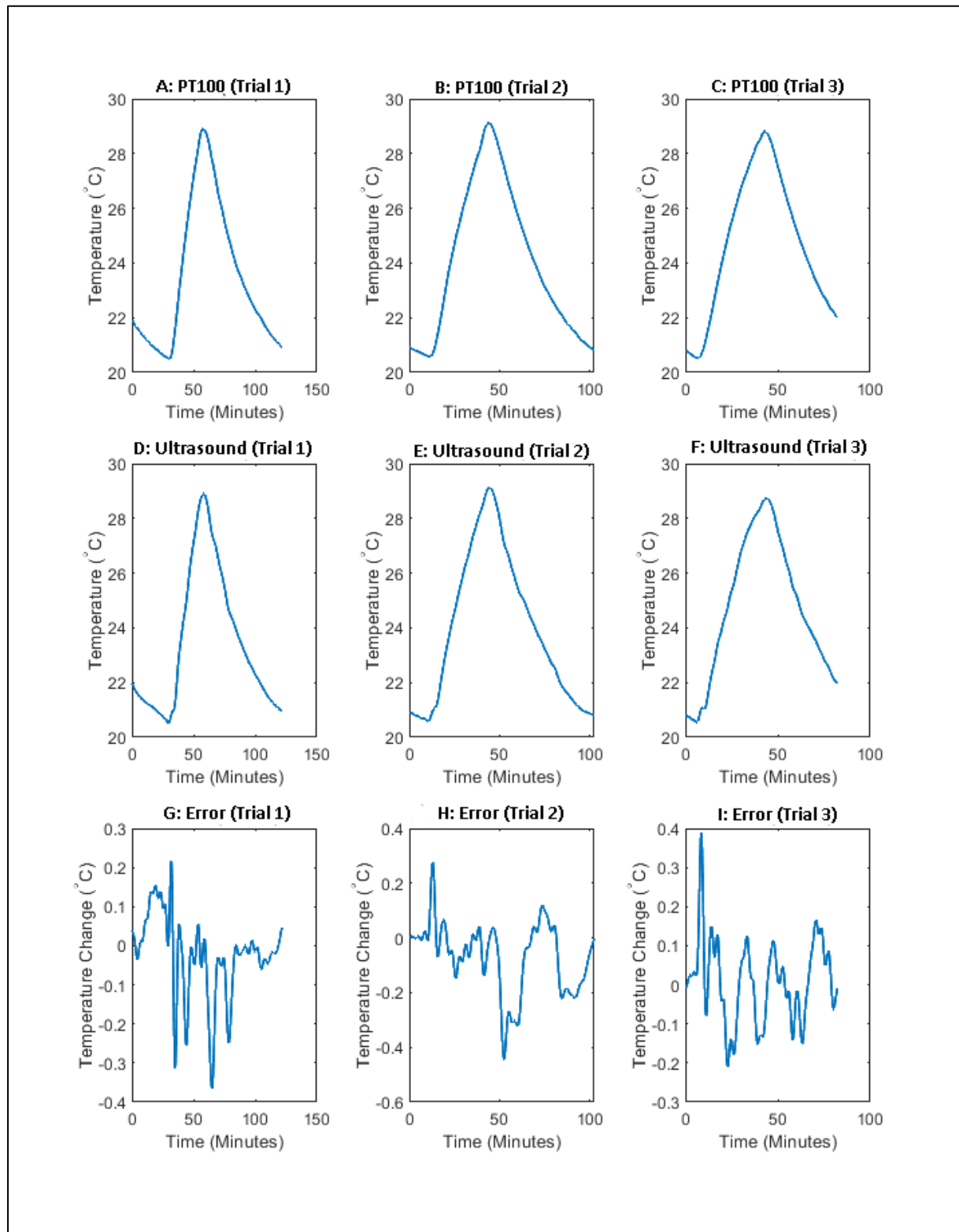


Figure 6.8: Results of ultrasonic thermometry on aluminium trials 1-3

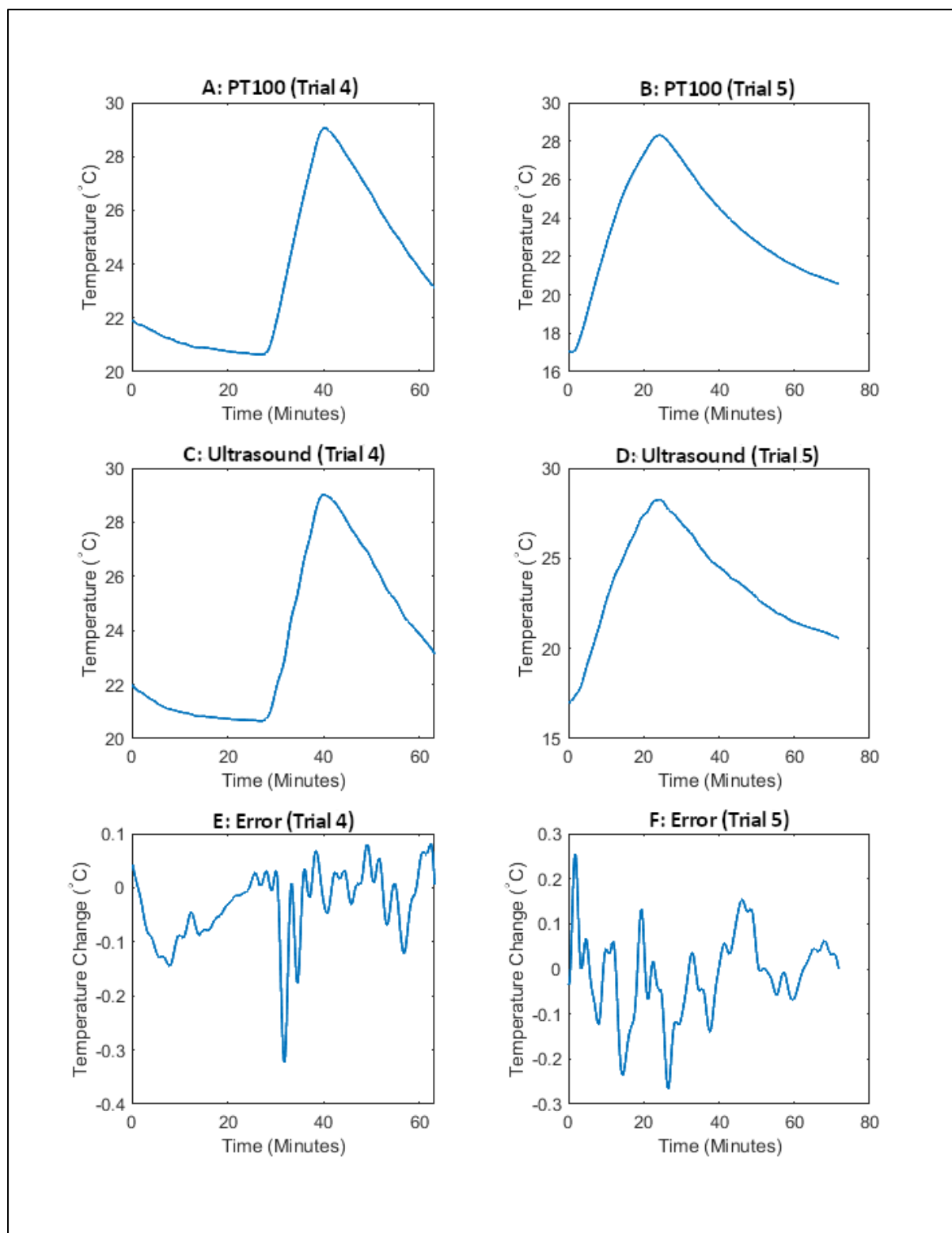


Figure 6.9: Results of ultrasonic thermometry on aluminium (trials 3-4)

Table 6.1: Aluminium trial errors

Cutting Trial #	Unfiltered Results		Filtered Results	
	Error Range (°C)	Standard Deviation (°C)	Error Range (°C)	Standard Deviation (°C)
1	-0.3752/+0.2361	0.1081	-0.3650/+0.2163	0.1068
2	-0.4588/+0.2754	0.1298	-0.4420/+0.2767	0.1286
3	-0.2118/+0.3818	0.1068	-0.2087/+0.3891	0.1058
4	-0.3315/+0.1372	0.0695	-0.3236/+0.0815	0.0678
5	-0.2515/+0.2905	0.0981	-0.2665/+0.2565	0.0914

The results show that the ultrasonic thermometry method measures the core temperature of aluminium with deviations of less than 0.45 °C from the reference temperature readings in all the trials. The results also show high repeatability with the standard deviations values below 0.13 °C.

6.3 Summary

In this chapter, an experiment was carried out on the CMM to study the relationship between surface and core temperature and the expansion of the material. The core temperature of the workpiece was measured using an ultrasonic transducer with PT100 as reference. The surface temperature was measured with the temperature sensor on the CMM. Expansion of the part was measured with the CMM probe and compared with the calculated values based on the core and surface temperature values. The results show that the core temperature values predicted the expansion with mean absolute error of 0.58 µm while the surface temperature had a mean absolute error of 1.1 µm.

To study ultrasonic thermometry in another material different from steel, aluminium 5080 was used for an ultrasonic thermometry experiment. The aluminium part was heated up to get a temperature rise of 10 °C. The temperature of the part was recorded during the heating and

cooling cycles. The results of the experiment show that ultrasonic measurement agree with PT100 readings with standard deviation of approximately 0.1 °C and all errors within the range of ± 0.5 °C. The conclusion and summary of key findings from the thesis will be presented in Chapter 7.

Chapter 7

7 Conclusions and Suggestions for Future Research

In this chapter, the conclusions and suggestions for future research will be discussed.

7.1 Conclusions

The aim of this research is to create a novel temperature measurement system that measures the core workpiece temperature with accuracy and resolution that satisfy the requirements for precision manufacturing. To achieve this, the following were carried out.

Existing temperature measurement methods used during metal cutting processes were reviewed. From all the reviewed methods, none has been applied to core temperature measurement of metals during manufacturing. Based on the findings from the literature review, ultrasound was chosen for further analysis.

Ultrasonic simulations were performed in MATLAB to determine the suitability of ultrasound for core temperature measurement of metals. The k-Wave toolbox was redesigned for use as pulse-echo and phase-shift ultrasonic thermometry simulation tools. From the simulation results, it was found that the required resolution can be achieved with both techniques. However, upon review of the devices needed for the actual use of the techniques, the phase-shift method was found to be a more cost-effective method than the pulse-echo method. A simulation was also carried out to study the individual effects of ultrasonic velocity and part expansion on the time-of-flight. The result showed that the time-of-flight largely depends on the ultrasonic velocity.

A methodology was created for the use of the phase-shift method for temperature measurement. The created ultrasonic phase-shift thermometry system was tested in the laboratory with steel EN24T workpiece being the medium of ultrasonic propagation. The system was first tested with a 15 mm workpiece and thereafter a 100 mm workpiece. The results show that the created system measures core temperature with resolution of 0.1 °C.

After the bench tests, the setup was tested on the CNC. The method adopted was to progressively increase the number of uncertainties to the measurement system and study their individual effects on the measurement results. Measurements were taken with the CNC switched on but left in the static position. The results show that the ultrasonic thermometry measured the core temperature of the workpiece with good agreement with the reference temperature measurement. This experiment was then repeated over an extended period. The results show that the readings were stable over time.

After the static tests, two tests were carried out while the spindle of the CNC were running. The first was for a 1000 rpm speed and the second for a 5000 rpm spindle speed. Both tests had errors within ± 0.02 °C. A cutting fluid test was also carried out and the results showed that the presence of coolant reduced the accuracy of the measurement, however the setup was still able to obtain the workpiece temperature with errors within ± 0.1 °C.

Dry cutting trials were carried out with a 1 MHz transducer to get more range of temperature measurement. The results show that the ultrasonic thermometry system measures core temperature of workpiece with standard deviations of 0.1 °C. A wet cutting test was also carried out and although the error range increased relative to the range of measurement due to the inconsistent boundary formed by the cutting fluid with the workpiece, the standard deviations were less than 0.4 °C.

To study the effects of both core and surface temperature variations on workpieces, an expansion experiment was performed on a CMM. Ultrasonic transducer and PT100 were used to measure core temperature of a workpiece. The on-CMM temperature detector was used to measure the surface temperature and the CMM probe was used to measure the expansion of the part. The measured temperature values were used to calculate the expansion of the part. The results of the experiment show that the mean absolute error of the calculated expansion from the surface temperature values is 0.52 μm more than the error from the core temperature measurement.

Finally, an experiment was carried out to find out if the created system will work on other materials apart from steel. Aluminium was used as the medium of transmission. The results show high repeatability with the standard deviations approximately equal to 0.1 $^{\circ}\text{C}$.

7.1.1 Summary of the Key Findings

- Ultrasonic phase-shift technique offers a more cost-effective solution to core temperature measurement of metals during manufacturing than the pulse-echo method.
- Time-of-flight of ultrasonic wave is influenced mostly by the ultrasonic velocity with some influence from material expansion.
- An ultrasonic phase-shift system that measures core temperature of steel with accuracy of ± 1 $^{\circ}\text{C}$ and a resolution of better than 0.5 $^{\circ}\text{C}$ was created. The setup was also tested for aluminium and the measurement errors were within ± 0.5 $^{\circ}\text{C}$.
- The created ultrasonic phase-shift system works during subtractive manufacturing processes.
- The CMM experiment show that the mean absolute error of the calculated expansion from the surface temperature values is 0.52 μm more than the error from the core

temperature measurement. This is particularly significant due to growing decrease in tolerances as the CMM capability improves. The created method can reduce uncertainty even in the relatively small part tested and will be even more effective in larger components with the potential for greater gradients.

- The presence of cutting fluid during ultrasonic thermometry reduces the accuracy of the measurement results when the conventional dual element ultrasonic transducer is used.

7.1.2 Contributions to Knowledge

- Creation of a new method for precision core temperature measurement of metals using an ultrasonic phase-shift method: Previous temperature measurement methods used in manufacturing applications have only been used to measure the surface temperature of workpieces, the created method measures the core temperature of metals which represent the temperature of the material volume better than the surface temperature.
- Creation of MATLAB tools to simulate ultrasonic pulse-echo and phase-shift thermometry measurements: The k-Wave toolbox used for the simulations was not primarily designed for temperature measurement simulations. This toolbox was modified for use as pulse-echo and phase-shift thermometry simulation tool. This was achieved with the peak detection technique for pulse-echo and Hilbert transform for phase-shift simulations.
- Comparison of the effects of change in ultrasonic velocity and material dimension (expansion) on ultrasonic time-of-flight: Using the created simulation tool, the individual effects of ultrasonic velocity and expansion on ultrasonic time-of-flight was

quantified. This provides useful knowledge on the characteristics of ultrasonic waves in a medium of changing temperature.

- Evaluation of the suitability of phase-shift technique and pulse-echo technique for temperature measurement applications during manufacturing processes: With the created simulation tool, the two main ultrasonic techniques were evaluated for their suitability for the manufacturing processes. The phase-shift method was found to be more suitable for the intended application.
- Amplification of ultrasonic echo signals using high speed amplifier for phase-shift measurements.
- Application of core temperature measurement on coordinate measuring machines to reduce uncertainty during dimensional inspection: Using the ultrasonic thermometry method, it was shown that the core temperature of materials can be used to predict the material's expansion with higher accuracy than the surface temperature.
- Creation of a functional method for ultrasonic transducer coupling in manufacturing environment.

7.2 Avenues for Future Research

1. Increased range of measurement

In this research, the workpiece used was a 120 mm length steel. Some manufacturing applications require measurements to be carried out on larger parts which is not used in this thesis. To increase the range of measurement, multiple frequency continuous wave ultrasonic phase-shift method can be used to determine absolute temperature at ranges beyond those used in this research. This can also be of use in applications where high temperature variations are expected. Another way of achieving increased range of

measurement is with frequency switching algorithm which can be created to maintain the phase difference reading at the linear range of the AD8302 board by changing the signal frequency. For this, a wideband ultrasonic transducer should be used to accommodate changing frequencies.

2. Transducer coupling mechanism

In this research, epoxy was used for coupling the ultrasonic transducer to the workpiece. Because of the time epoxy bond needs to properly set, a measurement task cannot be carried out instantaneously. To aid a faster measurement process, a quick-release coupling mechanism can be created for use with the ultrasonic transducer and workpiece bonding. This will reduce the risk of damage to the transducers and provide more efficient use in actual manufacturing processes. Also, the effect of different couplants and their mode of application can be studied.

3. Ultrasonic thermometry on complex shapes

One of the limitations of the method used is the simple rectangular block. In a realistic manufacturing scenario, there may be a need to use more complex shapes. This will require calibration of the measurement system and possibly an adaptation of the system. This is also useful in processes where the path length of the ultrasonic wave may change over time.

4. Ultrasonic thermometry for elevated temperature

The scope of this research was limited to temperature measurement below 50 °C. The created ultrasonic thermometry system could be tested at elevated temperature. This test will require custom made transducers able to handle very high temperature.

5. Transducers for measurements during wet cutting processes

The results of the wet cutting trials show that there was reduction of the measurement accuracy. With the use of transducers adapted for liquid environments, more tests can be carried out to find out if the accuracy in a wet cutting process will increase.

References

- 1 O. İynen, A. Şahinoğlu, M. Özdemir, and V. Yilmaz, “Investigation of the Effect of Cutting Parameters on the Surface Roughness Value in the Machining of AISI 4140 Steel with Taquchi Method,” *J. Inst. Sci. Technol.*, vol. 10, no. 4, pp. 2840–2849, 2020.
- 2 O. Özbek and H. Saruhan, “The effect of vibration and cutting zone temperature on surface roughness and tool wear in eco-friendly MQL turning of AISI D2,” *J. Mater. Res. Technol.*, vol. 9, no. 3, pp. 2762–2772, 2020.
- 3 G. C. Verma, P. M. Pandey, and U. S. Dixit, “Estimation of workpiece-temperature during ultrasonic-vibration assisted milling considering acoustic softening,” *Int. J. Mech. Sci.*, vol. 140, no. January, pp. 547–556, 2018.
- 4 E. Mirkoohi, P. Bocchini, and S. Y. Liang, “Analytical temperature predictive modeling and non-linear optimization in machining,” *Int. J. Adv. Manuf. Technol.*, vol. 102, no. 5–8, pp. 1557–1566, 2019.
- 5 L. Chen *et al.*, “Core temperature estimation based on electro-thermal model of lithium-ion batteries,” *Int. J. Energy Res.*, vol. 44, no. 7, pp. 5320–5333, 2020.
- 6 N. S. Mian, S. Fletcher, and A. P. Longstaff, “Reducing the latency between machining and measurement using FEA to predict thermal transient effects on CMM measurement,” *Meas. J. Int. Meas. Confed.*, vol. 135, pp. 260–277, 2019.
- 7 J. Li *et al.*, “Study on the Effect of Coupling Materials on the Ultrasonic Signals Detection of Partial Discharge,” *IOP Conf. Ser. Earth Environ. Sci.*, vol. 440, no. 3, 2020.
- 8 S. Kocis and Z. Figura, “Ultrasonic measurements and technologies ,” vol. 4. Chapman & Hall , London , 1996.

- 9 M. Dobosz and M. Ściuba, “Ultrasonic measurement of air temperature along the axis of a laser beam during interferometric measurement of length,” *Meas. Sci. Technol.*, vol. 31, no. 4, 2020.
- 10 I. Ihara and M. Takahashi, “A novel ultrasonic thermometry for monitoring temperature profiles in materials,” *19th IMEKO World Congr. 2009*, vol. 3, pp. 1635–1639, 2009.
- 11 R. Queirós, R. C. Martins, P. S. Girão, and a C. Serra, “A New Method for High Resolution Ultrasonic Ranging in Air,” *Xviii Imeko World Congr.*, pp. 1–4, 2006.
- 12 M. Mareš, O. Horejš, and L. Havlík, “Thermal error compensation of a 5-axis machine tool using indigenous temperature sensors and CNC integrated Python code validated with a machined test piece,” *Precis. Eng.*, vol. 66, no. July, pp. 21–30, 2020.
- 13 T. Kizaki, K. Takahashi, T. Katsuma, J. Tanaka, L. Shu, and N. Sugita, “Effect of grinding fluid supply on workpiece temperature in continuous generating grinding,” *J. Manuf. Process.*, vol. 60, no. September, pp. 410–417, 2020.
- 14 M. Holub, O. Andrs, J. Kovar, and J. Vetiska, “Effect of position of temperature sensors on the resulting volumetric accuracy of the machine tool,” *Meas. J. Int. Meas. Confed.*, vol. 150, p. 107074, 2020.
- 15 A. S. Morris, *Measurement and instrumentation principles*. Butterworth-Heinemann, 2001.
- 16 P. R. N. Childs, J. R. Greenwood, C. A. Long, P. R. N. Childs, J. R. Greenwood, and C. A. Long, “Review of temperature measurement,” *Rev. Sci. Instrum.*, vol. 71, no. 8, 2000.
- 17 S. Li *et al.*, “Physical sensors for skin-inspired electronics,” *InfoMat*, vol. 2, no. 1, pp. 184–211, 2019.
- 18 J. P. Bentley, “Temperature Sensor Characteristics and Measurement System Design,”

- J Phys E*, vol. 17, pp. 430–443, 1984.
- 19 R. L. Rusby, “Introduction to temperature measurement,” *Meas. Good Pract. Guid. No. 125*, no. 125, 2015.
 - 20 K. Technologies, “Practical Temperature Measurements - Application Note,” *Keysight Technologies*, 2017. .
 - 21 P. R. N. Childs, *Practical temperature measurement*. Oxford: Butterworth-Heinemann, 2001.
 - 22 J. Daw, J. Rempe, S. Taylor, J. Crepeau, and S. C. Wilkins, “Ultrasonic thermometry for in-pile temperature detection,” *7th Int. Top. Meet. Nucl. Plant Instrumentation, Control. Human-Machine Interface Technol. 2010, NPIC HMIT 2010*, vol. 2, pp. 764–774, 2010.
 - 23 J. Williams and O. Sanchez-Felipe, *An introduction to acoustic thermometry: An air filled olive jar teaches signal conditioning*. Elsevier Inc., 2013.
 - 24 Olympus NDT, “Ultrasonic transducers technical notes,” *Technical brochure: Olympus NDT, Waltham, MA*. pp. 39–49, 2006.
 - 25 M. Bacci da Silva and J. Wallbank, “Cutting temperature: prediction and measurement methods—a review,” *J. Mater. Process. Technol.*, vol. 88, no. 1–3, pp. 195–202, 1999.
 - 26 E. G. Herbert, “The measurement of cutting temperatures,” *Proc. Inst. Mech. Engrs*, vol. 110, no. September 1925, pp. 289–329, 1926.
 - 27 N. Dhar, S. Islam, M. Kamruzzaman, and T. Ahmed, “The Calibration of Tool-Work Thermocouple in Turning Steels,” in *Proceedings of National Conference on Industrial Problems on Machines and Mechanisms (IPROMM-2005)*, 2005.

- 28 M. C. Santos, J. S. Araújo Filho, M. A. S. Barrozo, M. J. Jackson, and A. R. Machado, “Development and application of a temperature measurement device using the tool-workpiece thermocouple method in turning at high cutting speeds,” *Int. J. Adv. Manuf. Technol.*, vol. 89, no. 5–8, pp. 2287–2298, 2017.
- 29 C. W. Wu, C. H. Tang, C. F. Chang, and Y. S. Shiao, “Thermal error compensation method for machine center,” *Int. J. Adv. Manuf. Technol.*, vol. 59, no. 5–8, pp. 681–689, 2012.
- 30 J. A. Ramirez-Nunez, M. Trejo-Hernandez, R. J. Romero-Troncoso, G. Herrera-Ruiz, and R. A. Osornio-Rios, “Smart-sensor for tool-breakage detection in milling process under dry and wet conditions based on infrared thermography,” *Int. J. Adv. Manuf. Technol.*, vol. 97, no. 5–8, pp. 1753–1765, 2018.
- 31 U. National Physical Laboratory, “Reliable harsh environment thermometry,” *Temperature and Humidity*, 2020. [Online]. Available: <https://www.npl.co.uk/temperature-humidity/harsh-environment-thermometry>. [Accessed: 27-Apr-2021].
- 32 T. Cai *et al.*, “Phosphorescence-Based Flexible and Transparent Optical Temperature-Sensing Skin Capable of Operating in Extreme Environments,” *ACS Appl. Polym. Mater.*, Apr. 2021.
- 33 N. Arunkumar, A. Thanikasalam, V. Sankaranarayanan, and E. Senthilkumar, “Parametric optimization of deep-hole drilling on AISI 1045 steel and online tool condition monitoring using an accelerometer,” *Mater. Manuf. Process.*, vol. 33, no. 16, pp. 1751–1764, 2018.
- 34 M. Takahashi and I. Ihara, “Ultrasonic monitoring of internal temperature distribution in a heated material,” *Jpn. J. Appl. Phys.*, vol. 47, no. 5 PART 2, pp. 3894–3898, 2008.

- 35 S. W. Rienstra and A. Hirschberg, “An introduction to acoustics,” *Eindhoven Univ. Technol.*, vol. 18, 2004.
- 36 C. Meola, *Recent Advances in Non-Destructive Inspection*. New York, UNITED STATES: Nova Science Publishers, Incorporated, 2010.
- 37 L. Koval, J. Vaňuš, and P. Bilík, “Distance Measuring by Ultrasonic Sensor,” *IFAC-PapersOnLine*, vol. 49, no. 25, pp. 153–158, 2016.
- 38 S. L. Hill, B. Bury, and J. O. Gray, “A Multifrequency AM-Based Ultrasonic System for Accuracy Distance Measurement,” *IEEE Trans. Instrum. Meas.*, vol. 43, no. 6, pp. 861–866, 1994.
- 39 F. E. Gueuning, M. Varlan, C. E. Eugène, and P. Dupuis, “Accurate distance measurement by an autonomous ultrasonic system combining time-of-flight and phase-shift methods,” *IEEE Trans. Instrum. Meas.*, vol. 46, no. 6, pp. 1236–1240, 1997.
- 40 Y. P. Huang, J. S. Wang, K. N. Huang, C. T. Ho, J. D. Huang, and M. S. Young, “Envelope pulsed ultrasonic distance measurement system based upon amplitude modulation and phase modulation,” *Rev. Sci. Instrum.*, vol. 78, no. 6, pp. 1–8, 2007.
- 41 D. Webster, “A Pulsed Ultrasonic Distance Measurement System based upon Phase Digitizing,” *Instrumentation*, vol. 43, no. 4, pp. 578–582, 1994.
- 42 R. S. C. Cobbold, *Foundations of biomedical ultrasound*. Oxford university press, 2006.
- 43 D. Dalecki, “Mechanical bioeffects of ultrasound,” *Annu. Rev. Biomed. Eng.*, vol. 6, pp. 229–248, 2004.
- 44 G. Ter Haar, “Therapeutic applications of ultrasound,” *Prog. Biophys. Mol. Biol.*, vol. 93, no. 1–3, pp. 111–129, 2007.

- 45 T. J. Mason, "Ultrasound in synthetic organic chemistry," *Chem. Soc. Rev.*, vol. 26, no. 6, pp. 443–451, 1997.
- 46 K. Hodgson, R. S. Dwyer-Joyce, and B. W. Drinkwater, "Ultrasound as an experimental tool for investigating engineering contacts," *Tribologia*, vol. 19, no. 4, pp. 9–17, 2000.
- 47 W. Y. Tsai, H. C. Chen, and T. L. Liao, "High accuracy ultrasonic air temperature measurement using multi-frequency continuous wave," *Sensors Actuators, A Phys.*, vol. 132, no. 2, pp. 526–532, 2006.
- 48 W.-Y. Tsai, H.-C. Chen, and T.-L. Liao, "An ultrasonic air temperature measurement system with self-correction function for humidity," *Meas. Sci. Technol.*, vol. 16, no. 2, p. 548, 2005.
- 49 K. N. Huang, C. F. Huang, Y. C. Li, and M. S. Young, "High precision, fast ultrasonic thermometer based on measurement of the speed of sound in air," *Rev. Sci. Instrum.*, vol. 73, no. 11, p. 4022, 2002.
- 50 M. Pernot, M. Tanter, J. Bercoff, K. R. Waters, and M. Fink, "Temperature estimation using ultrasonic spatial compound imaging," *IEEE Trans. Ultrason. Ferroelectr. Freq. Control*, vol. 51, no. 5, pp. 606–615, May 2004.
- 51 C. Zhou, Y. Wang, C. Qiao, S. Zhao, and Z. Huang, "High-accuracy ultrasonic temperature measurement based on MLS-modulated continuous wave," *Measurement*, vol. 88, pp. 1–8, 2016.
- 52 I. Ihara and M. Takahashi, "A New Method for Internal Temperature Profile Measurement by Ultrasound," in *2007 IEEE Instrumentation Measurement Technology Conference IMTC 2007*, 2007, pp. 1–5.
- 53 Y. Wei, Y. Gao, Z. Xiao, G. Wang, M. Tian, and H. Liang, "Ultrasonic Al₂O₃ ceramic

- thermometry in high-temperature oxidation environment,” *Sensors (Switzerland)*, vol. 16, no. 11, pp. 1–10, 2016.
- 54 L. Iglesias, P. Shanmugam, J.-F. Michaud, D. Alquier, D. Certon, and I. Dufour, “CMUT Time of Flight Gas Sensor By Phase Shift Measurement,” in *ECS Meeting Abstracts*, 2020, no. 31, p. 2323.
 - 55 C. F. Huang, M. S. Young, and Y. C. Li, “Multiple-frequency continuous wave ultrasonic system for accurate distance measurement,” *Rev. Sci. Instrum.*, vol. 70, no. 2, pp. 1452–1458, 1999.
 - 56 M. Abdelmejeed, J. C. Kuo, and A. Lal, “A CMOS compatible GHz ultrasonic pulse phase shift based temperature sensor,” *Proc. IEEE Int. Conf. Micro Electro Mech. Syst.*, vol. 2018-Janua, no. January, pp. 1108–1111, 2018.
 - 57 B. Barshan, “Fast processing techniques for accurate ultrasonic range measurements,” *Meas. Sci. Technol.*, vol. 11, no. 1, pp. 45–50, 2000.
 - 58 K. N. Huang and Y. P. Huang, “Multiple-frequency ultrasonic distance measurement using direct digital frequency synthesizers,” *Sensors Actuators, A Phys.*, vol. 149, no. 1, pp. 42–50, 2009.
 - 59 D. Rodríguez, A. Jiménez, R. Pérez, L. Leija, A. Vera, and E. Moreno, “A microprocessor-based system for pulse-echo overlap measurement of ultrasonic velocity,” *2nd Int. Conf. Electr. Electron. Eng. ICEEE XI Conf. Electr. Eng. CIE 2005*, vol. 2005, no. Cie, pp. 140–143, 2005.
 - 60 C. Pantea *et al.*, “Digital ultrasonic pulse-echo overlap system and algorithm for unambiguous determination of pulse transit time,” *Rev. Sci. Instrum.*, vol. 76, no. 11, pp. 1–9, 2005.

- 61 H. J. McSkimin, "Pulse Superposition Method for Measuring Ultrasonic Wave Velocities in Solids," *J. Acoust. Soc. Am.*, vol. 33, no. 1, pp. 12–16, 1961.
- 62 A. Manbachi and R. S. C. Cobbold, "Development and application of piezoelectric materials for ultrasound generation and detection," *Ultrasound*, vol. 19, no. 4, pp. 187–196, 2011.
- 63 A. Abdullah, M. Shahini, and A. Pak, "An approach to design a high power piezoelectric ultrasonic transducer," *J. Electroceramics*, vol. 22, no. 4, pp. 369–382, 2009.
- 64 C. Fei *et al.*, "Ultrahigh frequency (100 MHz-300 MHz) ultrasonic transducers for optical resolution medical imaging," *Sci. Rep.*, vol. 6, no. June, pp. 1–8, 2016.
- 65 NDT Resource Center, "Transducer Types." [Online]. Available: <https://www.nde-ed.org/EducationResources/CommunityCollege/Ultrasonics/EquipmentTrans/transducertypes.htm>. [Accessed: 17-Jul-2020].
- 66 K. Sharma, S. Singh, and P. K. Dubey, "Design of Low Cost Broadband Ultrasonic Pulser–Receiver," *Mapan - J. Metrol. Soc. India*, vol. 32, no. 2, pp. 95–100, 2017.
- 67 K. N. Huang, C. F. Huang, Y. C. Li, and M. S. Young, "Temperature measurement system based on ultrasonic phase-shift method," in *IEEE EMBS Asian-Pacific Conference on Biomedical Engineering, 2003.*, 2003, pp. 294–295.
- 68 P. Kumar, V. Kumar, and R. Pratap, "Design and implementation of phase detector on FPGA," *2017 6th Int. Conf. Comput. Appl. Electr. Eng. - Recent Adv. CERA 2017*, vol. 2018-Janua, pp. 108–110, 2018.
- 69 T. Reddyhoff, S. Kasolang, R. S. Dwyer-Joyce, and B. W. Drinkwater, "The phase shift of an ultrasonic pulse at an oil layer and determination of film thickness," *Proc. Inst. Mech. Eng. Part J J. Eng. Tribol.*, vol. 219, no. 6, pp. 387–400, 2005.

- 70 P. N. T. Wells and F. G. M. Ross, "A time-to-voltage cardiology," no. July, pp. 171–176, 1969.
- 71 Texas Instruments, "TDC7200 Time-to-Digital Converter for Time-of-Flight Applications in LIDAR, Magnetostrictive and Flow Meters," no. 1, p. 50, 2016.
- 72 F. Foucher, S. Mahaut, S. Chatillon, and A. Carnot, "An overview of validation campaigns of the CIVA simulation software 2 . Models implemented in the CIVA simulation platform," *12th ECNDT*, no. 1, pp. 1–9, 2018.
- 73 K. Jezzine, A. Imperiale, E. Demaldent, F. Le Bourdais, P. Calmon, and N. Dominguez, "Modeling approaches for the simulation of ultrasonic inspections of anisotropic composite structures in the CIVA software platform," *AIP Conf. Proc.*, vol. 1949, 2018.
- 74 B. Treeby, B. Cox, and J. Jaros, "k-Wave: A MATLAB toolbox for the time domain simulation of acoustic wave fields - User Manual," vol. 1. 2016.
- 75 E. Martin, J. Jaros, and B. E. Treeby, "Experimental validation of k-Wave: Nonlinear wave propagation in layered, absorbing fluid media," *IEEE Trans. Ultrason. Ferroelectr. Freq. Control*, vol. 67, no. 1, pp. 81–91, 2020.
- 76 D. Hladky and J. Mikulka, "Modeling the propagation of a modulated ultrasonic wave in a nonlinear medium," in *2017 Progress In Electromagnetics Research Symposium-Spring (PIERS)*, 2017, pp. 759–762.
- 77 S. Rooney and K. Pochiraju, "Simulations of Online Non-Destructive Acoustic Diagnosis of 3D-Printed Parts Using Air-Coupled Ultrasonic Transducers," in *ASME International Mechanical Engineering Congress and Exposition*, 2019, vol. 59377.
- 78 A. Coila and M. Oelze, "Nonlinearity parameter estimation based on quantifying excess ultrasonic attenuation," in *2020 IEEE International Ultrasonics Symposium (IUS)*, 2020,

pp. 1–4.

- 79 M. Semenova, G. Persson, and H. Wirdelius, “A 2D hybrid approach to model a complexed shaped defect in an ultrasonic inspection situation,” *Rev. Prog. Quant. Nondestruct. Eval.*, 2019.
- 80 D. Kurniadi and others, “Modelling and Simulation 3D Ultrasound Wave Propagation using k-space Pseudospectral Method in the Railway Track Geometry,” in *2019 6th International Conference on Instrumentation, Control, and Automation (ICA)*, 2019, pp. 153–157.
- 81 E. Bossy, “SimSonic Suite user’s guide for SimSonic2D.” Technical report, 2012.
- 82 F. Lingvall, “User Manual for the DREAM Toolbox: An ultrasound simulation software for use with Matlab and GNU Octave.” 2009.
- 83 J. A. Jensen, “User’s guide for the Field II program,” 2014.
- 84 Otai Special Steel, “AISI 4340 Steel | 36CrNiMo4 | 1.6511 | EN24 | 817M40 | SNCM439,” 2021. [Online]. Available: <https://www.astmsteel.com/product/4340-steel-aisi/#>. [Accessed: 21-Feb-2021].
- 85 F. R. Kschischang, “The Hilbert Transform.” The Edward S. Rogers Sr. Department of Electrical and Computer Engineering University of Toronto, pp. 1–12, 2006.
- 86 Y.-W. Liu, “Hilbert Transform and Applications,” *Fourier Transform Appl.*, no. April 2012, 2012.
- 87 MathWorks, “Hilbert Transform.” [Online]. Available: <https://uk.mathworks.com/help/signal/ug/hilbert-transform.html>. [Accessed: 14-Sep-2020].

- 88 P. Theobald, “Guide on Acoustic Emission Sensor Couplants,” *Natl. Phys. Lab. ,UK*, pp. 7–9, 2015.
- 89 ASTM E650 / E650M-17, “Standard Guide for Mounting Piezoelectric Acoustic Emission Sensors.” ASTM International, West Conshohocken, PA, 2017.
- 90 M. O. Culjat, R. S. Singh, S. N. White, R. R. Neurgaonkar, and E. R. Brown, “Evaluation of gallium-indium alloy as an acoustic couplant for high-impedance, high-frequency applications,” *Acoust. Res. Lett. Online*, vol. 6, no. 3, pp. 125–130, 2005.
- 91 K. Dugmore, D. Jonson, and M. Walker, “A comparison of signal consistency of common ultrasonic couplants used in the inspection of composite structures,” *Compos. Struct.*, vol. 58, no. 4, pp. 601–603, 2002.
- 92 S. Colombo, M. Forde, O. Das, and J. Halliday, “AE experiments on concrete beams: general overview and research in progress on bridges,” in *Ninth International Conference on Structural Faults and Repair*, 2001.
- 93 S. Colombo, “Feasibility study of the application of the acoustic emission technique to concrete bridges,” The University of Edinburgh, 2003.
- 94 S. Colombo, A. Giannopoulos, M. C. Forde, R. Hasson, and J. Mulholland, “Frequency response of different couplant materials for mounting transducers,” *NDT E Int.*, vol. 38, no. 3, pp. 187–193, 2005.
- 95 K. T. Son and C. C. Lee, “Bonding and impedance matching of acoustic transducers using silver epoxy,” *Ultrasonics*, vol. 52, no. 4, pp. 555–563, 2012.
- 96 K. Ono, “Through-Transmission Characteristics of AE Sensor Couplants,” *J. Acoust. Emiss.*, vol. 34, p. 1, 2017.
- 97 P. P. L. Regtien and E. Dertien, “Acoustic Sensors,” in *Sensors for mechatronics*, 2nd

- ed., Elsevier, 2018, pp. 267–303.
- 98 H. J. Hilke, “Piezoelectric transducer vibrations in a one-dimensional approximation,” *Appl. Phys.*, vol. 1, no. 6, pp. 317–329, 1973.
 - 99 T. S. Ramotowski, “Method for improving acoustic impedance of epoxy resins.” Google Patents, 2012.
 - 100 Spectrum Instrumentation, “M2i.60xx - 14 bit 125 MS/s Arbitrary Waveform Generator,” 2019. [Online]. Available: https://spectrum-instrumentation.com/sites/default/files/download/m2i60_datasheet_english.pdf. [Accessed: 24-Sep-2019].
 - 101 Analog Devices, “LF–2.7 GHz RF/IF Gain and Phase Detector AD8302,” 2018. [Online]. Available: <https://www.analog.com/media/en/technical-documentation/data-sheets/ad8302.pdf>. [Accessed: 13-Aug-2020].
 - 102 Y. F. Yee and C. K. Chakrabarty, “Phase detection using AD8302 evaluation board in the superheterodyne microwave interferometer for line average plasma electron density measurements,” *Measurement*, vol. 40, no. 9–10, pp. 849–853, 2007.
 - 103 J. Cowles and B. Gilbert, “Accurate gain/phase measurement at radio frequencies up to 2.5 GHz,” *Analog Dialogue*, vol. 35, no. 05, pp. 1–4, 2001.
 - 104 E Instruments, “TCS 140 Instruction Manual.” .
 - 105 B. Carter, “Chapter 7 - Using Op Amps for Radio frequency Design,” in *Op Amps for Everyone (Fourth Edition)*, Fourth Edi., B. Carter, Ed. Boston: Newnes, 2013, pp. 105–118.
 - 106 Texas Instruments, “2-GHz, Low Distortion, Dual Current-Feedback Amplifiers THS3202,” pp. 1–26, 2010.

- 107 Analog Devices, “Evaluation Board User Guide UG-128.” pp. 1–8, 2000.
- 108 K. K. Gajrani and M. R. Sankar, “Sustainable Cutting Fluids: Thermal, Rheological, Biodegradation, Anti-Corrosion, Storage Stability Studies and its Machining Performance,” in *Encyclopedia of Renewable and Sustainable Materials*, S. Hashmi and I. A. Choudhury, Eds. Oxford: Elsevier, 2020, pp. 839–852.
- 109 Quaker, “QUAKERCOOL 7101 BFF Safety Data Sheet.” 2018.

Appendix A

MATLAB Code and Results for the Pulse-Echo Thermometry Simulation

```
% =====
% NOTE:
% This script computes time of flight of ultrasonic wave through
% the material for the specified length, temperature, speed and density.
% Visualization of simulation as well as plot of result are then generated.

% Functions kWaveGrid,toneBurst,kspaceFirstOrder1D are provided in the
% k-Wave MATLAB toolbox and are called from this script.
% =====
% SIMULATION
% =====
clearvars;

%Getting user input for temperature

sampling_data = zeros(7,6); % creates array for storing tof results
j=1; %used for array index
k = 5; % passed to simulate function to represent sampling frequency

% For loop for calling the 'simulate' function
for temp = 25:0.1:25.5
    duration = simulate(k,temp);
    sampling_data(j,1) = temp;
    sampling_data(j,2) = str2double(duration);
    j=j+1;
end

% The simulate function computes the time of flight and plots the results.
function duration = simulate(Factor,Temp)

% Create the computational grid
Nx = 7.776e+03; % number of grid points in the x (row) direction
dx = 1.023e-04; % grid point spacing in the x direction [m]
kgrid = kWaveGrid(Nx, dx);

% Material length
Length = 200;

% Estimates Coordinates
cv = 1000;
p1 = round(299/(dx*cv));
p2 = round(300/(dx*cv));
p3 = round((Length+300)/(dx*cv));

% Defines the properties of the propagation medium
medium.sound_speed = 3070 * ones(Nx, 1); % [sound speed in epoxy m/s]
medium.sound_speed(p2:p3) = ...
    ((-0.636*Temp)+5917.6); % [sound speed in steel m/s]
medium.density = 1800 * ones(Nx, 1); % [Density of epoxy kg/m^3]
medium.density(p2:p3) = 8030; % [Density of steel kg/m^3]

%Creates time array
dt = (1/Factor)*1e-9;
t_end = 100e-6;
kgrid.t_array = 0:dt:t_end;
```



```

% Defines a tone burst
source.p_mask = zeros(Nx,1);
source.p_mask(p1) =1;
sampling_freq = Factor*1e9;           % [Hz]
tone_burst_freq = 5e6;                % [Hz]
tone_burst_cycles = 1;
source.p = toneBurst(sampling_freq, tone_burst_freq, tone_burst_cycles);

%Create a sensor mask
sensor.mask = zeros(Nx,1);
sensor.mask(p2) = 1; %First sensor at 25mm
sensor.mask(p3) = 1; %Second sensor at 225mm (200mm length)

% Runs the simulation
display_mask = source.p_mask +sensor.mask;
sensor_data = kspaceFirstOrder1D(kgrid, medium,source,sensor,...
'DisplayMask',display_mask,'RecordMovie',false);

% =====
% VISUALISATION
% =====

% Plots the recorded time signals
figure;
plot(kgrid.t_array*1e6, sensor_data(1, :), 'b-');
hold on;
plot(kgrid.t_array*1e6, sensor_data(2, :), 'r-');
xlabel('Time [\mus]');
ylabel('Amplitude (arb. unit)');
legend('Sensor Position 1', 'Sensor Position 2');
title('Recorded Tone Burst');
set(gca,'Xtick',0:10:150)

% Finds peaks of signals on both sensors to calculate time of flight
% Re-assigns values to x, y1 and y2
x = kgrid.t_array*1e6;
y1 = sensor_data(1, :);
y2 = sensor_data(2, :);

% Finds the max for sensor 1
sensor_1_peak = find(max(y1) == y1);
x_peak_1 = x(sensor_1_peak);
y_peak_1 = y1(sensor_1_peak);
max1 = ['\leftarrow',num2str(x_peak_1),' \mus'];
text(x_peak_1,y_peak_1,max1);

% Finds the max for sensor 2
sensor_2_peak = find(max(y2) == y2);
x_peak_2 = x(sensor_2_peak);
y_peak_2 = y2(sensor_2_peak);
max2 = ['\leftarrow',num2str(x_peak_2),' \mus'];
text(x_peak_2,y_peak_2,max2);

% Calculates time of flight
tof = x_peak_2 - x_peak_1;
tof_txt = {'Time of flight = ',num2str(tof), ' \mus'},{'@ Temp '...
,num2str(Temp),'\circC'};
text(30,(min(sensor_data(1,:))),tof_txt)
duration = num2str(tof);
end

```

Running k-Wave simulation...

start time: 22-Jun-2021 20:29:50

reference sound speed: 5901.7m/s

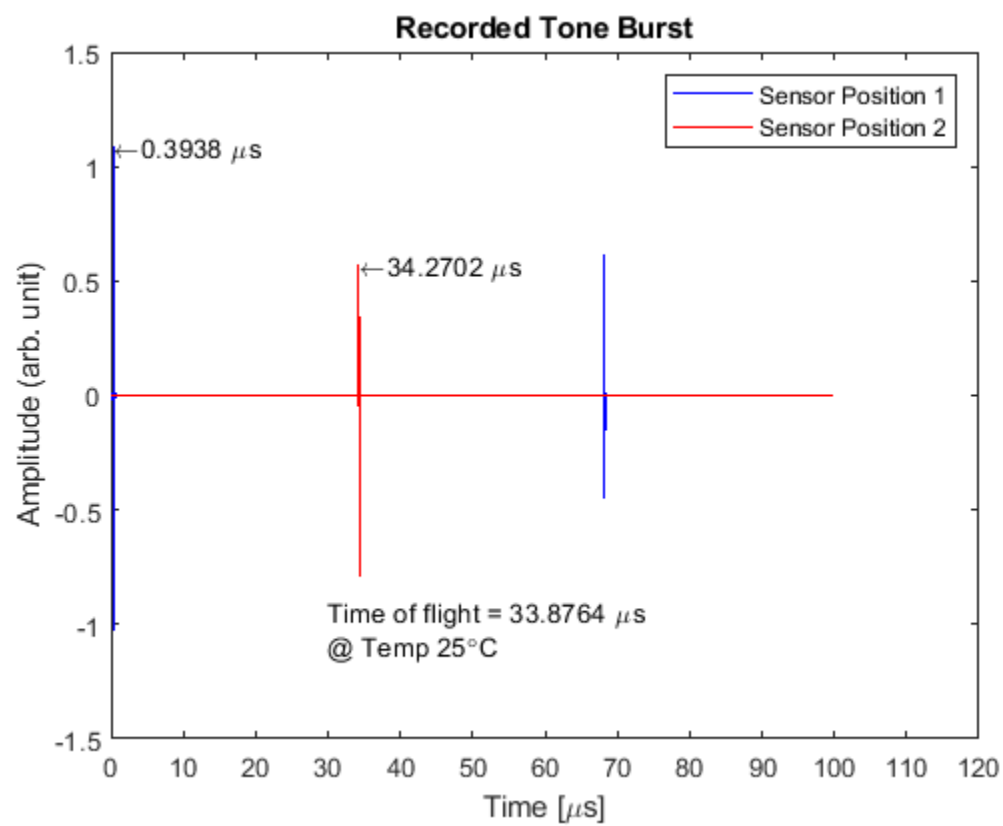
dt: 200ps, t_end: 100us, time steps: 500001

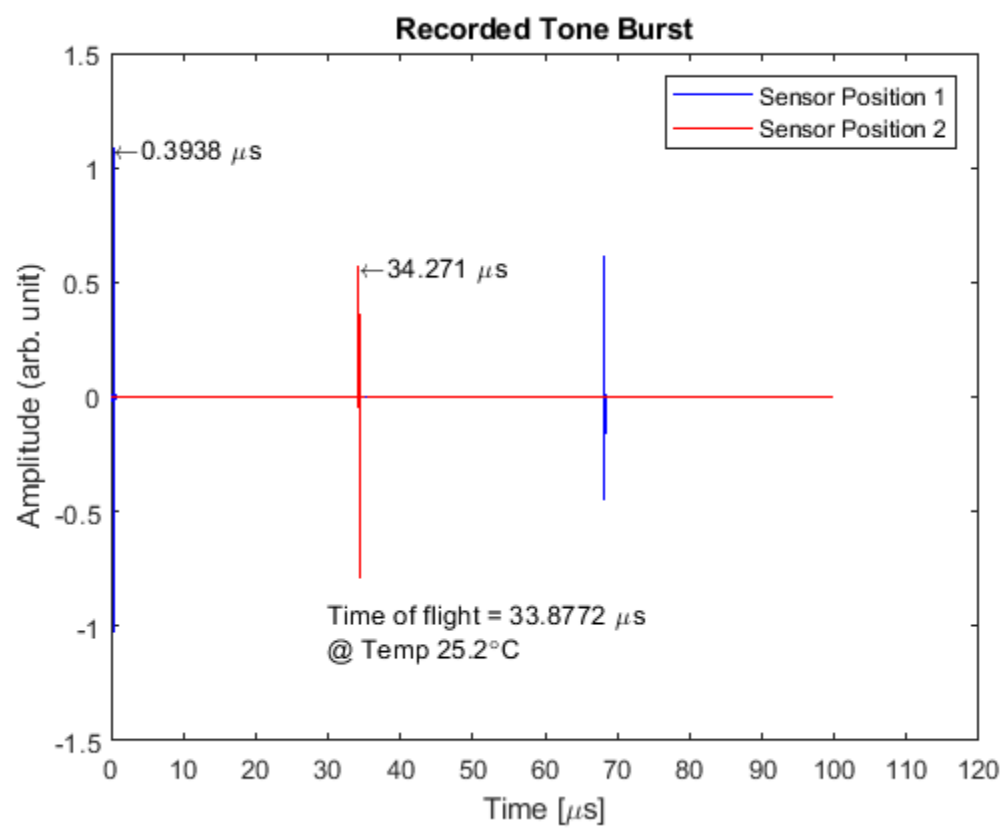
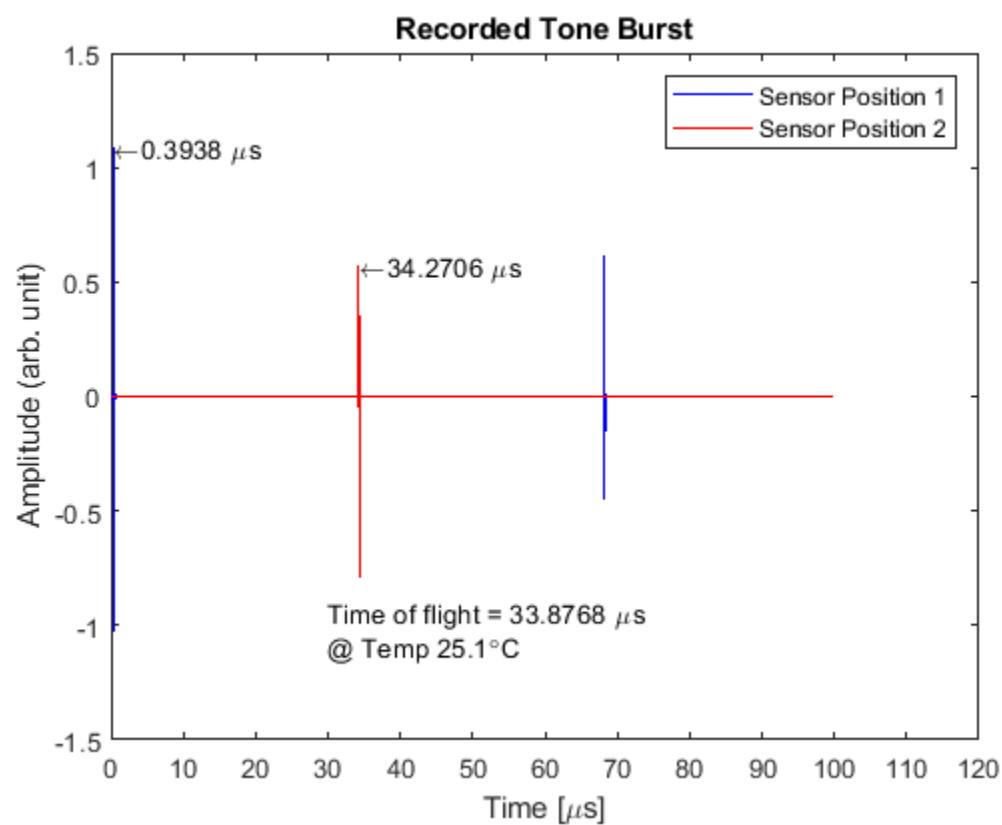
```

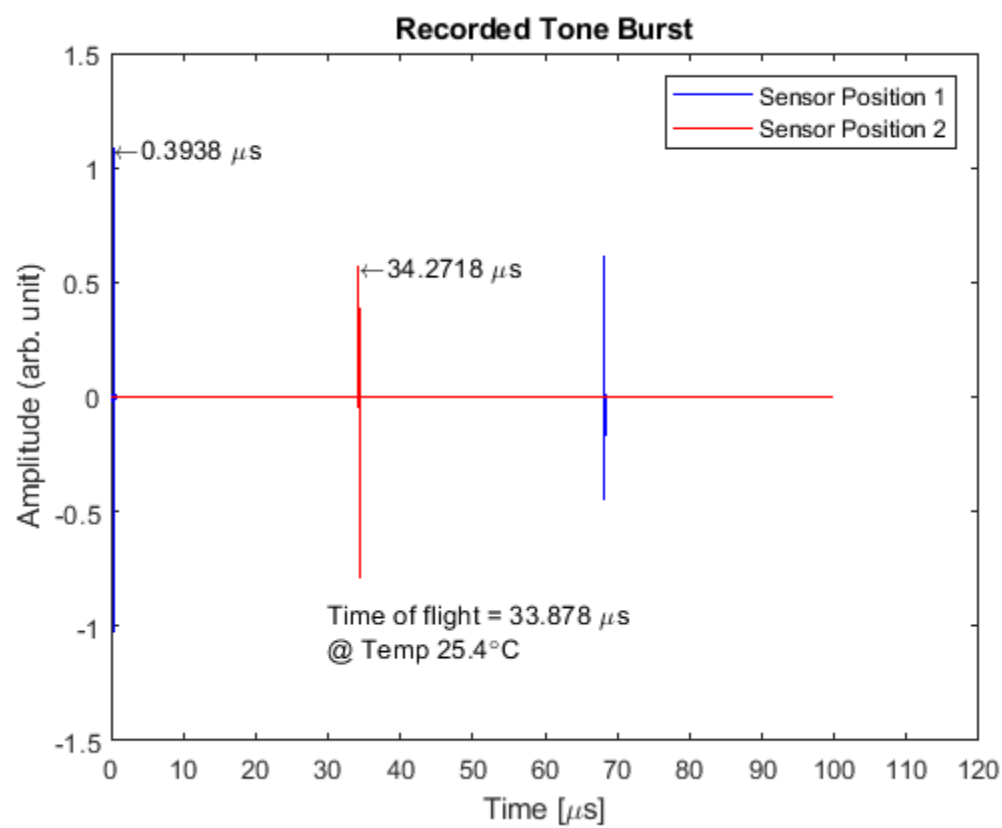
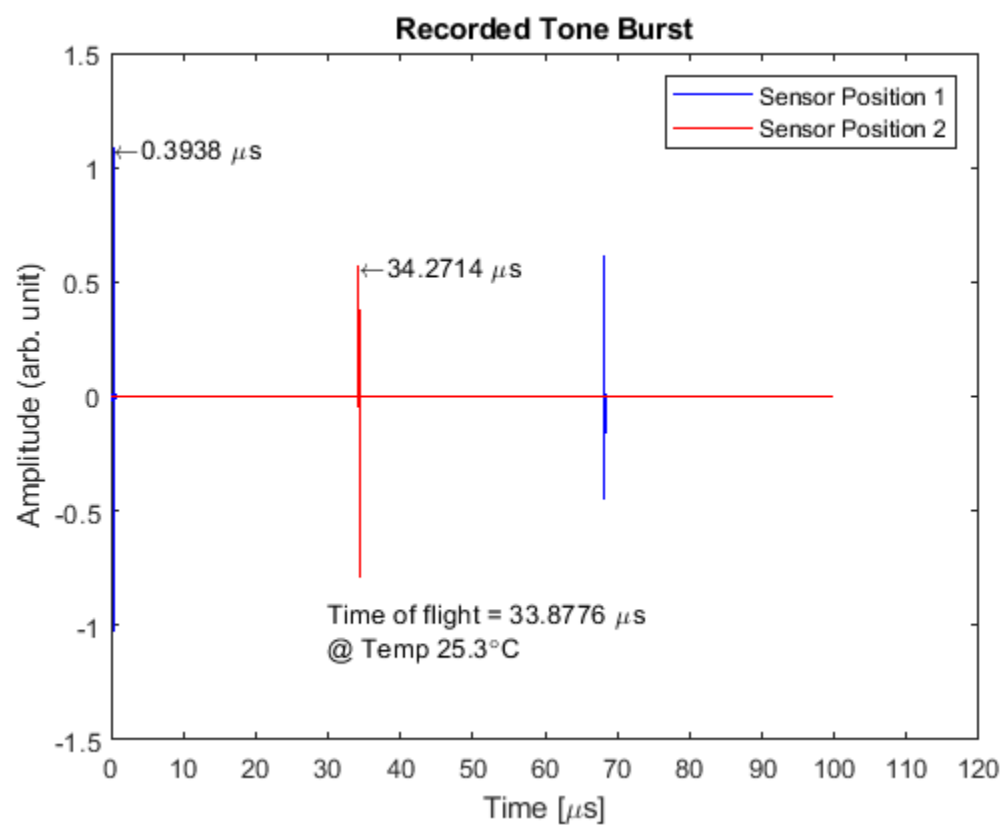
input grid size: 7776 grid points (795.4848mm)
maximum supported frequency: 15.0049MHz
precomputation completed in 0.13644s
starting time loop...
estimated simulation time 18min 10.0022s...
simulation completed in 23min 45.7982s
total computation time 23min 45.985s
Running k-Wave simulation...
start time: 22-Jun-2021 20:53:36
reference sound speed: 5901.6364m/s
dt: 200ps, t_end: 100us, time steps: 500001
input grid size: 7776 grid points (795.4848mm)
maximum supported frequency: 15.0049MHz
precomputation completed in 0.26117s
starting time loop...
estimated simulation time 18min 30.0022s...
simulation completed in 23min 40.0995s
total computation time 23min 40.404s
Running k-Wave simulation...
start time: 22-Jun-2021 21:17:17
reference sound speed: 5901.5728m/s
dt: 200ps, t_end: 100us, time steps: 500001
input grid size: 7776 grid points (795.4848mm)
maximum supported frequency: 15.0049MHz
precomputation completed in 0.24696s
starting time loop...
estimated simulation time 21min 30.0026s...
simulation completed in 23min 45.3342s
total computation time 23min 45.626s
Running k-Wave simulation...
start time: 22-Jun-2021 21:41:02
reference sound speed: 5901.5092m/s
dt: 200ps, t_end: 100us, time steps: 500001
input grid size: 7776 grid points (795.4848mm)
maximum supported frequency: 15.0049MHz
precomputation completed in 0.25756s
starting time loop...
estimated simulation time 21min 30.0026s...
simulation completed in 23min 45.5962s
total computation time 23min 45.895s
Running k-Wave simulation...
start time: 22-Jun-2021 22:04:48
reference sound speed: 5901.4456m/s
dt: 200ps, t_end: 100us, time steps: 500001
input grid size: 7776 grid points (795.4848mm)
maximum supported frequency: 15.0049MHz
precomputation completed in 0.24915s
starting time loop...
estimated simulation time 18min 40.0022s...

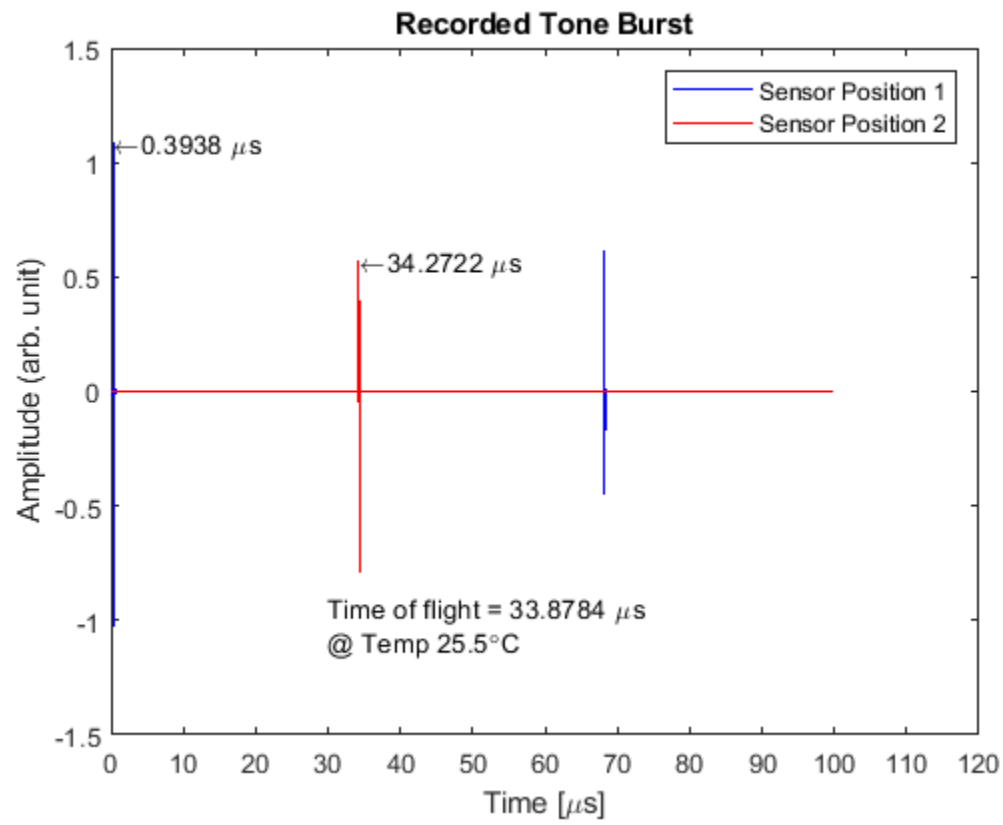
```

simulation completed in 26min 35.6817s
total computation time 26min 35.999s
Running k-Wave simulation...
start time: 22-Jun-2021 22:31:25
reference sound speed: 5901.382m/s
dt: 200ps, t_end: 100us, time steps: 500001
input grid size: 7776 grid points (795.4848mm)
maximum supported frequency: 15.0049MHz
precomputation completed in 0.2652s
starting time loop...
estimated simulation time 25min 0.003s...
simulation completed in 24min 48.0631s
total computation time 24min 48.386s









Published with MATLAB® R2019a

MATLAB Code for Speed of Sound/Expansion Effects on Time-of-flight

Simulation

```
% =====  
% NOTE:  
% This script takes simulates the effects of speed and expansion on time of  
% flight of ultrasonic wave.  
% Visualization of simulation as well as plot of result are then generated.  
  
% Functions kWaveGrid,toneBurst,kspaceFirstOrder1D are provided in the  
% k-Wave MATLAB toolbox and are called from this script.  
% =====  
% =====  
% SIMULATION  
% =====  
clearvars;  
  
%Speed simulation  
speed_data = zeros(2,20);  
expan_data = zeros(2,20);  
j = 1;  
for i = 0:10:200  
    temp = i;  
    d_L = 0;  
    length = 200;  
    speed = ((-0.636*temp)+5917.6);  
    tof = simulate(temp,length,d_L,speed);  
    speed_data(1,j) = temp;  
    speed_data(2,j) = tof;  
    j = j+1;  
    close;  
end  
  
% Expansion simulation  
j = 1;  
for i = 0:10:200  
    temp = i;  
    length = 200;  
    d_L = (10e-6*(temp-23)*length);  
    speed = 5917.6;  
    tof = simulate(temp,length,d_L,speed);  
    expan_data(1,j) = temp;  
    expan_data(2,j) = tof;  
    j = j+1;  
    close;  
end
```

```

% The 'simulate' function is called for speed and expansion simulation
function tof = simulate(Temp,Length,dL,Speed)

% create the computational grid
Nx = 6.561e+03;           % number of grid points in the x (row) direction
dx = 1.2e-04;             % grid point spacing in the x direction [m]
kgrid = kWaveGrid(Nx, dx);

% Estimates Coordinates
cv = 1000;
p1 = round(49/(dx*cv));
p2 = round(50/(dx*cv));
p3 = round((Length+dL+50)/(dx*cv));
p4 = round((Length+dL+51)/(dx*cv));

% Defines the properties of the propagation medium
medium.sound_speed = 346 * ones(Nx, 1);           % [sound speed in air m/s]
medium.sound_speed([p1:p2 p3:p4]) = 3070;         % [sound speed in epoxy m/s]
medium.sound_speed(p2:p3) = Speed;                 % [sound speed in steel m/s]
medium.density = 1800 * ones(Nx, 1);               % [Density of steel kg/m^3]
medium.density([p1:p2 p3:p4]) = 1800;             % [Density of epoxy kg/m^3]
medium.density(p2:p3) = 8030;                      % [Density of steel kg/m^3]

% Creates time array
dt = 0.4e-9;
t_end = 150e-6;
kgrid.t_array = 0:dt:t_end;

% Defines a tone burst
source.p_mask = zeros(Nx,1);
source.p_mask(p1) = 1;
sampling_freq = 4/dt;           % [Hz]
tone_burst_freq = 1.2e6;        % [Hz]
tone_burst_cycles = 2;
source.p = toneBurst(sampling_freq, tone_burst_freq, tone_burst_cycles);

% Creates a sensor mask
sensor.mask = zeros(Nx,1);
sensor.mask(p2) = 1; %First sensor at 25mm
sensor.mask(p3) = 1; %Second sensor at 225mm (200mm length)

% Runs the simulation

display_mask = source.p_mask + sensor.mask;
sensor_data = kspaceFirstOrder1D(kgrid, medium, source, sensor, ...
'DisplayMask', display_mask, 'RecordMovie', false);

```



```

% =====
% VISUALISATION
% =====

% Plots the recorded time signals
figure;
plot(kgrid.t_array*1e6, sensor_data(1, :), 'b-');
hold on;
plot(kgrid.t_array*1e6, sensor_data(2, :), 'r-');
xlabel('Time [\mus]');
ylabel('Amplitude (arb. unit)');
legend('Sensor Position 1', 'Sensor Position 2');
title('Recorded Tone Burst');
set(gca, 'Xtick', 0:10:150)

% Finds peaks of both sensors to calculate time of flight
% Re-assign values to x, y1 and y2
x = kgrid.t_array*1e6;
y1 = sensor_data(1, :);
y2 = sensor_data(2, :);

% Finds the max for Sensor 1
sensor_1_peak = find(max(y1) == y1);
x_peak_1 = x(sensor_1_peak);
y_peak_1 = y1(sensor_1_peak);
max1 = ['\leftarrow', num2str(x_peak_1), ' \mus'];
text(x_peak_1, y_peak_1, max1);

% Find the max for Sensor 2
sensor_2_peak = find(max(y2) == y2);
x_peak_2 = x(sensor_2_peak);
y_peak_2 = y2(sensor_2_peak);
max2 = ['\leftarrow', num2str(x_peak_2), ' \mus'];
text(x_peak_2, y_peak_2, max2);

% Calculates time of flight
tof = x_peak_2 - x_peak_1;
tof_txt = {'Time of flight = ', num2str(tof, 6), ' \mus'}, {'@ Temp', num2str(Temp), '\circC'};
text(80, (min(sensor_data(1, :))/2), tof_txt)
end

```

Running k-Wave simulation...

```

start time: 23-Feb-2021 10:25:44
reference sound speed: 5917.6m/s
dt: 400ps, t_end: 150us, time steps: 375001
input grid size: 6561 grid points (787.32mm)
maximum supported frequency: 1.4414MHz
precomputation completed in 0.19926s

```

```

starting time loop...
estimated simulation time 11min 15.0018s...
simulation completed in 12min 10.2458s
total computation time 12min 10.572s
Running k-Wave simulation...
start time: 23-Feb-2021 10:37:54
reference sound speed: 5911.24m/s
dt: 400ps, t_end: 150us, time steps: 375001
input grid size: 6561 grid points (787.32mm)
maximum supported frequency: 1.4414MHz
precomputation completed in 0.17788s
starting time loop...
estimated simulation time 12min 52.5021s...
simulation completed in 12min 29.138s
total computation time 12min 29.41s
.
.
.
Running k-Wave simulation...
start time: 23-Feb-2021 17:29:49
reference sound speed: 5917.6m/s
dt: 400ps, t_end: 150us, time steps: 375001
input grid size: 6561 grid points (787.32mm)
maximum supported frequency: 1.4414MHz
precomputation completed in 0.12841s
starting time loop...
estimated simulation time 7min 15.0012s...
simulation completed in 8min 57.6185s
total computation time 8min 57.838s

```

Published with MATLAB® R2020b

MATLAB Code and Results for the 5 MHz Phase-shift Thermometry

Simulations

```
% =====
% NOTE:
% This script computes phase-shift of ultrasonic wave through
% the material for the specified length, temperature, speed and density.
% Visualization of simulation as well as plot of result are then generated.

% Functions kWaveGrid,toneBurst,kspaceFirstOrder1D are provided in the
% k-Wave MATLAB toolbox and are called from this script.
% =====
% =====
% SIMULATION
% =====
clearvars;

%Placeholders for the phase-shift results
speed_data = zeros(3,6);

%array index
j = 1;

%Defines length of material
length = 200;

%For loop for calling the 'simulate' function
for temp = 25:0.1:25.5
    speed = ((-0.636*temp)+5917.6);
    phase = simulate(length,speed,temp);
    speed_data(1,j)= temp;
    speed_data(2,j) = phase;
    speed_data(3,j)= speed;
    j = j+1;
end

%Function for computing ultrasonic phase-shift.
function phase = simulate(Length,Speed,Temp)

% define the properties of the propagation medium and computational grid

Nx = 10e+03;
dx = 0.4e-4;
kgrid = kWaveGrid(Nx,dx);

% Material density and transducer frequency
density = 8030;
freq = 5e6;

% Estimates Coordinates
cv = 1000;
p1 = round(49/(dx*cv));
p2 = round(50/(dx*cv));
p3 = round((Length+50)/(dx*cv));
p4 = round((Length+51)/(dx*cv));

% Defines medium density and speed
medium.sound_speed = Speed * ones(Nx, 1);
medium.sound_speed([p1:p2 p3:p4]) = Speed;
medium.sound_speed(p2:p3) = Speed;
medium.density = density * ones(Nx, 1);
```

```

medium.density([p1:p2 p3:p4]) = density;
medium.density(p2:p3) = density;

% Defines time array
t_end = 100e-6;
kgrid.t_array = makeTime(kgrid, medium.sound_speed, [], t_end);

% create initial pressure distribution using a smoothly shaped sinusoid
source.p_mask = zeros(Nx,1);
source.p_mask(p1-1) = 1;
source.p = 0.25*sin(2*pi*freq*kgrid.t_array);

% create 2 sensor mask
sensor.mask = zeros(Nx, 1);
sensor.mask(p2) = 1;
sensor.mask(p3) = 1;

% define the time array
kgrid.makeTime(medium.sound_speed, [], t_end);

% run the simulation

display_mask = source.p_mask + sensor.mask;
sensor_data = kspaceFirstOrder1D(kgrid, medium, source, sensor,...
    'DisplayMask',display_mask,'RecordMovie',false);

% =====
% VISUALISATION
% =====

% plot the recorded time signals
starting = find(abs(kgrid.t_array - 50e-6)<= 2e-8);

ending = find(abs(kgrid.t_array - 80e-6)<= 2e-8);

figure;
plot(kgrid.t_array*1e6,...
    sensor_data(1,:), 'b-');
hold on;
plot(kgrid.t_array*1e6,...
    sensor_data(2,:), 'r-');
xlabel('Time [\mus]');
ylabel('Amplitude (arb. unit)');
legend('Sensor Position 1', 'Sensor Position 2');
title('Recorded Signal');
set(gca,'Xtick',0:10:150,'XTickLabelRotation',45)

%Performs Hilbert transform
y1_h = hilbert(sensor_data(1,starting:ending));
y2_h = hilbert(sensor_data(2, starting:ending));
prad1 = (unwrap(angle(y1_h)))';
prad2 = (unwrap(angle(y2_h)))';

%Computes the phase-shift and outputs the result
phase_rad = prad1 - prad2;
phase_diff = mean(phase_rad);
phase_deg = rad2deg(phase_diff);
path_len = 1e3*dx*(p3 - p2);
text(10,-0.28,['Material Length = ', num2str(path_len,4), ' mm,'])
text(50,0.28,['Temp = ',num2str(Temp,3),'\circC'])
text(50,-0.28,['Phase Shift = ',num2str(phase_deg,5),'\circ'])
text(10,0.28,['Frequency = ', num2str((freq/1e6),3), ' MHz'])
phase = phase_deg;

```

end

Running k-Wave simulation...

start time: 22-Jun-2021 12:45:06
reference sound speed: 5901.7m/s
dt: 2.0333ns, t_end: 99.9983us, time steps: 49181
input grid size: 10000 grid points (400mm)
maximum supported frequency: 73.7713MHz
precomputation completed in 0.32034s
starting time loop...
estimated simulation time 2min 9.8378s...
simulation completed in 1min 48.1523s
total computation time 1min 48.636s

Running k-Wave simulation...

start time: 22-Jun-2021 12:46:55
reference sound speed: 5901.6364m/s
dt: 2.0333ns, t_end: 99.9994us, time steps: 49181
input grid size: 10000 grid points (400mm)
maximum supported frequency: 73.7705MHz
precomputation completed in 0.73411s
starting time loop...
estimated simulation time 1min 54.0999s...
simulation completed in 1min 49.8411s
total computation time 1min 50.752s

Running k-Wave simulation...

start time: 22-Jun-2021 12:48:47
reference sound speed: 5901.5728m/s
dt: 2.0334ns, t_end: 99.9984us, time steps: 49180
input grid size: 10000 grid points (400mm)
maximum supported frequency: 73.7697MHz
precomputation completed in 0.53982s
starting time loop...
estimated simulation time 1min 51.1468s...
simulation completed in 1min 54.2638s
total computation time 1min 55.073s

Running k-Wave simulation...

start time: 22-Jun-2021 12:50:42
reference sound speed: 5901.5092m/s
dt: 2.0334ns, t_end: 99.9995us, time steps: 49180
input grid size: 10000 grid points (400mm)
maximum supported frequency: 73.7689MHz
precomputation completed in 0.39744s
starting time loop...
estimated simulation time 1min 40.3272s...
simulation completed in 1min 52.4084s
total computation time 1min 52.977s

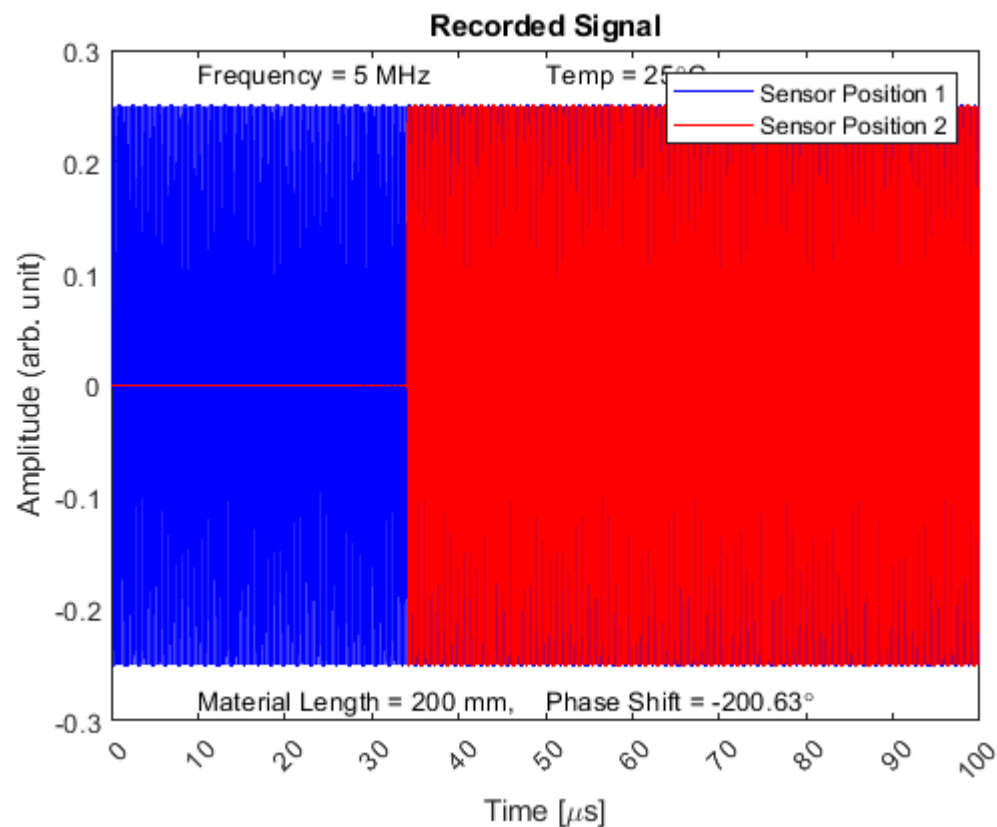
Running k-Wave simulation...

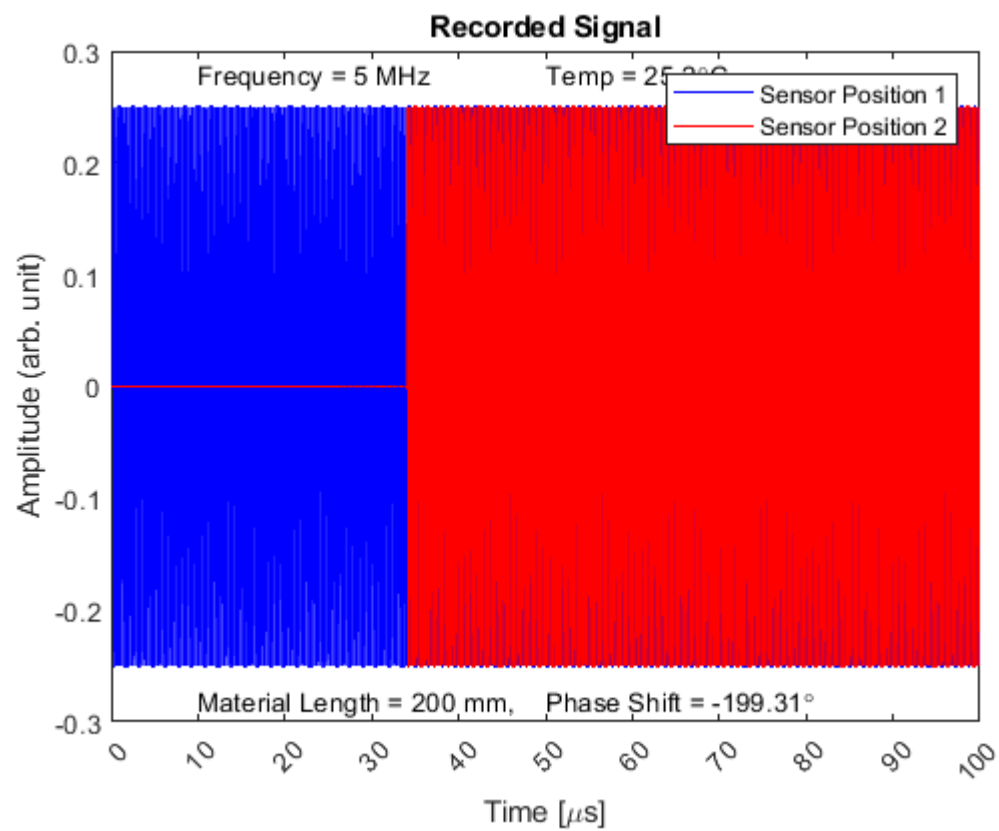
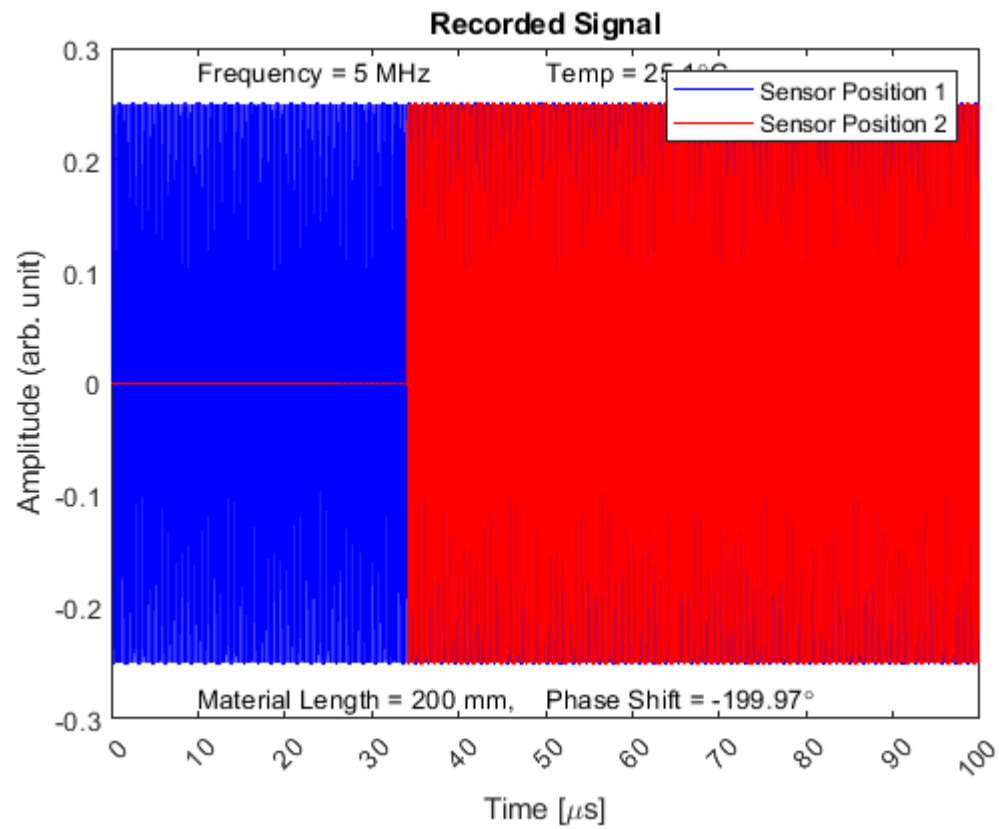
start time: 22-Jun-2021 12:52:35
reference sound speed: 5901.4456m/s

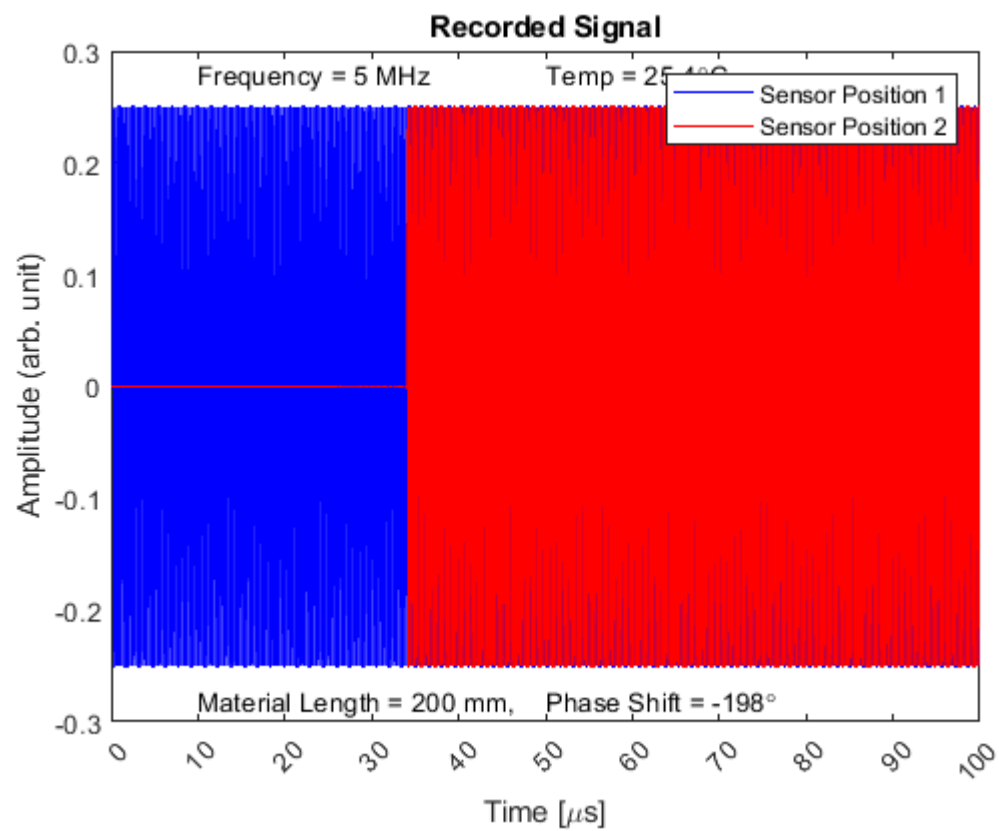
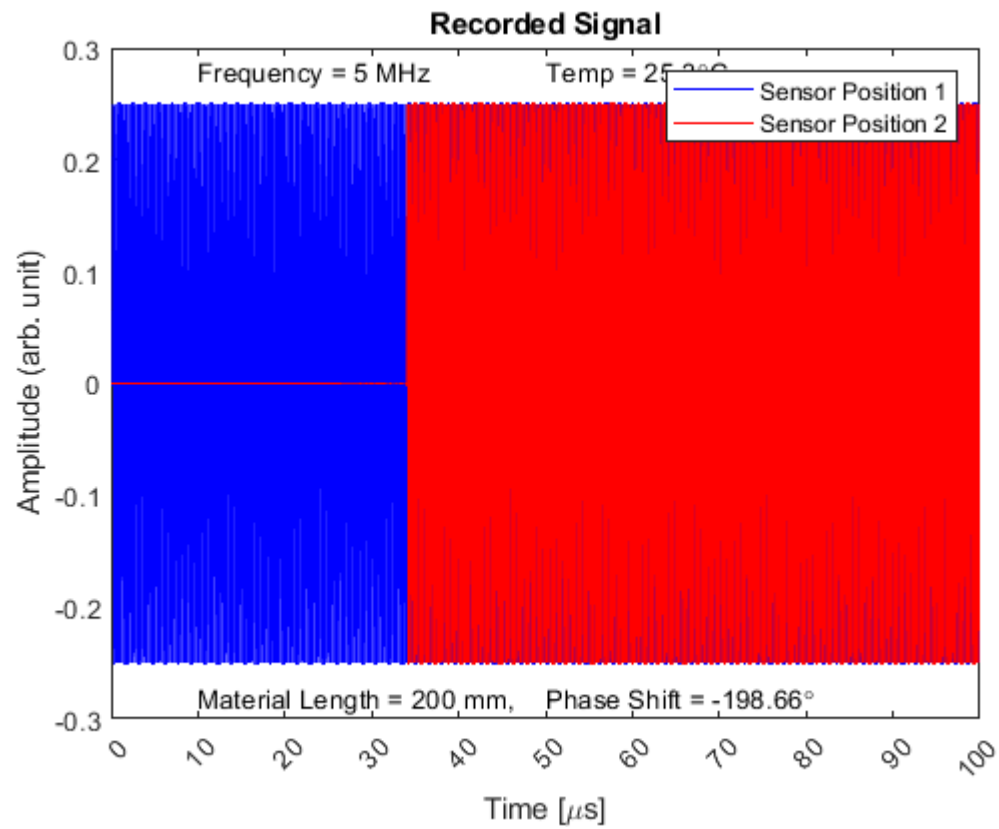
```

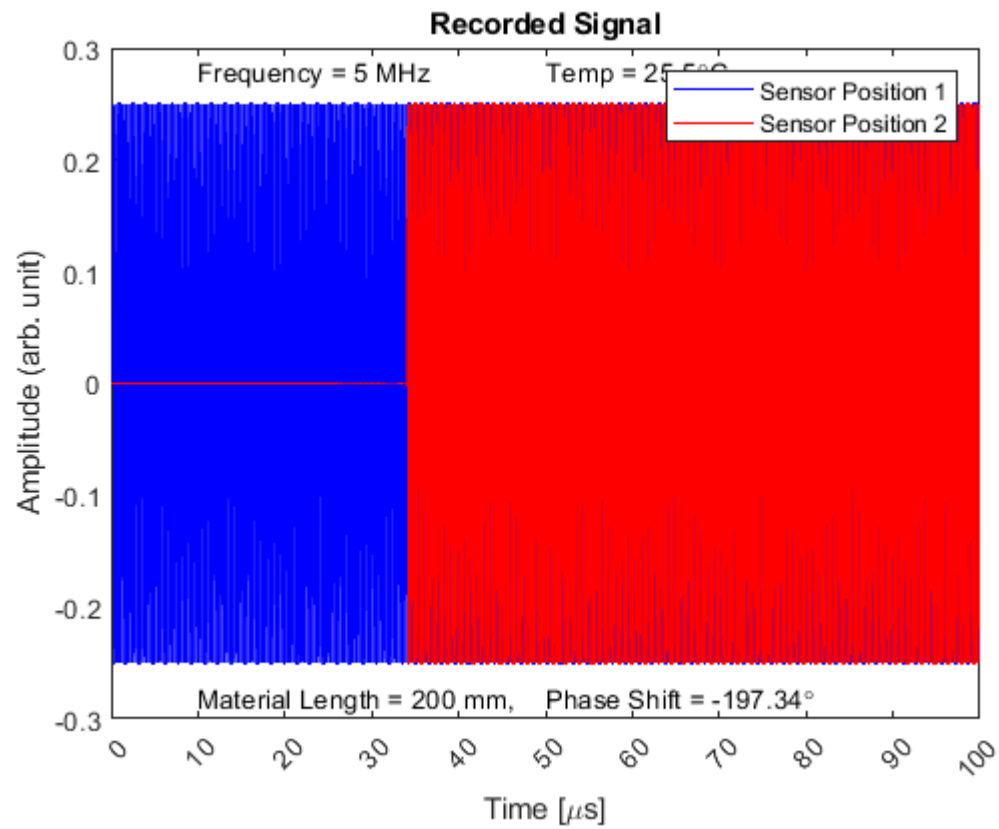
dt: 2.0334ns, t_end: 99.9985us, time steps: 49179
input grid size: 10000 grid points (400mm)
maximum supported frequency: 73.7681MHz
precomputation completed in 0.43418s
starting time loop...
estimated simulation time 1min 42.2923s...
simulation completed in 1min 53.3993s
total computation time 1min 54.014s
Running k-Wave simulation...
start time: 22-Jun-2021 12:54:30
reference sound speed: 5901.382m/s
dt: 2.0334ns, t_end: 99.9996us, time steps: 49179
input grid size: 10000 grid points (400mm)
maximum supported frequency: 73.7673MHz
precomputation completed in 0.39718s
starting time loop...
estimated simulation time 1min 56.0624s...
simulation completed in 1min 54.8746s
total computation time 1min 55.436s

```



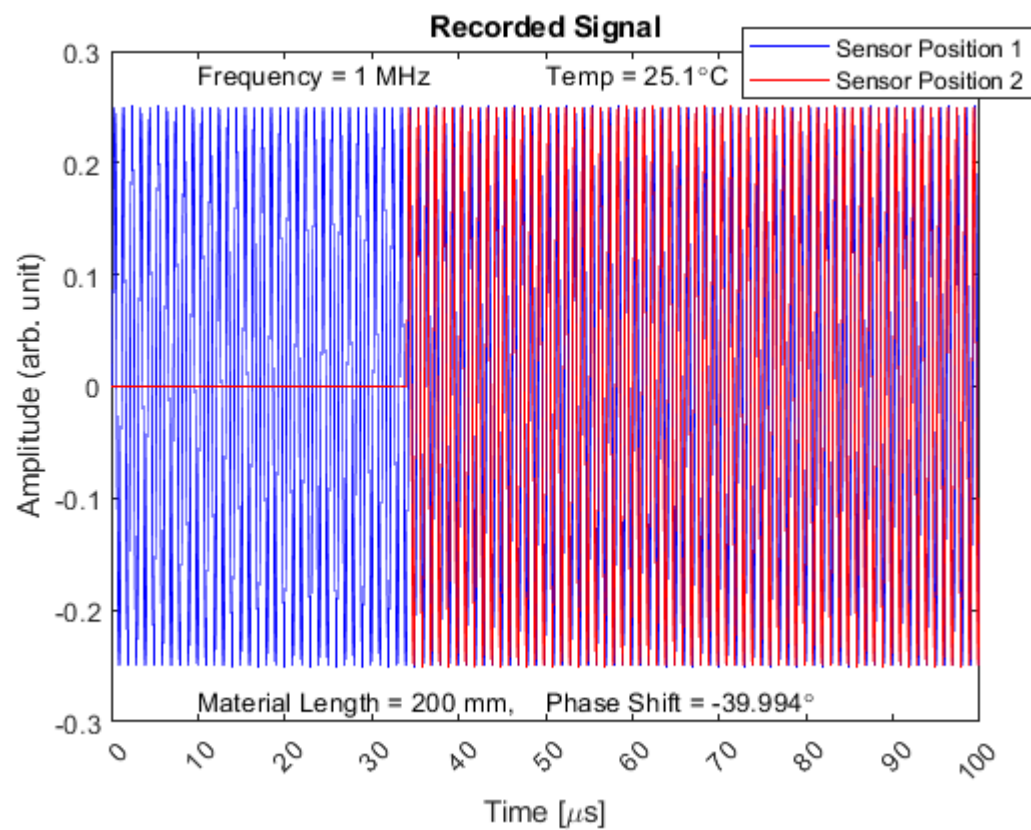
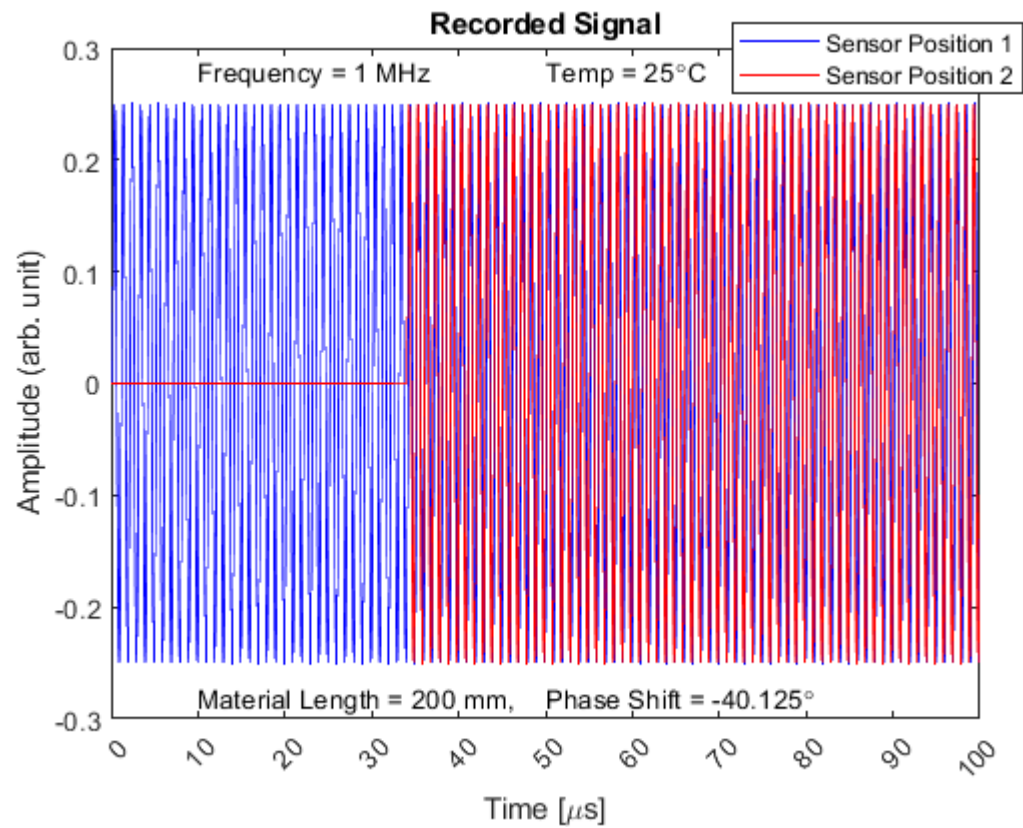


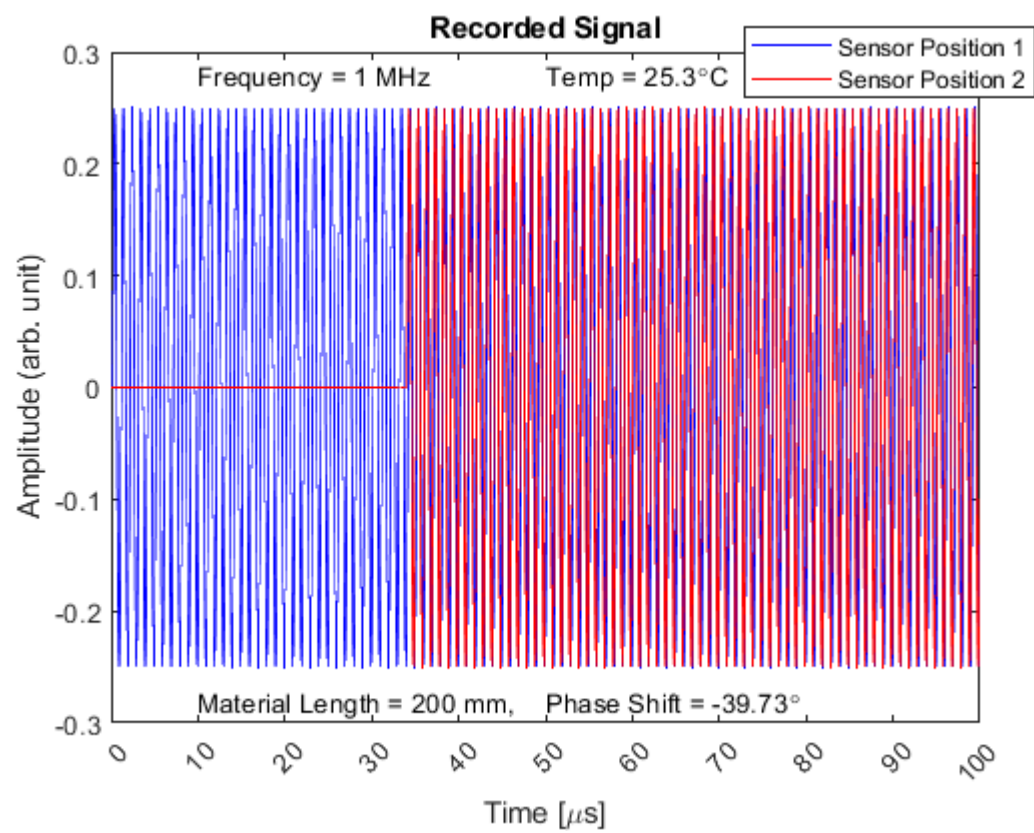
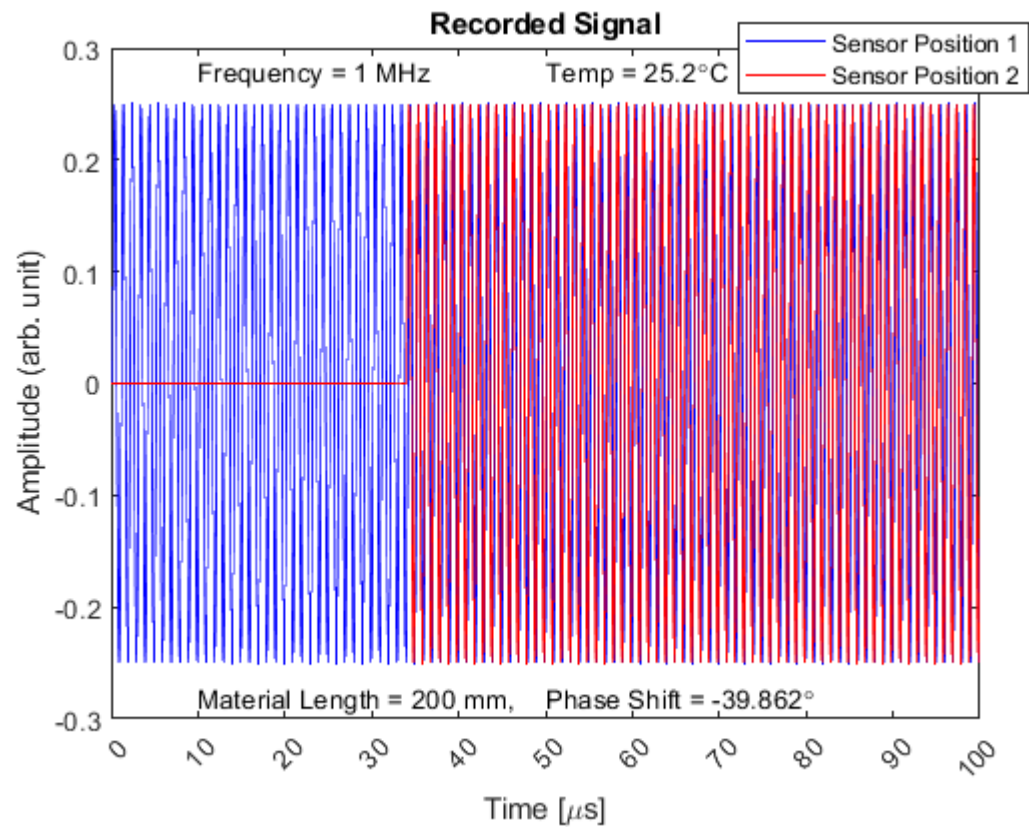


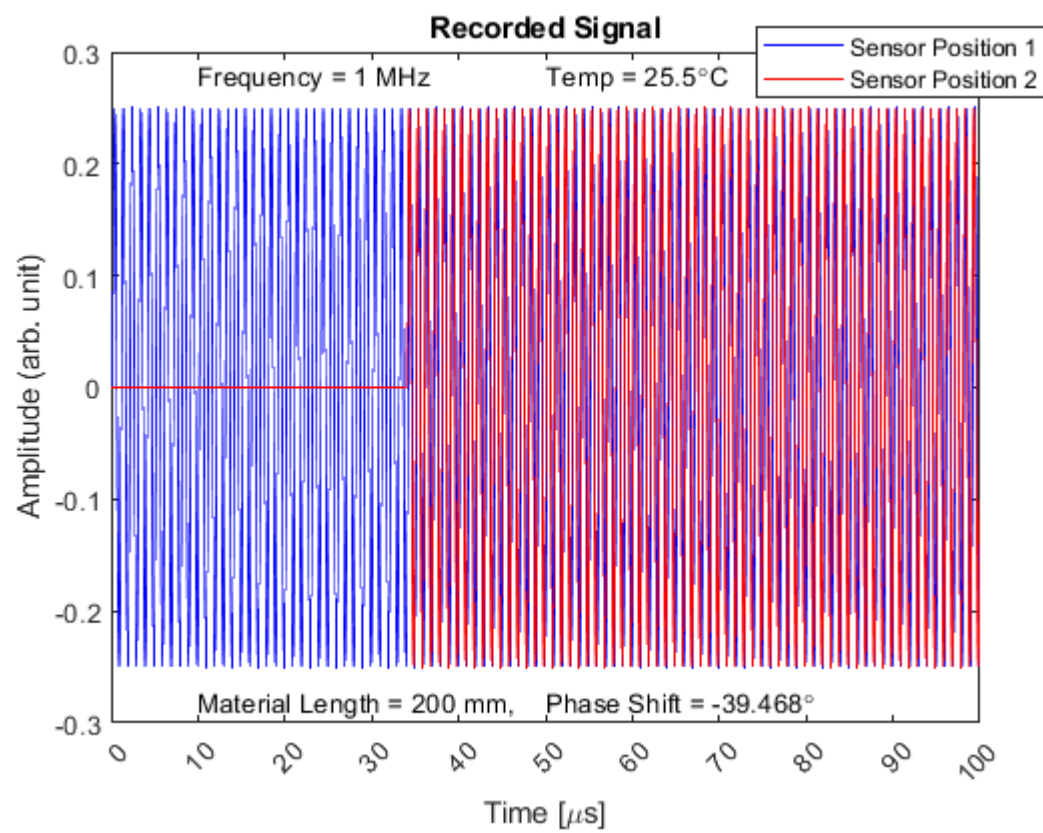
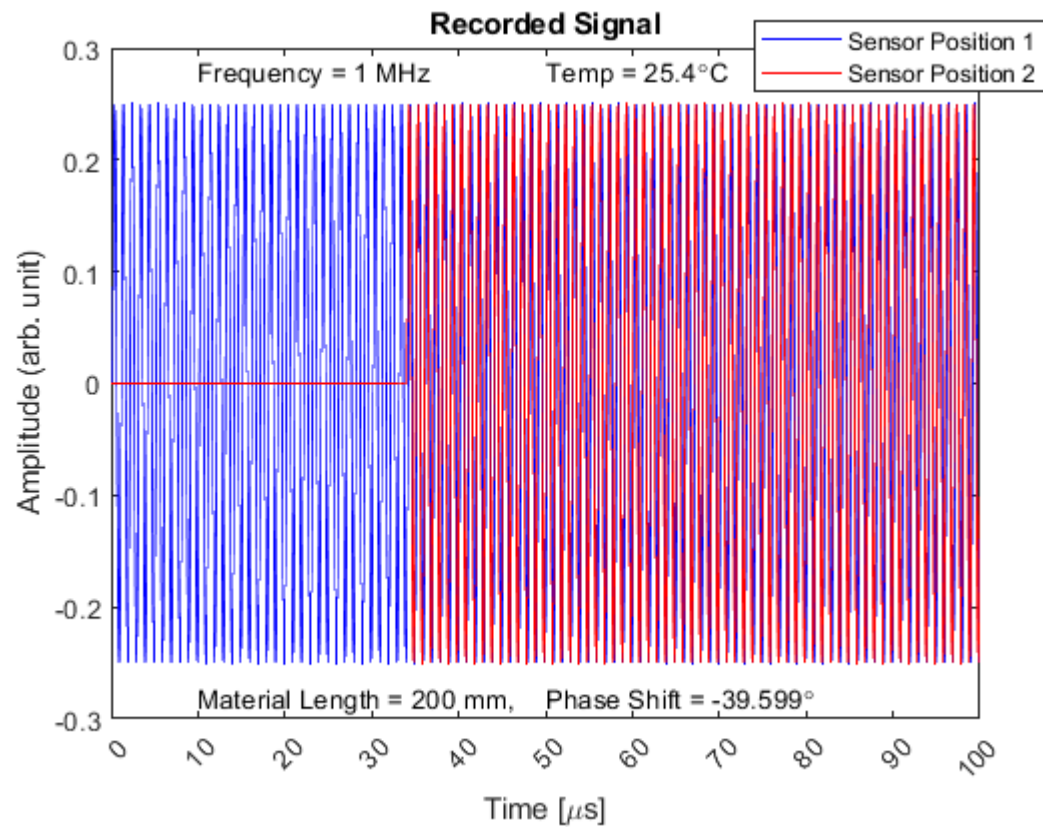


Published with MATLAB® R2020b

MATLAB Plots for the 1 MHz Phase-shift Thermometry Simulations

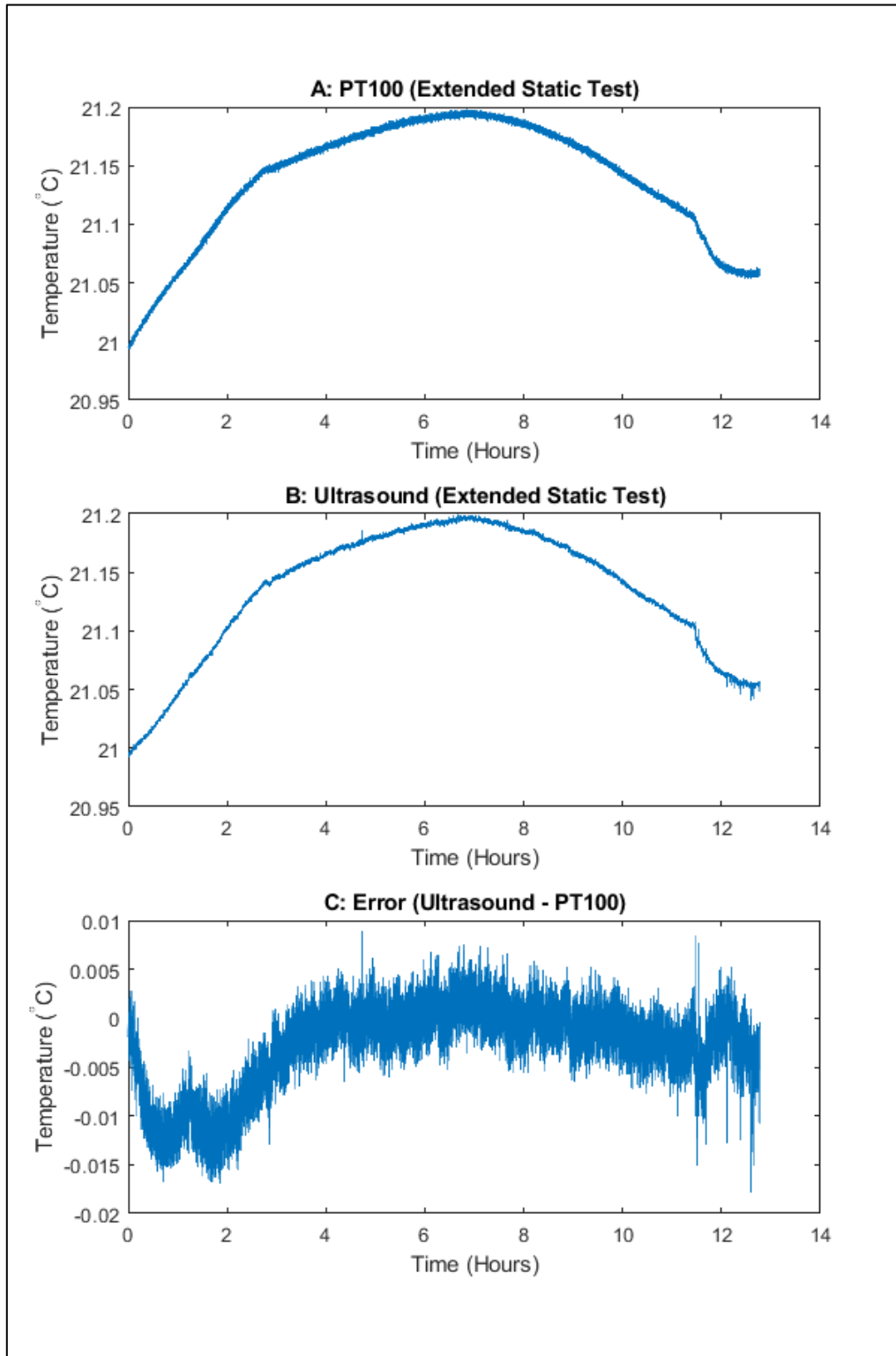




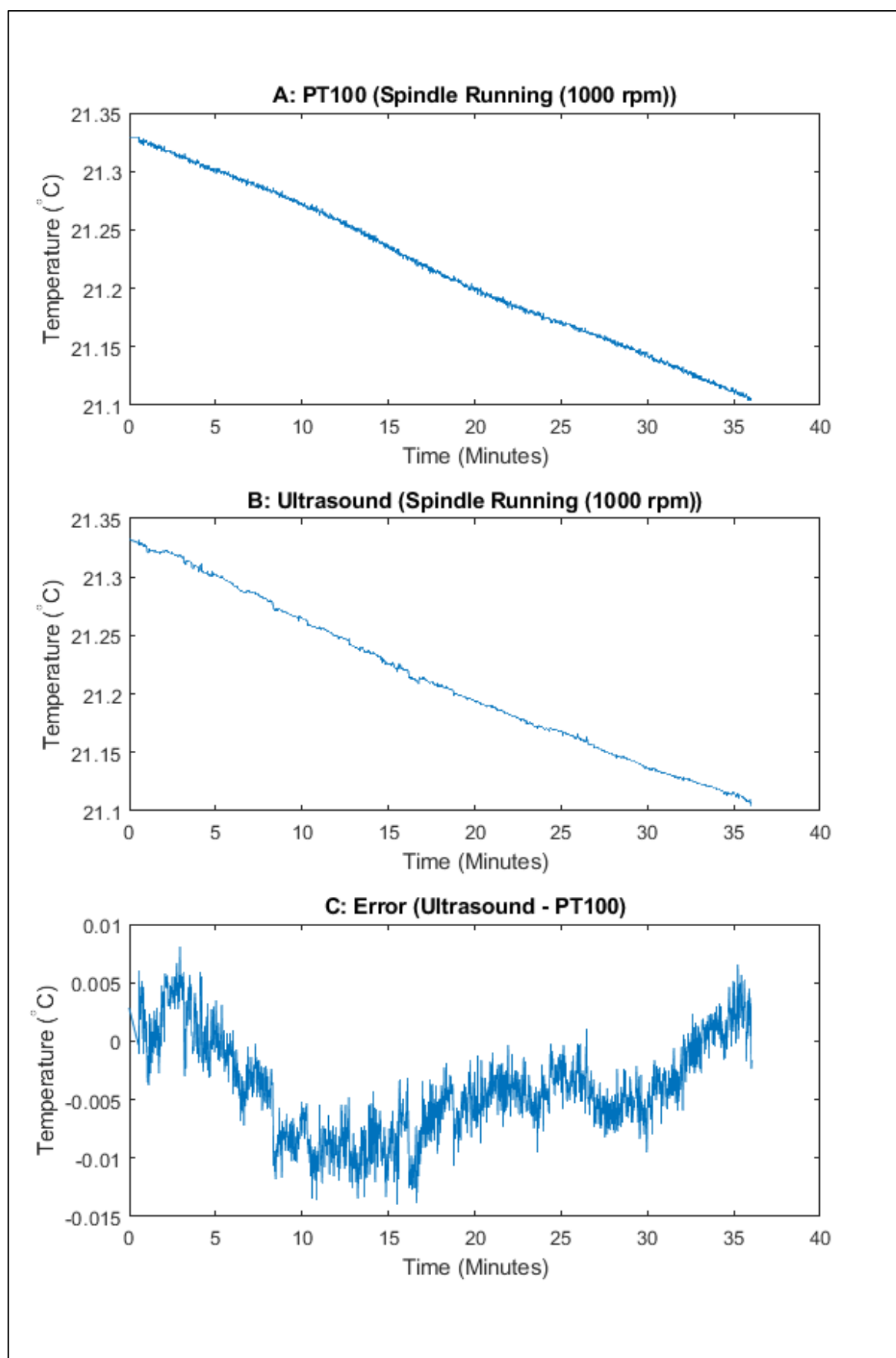


Appendix B

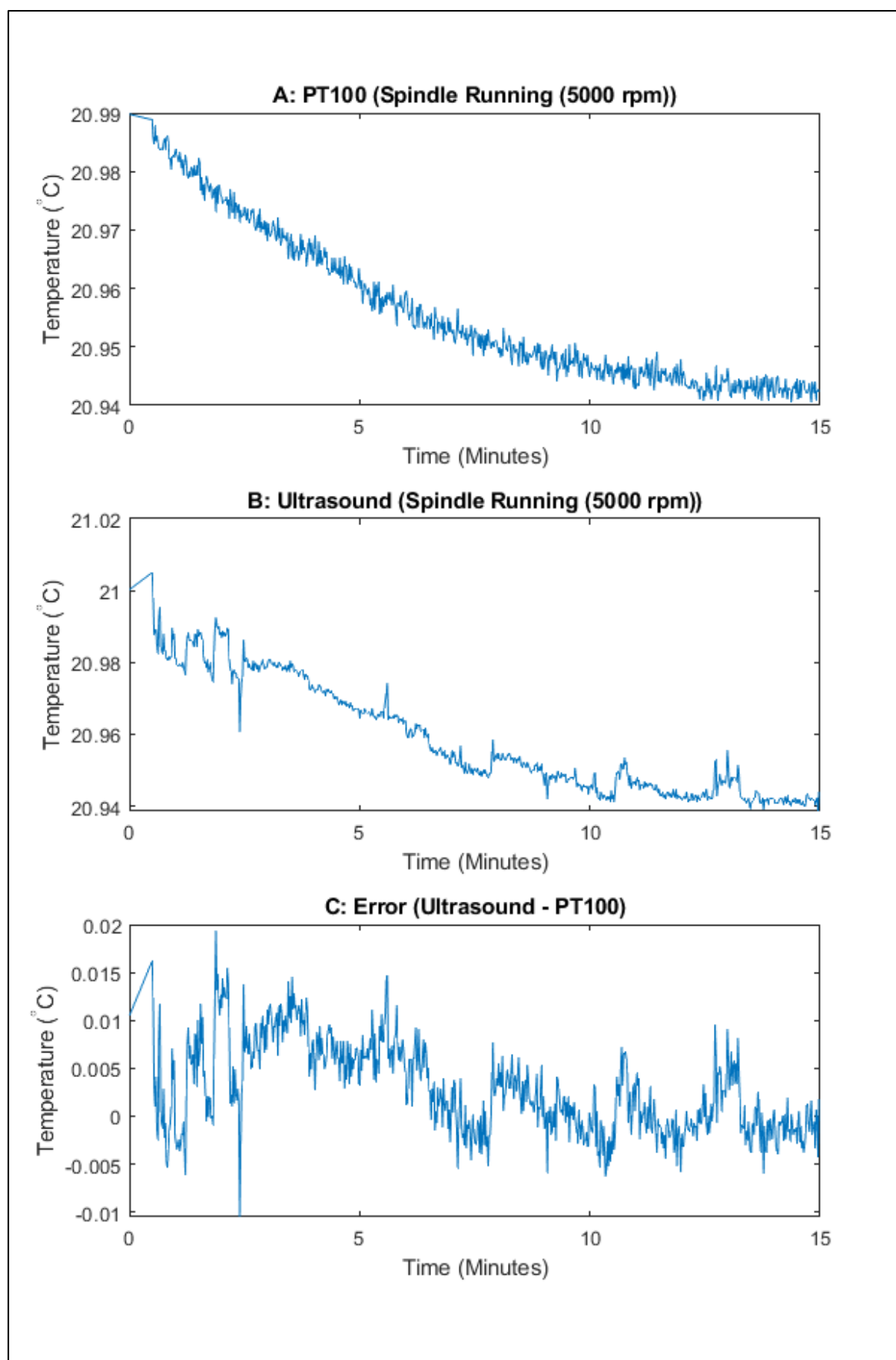
Unfiltered Results of In-process Ultrasonic Tests



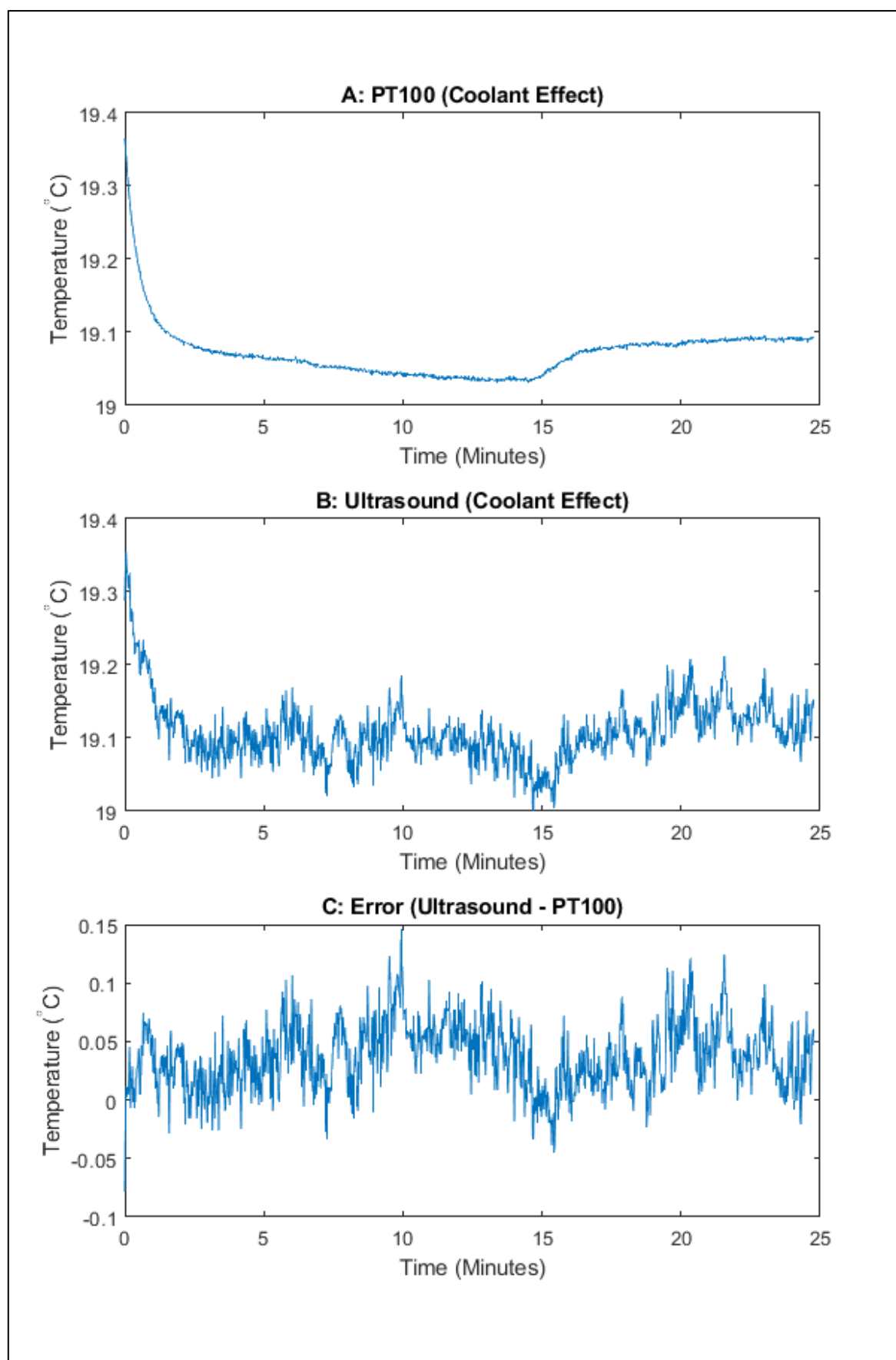
Unfiltered results of extended static test



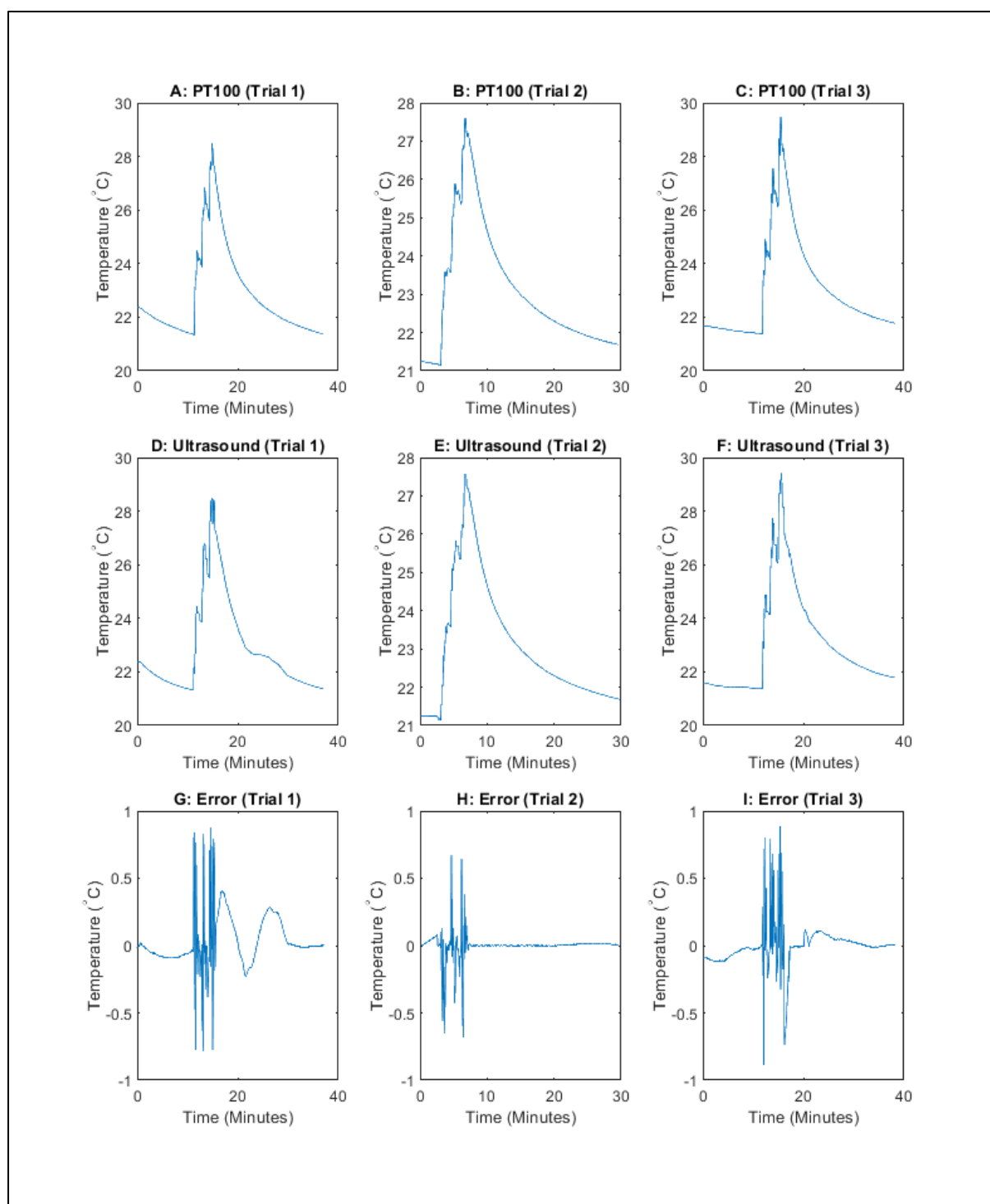
Unfiltered results of spindle running at 1000 rpm



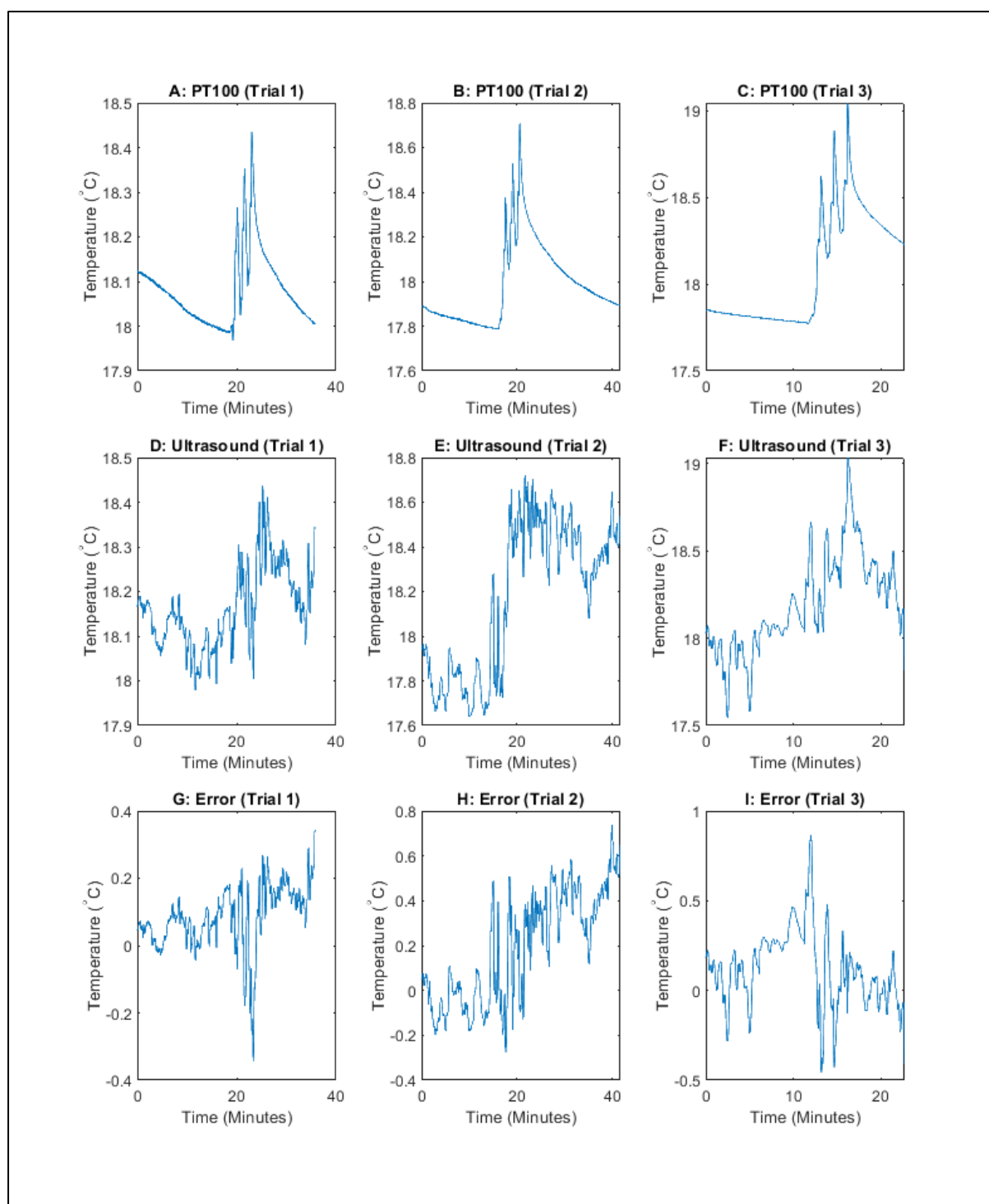
Unfiltered results of spindle running at 5000 rpm



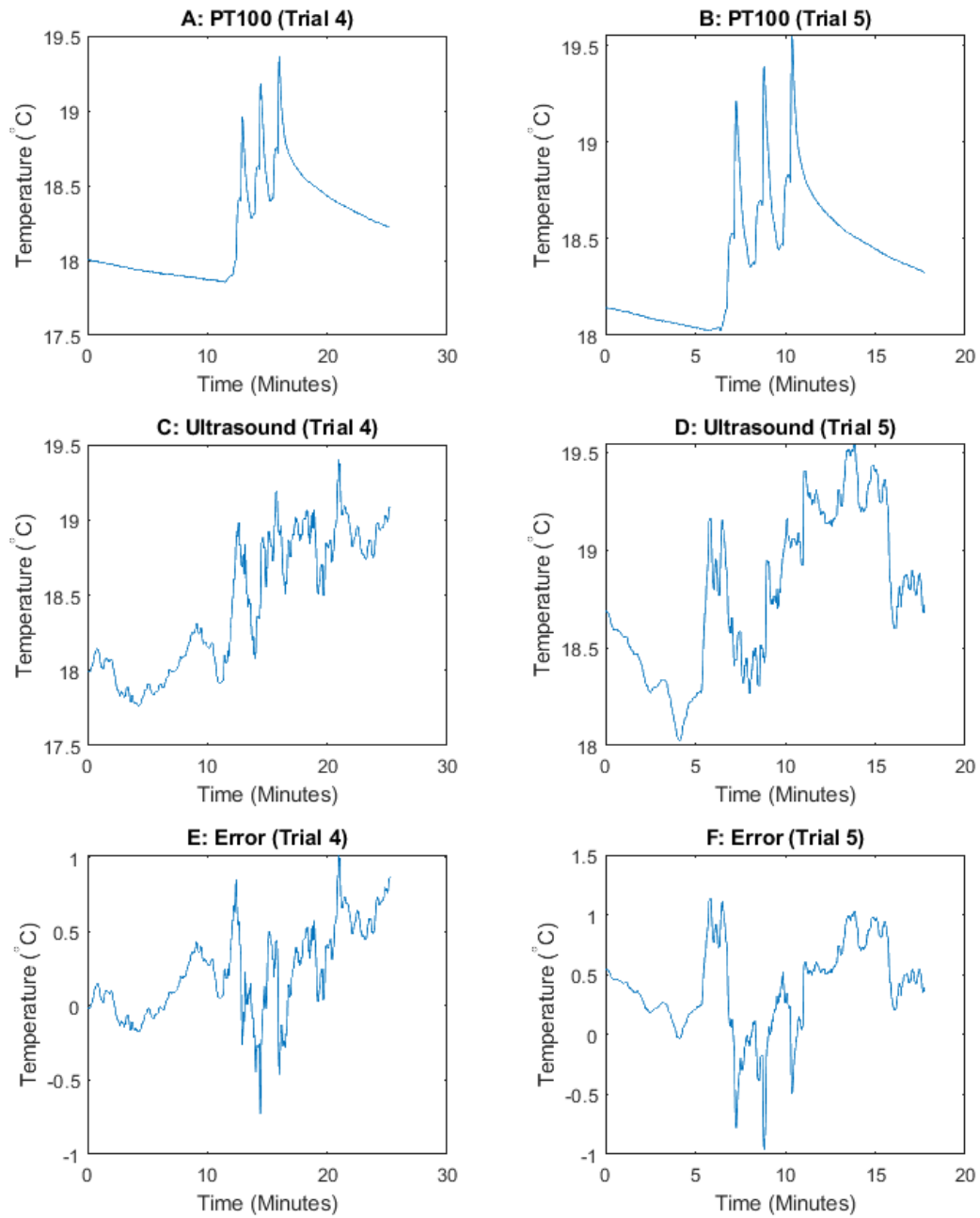
Unfiltered results of coolant effect on ultrasonic thermometry



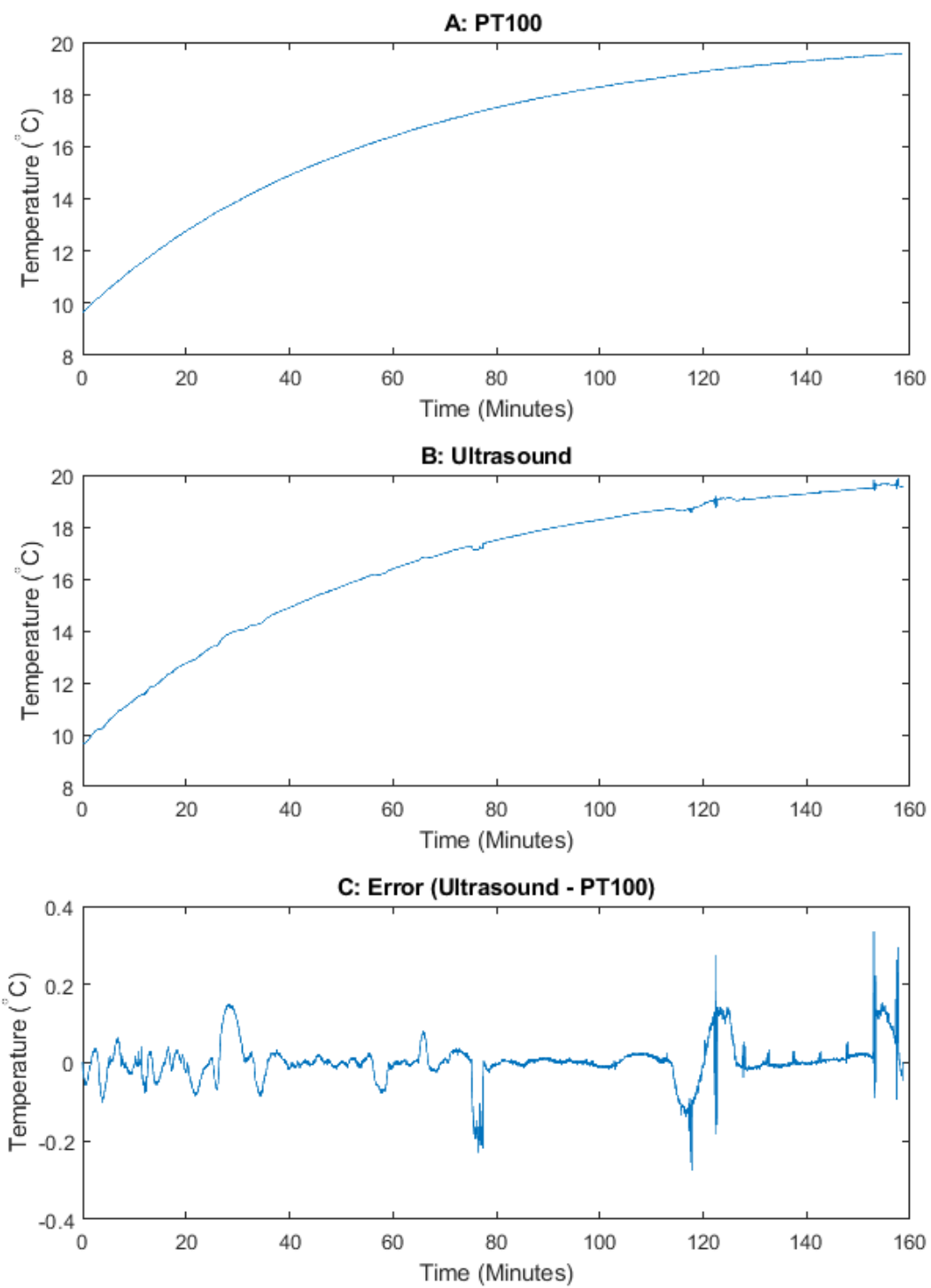
Unfiltered results for dry cutting trials



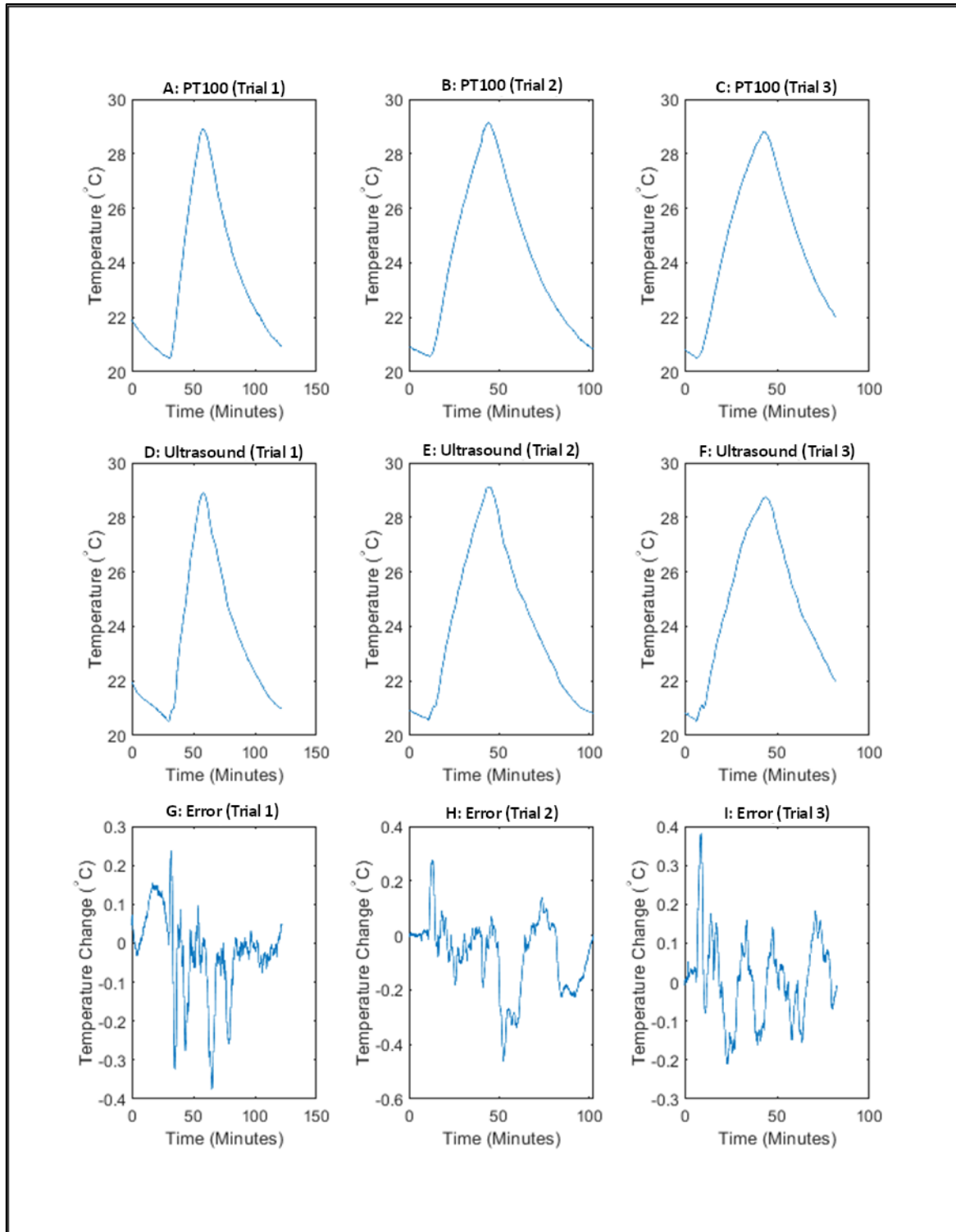
Unfiltered results of wet cutting trials 1-3



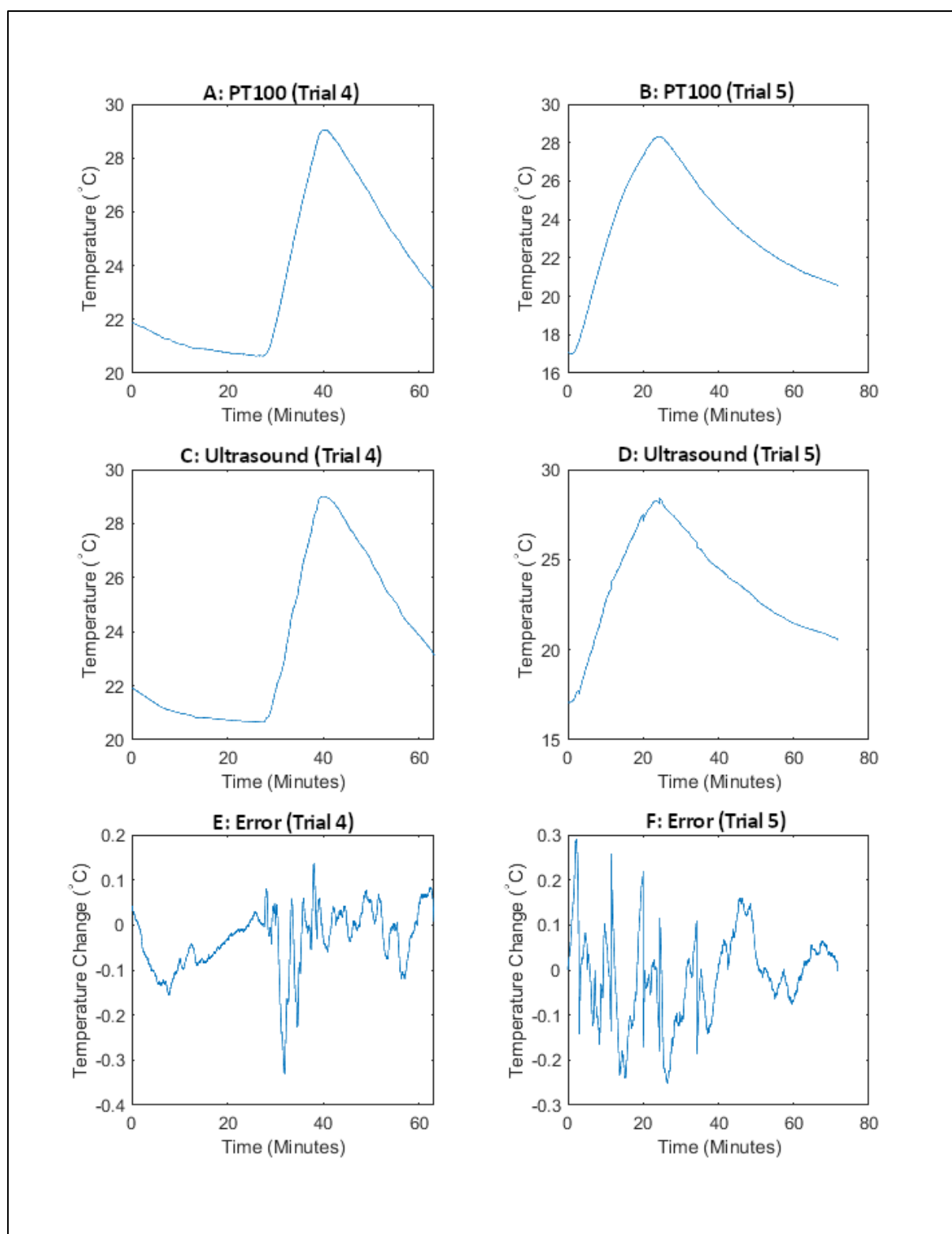
Unfiltered results of wet cutting trials 4-5



Unfiltered on CMM PT100 and ultrasound results

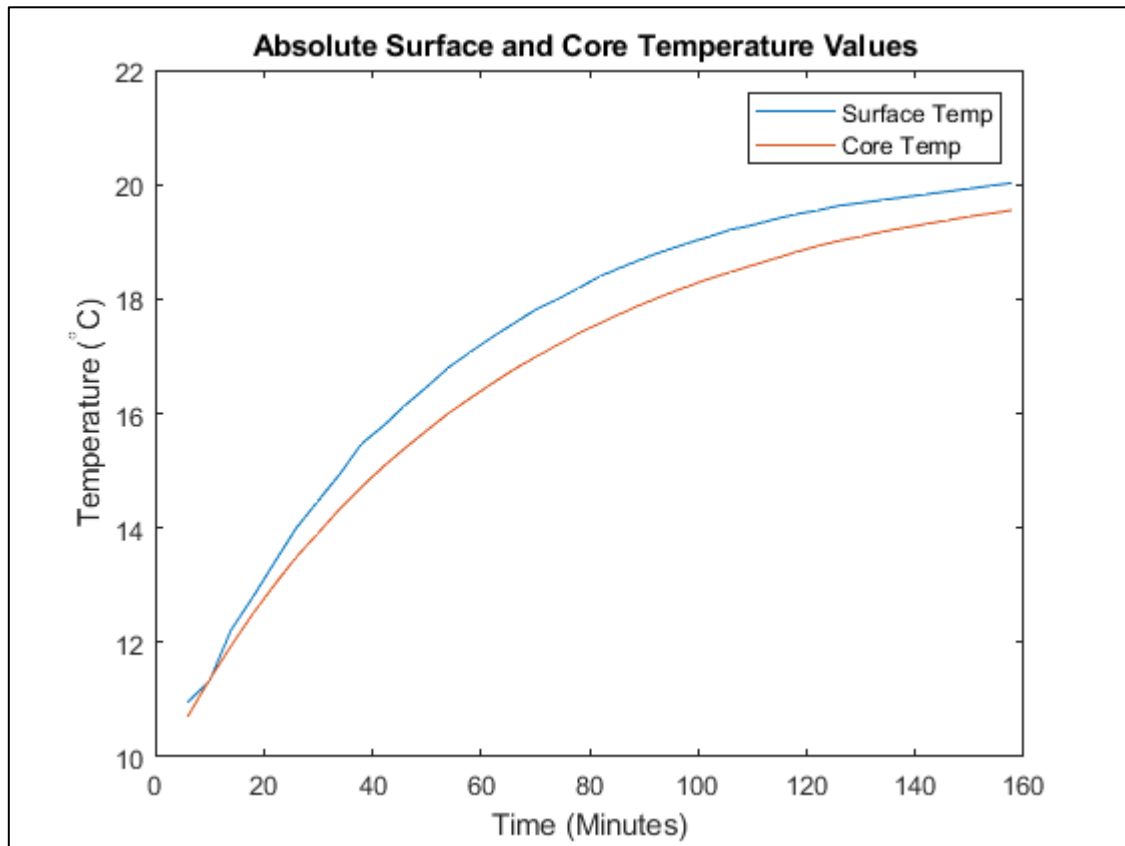


Unfiltered results of aluminium trials 1-3



Unfiltered results of aluminium trials 4-5



Absolute Temperature Measurement for the On-CMM Experiment



Absolute core and surface temperature measurement for the on-CMM experiment

Appendix C

1 MHz Transducer Certificate of Conformance

		NDT Systems		
		Worldwide Excellence In Ultrasonics		
5542 Buckingham Dr. • Huntington Beach • CA 92649 • Phone 714-893-2438 • Fax 714-897-3840				
Web Site http://www.ndt-systems.com				
CERTIFICATE OF CONFORMANCE				
ADVANCED NDT LIMITED UNIT 4, ELGAR BUSINESS CENTRE WORCESTER, WR2 6NJ UK		Date Date due P.O.#: NDTS#	12/18/2020 12/18/2021 05285 68032	
Quantity	Model No	Description	Serial No	
1	DVF014	UT Transducer	S/N 1220069	
Transducer Type	Nominal Frequency	Element Size		
Dual Element	1.00 MHz	.50"		
NDT Systems hereby certifies that the above Instrument(s) meet/or exceed manufacturer's applicable performance specifications and is/are in good working order. The equipment(s) used to calibrate these instruments is traceable to the National Institute of Standard and Technology within limitation of the N.I.S.T.'s calibration service. The policies and procedures at this facility comply with ANSI Z540 and Mil-Std 45662A. The above stated results are applicable only to the items listed on this Certificate. This Certificate may not be reproduced, except in full, without the written approval of NDT Systems, Inc.				
The Equipment Used:	S/N	N.I.S.T. Trace No.	Cal Date	Cal Due
SCOPE 11401	B010502	67971-23	4/07/2020	4/07/2021
SCOPE 11401	B010538	67971-26	4/07/2020	4/07/2021
SCOPE 11403	B010496	67971-29	4/07/2020	4/07/2021
AMP 11A32	B010817	67971-27	4/07/2020	4/07/2021
AMP 11A32	B084898	67971-28	4/07/2020	4/07/2021
AMP 11A32	B010728	67971-24	4/07/2020	4/07/2021
AMP 11A32	B020858	67971-25	4/07/2020	4/07/2021
AMP 11A34	B020979	67971-31	4/07/2020	4/07/2021
AMP 11A34	B043860	67971-30	4/07/2020	4/07/2021
5 STEP BLOCK	11-2537	76448-02		
5 STEP BLOCK	11-2538	76474-02		
5 STEP BLOCK	11-2539	76474-03		
7 STEP BLOCK	08-5995	76448-01		
7 STEP BLOCK	08-5997	76474-01		
Temperature:	72 Deg. F	Humidity:	40% RH	
Signed: 				
Quality Control				

1 MHz Transducer Characterization



NDT Systems, Inc.
5542 Buckingham Drive
Huntington Beach, CA



Transducer		Test Setup		Time Domain Results		Frequency Domain Results	
Part Number	DVF014	Test Target	1" BLOCK	-20dB Pulse Width(us)	1.720	Peak Frequency(MHz)	1.038
Serial Number	1220069	Test Material	STEEL	-40dB Pulse Width(us)	1.720	Center Frequency(MHz)	1.038
Nominal Frequency(MHz)	1.0	Pulse/Receiver Type	SPIKE	Received Voltage(Vpp)	0.842	-6dB Low Frequency(MHz)	0.305
Element Dimension(In)	0.5	High Voltage(Vpp)	100.0	Loop Gain(dB)	-83.898	-6dB High Frequency(MHz)	1.770
Focal Type	N/A	Damping(Ohms)	100.0	Water Path(us)	14.598	-6dB Bandwidth(MHz)	1.465
Focal Length(In)	0.0	Energy Level	470.0	Water Path Length(In)	0.431	-6dB Bandwidth(%)	141.176
Connector Type	BNC	Gain(dB)	42.4			-12dB Low Frequency(MHz)	0.122
		High Pass Filter(MHz)	0.1			-12dB High Frequency(MHz)	1.953
		Low Pass Filter(MHz)	32.0			-12dB Bandwidth(MHz)	1.831
						-12dB Bandwidth(%)	176.471

This test conforms to ASTM E1065

A. M. M. 12-11-20

Tech/Date

Appendix D

Cutting Routine G-Code

DEF REAL DEPTH = -13

DEF REAL PASSES = 3

;MULTIPLE PASSES PERPENDICULAR TO SENSOR FOR TEMPERATURE MEASUREMENT

;1MM DOC

TRANS X0 Y0 Z-0 ;45/30/15/5 15MM STEPS MEANS 5MM FROM PT100

T20

M6

G53 G40 G90

G54

S3500 M3

F750

LABEL01:

G0 X85 Y80

G0 Z2 ;M8

G1 Z=DEPTH

G41 X45

Y-70

G40 X85

G0 Z20

X85 Y80

G1 Z=DEPTH

G41 X30

Y-70

G40 X85

G0 Z20

X85 Y80

G1 Z=DEPTH

G41 X15

Y-70

G40 X85

G0 Z20

X85 Y80

G1 Z=DEPTH

G41 X10

Y-70

G40 X85

G0 Z20

DEPTH=DEPTH-1

PASSES=PASSES-1

IF PASSES>0 GOTOB LABEL01

G0 Z150

M9

M5

M30